Utah State University

DigitalCommons@USU

All Graduate Theses and Dissertations | Graduate Studies

5-2019

River Hydrology, Morphology, and Dynamics in an Intensively Managed, Transient Landscape

Sara Ann Kelly
Utah State University

Follow this and additional works at: https://digitalcommons.usu.edu/etd

 Part of the Physical Sciences and Mathematics Commons

Recommended Citation

Kelly, Sara Ann, "River Hydrology, Morphology, and Dynamics in an Intensively Managed, Transient Landscape" (2019). *All Graduate Theses and Dissertations*. 7479.
https://digitalcommons.usu.edu/etd/7479

This Dissertation is brought to you for free and open access by the Graduate Studies at DigitalCommons@USU. It has been accepted for inclusion in All Graduate Theses and Dissertations by an authorized administrator of DigitalCommons@USU. For more information, please contact digitalcommons@usu.edu.

RIVER HYDROLOGY, MORPHOLOGY, AND DYNAMICS IN AN INTENSIVELY MANAGED, TRANSIENT LANDSCAPE

by

Sara Ann Kelly

A dissertation submitted in partial fulfillment
of the requirements for the degree

of

DOCTOR OF PHILOSOPHY

in

Watershed Science

Approved:

_____	_____
Patrick Belmont, Ph.D. Major Professor	Peter Wilcock, Ph.D. Committee Member
_____	_____
Efi Foufoula-Geogiou, Ph.D. Committee Member	Joseph Wheaton, Ph.D. Committee Member
_____	_____
Jiming Jin, Ph.D. Committee Member	Richard S. Inouye, Ph.D. Vice Provost for Graduate Studies

UTAH STATE UNIVERSITY
Logan, Utah

2019

Copyright © Sara Ann Kelly 2019

All Rights Reserved

ABSTRACT

River Hydrology, Morphology, and Dynamics in an Intensively Managed, Transient Landscape

by

Sara Ann Kelly, Doctor of Philosophy

Utah State University, 2019

Major Professor: Dr. Patrick Belmont
Department: Watershed Sciences

Rivers sculpt Earth's surface, and carry with them eroded and dissolved materials from the landscape. Deconvolving the fraction of material carried by rivers that is natural versus those that are caused by humans remains a challenging task for river science and management. Many rivers in the US and globally are impaired for excessive amounts of sediment, which limits the ecological integrity, recreation potential, and municipal, agricultural, and industrial water use. To inform water quality policy and management strategies, advances are needed to better understand factors influencing delivery of water and sediment to rivers, and the response of rivers to changes in those factors . Here, I study the Minnesota River Basin (MRB), where geologic history, land use, and recent streamflow increases have created rapidly adjusting and exceedingly muddy rivers. I answer three overarching questions: 1) have agricultural drainage practices contributed to streamflow increases in the upper Midwest?, 2) which flood events accomplish the most erosion in incising tributaries of the MRB?, and 3) where does most of the sediment come

from and get transported to in the lower Minnesota River? Chapter 2 demonstrates that drainage practices are partly responsible for increasing streamflows in three intensively agricultural basins. Chapter 3 demonstrates that increased runoff in tributary basins has accelerated erosion of near-channel sources, such as bluffs. Further, I demonstrate that the 1.2 year return period floods cause the most erosion. Chapter 4 examines the downstream impacts of excessive sediment loading on the morphodynamics of the mainstem Minnesota River. I demonstrate that portions of the mainstem Minnesota River receiving excessive loading of coarse sediment from tributaries build broad alternate bars that create cross stream hydraulics favorable for meander migration and channel widening. Portions of the Minnesota River lacking significant bedload exhibit narrow bars that are less effective at driving meander migration and channel widening. The combined results suggest that agricultural drainage is increasing runoff, creating more erosive rivers, and recruiting material more readily from near-channel sources. These results support the notion that retention of agricultural drainage water would be an effective sediment reduction strategy.

(242 pages)

PUBLIC ABSTRACT

River Hydrology, Morphology, and Dynamics in an Intensively Managed, Transient Landscape

Sara Ann Kelly

Rivers create beautiful patterns and provide drinking water to millions. However an alarming number of rivers in the US and globally are threatened by excess sediment and nutrients. Agricultural rivers draining erodible soils are particularly vulnerable. Rivers of southern Minnesota provide a unique opportunity to study water and sediment dynamics in a naturally vulnerable system. Sediment reduction strategies are needed to ensure biological integrity and adequate water quality. Here, I address the questions: 1) have climate, land use practices, or both affected streamflows in Midwest agricultural rivers?, 2) which streamflows set the rate of river bluff erosion?, and 3) how do sediment supply and transport influence the form and behavior of the lower Minnesota River? Chapter 2 demonstrates, in three agricultural basins, that artificial drainage practices have decreased soil moisture, contributing to increases in streamflow. Chapter 3 quantifies river bluff erosion and identifies erosion by streamflows as the dominant erosion process. Erosion by common floods accomplishes the most cumulative bluff erosion. Bluff erosion contributes sediment to the Minnesota River. Chapter 4 shows how this coarse sediment influences the form and behavior of the Minnesota River. Therefore if flows were reduced, bluff erosion would slow, and the supply sediment to the Minnesota would slow, leading to less streambank erosion. Since streamflows have been increased by agricultural drainage practices, water retention solutions are needed to reduce high flows.

ACKNOWLEDGMENTS

First I would like to thank my major advisor, Dr. Patrick Belmont for believing that a 22 year old would one day finish her PhD. Patrick was always my biggest fan and mentor during this journey; I still tell myself, "you got this Kelly!" Thanks to Patrick, I had several amazing opportunities during my PhD including traveling to Ireland to attend a scientific meeting and prepare for teaching. Patrick rarely said no to extracurricular workshops and conference presentations, where he encouraged and supported me to give oral talks to further my presentation skills. Thank you for the opportunity to practice.

I would also like to thank my committee members and collaborators Efi Foufoula-Georgiou, Peter Wilcock, Joe Wheaton, Jiming Jin, Karen Gran, and Phil Larson. Efi and Karen, thank you for being strong female role models for me to look up to. Peter, thank you for always making yourself available to meet with me. Many, many thanks for the use of your secret office during my final weeks of writing.

I would also like to thank the many undergraduate and graduate students who helped with fieldwork over the years, including: Shayler Levine, Jay Hemmis, Michael Souffront, Keeling Schaffrath, Adam Fisher, Bruce Call, Angus Vaughan, Devon Libby, and Zachary Hilgendorf. I would also like to thank post-doctoral fellows Karthik Kumarasamy and Brendan Murphy for appreciated insight and assistance over the years. Zeinab Takbiri co-authored chapter 2 with me and was a pleasure to work with.

Finally I would like to thank my family. Mom and Jen, I know it wasn't easy living with me while I worked on my PhD. Thanks for always being supportive. Mike and Dad, while I don't see you often I know you're always there for me. Corey, thank you for your support and friendship.

The material in chapter 2 is based upon work supported by the National Science Foundation (Grant No. EAR-1209402) under the Water Sustainability and Climate Program (WSC): REACH (REsilience under Accelerated CHange), and by the National Science Foundation Graduate Research Fellowship Program under Grant No. 1147384. This research was supported by the Utah Agricultural Experiment Station, Utah State University, and approved as journal paper number 8938. The authors would like to thank Jon Czuba at Indiana University, and Karthik Kumarasamy, Eden Furtak-Cole, and Mitchell Donovan at Utah State University for their input. Thank you to Alexander Bryan at the Northeast Climate Science Center for generously providing evapotranspiration data from Bryan et al. 2015. Funding for AmeriFlux data resources was provided by the U.S. Department of Energy's Office of Science.

The material in chapter 3 is based upon work supported by the Geological Society of America Graduate Student Research Grant, the National Science Foundation (NSF) Graduate Research Fellowship Program (grant no. 1147384), the NSF Water Sustainability and Climate (WSC) – Category 2 grant (EAR- 1209445). Authors thank Peter Wilcock, Jack Schmidt, Joe Wheaton, and Jiming Jin, as well as current and former members of the Belmont Hydrology and Fine Sediment Laboratory for discussions. Two anonymous reviewers provided useful feedback. We thank Brendan Murphy for writing a Matlab script for point cloud rotation (Appendix B). Additional gratitude is extended to Se Jong Cho, St. Anthony Falls Research Laboratory; Stephanie Day, North Dakota State University; Karen Gran, University of Minnesota, Duluth; Philip Larson, Ben Von Korff, and many Geography Department undergraduate and graduate students, Minnesota State University, Mankato; Andy Wickert University of Minnesota, Minneapolis; Efi

Foufoula-Georgiou, University of California Irvine; and many Blue Earth County, MN landowners.

The material in chapter 4 is based upon work supported by the Geological Society of America Graduate Student Research Grant, the National Science Foundation (NSF) Graduate Research Fellowship Program (Grant No. 1147384), and the NSF Water Sustainability and Climate (WSC)—Category 2 grant (EAR-1209445). The authors are thankful for codes written by Bruce Call and Brendan Murphy. Additional gratitude is extended to Adam Fisher, Shayler Levine, Jack Trice, Jay Hemmis, and Michael Souffront for field assistance.

CONTENTS

Page

LIST OF TABLES

LIST OF FIGURES

CHAPTER 1

INTRODUCTION

Rivers act as Earth's arteries, draining water from Earth's surface. Water carries with it dissolved material as well as sediment particles that have been detached and transported from the terrestrial surface. In this way, rivers are largely responsible for sculpting Earth's surface. Rivers act as 'jerky' sediment conveyor belts, transporting sediment in an unsteady and non-uniform manner from uplands and hillslopes to depositional basins such as lowlands and the oceans, typically picking up, depositing, and re-suspending sediments many times along the way (Allen, 2008; Burt and Allison, 2010; Ferguson, 1981; Fryirs and Brierley, 2013; Harvey, 2010). While sediment is a natural component of river ecosystems, in excess or deficit it can create problems for water quality and impair biological integrity. Although some rivers are naturally prone to carry high sediment loads, many rivers transport excessive amounts of sediment as a result of human disturbance in the watershed.

Humans alter rivers both directly and indirectly for municipal, agricultural, industrial, navigational, recreational, and hydropower uses. As a direct result of such river alterations, a growing number of US rivers (44% and 55% of river miles assessed in 2004 and 2008/9, respectively) do not meet their designated uses, many of which are impaired for sediment, especially excessive amounts of fine sediment (United States Environmental Protection Agency, 2017, 2009). For many Midwestern agricultural watersheds, identifying the cause of excess sediment and understanding how to reduce fine sediment loading is a high priority, as many of these rivers are impaired for turbidity and total suspended solids under the Clean Water Act of 1972, Section 303d. Effective

strategies for reducing sediment loads, especially when sources are diffuse and distributed across vast areas, are urgently needed to restore degraded rivers.

Billions of dollars are spent each year on river restoration efforts to increase public safety from flooding and/or infrastructure damage, improve aquatic and riparian habitat for threatened and endangered species, decrease nutrient loading and delivery rates, and increase the aesthetic value of rivers (Bernhardt et al., 2005; Wohl et al., 2015). Basic scientific understanding of river processes involving water and sediment is critical to successful river restoration (Wohl et al., 2015). Restoration efforts may be tenuous given that we currently lack a unified theory to predict how, where and when rivers meander and how river channels adjust to changing water and sediment boundary conditions. Predicting river dynamics, especially over large scales, remains one of the grand challenges of Earth Surface Science (National Research Council, 2010).

Decades of research have yielded much progress towards theoretical and mechanistic understanding of river processes, such as meander migration (Braudrick et al., 2009; Ikeda and Parker, 1989), sediment transport (Garcia, 1999; van Rijn, 1984a, 1984b; Wilcock and Crowe, 2003; Wright and Parker, 2005), bank erosion (Simon et al., 2000), and bedform development (Bennett and Best, 1995; Dietrich and Smith, 1983; Nelson et al., 1995; Venditti et al., 2005; Venditti and Bennett, 2000). While significant advances towards understanding river and sediment dynamics have been achieved through flume experiments (Best, 1988; Blanckaert, 2010; Friedkin, 1945; Gran and Paola, 2001; Menard, 1950; Podolak and Wilcock, 2013; Van Dijk et al., 2012; Venditti et al., 2012), relatively few studies have applied this physical understanding to large, alluvial rivers with non-uniform and non-stationary boundary conditions. This is in part

due to the challenges in locating an appropriate study system and difficulties obtaining field measurements that constrain spatial and temporal variability.

Our ability to monitor landscapes remotely and make measurements across a wide range of temporal and spatial scales has increased significantly over the past decade (Palmer et al., 2015; Passalacqua et al., 2015). Most notably, our constraints on the fluxes and boundary conditions of geomorphic systems has been greatly enhanced via increased availability of high resolution aerial imagery (e.g., satellite, fixed-wing aircraft photo surveys, and remote controlled aerial vehicles), high resolution topography data (e.g., aerial and terrestrial lidar, real-time-kinematic GPS, structure-from-motion photogrammetry, multi-beam bathymetry data), and high resolution monitoring of hydrologic fluxes (satellite and terrestrial radar systems, remotely sensed groundwater monitoring, acoustic Doppler velocimetry). Increases in computational processing power enable geomorphologists to analyze these large datasets on standard desktop computers. Thus, the field of geomorphology is well positioned to connect recent advances in theoretical understanding with these high resolution empirical datasets to substantially improve our understanding of how natural systems function and predict how they might respond to perturbations.

This dissertation uses a wide variety of datasets to study river hydrologic, morphologic, and dynamic change in a large, intensively managed, transient landscape over the past 80 years. The Minnesota River basin has been heavily altered for agriculture and is currently impaired for sediment, nutrients, and aquatic life. Furthermore, pervasive increases in hydrology are exacerbating erosion and water quality problems. Basins similar to the Minnesota River are common throughout large swaths of the central USA

and other temperate, agricultural regions around the world. Scientifically, this research improves our understanding of and ability to predict sediment supply and transport in perturbed river-floodplain networks. This work also has societal importance, as it provides federal, state, and local agencies with essential context regarding the historical range of streamflows and channel variability, as well as insights regarding the implications for landscape erosion, sediment transport, and channel morphology and dynamics. Such information is vital for development of restoration plans for the Minnesota River and its tributaries.

The main thrust of this dissertation is exploring the cascade of potential linkages between agricultural drainage, increases in streamflow (chapter 2), accelerated erosion of near-channel features (chapter 3), and river channel dynamics (chapter 4). Understanding the extent to which each link in this cascade influences the next is essential for developing a strategy to reduce sediment loading in the Minnesota River Basin. Specifically, if we were to find that agricultural drainage has not influenced streamflows, or if increased streamflows are not responsible for accelerated erosion of near-channel features, then development of water storage capacity may not be an effective conservation practice for reducing sediment loading in the Minnesota River Basin. Alternatively, if we find that there are clear and direct linkages between agricultural drainage, increased streamflows, accelerated erosion of near-channel features and amplification of river channel dynamics, then gains in water quality will likely require flow reductions and cooperation with agricultural drainage districts (chapter 5).

Chapter 2 addresses an ongoing scientific debate over the influence of climate versus land use practices on Midwestern streamflows (Belmont et al., 2016; Foufoula-

Georgiou et al., 2016, 2015; Gupta et al., 2015; Schottler et al., 2014). We develop a water budget and use statistical techniques to investigate whether precipitation changes alone can explain streamflow change in four agricultural river basins. Other factors, such as land cover change, specifically extensive lake, wetland and field tile drainage for row crop agriculture, can also alter runoff. Daily, monthly, and annual flow metrics document increasing streamflow. These streamflow observations, in combination with precipitation, evapotranspiration, and land use data reveal that climate factors alone cannot explain increasing streamflow. Increased tile drainage installation as well as increased precipitation both appear to play a role to increase streamflows and therefore potentially affect downstream flood risk, channel adjustment, and sediment and nutrient transport. The following chapters (3 & 4) explore the sediment related implications of increasing streamflow.

Achieving sediment reduction targets requires understanding of sediment sources and processes of erosion. In Minnesota River basin tributaries, easily erodible near channel sources dominate the watershed sediment budget, with river bluffs contributing the most sediment (Belmont et al., 2011; Day et al., 2013). However, previously little was known about the relative importance of fluvial processes over other processes, such as freeze-thaw. Additionally, it is useful to consider streamflow magnitude and frequency, to determine which flows cause the greatest amount of erosion over decadal timescales? In chapter 3, I evaluate the magnitude of bluff erosion processes and frequency of flows that cause erosion to determine floods that cause the most cumulative bluff erosion. I use a combination of Structure from Motion and time lapse photogrammetry to observe failures at a daily time-step and measure rapid river bluff

erosion in muddy tributaries of the Minnesota River. Specifically, I document the importance of fluvial scour, precipitation, freeze–thaw, as well as other drivers of bluff erosion.

Chapter 4 addresses the question 'what dictates channel form and dynamics in a perturbed sand bed river?' Previous research and qualitative observations from the field and aerial photographs indicate that the Minnesota River exhibits some differences in form and dynamics along its length from Mankato to Fort Snelling, but the cause was unclear (Groten et al., 2016; Lenhart et al., 2013; Libby, 2018; Lauer et al., 2017). Leveraging this knowledge and existing data with additional field samples and analyses I characterize river slope, bed grain size, bar topography, channel migration, channel widening, and aggradation/degradation. I explain channel form and dynamics using a sediment budget, calculations of sediment transport, floodplain characteristics, and downstream hydraulic controls. The results of this work shed light on the sediment dynamics of the lower Minnesota River and urge future research to investigate mechanistic links between sediment transport, bar form, and meander migration.

In chapter 5, I synthesize the results of all three chapters, discuss sediment reduction targets for the Minnesota River, and make recommendations to Minnesota's pollution regulatory agency based on these findings.

References

Allen, P.A., 2008. From landscapes into geological history. Nature 451, 274–276. https://doi.org/10.1038/nature06586

Belmont, P., Gran, K.B., Schottler, S.P., Wilcock, P.R., Day, S.S., Jennings, C., Lauer, J.W., Viparelli, E., Willenbring, J.K., Engstrom, D.R., Parker, G., 2011. Large shift in source of fine sediment in the upper Mississippi River. Environ. Sci. Technol. 45, 8804–8810. https://doi.org/10.1021/es2019109

Belmont, P., Stevens, J.R., Czuba, J.A., Kumarasamy, K., Kelly, S.A., 2016. Comment on "Climate and agricultural land use change impacts on streamflow in the upper midwestern United States," by Satish C. Gupta et al. Water Resour. Res. 52, 7523–7528. https://doi.org/10.1002/2015WR018476

Bennett, S.J., Best, J.L., 1995. Mean flow and Turbulence structure over fixed, two-dimensional dunes: implications for sediment transport and bedform stability. Sedimentology 42, 491–513.

Bernhardt, E.S., Palmer, M.A., Allan, J.D., Alexander, G., Barnas, K., Brooks, S., Carr, J., Clayton, S., Dahm, C., Follstad-Shah, J., Galat, D., Gloss, S., Goodwin, P., Hart, D., Hassett, B., Jenkinson, R., Katz, S., Kondolf, G.M., Lake, P.S., Lave, R., Meyer, J.L., Donnell, T.K.O., Pagano, L., Powell, B., Sudduth, E., 2005. Sythesizing U.S. River Restoration Efforts. Science (80-.). 308, 636–637. https://doi.org/10.1126/science.1109769

Best, J.L., 1988. Sediment transport and bed morphology at river channel confluences. Sedimentology 35, 481–498.

Blanckaert, K., 2010. Topographic steering, flow recirculation, velocity redistribution, and bed topography in sharp meander bends. Water Resour. Res. 46, 1–23. https://doi.org/10.1029/2009WR008303

Braudrick, C.A., Dietrich, W.E., Leverich, G.T., Sklar, L.S., 2009. Experimental evidence for the conditions necessary to sustain meandering in coarse-bedded rivers. Proc. Natl. Acad. Sci. 106, 16936–16941. https://doi.org/10.1073/pnas.0909417106

Burt, T.P., Allison, R.J., 2010. Sediment Cascades in the Environment: An Integrated Approach, in: Burt, T.P., Allison, R.J. (Eds.), Sediment Cascades : An Integrated Approach. John Wiley and Sons Ltd, Hoboken, New Jersey, pp. 1–15.

Day, S.S., Gran, K.B., Belmont, P., Wawrzyniec, T., 2013. Measuring bluff erosion part 1: Terrestrial laser scanning methods for change detection. Earth Surf. Process. Landforms 38, 1055–1067. https://doi.org/10.1002/esp.3353

Dietrich, W.E., Smith, J.D., 1983. Influence of the point bar on flow through curved channels. Water Resour. Res. 19, 1173–1192.

Ferguson, R.I., 1981. Channel form and channel changes, in: Lewin, J. (Ed.), British Rivers. Allen and Unwin, London, pp. 90–125.

Foufoula-Georgiou, E., Belmont, P., Wilcock, P., Gran, K., Finlay, J.C., Kumar, P., Czuba, J.A., Schwenk, J., Takbiri, Z., 2016. Comment on "Climate and agricultural land use change impacts on streamflow in the upper midwestern

United States" by Satish C. Gupta et al. Water Resour. Res. 52, 7536–7539. https://doi.org/10.1002/2015WR018494

Foufoula-Georgiou, E., Takbiri, Z., Czuba, J.A., Schwenk, J., 2015. The change of nature and the nature of change in agricultural landscapes: Hydrologic regime shifts modulate ecological transitions. Water Resour. Res. 51, 6649–6671. https://doi.org/10.1002/2015WR017637

Friedkin, J.F., 1945. A Laboratory Study of the Meandering of Alluvial Rivers. Vicksburg, Mississippi.

Garcia, M.H., 1999. Sedimentation and Erosion Hydraulics, in: Mays, L. (Ed.), Hydraulic Design Handbook. McGraw-Hill Inc.

Gran, K., Paola, C., 2001. Riparian vegetation controls on braided stream dynamics. Water Resour. Res. 37, 3275–3283.

Groten, J.T., Ellison, C.A., Hendrickson, J.S., 2016. Suspended-Sediment Concentrations, Bedload, Particle Sizes, Surrogate Measurements, and Annual Sediment Loads for Selected Sites in the Lower Minnesota River Basin, Water Years 2011 through 2016, U.S. Geological Survey Scientific Investigations Report 2016-5174. Reston, VA.

Gupta, S.C., Kessler, A.C., Brown, M.K., Zvomuya, F., 2015. Climate and agricultural land use change impacts on streamflow in the upper midwestern United States. Water Resour. Res. 51, 5301–5317. https://doi.org/10.1002/2015WR017323

Harvey, A.M., 2010. Local buffers to the sediment cascade: debris cones and alluvial fans, in: Burt, T.P., Allison, R.J. (Eds.), Sediment Cascades: An Integrated Approach. John Wiley and Sons Ltd, West Sussex, United Kingdom, pp. 153–180.

Ikeda, S., Parker, G. (Eds.), 1989. River Meandering. American Geophysical Union, Washington, D.C.

Lauer, J.W., Echterling, C., Lenhart, C., Belmont, P., Rausch, R., 2017. Air-photo based change in channel width in the Minnesota River basin: Modes of adjustment and implications for sediment budget. Geomorphology 297, 170–184. https://doi.org/https://doi.org/10.1016/j.geomorph.2017.09.005

Lenhart, C.F., Titov, M.L., Ulrich, J.S., Nieber, J.L., Suppes, B., 2013. The Role of Hydrologic Alteration and Riparian Vegetation Dynamics in Channel Evolution along the Lower Minnesota River. Trans. Am. Soc. Agric. Biol. Eng. 56, 549–561.

Libby, D., 2018. Assessing historical planform channel change in an altered watershed with quantification of error and uncertainty present in a GIS/aerial photography-based analysis; case study: Minnesota River, Minnesota, USA. Minnesota State University.

Menard, H.W., 1950. Sediment Movement in Relation to Current Velocity. J. Sediment. Petrol. 20, 148–160.

National Research Council, 2010. Landscapes on the Edge: New Horizons for Research on Earth's Surface. The National Academies Press, Washington D.C.

Nelson, J.M., Shreve, R.L., Mclean, S.R., Drake, G., 1995. Role of near-bed turbulence structure in bed load transport and bed form mechanics. Water Resour. Res. 31, 2071–2086.

Palmer, S.C.J., Kutser, T., Hunter, P.D., 2015. Remote sensing of inland waters: Challenges, progress and future directions. Remote Sens. Environ. 157, 1–8. https://doi.org/10.1016/j.rse.2014.09.021

Passalacqua, P., Belmont, P., Staley, D.M., Simley, J.D., Arrowsmith, J.R., Bode, C.A., Crosby, C., DeLong, S.B., Glenn, N.F., Kelly, S.A., Lague, D., Sangireddy, H., Schaffrath, K., Tarboton, D.G., Wasklewicz, T., Wheaton, J.M., 2015. Analyzing high resolution topography for advancing the understanding of mass and energy transfer through landscapes: A review. Earth-Science Rev. 148, 174–193. https://doi.org/10.1016/j.earscirev.2015.05.012

Podolak, C.J.P., Wilcock, P.R., 2013. Experimental study of the response of a gravel streambed to increased sediment supply. Earth Surf. Process. Landforms 38, 1748–1764. https://doi.org/10.1002/esp.3468

Schottler, S.P., Urlich, J., Belmont, P., Moore, R., Lauer, J.W., Engstrom, D.R., Almendinger, J.E., 2014. Twentieth century agricultural drainage creates more erosive rivers. Hydrol. Process. 28, 1951–1961. https://doi.org/10.1002/hyp.9738

Simon, A., Curini, A., Darby, S.E., Langendoen, E.J., 2000. Bank and near-bank processes in an incised channel. Geomorphology 35, 193–217. https://doi.org/10.1016/S0169-555X(00)00036-2

United States Environmental Protection Agency, 2009. The National Water Quality Inventory: Report to Congress for the 2004 Reporting Cycle, EPA 841-R-08-001. Washington, D.C.

United States Environmental Protection Agency, 2017. National Water Quality Inventory: Report to Congress, EPA 841-R-16-011. Washington, DC.

Van Dijk, W.M., Van De Lageweg, W.I., Kleinhans, M.G., 2012. Experimental meandering river with chute cutoffs. J. Geophys. Res. 117, 1–18. https://doi.org/10.1029/2011JF002314

van Rijn, L.C., 1984. Sediment Transport, Part I: Bed Load Transport. J. Hydraul. Eng. https://doi.org/10.1061/(ASCE)0733-9429(1984)110:10(1431)

van Rijn, L.C., 1984. Sediment transport, Part II: Suspended load transport. J. Hydraul. Eng. 110, 1613–1641. https://doi.org/10.1061/(ASCE)0733-9429(1987)113:9(1187)

Venditti, J.G., Nelson, P.A., Minear, J.T., Wooster, J., Dietrich, W.E., 2012. Alternate bar response to sediment supply termination. J. Geophys. Res. 117, 1–18. https://doi.org/10.1029/2011JF002254

Venditti, J.G., Church, M.A., Bennett, S.J., 2005. Bed form initiation from a flat sand bed. J. Geophys. Res. Earth Surf. 110, 1–19. https://doi.org/10.1029/2004JF000149

Venditti, J.G., Bennett, S.J., 2000. Spectral Analysis of Turbulent Flow and Suspended Sediment Transport Over Fixed Dunes. J. Geophys. Res. 105, 22035–22047.

Wilcock, P.R., Crowe, J.C., 2003. Surface-based Transport Model for Mixed-Size Sediment. J. Hydraul. Eng. 129, 120–128. https://doi.org/10.1061/(ASCE)0733-9429(2003)129:2(120)

Wohl, E., Lane, S., Wilcox, A., 2015. The Science and Practice of River Restoration. Water Resour. Res. 51, 5974–5997. https://doi.org/10.1002/2014WR016874.Received

Wright, S., Parker, G., 2005. Modeling downstream fining in sand-bed rivers. II: application. J. Hydraul. Res. 43, 621–631. https://doi.org/10.1080/00221680509500382

CHAPTER 2

HUMAN AMPLIFIED CHANGES IN PRECIPITATION-RUNOFF PATTERNS IN LARGE RIVER BASINS OF THE MIDWESTERN UNITED STATES[1]

Abstract

Complete transformations of land cover from prairie, wetlands, and hardwood forests to row crop agriculture and urban centers are thought to have caused profound changes in hydrology in the Upper Midwestern US since the 1800s. In this study, we investigate four large (23,000-69,000 km2) Midwest river basins that span climate and land use gradients to understand how climate and agricultural drainage have influenced basin hydrology over the last 79 years. We use daily, monthly, and annual flow metrics to document streamflow changes and discuss those changes in the context of precipitation and land use changes. Since 1935, flow, precipitation, artificial drainage extent, and corn and soybean acreage have increased across the region. In extensively drained basins, we observe 2 to 4 fold increases in low flows and 1.5 to 3 fold increases in high and extreme flows. Using a water budget, we determined that the storage term has decreased in intensively drained and cultivated basins by 30%-200% since 1975, but increased by roughly 30% in the less agricultural basin. Storage has generally decreased during spring and summer months and increased during fall and winter months in all watersheds. Thus, the loss of storage and enhanced hydrologic connectivity and efficiency imparted by artificial agricultural drainage appear to have amplified the streamflow response to

[1]Kelly, S. A., Takbiri, Z., Belmont, P., & Foufoula-Georgiou, E. (2017). Human amplified changes in precipitation-runoff patterns in large river basins of the Midwestern United States. Hydrology and Earth System Sciences, 1–37. https://doi.org/10.5194/hess-2017-133

precipitation increases in the Midwest. Future increases in precipitation are likely to further intensify drainage practices and increase streamflows. Increased streamflow has implications for flood risk, channel adjustment, and sediment and nutrient transport and presents unique challenges for agriculture and water resource management in the Midwest. Better documentation of existing and future drain tile and ditch installation is needed to further understand the role of climate versus drainage across multiple spatial and temporal scales.

1 Introduction

1.1 Whether humans, climate or both have caused streamflow change matters for water quality and watershed management

The magnitude, frequency, duration and timing of streamflows strongly influence water quality, sediment and nutrient transport, channel morphology, and habitat conditions of a river channel. While streamflows fluctuate naturally over event to millennial timescales, humans have also altered rainfall-runoff processes in pervasive and profound ways (Vörösmarty et al., 2004). For example, humans have substantially altered the timing and magnitude of evapotranspiration, have dammed, channelized and leveed waterways, and have installed artificial drainage networks in former wetlands (Boucher et al., 2004; Dumanski et al., 2015; Rockström et al., 2014; Schottler et al., 2014; Vörösmarty et al., 2004) . While it is inevitable that wetland removal and artificial drainage will change rainfall-runoff processes, the effects of drainage on the hydrologic cycle may be subtle and difficult to discern, and may manifest differently at different spatial scales and times of year (e.g., Bullock and Acreman, 2003; Foufoula-Georgiou et al., 2016; Irwin and Whiteley, 1983; O'Connell et al., 2007).

Systematic increases in peak, mean, total, and base flows are widely reported in the Midwestern USA. Such increases have been attributed to changes in climate, such as increasing precipitation and earlier snowmelt, and land use, including widespread conversion from perennial vegetation, such as grasses, to annual row crops, primarily corn and soybean, and the addition of artificial drainage (e.g. Foufoula-Georgiou et al., 2015; Frans et al., 2013; Gerbert and Krug, 1996; Juckem et al., 2008; Novotny and Stefan, 2007; Schilling and Libra, 2003; Schottler et al., 2014; Xu et al., 2013; Zhang and Schilling, 2006). Furthermore large-scale, land use land cover (LULC) changes influence surface energy fluxes and thus have feedbacks on climate and water balances. As a result of the Green Revolution, net primary production increased during the 20th Century in the Midwestern US, which subsequently increased ET demands, especially during the peak growing season (Mueller et al., 2015). Corn yields (bushels per acre) tripled in the US between 1949 and 1989 (U.S. Department of Agriculture Bureau of Agricultural Economics Crop Reporting Board, 1949; U.S. Department of Agriculture National Agricultural Statistics Service Agricultural Statistics Board, 1990). However, any increase in ET demand due to crop yield increases may have been offset during this time by the addition and replacement of agricultural drainage. Regional studies have reported increases in Midwestern crop yields and yet simultaneously decreases in ET for artificially drained agricultural basins, where streamflows have subsequently increased during the 20th Century. (Frans et al., 2013; Schottler et al., 2014). Therefore, the question remains: how have combined climate and land use changes affected streamflows in very large (>104 km2) watersheds, the scale at which many states and federal programs are often tasked with monitoring and evaluating water quality?

Many basins across the Midwestern Corn Belt and around the world are experiencing greater runoff, higher sediment and nutrient loads, and accelerated loss of habitat than in the past (Blann et al., 2009). Linkages between artificial agricultural drainage and increased nutrient export have been well documented (David et al., 1997; Goolsby et al., 1999; Kreiling and Houser, 2016; Letey et al., 1977; Randall and Mulla, 2001; Royer et al., 2006; Schilling et al., 2017; Sims et al., 1998). Less research has focused on the implications of hydrologic change for sediment loads in agricultural landscapes. For waters impaired by sediment under the US Clean Water Act (CWA), EU Water Framework Directive, and similar regulations around the world, loads often consist of both natural and human-derived sediment sources (Belmont et al., 2011; Gran et al., 2011; Belmont and Foufoula-Georgiou, 2017). Differentiating between these two sources is often very difficult, and yet essential for identifying and achieving water quality standards (Belmont et al., 2014; Trimble and Crosson, 2000; Wilcock, 2009). Sediment sources derived from near or within the channel itself (e.g., bank erosion from channel widening) are particularly sensitive to changes in streamflows (Lauer et al., in review; Schottler et al., 2014; Lenhart et al., 2013). Bank erosion is a significant sediment source in many alluvial rivers, contributing as much as 80% to 96% of the sediment that comprise a river's total sediment load (Kronvang et al., 2013; Palmer et al., 2014; Schaffrath et al., 2015; Simon et al., 1996; Stout et al., 2014; Willett et al., 2012). For some agricultural basins, erosion of near-channel sources contributes more fine sediment than does agricultural field erosion (Belmont et al., 2011; Lenhart et al., 2012; Trimble, 1999). However, if artificial drainage practices act to amplify streamflows, then the source of accelerated bank erosion may still be linked to agriculture. Artificial drainage is

currently unregulated at the federal level in the US and many countries around the world. Therefore, in stark contrast to urban hydrology, progress in understanding the effects of agricultural drainage has been hindered by the fact that accurate data regarding the location, size, depth, efficiency and connectivity of sub-surface drainage systems are rarely available.

1.2 Artificial drainage improves agricultural productivity but may amplify streamflows in large watersheds

The United States is the largest producer of corn and soybeans in the world (Boyd and McNevin, 2015; Guanter et al., 2014). Exceptionally high agricultural productivity over the past century and a half required massive conversion of grasslands, wetlands, and forests to agricultural lands (Dahl, 1990; Dahl and Allord, 1996; Marschner, 1974). Although many advances in cropping practices have led to the modern day prosperity of the Corn Belt, artificial drainage has played a critical role for agriculture in the Midwestern USA. Throughout this paper "artificial drainage" is used as a general term that refers to both human installed surface ditches and subsurface tile drainage. Tile drains and ditch networks are installed to ameliorate water-logged soils, which are known to limit crop growth (Hillel, 1998; Sullivan et al., 2001; Wuebker et al., 2001). Modern tile drains are composed of corrugated plastic tubing and are typically installed at depths of 1-2 m to control the elevation of the water table below the soil surface (Hillel, 1998).

The economic benefits of artificial drainage are well understood by Midwestern farmers, who have invested heavily in drainage systems to reduce soil moisture, surface overland flow, and soil erosion, and increase land value, ease of equipment operation, and production of first class crops such as corn and soy (Burns, 1954; Fausey et al., 1987;

Hewes and Frandson, 1952; Johnston, 2013; McCorvie and Lant, 1993). Installation or enhancement of tile drainage systems often occurs simultaneously with land conversion from wild hay and small grains to soybeans, as Fig. A1 demonstrates in the Supplement (Blann et al., 2009; Burns, 1954; Hewes and Frandson, 1952). Conversion of perennial grasses to corn and soybean rotations doesn't necessarily lead to a reduction in evapotranspiration (ET) over the course of an entire growing season, at least for well drained soils (Hamilton et al., 2015). However, several studies report a reduction of ET early in the growing season (Hickman et al., 2010; McIsaac et al., 2010; Schottler et al., 2014; Zeri et al., 2013) and greater evapotranspiration rates than native prairie during the peak growing season (Wolf and Market, 2007; Zeri et al., 2013). Thus changes in land cover (and ET) and drainage expansion have been found to alter watershed hydrology and increase mean annual flows (Harrigan et al., 2014; Kibria et al., 2016), base flows (Juckem et al., 2008; Robinson, 1990; Schilling and Libra, 2003; Xu et al., 2013), annual peak flows (Dumanski et al., 2015; Magner et al., 2004; Skaggs et al., 1980, 1994), and total flow volumes (Dumanski et al., 2015; Frans et al., 2013; Lenhart et al., 2011). While it seems inevitable that altering ET and subsurface drainage efficiency should have measureable effects on streamflow, the combined effects have proven difficult to isolate empirically, especially across scales, due to measurement uncertainties, high temporal and spatial variability in antecedent moisture conditions and runoff processes, a shift towards a wetter climate today than in the historical past, as well as limited documentation of artificial drainage installation in the US.

1.3 Research questions

In this paper we couple analysis of historical patterns in large (>104 km2) river basin hydrology in the Midwestern USA with historical climate and land use data to identify how each of these factors have influenced streamflow patterns. Specifically, we address the following questions: (1) how have LULC, climate, and streamflows changed during the 20th and 21st centuries; (2) what are the timing, time scales and times of year that changes are most prominent; and (3) can changes in climate alone explain changes in streamflow? We hypothesize that in the most intensively managed agricultural basins, climate alone cannot explain streamflow patterns, and that land use changes in the Midwestern USA have amplified the expected hydrologic change associated with climate. We test this hypothesis in four large river basins with different histories and climates using a suite of quantitative methods that test the statistical significance of changes in streamflow and precipitation at multiple time scales. Finally, we present a water budget for each basin.

We acknowledge that the conversion of precipitation to streamflow occurs by a complex suite of physical processes. Inevitably, we lack temporal and spatial coverage/resolution of all of the relevant hydrologic fluxes (e.g., groundwater, actual evapotranspiration, infiltration, soil water flux rates) to characterize the system completely and have limited ability to ascribe subtle changes to any given physical process, especially at large scales. Yet, with increasing concerns about water quality and aquatic biota, disentangling the effects of artificial drainage and changing precipitation patterns is important for evaluating economic costs, benefits and risks, predicting the effects of future land and water management and informing future policy.

2 Study areas: large river basins of the Midwest with varying degrees of climate and land use change

We analyze hydrologic and land use change in four large Midwestern watersheds during 1935-2013. We selected these basins for the following reasons: all are agricultural, to various degrees, primarily producing corn and soybeans; all are located mainly within the Central Lowland physiographic province and were affected by continental glaciation resulting in mostly flat, poorly drained uplands and incised river valleys (Arnold et al., 1999; Barnes, 1997; Belmont et al., 2011; Day et al., 2013; Gran et al., 2009; Groschen et al., 2000; Rosenberg et al., 2005; Stark et al., 1996); and all are characterized by a humid, temperate climate (Kottek et al., 2006). Additionally, all four basins also contain waters impaired for excessive sediment under the US Clean Water Act. Therefore, deconvolving climate and land use effects on basin hydrology is essential for developing and attaining sediment- and nutrient-related water quality standards. Despite the broad similarities between basins, we have intentionally selected watersheds that span a gradient of climate and land use change. From northwest to southeast, these include: the Red River of the North basin (RRB), upstream of Grand Forks, ND (67,005 km2), Minnesota River basin (MRB), upstream of Jordan, MN (42,162 km2), Chippewa River basin (CRB), upstream of Durand, WI (23,444 km2), and Illinois River basin (IRB), upstream of Valley City, IL (69,268 km2) (Fig. 2-1).

Soils in the Minnesota River basin consists of organic rich, but poorly drained mollisols with a very small area consisting of alfisols and entisols (Stark et al., 1996). The Illinois River basin is generally dominated mollisols, containing around 1% organic matter and generally of low to very low permeability, with some presence of more permeable alfisols and entisols (Arnold et al., 1999; Groschen et al., 2000). The

dominant soil orders found in the Red River of the North basin include mollisols and alfisols with some areas underlain by entisols and histosols (Stoner et al., 1993). In the Chippewa River basin, alfisols and spodosols are most prevelant, with occasional pockets of entisols, mollisols, and histosols (Hartemink et al., 2012; Soil Survey Staff, NRCS).

There is a broad northwest to southeast precipitation and temperature gradient across the region (Fig. A2). The RRB is the coldest and driest of all four study basins, although the last two decades (1990's and 2000's) have been the wettest in historical times. Precipitation records, lake level elevations, and paleoclimate studies indicate that the basin is prone to extreme climate variability (Fritz et al., 2000; Miller and Frink, 1984). Much like the RRB, the adjacent MRB is uniquely situated at a "climatic triple junction" where warm moist air from the Gulf of Mexico, cold dry air from the Artic, and dry Pacific air dominate at different times of the year and have varied in relative dominance in the past (Dean and Schwalb, 2000; Fritz et al., 2000). Temperature and humidity in the CRB are more strongly influenced by the Great Lakes than in the other basins. The southwest IRB generally receives more precipitation than the northeast in all months. On average each basin from northwest to southeast receives 589 mm, 716 mm, 822 mm, and 960 mm annually, with 59%-68% of the annual precipitation falling in the spring (MAM) and summer (JJA) months based on annual long term means, 1981-2010 (Fig. A2). Recent increases in precipitation and streamflows have been reported across the region during the last few decades (Foufoula-Georgiou et al., 2015; Frans et al., 2013; Gerbert and Krug, 1996; Groisman et al., 2001; Juckem et al., 2008; Novotny and Stefan, 2007; Schottler et al., 2014).

Settlement, agricultural intensification, and development differ in timing and intensity among basins but are generally similar. During the early to mid-nineteenth century, permanent occupation of the Midwest was difficult without the aid of artificial drainage (Beauchamp, 1987). Beginning in the mid-1800s, organized drainage districts and enterprises installed ditches and tile to drain many permanently or seasonally wet areas and create more arable land (Beauchamp, 1987; Skaggs et al., 1994). Between 1850 and 1930 Illinois, Minnesota, and Wisconsin lost an estimated 90%, 53%, and 32% of state wetlands, respectively (McCorvie and Lant, 1993). Enormous tracts of wetlands and tall grass prairie (millions of acres) were levelled and drained, mainly by surface ditches and canals, in the RRB during this same time (Miller and Frink, 1984). Artificial drainage increased property value, and as corn and soybean commodity prices increased, as they did following WWII, in the mid-1970's, and most recently a tripling of commodity prices between 2002-2012 (Glaser, 2016; Johnston, 2013), lands previously cultivated for small grains or left as wet meadows were drained and converted to soybean and corn fields (Blann et al., 2009; Burns, 1954; Wright and Wimberly, 2013). Although many advances in cropping practices have led to the modern day prosperity of the Corn Belt, drainage installation and intensification has played a critical role for agriculture in the Midwestern US. Today the RRB, MRB, CRB, and IRB respectively contain 45%, 78%, 12% and 60% of land cultivated for corn and soybeans, yet estimates of tile drainage in these basins remain poorly constrained (Fig. 2-1). Within the Bois de Sioux watershed, a sub-basin of the RRB where permits are required for drain tile installation, annual installation has increased from 5 km in 1999 to 3,096 km in 2015 for a cumulative total of 24,304 km of

new tile installed since 1999 (Bois de Sioux Watershed District, 2015). Tile drainage installation in all basins continues to this day.

The other major anthropogenic impact that affects all basins is dams installed for hydropower, navigation, water resources, and recreation. Most of the dams in our study basins are small and were constructed in the late 1800's and early 1900's (Barnes, 1997; Delong, 2005; Graf, 1999; Hyden, 2010; Lian et al., 2012; Martin, 1965; Stoner et al., 1993; United States Army Corps of Engineers, 2016). Therefore, the effects of these dams would have been established well before our study period. For example, in the Illinois River basin all major dams had been completed by 1939. Based on work by Lian et al. (2012), streamflow changes post 1938, specifically peak flows, have been influenced more by climate than dam operations, though they did not consider the effects of drain tile. One exception might be the uppermost Illinois River basin, which has been influenced by expansion of the Chicago metropolitan area. Though historical and present water withdrawals are largely unknown, increased water use for industry, agriculture, and public drinking supply may offset some of the climate impacts of increased precipitation. Urban and suburban detention basins may also limit how much precipitation is converted to runoff. We expect that other water development projects in each basin have minimally affected streamflows at the basin outlet. Conversion of hay and small grains to corn and soybeans accompanied by artificial drainage expansion are likely the largest LULC changes in these basins since the early to mid-twentieth century.

3 Data and Methods: LULC, climate, and streamflow

We explain our methods for addressing how LULC, climate, and streamflows have changed during the 20th and 21st centuries in sections 3.1 thru 3.3. In section 3.4 we

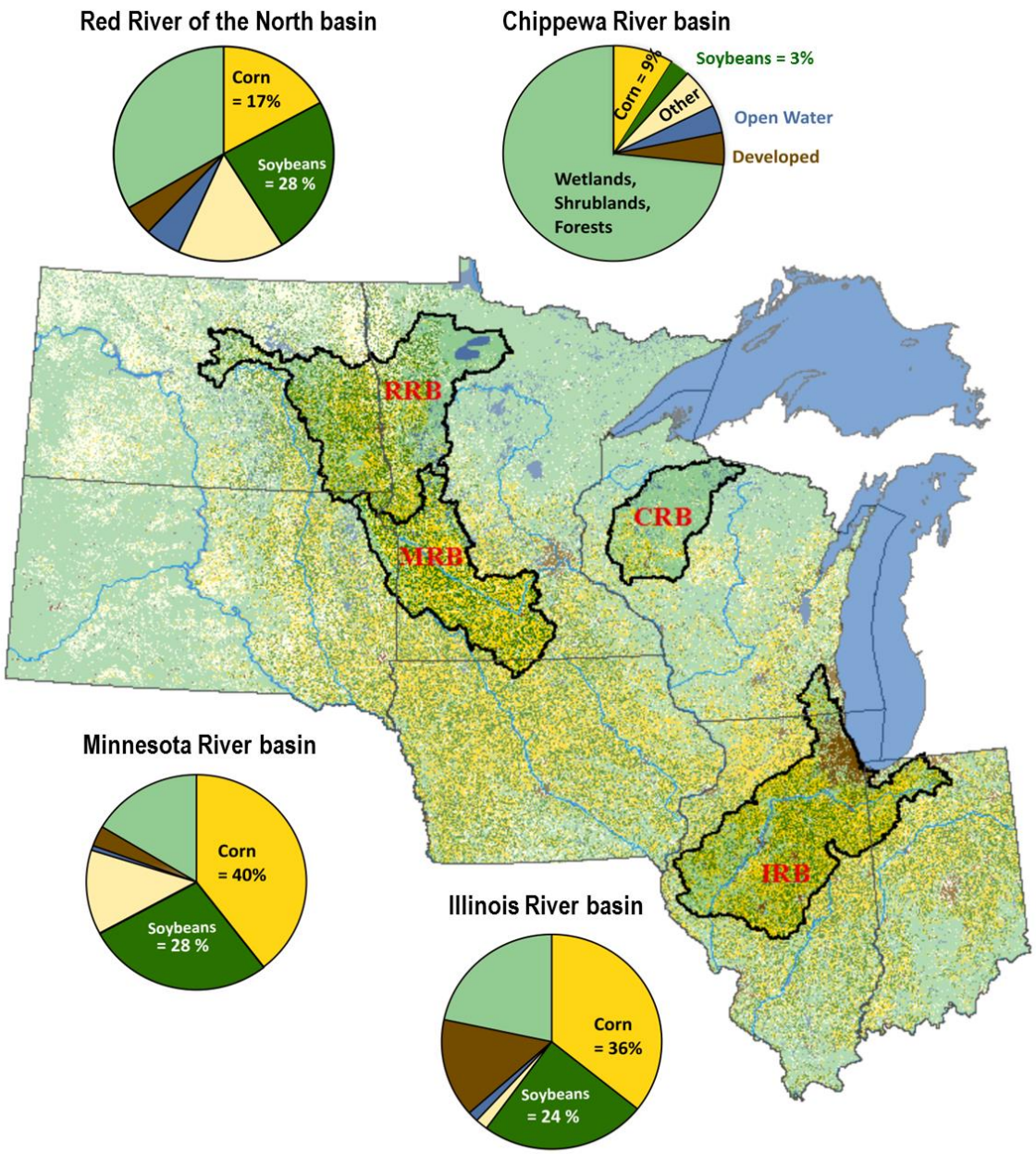

Figure 2-1. 2013 Relative proportion of each land cover class for the four study watersheds, Red River of the North basin (RRB), Minnesota River basin (MRB), Chippewa River basin (CRB), and Illinois River basin (IRB). Data from USDA National Agricultural Statistics Service Cropland Data Layer (2013).

explain how the timing and timescales of prominent change were determined. We use a water budget to determine whether precipitation and evapotranspiration alone can explain runoff trends in section 3.5.

3.1 Records of LULC change during the 20th and 21st centuries

We compiled county-level US Census of Agriculture drainage data from 1940, 1950, 1960, 1978, and 2012 for each study watershed, weighing partial counties by area (U.S. Bureau of the Census, 1942, 1952, 1961, 1981; U.S. Department of Agriculture, 2014a). Tabulations of drainage enterprises exclude lands draining less than 500 acres in all years except 1940 (U.S. Bureau of the Census, 1952, 1922). In 1940 and 2012, acres drained by ditches and tile were reported individually. To normalize the land area across basins of different sizes, we report the percentage of watershed area drained. While the uncertainties in these data are high, they are the best data available on a national scale for our study period. Some studies (e.g. David et al., 2010) have taken advantage of other drainage estimates, such as those from Sugg, (2007). However, the Sugg (2007) method was calibrated and validated using data from 1987 and 1992 drainage census reports. Therefore it is unclear whether this approach could be used to estimate historical or current drainage extents. Furthermore, the drainage estimates are based on soil type, class, and crop type and assume that state percentages of average cropland area drained are uniform for every county in each state and have remained static through time (Sugg, 2007). Although somewhat tedious, we use U.S. Census of Agriculture drainage data as the best available proxy for the relative drainage extent and expansion through time in each of the four large study basin, the smallest of which is still larger than 20 counties.

County level agricultural census drainage data are only available for five census years. Therefore, we also compiled annual USDA National Agricultural Statistics Service (NASS) crop acreage harvested in each basin following the methods of Foufoula-Georgiou et al. (2015). We report the percentage of corn, soybeans, and hay and small grains grown in each watershed from 1915 to 2015. Artificial drainage installation has typically coincided with the replacement of hay and small grains for soybeans as shown in Fig. A1 in the Supplement (Burns, 1954; Hewes and Frandson, 1952). Therefore we use these annual crop data as another indication of LULC changes.

3.2 Climate records: precipitation and evapotranspiration

Monthly Parameter elevation Regression on Independent Slopes Model (PRISM) precipitation rasters produced by PRISM Climate Group (2004) and modeled actual evapotranspiration (ET_a) produced by Livneh et al. (2013) are readily available, reproducible, and defensible climatology data that provide continuous spatial and temporal coverage of our study areas. We compiled spatially-averaged monthly and annual precipitation and evapotranspiration depths for each watershed for 1935-2013 and 1935-2011, respectively.

Livneh et al. (2013) evapotranspiration was produced for the continental United States using the Variable Infiltration Capacity (VIC) model run at 3-hr time steps in energy balance mode, consistent with methods of Maurer et al. (2002). Hereafter we refer to Livneh et al. (2013) and Maurer et al. (2002) as L13 and M02. We have chosen L13 data over other available estimates of evapotranspiration because they cover a large spatial and temporal domain necessary for the study, i.e. the contiguous US from 1915-2011, at reasonable spatial ($1/16^{\circ}$) and temporal (monthly) resolution, unlike other global

and North American reanalysis products such as ERA-Interim (data available from 1979-2013 at 0.7°) and NARR (data available from 1979-2015 at 0.3°).

Although the precipitation input used to generate the ET_a data was gridded NCDC COOP station data, Livneh et al. (2013) scaled monthly gridded precipitation to match the PRISM long term mean (1961-1990). We directly compared monthly precipitation from L13 and PRISM (1935-2011) and found that for each of the four study basins the mean error was 1% (Fig. A3). Further discussion of potential biases in using the ET_a estimates from L13 are discussed in the Supplement.

3.3 Streamflow gauge records

We evaluated annual (seasonal), monthly and daily flow metrics for each of the four river basins. Using multiple gauges for a single basin, we compiled seven annual flow metrics: mean annual flow, 7-day average annual low flow winter (November-April), 7-day average annual low flow summer (May-October), peak mean daily flow spring (March-May), peak mean daily flow summer and fall (June-November), high flow days, and extreme flow days using mean daily flow data from USGS gauges within each basin (Fig. A2; Table 2-1) following the methods of Novotny and Stefan (2007). The number of high and extreme flow days refers to the number of days in a given year that are one and two standard deviations above the 1950-2010 mean. For each gauge, we normalized the annual flow metric by the 1950-2010 mean to facilitate comparisons among basins and to observe similarities in trends among metrics. Each gauge record included a minimum of 62 years, and of the 63 gauges analysed 53 gauges had continuous records. Of the 10 non-continuous records, 4, 2, 2, 1, and 1 gauges were

missing 2, 4, 6, 8, and 14 years of data respectively during the period 1929-2013 (Table 2-1).

For the downstream outlet gauge in each basin (Table 2-1) we computed annual and monthly streamflow average depths (cm $month^{-1}$) and volumes (km^3 $month^{-1}$) for 1935-2013 for the MRB, RRB, and CRB, and 1939-2013 for the IRB due to missing gauge data prior to 1939. We also calculated daily streamflow change exceedance probabilities, where $dQ/dt>0$ characterizes the rising limbs of daily hydrographs and $dQ/dt<0$ the falling limbs.

3.4 Determining the timing and time-scales of prominent LULC, climate, and runoff changes

In order to determine whether observed changes in climate and streamflow are statistically meaningful and potentially coincident with LULC change, we first determined the timing of climate, streamflow, and LULC change. Annual crop data reveal the timing of rapid expansion of soybean acreage and indicate land use land cover transitions (LCTs) when soybean acreage exceeds hay and small grains (Foufoula-Georgiou et al., 2015). We identified the timing of precipitation and streamflow change using wavelets and by fitting a piecewise linear regression (PwLR) using a least-squares approach to the monthly streamflow and precipitation volume time series in each basin (Liu et al., 2010; Tomé and Miranda, 2004; Verbesselt et al., 2010; Zeileis et al., 2003).

A common method for detecting and quantifying changes in the magnitude/frequency content of a time series is via a localized time-frequency analysis using wavelets. The Continuous Wavelet Transform (CWT) of a signal $x(t)$ is defined as

the convolution of the signal with scaled and translated versions of a mother wavelet $\psi(t)$:

$$T(a,b) = \frac{1}{\sqrt{a}} \int_{-\infty}^{+\infty} x(t) \psi^* \left(\frac{t-b}{a}\right) dt \quad (1)$$

where $\psi\left(\frac{t-b}{a}\right)$ is the mother wavelet scaled by parameter a and translated by parameter b, and * denotes the complex conjugate. By changing a and b the CWT quantifies the localized energy or variance of a signal at different times and scales (frequencies). To every scale there is a corresponding frequency assigned as the central frequency of the Fourier transform of the wavelet at that scale. This relationship is analytically computable depending on the chosen mother wavelet. In this paper, we use the Morlet wavelet (Addison, 2002; Daubechies, 1992; Seuront and Strutton, 2003), which has been proven effective for analyzing climate signals such as El Niño, streamflow, and precipitation among others (e.g., Anctil and Coulibaly, 2004; Foufoula-Georgiou et al., 2015; Labat et al., 2001; Torrence and Compo, 1998 and the references therein). The Morlet wavelet is simply a complex wave within a Gaussian envelope and by choosing the central frequency f_0 appropriately it simplifies to the form:

$$\psi(t) = \frac{1}{\pi^{1/4}} e^{i2\pi f_0 t} \, e^{-t^2/2} \quad . \quad (2)$$

Here we used $f_0 = 0.849$ as this achieves the best time-frequency localization (Addison, 2002).

We also evaluated precipitation and streamflow change using two statistical tests and three breakpoints. We selected 1974/75 as a breakpoint for the pre-period and post-period because it lumps the time series data into two roughly equal periods (40/39 years), coincides with the timing of widespread acceptance of cheaper and easier to install

corrugated plastic tile (Fouss and Reeve, 1987), and other studies in the MRB and IRB have identified hydrologic change occurring around that time (e.g. Foufoula-Georgiou et al., 2015; Lian et al., 2012; Schottler et al., 2014). Acknowledging that 1974/75 may not be the hydrologically relevant breakpoint in all basins at this large scale, we ran statistical tests using 1974/1975 as well as the breakpoints identified for each basin from the PwLR and LCT.

We performed one-tailed student's t-tests or Wilcoxon Rank Sum tests when data did not meet parametric assumptions after testing log, square root, and arcsine transformations, and Kolmogorov–Smirnov (KS) tests using the statistical program R to analyze changes in the mean and distribution of annual and monthly total flow (Q) at the basin outlet and spatially averaged basin precipitation (P) volumes between each pre-period and post-period (R Core Team, 2013). We test the hypothesis that mean monthly water volumes have increased and their distributions have shifted right during the post-period. We selected an alpha value of 0.05 (95% confidence level) for all statistical tests performed. Thus we performed 312 t-test and 312 KS-test using the annual and monthly P and Q data for each basin, as well as 28 t-tests on the seven streamflow metrics described in section 3.3 for a total of 652 statistical tests. In general the results of the statistical tests are not sensitive to the timing of different breakpoints, spanning nearly four decades, and therefore we generally report statistical results for the pre-period (1935-1974) and post-period (1975-2013), though all results are presented in Table A1 in the Supplement.

3.5 Determining the role of climate versus LULC change on streamflows using a water budget

For given watershed over a specified time period of integration, water inputs minus water outputs are equal to the change in storage per unit time:

$$P - ET - Q = \frac{dS}{dt} \quad (3)$$

where P is average watershed precipitation (cm month^{-1}), ET is estimated average watershed actual evapotranspiration (cm month^{-1}), Q is runoff depth at the basin outlet (cm month^{-1}), and $\frac{dS}{dt}$ is the depth of change in soil water, groundwater, and lake/reservoir storage per unit time.

We have computed average annual water budgets for each basin by accumulating monthly P, ET, and Q during the pre-period and post-period determined by the land cover transition (LCT) and 1974/75 in each basin, to solve for the change in storage. If the change in storage term increases from the pre-period to post-period we conclude that soil moisture, groundwater, and/or lake/reservoir storage has also increased and that climate likely explains most of the increase in Q. However, if the change in storage term decreases from the pre-period to post-period, then we conclude that soil moisture, groundwater, and/or lake/reservoir storage has decreased despite precipitation increases, indicating that widespread LULC change has altered watershed storage and contributed, in addition to precipitation, to increased streamflows.

Livneh et al (2013) did not incorporate land use land cover changes, such as tile drainage expansion or crop changes, into the VIC model. The fact that LULC change is not included in the model is what allows us to test, external to the ET predictions, whether or not a LULC effect exists. There is no evidence of regional groundwater

change and the effects of dams and urbanization on streamflows are likely minimal as discussed in section 2. Comparing these data to other estimates of evapotranspiration including four AmeriFlux towers, two of which are in corn-soy agricultural areas, we demonstrate that they are sufficiently reliable modern estimates for our purposes (Table 2-2; Fig. A4; Fig. A5).

We acknowledge that there is uncertainty in the all of the input data and understand that the magnitude of the storage term is sensitive to estimates of ET. Livneh et al. (2013) reported 17% overestimation of ET_a during the summer months when compared with AmeriFlux station data. It is during summer months that ET is most likely limited by soil water availability. Therefore in addition to the raw water budgets, we present water budgets where we have reduced monthly ET_a by 17% during summer months (JJA). This lower estimate of ET effectively reduces the potential amount of streamflow change that could be attributed to land use and artificial drainage and is therefore a more conservative analysis. Overall, the data from Livneh et al. (2013) used in computing the monthly water budgets are consistent with other sources (Bryan et al., 2015; Diak et al., 1998) and provide reasonable modern estimates of ET_a, especially when reducing summer (JJA) ET_a by 17% (Figs. 2-S4 & 2-S5).

4 Results and Discussion

We present records of land use land cover in section 4.1 and discuss the timing of notable change in section 4.2. In section 4.2 we also present the timing, time scales and times of year when changes in precipitation, evapotranspiration, and streamflow magnitude are most prominent. Finally, we present the results of a water budget in section 4.3 to address whether change in climate variables alone can explain runoff

trends. Discussion of how the combined results address our three research questions can be found in section 5.

4.1 Drainage, corn and soybean expansion during the 20th and 21st centuries in the Upper Midwest

Across the Upper Midwest, the percent of land drained by tiles and ditches and cultivated for corn and soybeans has increased since the early twentieth century while land cultivated for hay and small grains has declined. Figure 2-2 shows the percent of each watershed drained by tiles and ditches from the Census of Agriculture data, as well as the percent of each county drained by tile in 1940 and 2012. Total drainage and tile drainage has increased in the MRB and IRB, while it has remained relatively unchanged from 1940 to 2012 in the CRB and RRB (Fig. 2-2). The drainage census data show that the MRB has the greatest percentage of the watershed area drained by tile, 19% in 1940 and 35% in 2012, and ditches, 7% in 1940 and 10% in 2012, followed closely by the IRB (Fig. 2-2). The Red River of the North basin has experienced very little increase in total drainage since 1940. Most artificial drainage in the RRB is ditches rather than tile drains. Although a dramatic increase in tile installation has been reported in the Red River Valley since the 1990's, the area of this expansion appears small relative to the watershed area. Acres reported to be drained by tile in 2012 represents only 2% of the total watershed area. The CRB has very little agricultural land and thus the 2012 census reports less than 1.5% of the watershed area drained by tile and ditches (Fig. 2-2).

The 1978 census data illustrate the uncertainty associated with reporting, as it is unlikely for total drainage to have decreased between 1960 and 1978 in the RRB and MRB (Fig. 2-2). Most county ditches and tile in Blue Earth County, Minnesota were

installed during the 1910's and 1920's with a noticeable drop off during WWII and a resurgence of drainage enterprises starting in the 1960's (Blue Earth County Minnesota, n.d.). Burns (1954) reported that the 1940 census data underestimated drainage enterprises in Blue Earth County by 8.5%, simply due to inaccuracies in reporting. According to one report, it was estimated that 27% of drained land in the United States was not included in the 1960 drainage census due to private drainage operations on lands less than 500 acres (Gain, 1967). Furthermore, 82%, 80%, 51%, and 91% of all farms in Minnesota, Illinois, North Dakota, and Wisconsin, respectively, were less than 500 acres in 2012, and therefore were not included in survey results (U.S. Department of Agriculture, 2014b). Therefore these estimates are likely to underestimate the area drained by tile and ditches. Although the 2012 census attempts to correct for incomplete and missing responses, because drainage enterprise records have traditionally been so poorly documented, it is difficult to know how much reported acreage underestimates the actual acreage.

We also note that acres drained by tile and ditches does not directly translate to effectiveness of artificial drainage. Several factors influence the flow rate from soils, including the hydraulic conductivity of the soil, macropores, depth of the water table, depths of the tile lines, tile diameter, slope of the tile or ditch, horizontal spacing, as well as precipitation intensity and duration and antecedent soil conditions (Hillel, 1998). We simply do not have this level of information regarding artificial drainage in the Midwestern USA and suspect that the spatial variability in drainage management practices may be high. For example, Naz et al. (2009) mapped tile drains in a 202 km^2 Indiana watershed and found tile spacing that ranged from 17-80 m.

While we expect that the drainage trends observed are relatively correct, we are cautious about drawing any definitive conclusions from the Census of Agriculture data regarding the actual extent of tile drainage and changes over time. It is clear that these estimates tend to underestimate the amount of drainage. Nevertheless, total drainage and tile drainage in the Minnesota River basin and Illinois River basin have increased considerably since 1940. It is known anecdotally, but not included in these data, that tile drainage spacing has decreased and intensity or drainage rate in mm h^{-1} has increased on agricultural lands, often by a factor of two, as was done at the Lamberton Research Station, MN (L. Klossner, personal communication, November 17, 2015).

Conversion from small grains to soybeans is often accompanied by increased sub-surface drainage installation (Foufoula-Georgoiu et al., 2015). Figure 2-3 displays the percent of each basin harvested for corn, soybean, and hay and small grains from 1915-2015. There has been a decline in hay and small grains and an increase in soybeans in all four of the watersheds over the period of record. The RRB is the only basin containing a significantly higher percentage of soybean acreage relative to corn; on average since 1995 soybean acreage in the RRB has been more than twice that of corn.

Overall, changes in crop type occurred gradually in the MRB and IRB, much more rapidly and recently in the RRB (Fig. 2-3). The CRB is largely non-agricultural, only 9% of the basin grew corn, soy, and hay and small grains in 2015, and the changes in the basin have been small during the period of record (Fig. 2-3). While we cannot directly ascribe these changes in crop type to changes in drainage practices or vice versa, they provide a relatively detailed history of LULC and whether the changes occurred gradually or rapidly and recently or long-ago in each basin.

4.2 Timing and magnitude of precipitation, evapotranspiration, and streamflow changes

4.2.1 Timing of streamflow change coincides more closely with precipitation change than LULC change

The land cover transition (LCT), precipitation, and streamflow breakpoints of change identified using piecewise linear regression (PwLR) and continuous wavelet transform (CWT) reveal that the timing of precipitation and streamflow change generally preceded LCT change (Table 2-3). This was true for all tests in the RRB and CRB. However, there are some chronological differences in the order of precipitation, streamflow, and LCT breakpoints. In the IRB, the timing of LCT precedes precipitation and streamflow breakpoints identified using PwLR and CWT by between 13 years and 20 years (Table 2-3). In the MRB, LCT follows precipitation by 20 years and streamflow by 11 years as identified using PwLR but precedes the streamflow breakpoint by one year identified using CWT (Table 2-3).

Land cover transition breakpoints shown in Fig. 2-3 are not exact; land cover change occurs gradually, and therefore LCT breakpoints represent when a large portion of each watershed was converted to from hay and small grains to soybeans. Land cover transition breakpoints are indicated two ways: 1) when percent watershed area harvested for soybeans exceeds hay and small grains, and 2) when the proportion of the total acreage harvested for the three commodity groups is dominated by corn and soybeans. The second criteria varies from basin to basin, as some basins may have historically grown more hay and small grains, while others more corn and soybeans. In the CRB and RRB, hay and small grains exceeded 50% of the total area harvested for corn, soybeans, and hay and small grains from 1915 until the year 2000 or later. However in the MRB

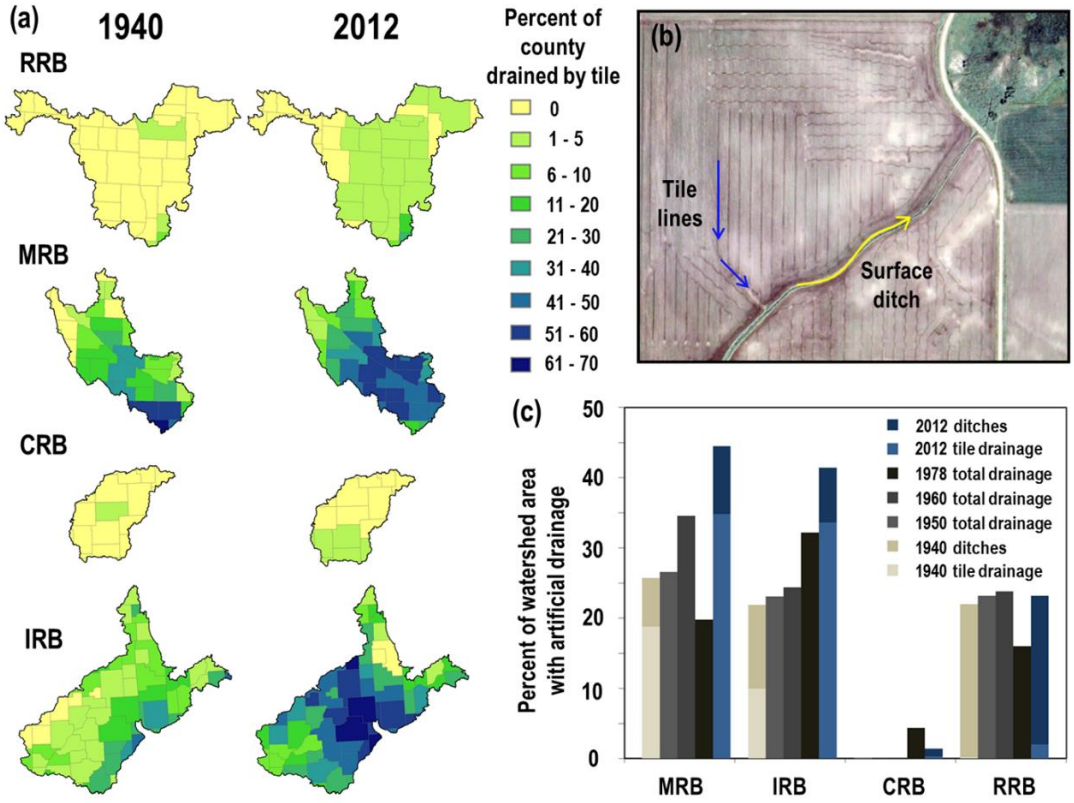

Figure 2-2. a) Spatial distribution of tile drainage patterns in 1940 and 2012 for each of the four study basins: Red River of the North basin (RRB), Minnesota River basin (MRB), Chippewa River basin (CRB), and Illinois River basin (IRB). b) Image showing an example field pattern that combines subsurface tile lines with a surface ditch. c) Percentage of the total watershed area with artificial drainage from 1940, 1950, 1960, 1978, and 2012 drainage census data. The magnitude of each bar indicates total drainage (ditches and tiles), and 1940 & 2012 bars are broken proportionally into drainage by ditches and tiles.

and IRB, hay and small grains only exceeded 50% of the total area harvested for the three commodity groups from 1915 until 1950 or earlier. The LCT breakpoints, indicated by the vertical dashed lines in Fig. 2-3, approximately coincide with the horizontal dashed lines, which represent a time when the percent of the total acres harvested for the three commodity groups exceeded 60% in RRB and CRB, where hay and small grains have historically dominated, and 75% in the MRB and IRB, where corn and soybeans have

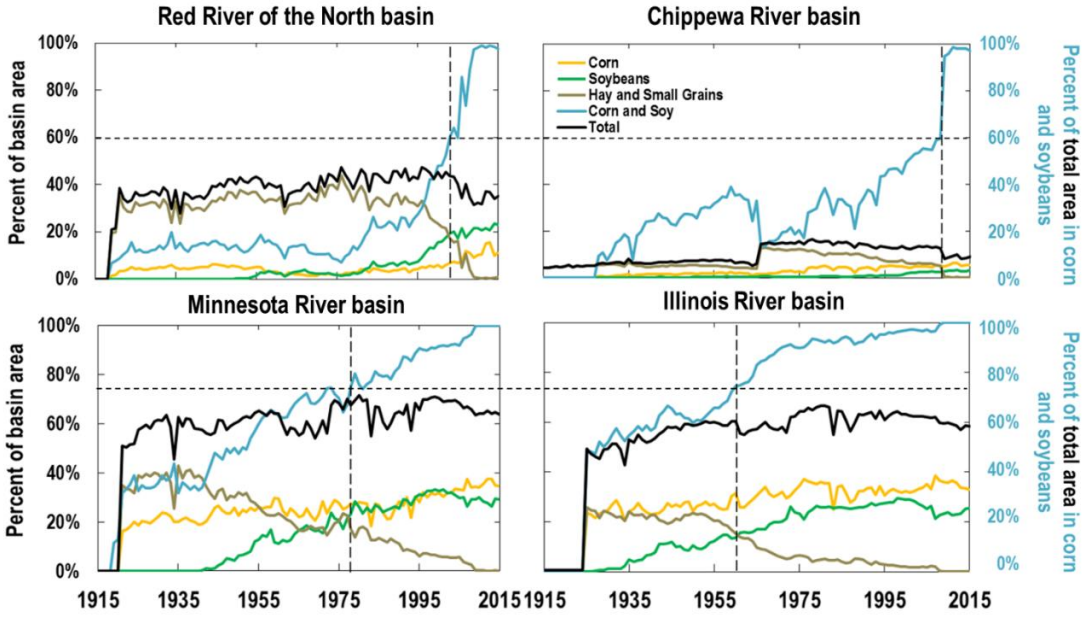

Figure 2-3. Acres harvested of corn, soybeans, and hay and small grains (barley, oats, wheat) expressed as percent watershed area for each of the basins based on county level data from USDA NASS. The sum of these three commodity groups is shown as a total in black and the percent of this total area in corn and soybeans is plotted in blue. Vertical dashed lines indicate when percent of basin area harvested for soybeans exceeds hay and small grains. Horizontal dashed lines indicate when the percent of total area harvested for corn and soybeans exceeds 60% in the Red River of the North basin and Chippewa River basin and 75% in the Minnesota River basin and Illinois River basin.

historically dominated. We acknowledge that these breakpoints do not consider the actual extent of soybeans, which is assumed to be a surrogate approximation for area of drained croplands. Soybean coverage is much higher for both MRB and IRB compared to RRB and CRB even before 1955. Considering the large proportion of the MRB and IRB watersheds cultivated for soybeans in the early 1950's combined with extensive (20-25%) drainage by 1940 and 1950 (Fig. 2-2), this suggests streamflow changes generally occurred after both precipitation and LCT changes.

We observe minimal changes in the energy of the annual and inter-annual precipitation signal for any basins during the period of record, and therefore could not

identify the timing of precipitation change in any basin using CWT (Fig. 2-4). However, Fig. 2-4 displays significant increases in the annual and inter-annual energy of the basin outlet streamflow signal around 1975, 1980, and 1995 for the IRB, MRB, and RRB respectively, while the CRB does not exhibit any striking changes in energy throughout the period of record. All decadal energy shifts in the precipitation signals are clearly translated into the decadal energy of the streamflow signals for all four basins (Fig. 2-4). The observed correlation between the decadal energy changes in streamflow and precipitation signals together with the lack of any significant correlation between their energies at the annual scale may signal the importance of factors other than precipitation, here artificial drainage, to streamflows in the MRB, RRB, and IRB at the annual scale.

In all basins, the timing of precipitation change coincided with or preceded streamflow breakpoints based on PwLR (Table 2-3). Similar temporal coincidence of precipitation and streamflow breakpoints in contrast to the LCT and streamflow breakpoints may suggest that streamflow changes are tightly coupled with precipitation changes. However, that interpretation fails to account for the potential effects of drainage, which could amplify the streamflow response to precipitation.

4.2.2 Seasonal and annual scale changes of precipitation, evapotranspiration, and streamflow

The raw timeseries of spatially averaged annual precipitation and streamflow depths (cm), reported in the Supplement, show an increasing trend in precipitation and streamflow in the RRB, MRB, and IRB and no trend in the CRB (Fig. A6). The magnitude of the precipitation and streamflow trends are on the order of 120-150 mm/century and 90-170 mm/century, respectively, and are consistent with those reported

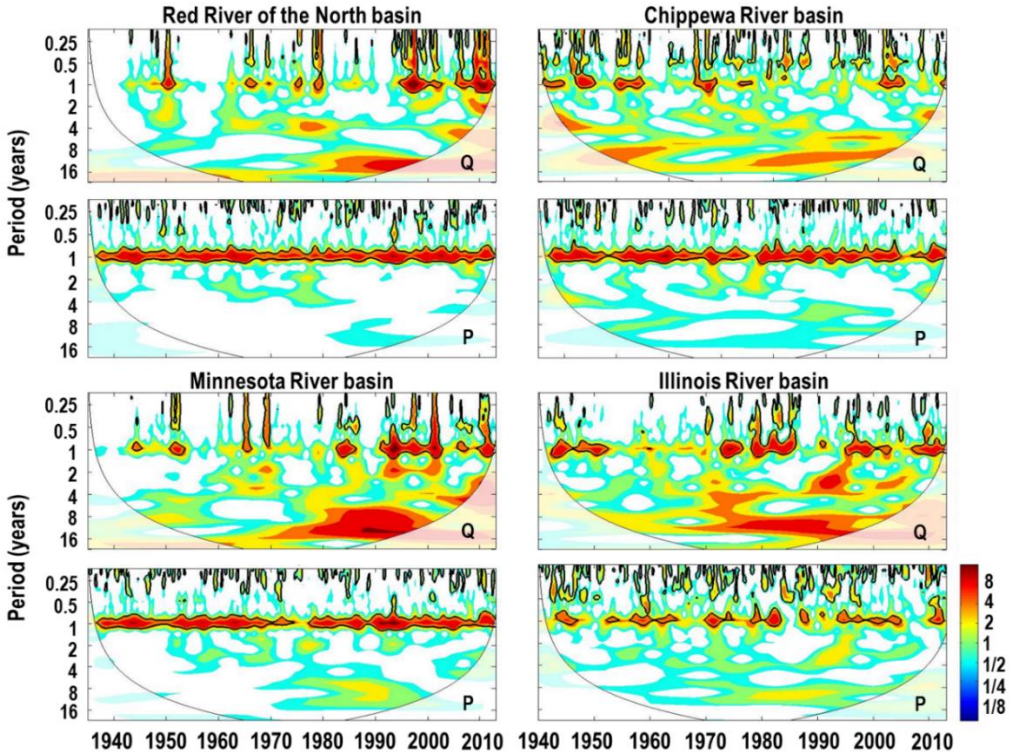

Figure 2-4. Continuous Wavelet Transform (CWT) energies for monthly volumetric streamflow (Q) and precipitation (P) time series.

for the entire Upper Mississippi River basin by Frans et al. (2013). Xu et al. (2013) report precipitation trends that are similar to our study and Frans et al. (2013) in 22% of the study watersheds (average size 489 km^2) in Iowa, Illinois, Indiana, and Ohio. Figure 2-5a shows five year running averages of seven annual streamflow metrics, where normalized values of 1 indicate that the annual value is equivalent to the mean (1950-2010) value. Stationary flow statistics vary around 1 for the entire time series, as is the case for the Chippewa River basin (Fig. 2-5). Non-stationary time series systematically deviate from 1, indicating that the mean condition has changed during the period of record. Qualitatively, all seven flow metrics in the CRB have remained stable since the 1930's,

except for seven day low flows in winter, which have increased 12% since 1975 ($p<0.01$) (Fig. 2-5).

Unlike the Chippewa, flow metrics in the Minnesota, Red, and Illinois river basins systematically increase in recent decades, with nearly a two-fold increase or greater in almost all flow metrics since 1975 (Fig. 2-5). Seven day low flows in summer and winter (i.e. the lowest annual flows) have increased most in these basins, where mean conditions have increased 67%-275% ($p<0.001$) since 1975 (Fig. 2-5b). In much smaller basins, Xu et al. (2013) also reported the greatest streamflow changes to baseflows. High flow and extreme flow days have also increased significantly in the MRB ($p<0.001$), IRB ($p<0.05$) and RRB ($p<0.001$). Spring peak daily flows have changed the least in all basins, indicating 14% ($p>0.05$), 37% ($p<0.05$), and 60% ($p<0.05$) increase in mean between 1934-1974 and 1975-2013 for the IRB, MRB, and RRB, respectively (Fig. 2-5b). The Minnesota River basin has seen the greatest percent increase in mean annual flow, peak daily flow summer & fall, 7 day low flow in winter, high flow days and extreme flow days (Fig 2-5b). Peak daily flow summer and 7 day low flow in summer have increased most in the Red River of the North basin (Fig. 2-5b).

All seven flow statistics in the Red River of the North basin increase dramatically after the mid-1990's (Fig. 2-5a). Low flows have increased 3.5-4 fold ($p<0.001$) and high and extreme flows have increased 2.5-3 fold ($p<0.001$) in the RRB since 1995 (Fig. 2-5b). Flows in Minnesota River basin have increased similarly, with a 3-4 fold increase in low flows ($p<0.001$) and 3 fold increase in high and extreme flows ($p<0.001$) since the timing of land cover transition. Changes in the Illinois River basin are less obvious, yet

still significant, with a 2 fold increase in low flows ($p<0.001$) and 1.5 fold increase in high and extreme flows ($p<0.05$) since LCT.

The MRB and RRB exhibit an increase not only in the magnitude but also in the cyclicity and synchronicity of these metrics after about 1980 (Fig. 2-5a). Cyclicity could imply that climate is playing a role in the observed increase in flows. However, the extent to which agricultural land and water management practices may be amplifying this climate effect cannot be ascertained from this figure alone. The Illinois River basin exhibits the most change in summer and winter 7 day low flows, which increase after 1970, and this trend is even more pronounced when only examining gauges within predominantly agricultural sub-basins that are unaffected by large dams (Fig. 2-5c). However, the changes in the RRB and MRB are much more obvious and statistically significant than those in the IRB.

Statistical results for annual changes in streamflow and precipitation for all breakpoints can be found in Table A1 in the Supplement. The following results are based on the 1974/75 breakpoint. Overall, average annual streamflow, precipitation, and evapotranspiration depths have increased significantly in the MRB and RRB, while only streamflow has increased significantly in the IRB; no significant changes are reported in the CRB. Average annual runoff depth at the outlet gauge of the MRB has increased 5.9 cm ($p<0.001$). Average annual precipitation and evapotranspiration depths in the MRB have also increased by 4.6 cm ($p=0.033$) and 3.3 cm ($p=0.021$), respectively. Average annual runoff ratio has increased from 0.11 to 0.18, equivalent to a 65% increase and consistent with the results of Vandegrift and Stefan (2010). In the RRB, the average annual runoff ratio has increased 65%, from 0.07 to 0.11 at the outlet gauge, which is

slightly greater than the 55% increase reported by Vandegrift and Stefan (2010). On average, annual runoff, precipitation, and evapotranspiration depths have increased by 2.9 cm ($p<0.01$), 4.1 cm ($p=0.019$), and 2.4 cm ($p=0.043$), respectively. Average annual runoff in the IRB has increased 5.4 cm ($p=0.011$). Precipitation and evapotranspiration are likely increasing in the IRB, however given the statistical power the apparent 4.2 cm ($p=0.086$) and 1.9 cm ($p=0.072$) increases were not significant. The average annual runoff ratio in the IRB has increased from 0.30 to 0.34, a 14% increase. The CRB average runoff ratio has decreased slightly (2%), from 0.37 to 0.36. On average, annual runoff depth in the CRB has not changed (0.00 cm; $p=0.499$). Average precipitation and evapotranspiration depths may have increased slightly, perhaps as much as 2.0 cm ($p=0.243$) and 0.9 cm ($p=0.209$) respectively, but these changes were not statistically significant.

The MRB and RRB exhibit the greatest change in the annual runoff ratio, followed by the IRB, with negligible change in the CRB. These findings are consistent with the fact that the MRB and RRB have relatively low runoff ratios comparted to the CRB and IRB, and are the only two basins where annual precipitation and evapotranspiration increases were statistically significant. On average, the fraction of annual precipitation that goes as ET has decreased 1.0%-2.4% in all four study basins, which is smaller in magnitude but consistent in direction of change with Schottler et al. (2014) who found the ratio of PET/P decreased 5.6% between 1940-1974 and 1975-2009 in a subbasin of the MRB. Schottler et al. (2014) considered the effects of both climate and cropping practices in calculations of PET while the Livneh et al. (2013) calculated

ET_a only considering climate. Modern decreases in PET/P ratios in Midwestern agricultural watersheds are also reported by Xu et al. (2013).

4.2.3 Monthly scale changes of precipitation and streamflow

Cumulative monthly precipitation, plotted in Fig. 2-6, indicates no systematic change in cumulative precipitation with time (i.e. constant slope) for any basin. However, cumulative monthly streamflow (1935-2013) plotted in Fig. 2-6 indicates a sudden change in slope around 1973 in the IRB, 1980 in the MRB, and 1995 in the RRB, without a distinct change in slope in the CRB. The visually identified change points are consistent with those identified from the CWT (Fig. 2-4).

Statistical tests of monthly streamflow and precipitation resulted in the same interpretations for 95% of the tests regardless of the breakpoint (Table A1); therefore Fig. 2-7 summarizes the results of these statistical tests for flow and precipitation in all basins using the 1974/75 breakpoint. Figure 2-7a illustrates the kernel density estimation, or non-parametric estimation of the probability density function, during the pre-period and post-period for June and September flows in each basin. Figure 2-7b reports 192 results (48 p-values reported per basin) from the monthly streamflow and precipitation t-tests and KS tests. Each color wheel displays 24 results, 2 results per month for each basin, and shows significant p-values for t-tests and KS tests based on color. Color is inversely related to p-value such that smaller p-values and thus more significant results are shown in increasingly darker colors, with p-values greater than 0.05 colored white. As such the streamflow color wheel in Fig. 2-7b for the Chippewa River basin is completely white, indicating there were no statistically significant changes in the mean or distribution of monthly streamflow volumes for any months, consistent with the

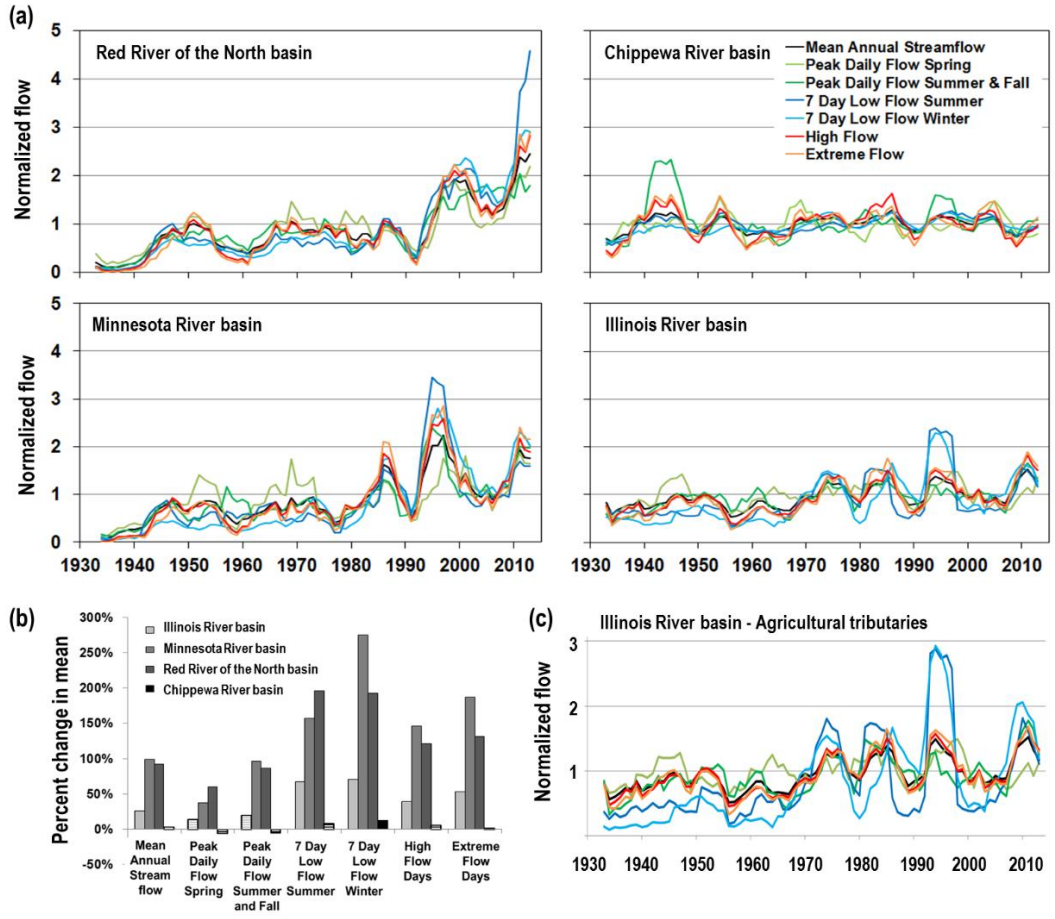

Figure 2-5. a) Seven normalized streamflow metrics presented as five year running averages based on annual and daily gauge analysis for the Red River of the North basin, 22 gauges; Chippewa River basin, 9 gauges; Minnesota River basin, 12 gauges; and Illinois River basin, 20 gauges. b) Percent change in flow metric mean between 1934-1974 and 1975-2013. Solid bars indicate significant increases in means (alpha=0.05). c) Streamflow metrics for 7 Illinois River basin tributary gauges that are predominately agricultural and not influenced by major dams. Annual flow metrics normalized by the 1950-2010 mean. Refer to Table 2-1 for gauge station details.

assessment of the seven annual streamflow metrics and cumulative streamflow (Figs 2-5 and 2-6). We report a significant increase in mean October precipitation in the CRB. Monthly results for flow and precipitation changes in the CRB are consistent with the annual changes reported earlier.

In stark contrast to the CRB, the streamflow color wheels for the MRB and RRB show significant changes in mean and distribution of monthly streamflow for nearly all months (22 out of 24 for MRB and 21 out of 24 for RRB) (Fig. 2-7b). In the RRB, mean precipitation in October has increased, and the precipitation distributions have shifted to the right for September and October (Fig. 2-7b). In the MRB, there has been a significant increase in mean March precipitation (Fig. 2-7b). The IRB exhibits fewer overall changes in streamflow than the RRB and MRB, with significant changes in monthly streamflow volumes for September, October, November, December and March, and significant changes in August and November precipitation (Fig. 2-7b).

We acknowledge that due to high variability and small sample sizes, we may not have sufficient power to detect small, but real changes in precipitation and streamflow using these statistical tests, and thus may be prone to Type II error (Belmont et al., 2016). However, these results are consistent with the qualitative assessment of CWT, results of the seven annual flow statistics, and cumulative precipitation and streamflow trends, which indicate only slight changes in total precipitation across all basins, large increases in total flow in the MRB and RRB, moderate flow increases in the IRB, and no streamflow changes in the CRB (Figs 2-4, 2-5, and 2-6).

To understand whether the cause and effect interconnection of streamflow (Q) and precipitation (P) has changed we plotted the joint probability distribution functions (joint PDF) of monthly P and Q, $f(P, Q)$, for each basin (Fig. 2-8). Joint PDF of pairs of monthly P and Q is the chance of their occurrence simultaneously. In Fig. 2-8 we illustrate three empirical quantiles of the joint PDFs through contour levels $\alpha \in \{0.1, 0.6, 0.9\}$, where each contour level represents the boundary of a discrete 2D space

in which the probability of each (P, Q) pair to fall inside that 2D space is alpha. A shift in the contour levels in the vertical, rather than diagonal, direction suggests that changes in precipitation magnitude alone cannot explain changes in streamflow, and some other component of the system must be amplifying the transformation of precipitation to runoff at the monthly timescale.

There is a shift toward larger monthly streamflow volume for the same volume of precipitation at each 10% and 60% quantile in the MRB and 60% and 90% quantile in the RRB (Fig. 2-8). However it appears the 90% exceedance contour for the MRB and 10% exceedance contour for the RRB have shifted up and to the right, indicating that an increase in precipitation in the driest months in the MRB and wettest months in the RRB could also be driving some of the change in flow (Fig. 2-8). Certainly the largest observable change in the MRB and RRB during this time is a shift from small grains to soybeans and an increase in the density and efficiency of drain tile networks. While analyses shown above documented significant changes in streamflow of IRB (Figs. 2-4, 2-5, 2-6, and 2-7b), this change is not as obvious in these joint PDF contours, which indicate only a slight vertical shift in all quantiles (Fig. 2-8). Consistent with other analyses, the CRB does not demonstrate any shift in the P-Q relation suggesting the streamflow has been largely unaffected by the observed slight increase in annual precipitation in the basin (Fig. 2-8).

4.2.4 Daily scale changes of streamflow

At the daily scale, we found an increase in the magnitude of streamflow change (hydrograph slopes) for both the daily rising limbs ($dQ/dt>0$) and falling limbs ($dQ/dt<0$)

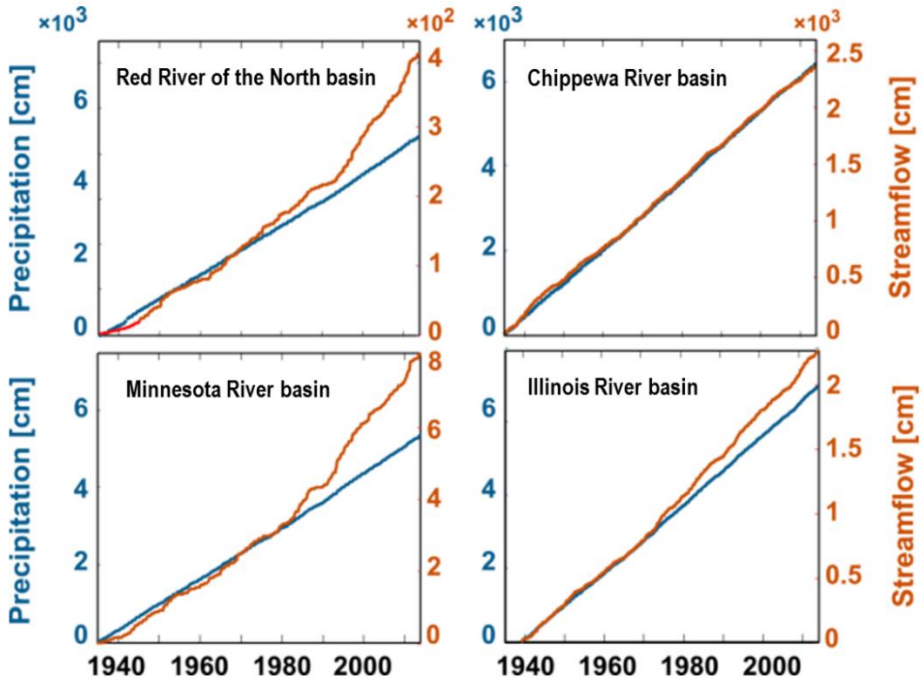

Figure 2-6. Cumulative monthly precipitation (blue) and streamflow (red) depths (cm) for each river basin. Breakpoints, where the streamflow-precipitation relationship starts to change, are hard to detect from the time series alone but can be clearly seen from the cumulative plots of the monthly data (i.e., when similar increments of monthly precipitation are translated into larger amounts of monthly streamflow).

of the hydrographs for RRB, MRB, and IRB outlet gauges, suggesting an increase in flashiness, or daily rate of change, of the hydrologic response (Fig. 2-9). Figure 2-9 shows a slight decrease in the post-period curve for the CRB, indicating that the rising limb and falling limb flows may actually be less flashy in recent times than in the past. May-June is approximately the start of the growing season for soybean and corn and it is the time that tiles are most active, as this time of year usually corresponds to high monthly rainfall, high antecedent moisture conditions from spring snowmelt, and lower ET rates than the peak growing season due to lower crop water demands, and air temperatures that precede the annual peak.

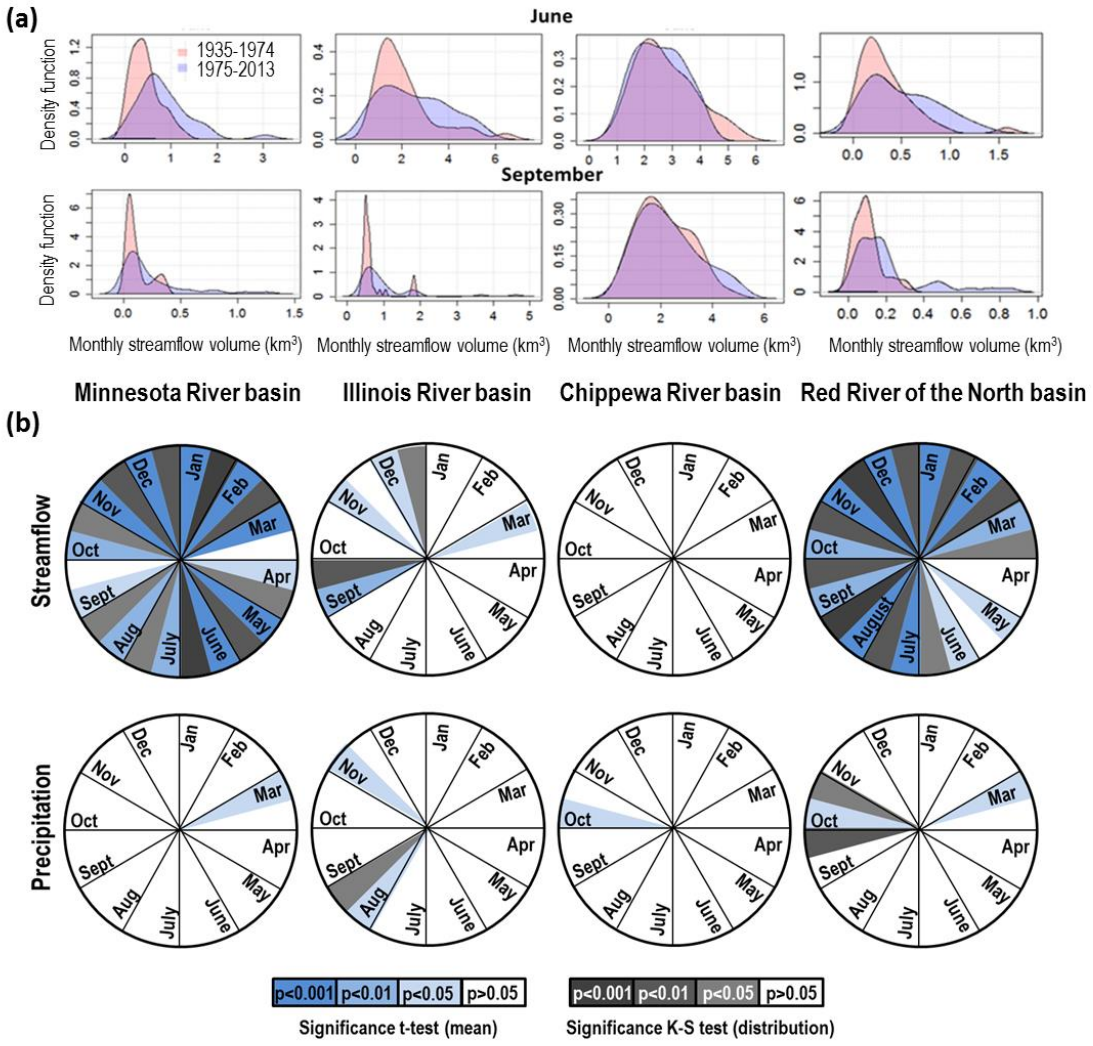

Figure 2-7. a) Kernel density plots of monthly streamflow volumes for June and September for each basin b) Corresponding significance results for t-tests and Kolmogorov–Smirnov (KS) tests (α=0.05) of monthly streamflow and precipitation volumes in each basin, where a significant result indicates a positive shift (increase) in the mean or distribution between 1935-1974 and 1975-2013; color wheels collectively display 192 individual p-values.

4.3 Hydrologic budgets suggest declining watershed storage in drained agricultural basins

While time series and statistical analyses reveal useful insights regarding the timing, magnitude, and significance of precipitation and streamflow changes, as well as

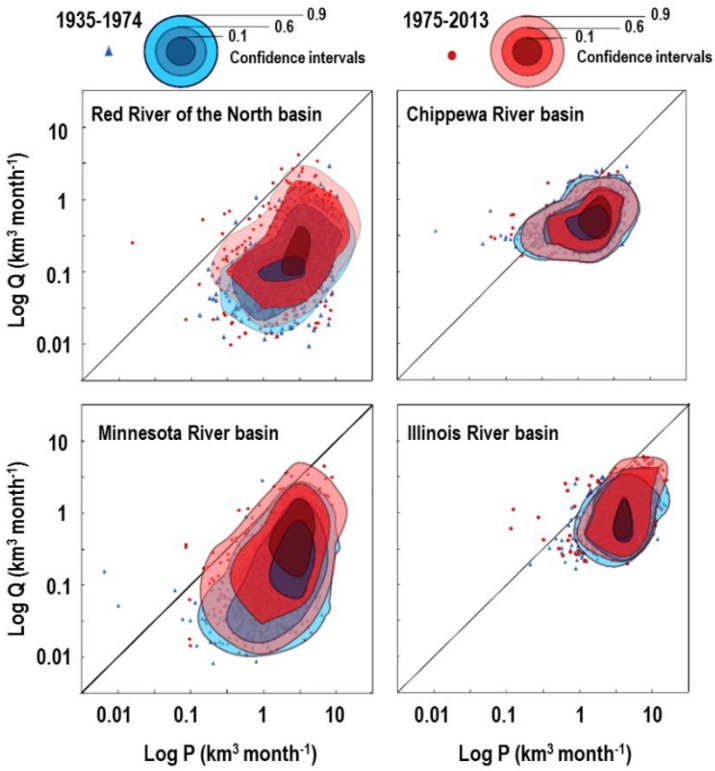

Figure 2-8. Log-log empirical quantiles of joint PDF plots of monthly streamflow (Q) versus monthly precipitation (P) volumes for each river basin during the pre-period (blue: 1935-1974) and post-period (red: 1975-2013); bulls eye shading represent the 0.1 (dark), 0.6 (medium), and 0.9 (light) confidence intervals.

provide a qualitative indication of whether or not changes in precipitation and streamflow may be correlated and proportional, they cannot fully deconvolve or attribute the influence of artificial drainage and climate on streamflows (Harrigan et al., 2014). Therefore, we calculate water budgets for each basin as a tool to understand whether the observed changes in precipitation are large enough to account for the changes in streamflow, and if there is more or less watershed storage in recent times than in the past (Healy et al., 2007).

Table 2-4 reports the calculated average annual water budget terms – precipitation, streamflow, evapotranspiration, and change in storage – during the periods

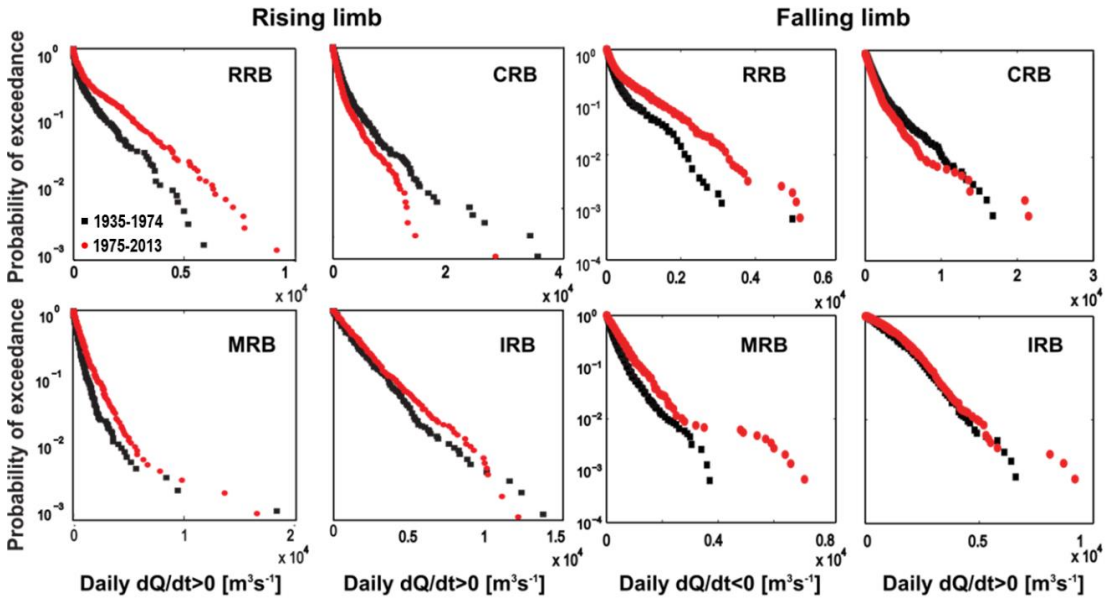

Figure 2-9. Daily streamflow change exceedance probabilities, where daily dQ/dt>0 characterizes rising limb flows and daily dQ/dt<0 characterizes falling limb flows. Study basin acronyms are defined as follows: Red River of the North basin (RRB), Minnesota River basin (MRB), Chippewa River basin (CRB), and Illinois River basin (IRB).

before and after the 1974/1975 and LCT breakpoint using raw and conservative (reduced by 17% in JJA) estimates of ET_a. We find that regardless of the breakpoint or raw vs. conservative estimates of ET_a there is a net reduction in water stored in soil, groundwater, and/or lakes, wetlands, or reservoirs between the pre period and post period in the MRB, RRB, and IRB (Table 4). The most parsimonious explanation for this reduction in water storage is the systematic removal of wetlands and lowering the water table, accomplished through tile drainage installation and expansion.

The CRB, which is not intensively drained (Fig. 2-2) and has experienced little change in crop type (Fig. 2-3), has been subject to an increase in precipitation, but does not exhibit an increase in runoff (Table 2-4), consistent with Figs. 2-8 & 2-9b. The overall trends in the CRB water budget indicate that water storage may have actually increased slightly between the pre-period and post-period, which could be accomplished

through increased soil moisture, groundwater recharge, or reservoir storage in recent times.

Using conservative estimates of summer ET_a the change in storage term has decreased by about 200%, 100%, and 30%, in the MRB, IRB, and RRB from the pre-LCT-period to post-LCT-period. In the CRB, change in storage has increased by roughly 30% from 1935-1974 to 1975-2011. These results are consistent with our hypothesis that increases in artificial drainage in the MRB, RRB, and IRB necessarily change how precipitation is transformed into streamflow and that increases in precipitation alone cannot explain changes in streamflow in these basins. Without pervasive artificial drainage in the CRB, while precipitation has increased slightly, flows have not changed, likely due to increases in soil moisture, groundwater, and/or lake, wetland and reservoir storage. Seasonal changes in storage shown in Fig. 2-10 suggest that soil moisture, groundwater, and/or lake, wetland, and reservoir storage in the spring and summer is negative, suggesting not enough P given ET_a to produce observed flows, and positive in the fall suggesting more P and ET_a than necessary to produce observed flows and thus an increase in storage during the fall.

The Red River of the North and Minnesota River basins have some of the poorest drained soils of the Upper Midwest and historically grew more hay and small grains than the other basins (Fig. 2-3). The introduction of artificial drainage combined with the replacement of hay and small grains with soybeans and the lack of major dams and municipal and industrial water use, has resulted in pronounced streamflow amplification in response to land use and climate changes in the RRB and MRB relative to the IRB and CRB (Fig. 2-4). Additionally these two basins have seen greater changes in annual and

even monthly precipitation (Figs. 2-7 and 2-8). However, the extensively drained Minnesota River Basin has seen the largest increases in flow and largest decrease in watershed storage for relatively similar climatic change to the IRB and RRB, and this is likely because of the high degree of watershed hydrologic alteration and connectivity from drainage and lack of other anthropogenic water uses.

5 Interpretations, implications, and conclusions

In this paper we address three research questions: (1) how have LULC, climate, and streamflows changed during the 20th and 21st centuries; (2) what are the timing, time scales and times of year that changes are most prominent; and (3) can changes in climate alone explain changes in streamflow? The combined results of this study lead us to several main conclusions. First, widespread drainage expansion and intensification, especially of tile drainage, coupled with conversion of hay and small grains to corn and soybeans is evident and continues to occur in agricultural river basins. Annual precipitation and evapotranspiration totals have increased since 1975, though we found these changes to only be statistically significant in the MRB and RRB. Monthly precipitation increases are generally not significant except in fall months for all basins.

Additionally, across multiple scales (daily, monthly , annual) and for a range of flows (low, mean, extreme) streamflows have increased at all times of the year in intensively managed agricultural watersheds (IRB, MRB, and RRB) and have remained stationary in the more forested CRB. The magnitude and timing of precipitation increases in each watershed suggests that precipitation contributes to recently observed increases in streamflow, consistent with other findings in the Midwestern USA (Frans et al., 2013; Xu et al., 2013). Despite this apparent correlation, the magnitude of precipitation increases

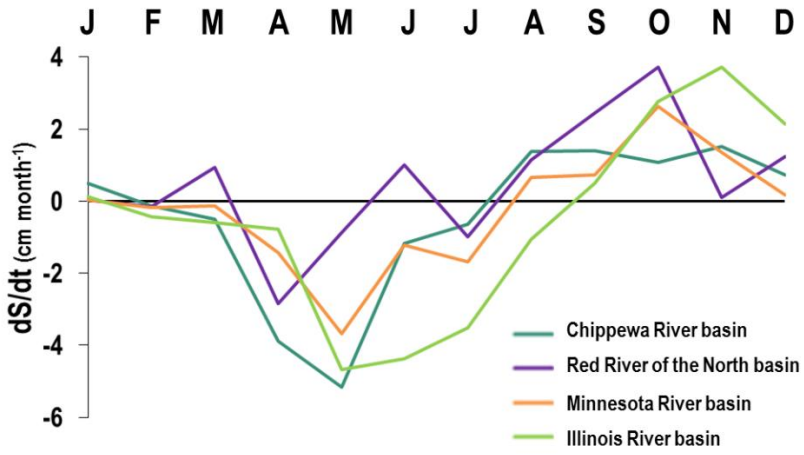

Figure 2-10. Average monthly (January – December) change in basin soil moisture, groundwater, and/or reservior storage (ds/dt), calculated after land cover transition (LCT) years (see Table 2-3 for Illinois River basin, Minnesota River basin, and Red River of the North basin LCT years), and after 1975 for Chippewa River basin assuming 17% reduction in ET_a for summer months.

alone cannot explain the observed increases in flow for agricultural basins according to the water balances. Therefore, it appears that the pervasive and extensive artificial drainage in agricultural basins has contributed to increased streamflow, not only at 10^2-10^3 km watershed scales (e.g. Foufoula-Georgiou et al., 2015; Harrigan et al., 2014; Schilling and Libra, 2003; Schottler et al., 2014; Xu et al., 2013, Zhang and Schilling, 2006), but also at the scale of very large basins studied here.

Harrigan et al. (2014) recognize that often multiple drivers explain hydrologic change. These drivers are not mutually exclusive and may even act synergistically to explain observed streamflow trends. In the Midwestern USA possible explanations that could explain substantial streamflow increases include: 1) changes in storm duration and intensity or the amount of precipitation falling as rain versus snow, have changed the characteristics of runoff generation while having little change on monthly or annual

precipitation magnitudes; 2) increases in precipitation have translated into increases in soil moisture, which contributes to amplified flows; and 3) artificial drainage more efficiently routes sub-surface flow to streams, an effect which could be amplified by increased precipitation.

First, it is theoretically possible to observe changes in streamflow while having no change in monthly or annual precipitation magnitudes. High intensity, short duration events yield higher runoff ratios in poorly drained soils. Additionally warmer winter temperatures, earlier snowmelt, and more days when winter precipitation falls as rain instead of snow should affect and even increase winter baseflows, decrease the timing of ice break-up, and affect the magnitude of snowmelt floods. Several studies have documented such hydroclimate changes in the Midwestern USA (Feng and Hu, 2007; Groisman et al., 2001; Higgins and Kousky, 2012) and the role of these hydroclimate changes could be explored by future investigations.

Second, increased soil moisture is known to cause a nonlinear increase in runoff generation for similar precipitation events. Meyles et al. (2003) and Penna et al. (2011) report a threshold response in runoff generation when antecedent soil moisture exceeds 65% of the soil porosity. It is possible that soil moisture has increased throughout the Midwestern US. However, no theory exists to predict how big this effect could be on landscape scales ($>10^4$ km^2). Furthermore, there are very limited data to determine whether or not soil moisture has in fact increased beyond such a threshold despite the immense amount of additional tile drainage that has been installed in the past few decades. Investigating this effect would be a good future step in this line of research.

Third, several previous studies have demonstrated that artificial drainage increases streamflow in moderate sized (10^2-10^3 km^2) watersheds (Schottler et al., 2014; Foufoula-Georgiou et al., 2015). Though we cannot fully rule out the first and second mechanisms discussed above, artificial drainage for corn-soy agriculture affects substantial swaths of land in all study watersheds except the Chippewa, and has almost doubled in area in the MRB and IRB since 1940 according to the US Census of Agriculture reports. It is known qualitatively that drainage has increased in density and efficiency during this same time. Using multiple lines of evidence from the analyses of very large basins and sub-basins it appears most likely that widespread agricultural drainage activities have amplified the streamflow response to relatively small changes in total precipitation. Frans et al. (2013) found that artificial drainage amplified annual runoff in the Upper Mississippi River basin in some cases by as much as 40% locally. Improved information regarding the size, spacing, depth, and extent of artificial drainage would greatly enhance our ability to model agricultural systems and predict downstream impacts.

Surface and subsurface drainage remains largely unregulated throughout the Midwestern USA and Canada (Cortus et al., 2011). Drainage census data are prone to reporting inconsistencies and errors, overall underestimation of drainage from excluding farms less than 500 acres, and do not provide the information necessary for modeling basin hydrology in large agricultural watersheds (such as drain size, depth, spacing, and extent). However, these are the most comprehensive inventory of drainage in the United States. This raises the question: why is such a widespread practice with such potentially profound and pervasive impacts on watershed hydrology and water quality so poorly

documented and regulated? Until we have the information necessary to calibrate and validate watershed models, it will be difficult to more precisely deconvolve proportional impacts of climate and artificial drainage on flows at large spatial scales.

Decreased residence time of water in the soil has substantially increased nutrient export from agricultural landscapes (Randall and Mulla, 2001; Kreiling and Houser, 2016; Schilling et al., 2017). Though artificial drainage reduces field erosion by reducing surface runoff, it has been shown to essentially have shifted the sediment source from fields to channels (Belmont, 2011; Belmont and Foufoula-Georgiou, 2017). Basins experiencing increases in streamflow due to natural (climate) and anthropogenic (drainage) factors have increased stream power available to erode and transport more sediments and sediment bound nutrients and contaminants. Improved runoff management, specifically increased residence time and damped peak flows, is most needed in spring and early summer when tiles are actively draining soils and precipitation events are large. Thus, substantial gains in water quality might only be achieved if some amount of the lost water storage capacity is reintroduced (e.g., wetlands, detention basins) into these agricultural watersheds.

6 Data availability

Precipitation and streamflow data are publically available and were accessed from the PRISM Climate Group, http://prism.oregonstate.edu/, and the United States Geological Survey, https://waterdata.usgs.gov/nwis, respectively. Livneh et al. 2013 evapotranspiration data provided by the NOAA/OAR/ESRL PSD, Boulder, Colorado, USA, from their website at http://www.esrl.noaa.gov/psd/. AmeriFlux evapotranispiration data are available at http://ameriflux.lbl.gov/. The Albert R. Mann Library at Cornell

University maintains historical archives of United States Department of Agriculture Census of Agriculture reports from 1840-2002, available at http://agcensus.mannlib.cornell.edu/AgCensus/homepage.do. The 2012 Census of Agriculture and National Cropland Data Layers are available from the United States Departement of Agricultural, National Agricultrual Statistics Service, https://www.agcensus.usda.gov/. For questions regarding data availability please contact the corresponding author.

References

Addison, P. S.: The Illustrated Wavelet Transform Handbook: Introductory Theory and Applications in Science, Engineering, Medicine and Finance, edited by: Revill, J. and Laurenson, S., Institute of Physics, Philadelphia, 2002.

Anctil, F. and Coulibaly, P.: Wavelet Analysis of the Interannual Variability in Southern Québec Streamflow, J. Climate, 17, 163–173, https://doi.org/10.1175/1520- 0442(2004)017<0163:WAOTIV>2.0.CO;2, 2004.

Arnold, T. L., Sullivan, D. J., Harris, M. A., Fitzpatrick, F. A., Scud- der, B. C., Ruhl, P. M., Hanchar, D. W., and Stewart, J. S.: Environmental Setting of the Upper Illinois River Basin and Implications for Water Quality, US Geol. Surv. Water-Resources Investig. Rep. 98–4268, 1999.

Barnes, W. J.: Vegetation Dynamics on the Floodplain of the Lower Chippewa River in Wisconsin, J. Torrey Bot. Soc., 124, 189–197, 1997.

Beauchamp, K. H.: A History of Drainage and Drainage Methods, in: Farm Drainage in the United States: History, Status, and Prospects, Miscellaneous Publication No. 1455, edited by: Pavelis, G. A., 13–29, U.S. Department of Agriculture, Wash-ington D.C., 1987.

Belmont, P.: Floodplain width adjustments in response to rapid base level fall and knickpoint migration, Geomorphology, 128, 92– 101, https://doi.org/10.1016/j.geomorph.2010.12.026, 2011.

Belmont, P. and Foufoula-Georgiou, E.: Solving water quality problems in agricultural landscapes: New approaches for these non-linear, multiprocess, multiscale systems, Water Resour. Res., 53, 2585–2590, https://doi.org/10.1002/2017WR020839, 2017.

Belmont, P., Gran, K. B., Schottler, S. P., Wilcock, P. R., Day, S. S., Jennings, C., Lauer, J. W., Viparelli, E., Willenbring, J. K., Engstrom, D. R., and Parker, G.: Large shift in source of fine sediment in the upper Mississippi River, Environ. Sci. Technol., 45, 8804–8810, https://doi.org/10.1021/es2019109, 2011.

Belmont, P., Willenbring, J. K., Schottler, S. P., Marquard, J., Kumarasamy, K., and Hemmis, J. M.: Toward generalizable sediment fingerprinting with tracers that are conservative and nonconservative over sediment routing timescales, J. Soils Sediments, 14, 1479–1492, https://doi.org/10.1007/s11368-014- 0913-5, 2014.

Belmont, P., Stevens, J. R., Czuba, J. A., Kumarasamy, K., and Kelly, S. A.: Comment on "Climate and agricultural land use change impacts on streamflow in the upper midwestern United States" by Satish C Gupta et al., Water Resour. Res., 52, 7523– 7528, https://doi.org/10.1002/2015WR018476, 2016.

Blann, K. L., Anderson, J. L., Sands, G. R., and Vondracek, B.: Effects of Agricultural Drainage on Aquatic Ecosystems: A Review, Crit. Rev. Env. Sci. Tec., 39, 909–1001, https://doi.org/10.1080/10643380801977966, 2009.

Blue Earth County Minnesota: Online Drainage Portal, available at: https://blueearth.drainagedb.net/portal/#portaldashboard.php, last access: 17 June 2016.

Bois de Sioux Watershed District: Calendar Year 2015 Annual Report, Wheaton, MN, available at: http://www.bdswd.com/ (last access: 19 September 2017), 2015.

Boucher, O., Myhre, G., and Myhre, A.: Direct human influence of irrigation on atmospheric water vapour and climate, Clim. Dynam., 22, 597–603, https://doi.org/10.1007/s00382-004-0402-4, 2004.

Boyd, C. and McNevin, A.: Aquaculture, Resource Use, and the Environment, Wiley-Blackwell, Hoboken, New Jersey, 2015.

Bryan, A. M., Steiner, A. L., and Posselt, D. J.: Regional modeling of surface-atmosphere interactions and their impact on Great Lakes hydroclimate, J. Geophys. Res. Atmos., 120, 1044–1064, https://doi.org/10.1002/2014JD022316, 2015.

Bullock, A. and Acreman, M.: The role of wetlands in the hydrological cycle, Hydrol. Earth Syst. Sci., 7, 358–389, https://doi.org/10.5194/hess-7-358-2003, 2003.

Burns, B. E.: Artificial Drainage in Blue Earth County, Minnesota, University of Nebraska, 1954.

Cortus, B. G., Jeffrey, S. R., Unterschultz, J. R., and Box- all, P. C.: The Economics of Wetland Drainage and Retention in Saskatchewan, Can. J. Agr. Econ., 59, 109–126, https://doi.org/10.1111/j.1744-7976.2010.01193.x, 2011.

Dahl, T. E.: Wetland losses in the United States 1780's to 1980's, US Department of the Interior, Fish and Wildlife Service, Washington DC, 1990.

Dahl, T. E. and Allord, G.: History of Wetlands in the Contermi- nous Unided States, in National Water Summary on Wetland Resources, United States Geological Survey Water Supply Paper 2425, US Government Printing Office, Reston, Va., 1996. Daubechies, I.: Ten Lectures on Wavelets, 61, available at: http: //epubs.siam.org/doi/book/10.1137/1.9781611970104 (last ac- cess: 22 April 2016), 1992.

David, M. B., Drinkwater, L. E., and McIsaac, G. F.: Sources of Nitrate Yields in the Mississippi River Basin, J. Environ. Qual., 39, 1657, https://doi.org/10.2134/jeq2010.0115, 2010.

David, M. M. B., Gentry, L. L. E., Kovacic, D. A., and Smith, K. M. K.: Nitrogen balance in and export from an agricultural watershed, J. Environ. Qual., 26, 1038–1048, https://doi.org/10.2134/jeq1997.00472425002600040015x, 1997.

Day, S. S., Gran, K. B., Belmont, P., and Wawrzyniec, T.: Measuring bluff erosion part 2: Pairing aerial photographs and terrestrial laser scanning to create a watershed scale sediment budget, Earth Surf. Proc. Land., 38, 1068–1082, https://doi.org/10.1002/esp.3359, 2013.

Dean, W. E. and Schwalb, A.: Holocene Evironmental and Climatic Change in the Northern Great Plains Recorded in the Geochemistry of Sediments in Pickeral Lake, South Dakota, Quaternary Int., 67, 5–20, 2000.

Delong, M. D.: Upper Mississippi River Basin, in Rivers of North America, edited by: Benke, A. C. and Cushing, C. E., Elsevier/Academic Press, Boston, 327–373, 2005.

Diak, G. R., Anderson, M. C., Bland, W. L., Norman, J. M., Mecikalski, J. M., and Aune, R. M.: Agricultural-Management Decision Aids Driven by Real-Time Satellite Data, B. Am. Meteorol. Soc., 79, 1345–1355, https://doi.org/10.1175/1520-0477(1998)079<1345:AMDADB>2.0.CO;2, 1998.

Dumanski, S., Pomeroy, J. W., and Westbrook, C. J.: Hydrological regime changes in a Canadian Prairie basin, Hydrol. Process., 29, 3893–3904, https://doi.org/10.1002/hyp.10567, 2015.

Fausey, N., Doering, E., and Palmer, M.: Purposes and benefits of drainage, in: Farm Drainage in the United States: History, Status, and Prospects, Miscellaneous

Publication No. 1455, edited by: Pavelis, G., US Department of Agriculture, Washington DC, 48– 51, 1987.

Feng, S. and Hu, Q.: Changes in winter snowfall/precipitation ratio in the contiguous United States, J. Geophys. Res., 112(D15), D15109, https://doi.org/10.1029/2007JD008397, 2007.

Foufoula-Georgiou, E., Takbiri, Z., Czuba, J. A., and Schwenk, J.: The change of nature and the nature of change in agricultural landscapes: Hydrologic regime shifts modulate ecological transitions, Water Resour. Res., 51, 6649–6671, https://doi.org/10.1002/2015WR017637, 2015.

Foufoula-Georgiou, E., Belmont, P., Wilcock, P., Gran, K., Fin- lay, J. C., Kumar, P., Czuba, J. A., Schwenk, J., and Takbiri, Z.: Comment on "Climate and agricultural land use change impacts on streamflow in the upper midwestern United States" by Satish C. Gupta et al., Water Resour. Res., 52, 7536–7539, https://doi.org/10.1002/2015WR018494, 2016.

Fouss, J. L. and Reeve, R. C.: Advances in Drainage Technology: 1955–1985, in Farm Drainage in the United States: History, Status, and Prospects, Miscellaneous Publication No. 1455, edited by: Pavelis, G. A., U.S. Department of Agriculture, Washington D.C., 30–47, 1987.

Frans, C., Istanbulluoglu, E., Mishra, V., Munoz-Arriola, F., and Lettenmaier, D. P.: Are climatic or land cover changes the dominant cause of runoff trends in the Upper Mississippi River Basin?, Geophys. Res. Lett., 40, 1104–1110, https://doi.org/10.1002/grl.50262, 2013.

Fritz, S. C., Ito, E., Yu, Z. C., Laird, K. R., and Engstrom, D. R.: Hydrologic variation in the northern Great Plains during the last two millennia, Quaternary Res., 53, 175–184, https://doi.org/10.1006/qres.1999.2115, 2000.

Gain, E. W.: Land drainage for production of food and fiber crops, in International Conference on Water for Peace, vol. 7, 451–461, Washington, DC, 1967.

Gerbert, W. A. and Krug, W. R.: Streamflow trends in Wisconsin's Driftless Area, J. Am. Water Resour. As., 32, 733–744, https://doi.org/10.1111/j.1752-1688.1996.tb03470.x, 1996.

Goolsby, D. A., Battaglin, W. A., Lawrence, G. B., Artz, R. S., Aulenbach, B. T., Hooper, R. P., Keeney, D. R., and Stensland, G. J.: Flux and Sources of Nutrients in the Mississippi-Atchafalaya River Basin: Topic 3 Report for the Integrated Assessment on Hypoxia in the Gulf of Mexico, Decision Analysis Series No. 17, NOAA Coastal Ocean Program, Silver Spring, MD, 1999.

Glaser, L.: Inflation-adjusted corn, wheat, and soybean prices, 1912–2014, USDA Econ. Res. Serv., available at: http://www.ers.usda.gov/data-products/chart-

gallery/detail. aspx?chartId=40093, last access: 1 January 2016.

Graf, W.: Dam nation: A geographic census of American dams and their large-scale hydrologic impacts, Water Resour. Res., 35, 1305–1311, 1999.

Gran, K. B., Belmont, P., Day, S. S., Jennings, C., Johnson, A., Perg, L. and Wilcock, P. R.: Geomorphic evolution of the Le Sueur River, Minnesota, USA, and implications for current sed- iment loading, in: Management and Restoration of Fluvial Systems with Broad Historical Changes and Human Impacts: Geological Society of America Special Paper 451, edited by: James, L. A., Rathburn, S. L., and Whittecar, G. R., 119–130, 2009.

Gran, K. B., Belmont, P., Day, S. S., Finnegan, N., Jennings, C., Lauer, J. W., and Wilcock, P. R.: Landscape evolution in south-central Minnesota and the role of geomorphic history on modern erosional processes, GSA Today, 21, 7–9, https://doi.org/10.1130/G121A.1, 2011.

Groisman, P. Y., Knight, R. W., and Karl, T. R.: Heavy precipitation and high streamflow in the contiguous United States: Trends in the twentieth century, B. Am. Meteorol. Soc., 82, 219–246, https://doi.org/10.1175/1520-0477(2001)082<0219:HPAHSI>2.3.CO;2, 2001.

Groschen, G. E., Harris, M., King, R., Terrio, P., and Warner, K.: Water quality in the lower Illinois River Basin, Illinois, 1995–98, U.S. Geol. Surv. Circ., 1209, 2000.

Guanter, L., Zhang, Y., Jung, M., Joiner, J., Voigt, M., Berry, J. A., Frankenberg, C., Huete, A. R., Zarco-Tejada, P., Lee, J.E., Moran, M. S., Ponce-Campos, G., Beer, C., Camps- Valls, G., Buchmann, N., Gianelle, D., Klumpp, K., Cescatti, A., Baker, J. M., and Griffis, T. J.: Global and time- resolved monitoring of crop photosynthesis with chlorophyll fluorescence, P. Natl. Acad. Sci. USA, 111, E1327–E1333, https://doi.org/10.1073/pnas.1320008111, 2014.

Hamilton, S. K., Hussain, M. Z., Bhardwaj, A. K., Basso, B., and Robertson, G. P.: Comparative water use by maize, perennial crops, restored prairie, and poplar trees in the US Midwest, Environ. Res. Lett., 10, 64015, https://doi.org/10.1088/1748- 9326/10/6/064015, 2015.

Harrigan, S., Murphy, C., Hall, J., Wilby, R. L., and Sweeney, J.: Attribution of detected changes in streamflow using multiple working hypotheses, Hydrol. Earth Syst. Sci., 18, 1935–1952, https://doi.org/10.5194/hess-18-1935-2014, 2014.

Hartemink, A. E., Lowery, B., and Wacker, C.: Soil maps of Wisconsin, Geoderma, 189–190, 451–461, https://doi.org/10.1016/j.geoderma.2012.05.025, 2012

Healy, R., Winter, T., LaBaugh, J., and Franke, L.: Water Budgets: Foundations for Effective Water-Resources and Environmental Management, U.S. Geological

Survey Circular 1308, 90 pp., available at: http://pubs.er.usgs.gov/publication/cir1308 (last access: 19 September 2017), 2007.

Hewes, L. and Frandson, P. E.: Occupying the Wet Prairie?: The Role of Artificial Drainage in Story County, Iowa, Ann. Assoc. Am. Geogr., 42, 24–50, 1952.

Hickman, G. C., Vanloocke, A., Dohleman, F. G., and Bernacchi, C. J.: A comparison of canopy evapotranspiration for maize and two perennial grasses identified as potential bioenergy crops, GCB Bioenergy, 2, 157–168, https://doi.org/10.1111/j.1757- 1707.2010.01050.x, 2010.

Higgins, R. W. and Kousky, V. E.: Changes in Observed Daily Precipitation over the United States Between 1950– 1979 and 1980–2009, J. Hydrometeorol., 120822104745000, https://doi.org/10.1175/JHM-D-12-062.1, 2012.

Hillel, D.: Groundwater drainage and pollution, in: Environmental Soil Physics, Academic Press, San Diego, CA, 471–505, 1998.

Hyden, J.: Wisconsin Dams, Univ. Wisconsin – Milwaukee, available at: http://uwmmap.com/dams.html (last access: 9 June 2016), 2010.

Irwin, R. W. and Whiteley, H. R.: Effects of land drainage on stream flow, Can. Water Resour. J., 8, 88–103, https://doi.org/10.4296/cwrj0802088, 1983.

Johnston, C. A.: Wetland losses due to row crop expansion in the dakota prairie pothole region, Wetlands, 33, 175–182, https://doi.org/10.1007/s13157-012-0365-x, 2013.

Juckem, P. F., Hunt, R. J., Anderson, M. P., and Robertson, D. M.: Effects of climate and land management change on streamflow in the driftless area ofWisconsin, J. Hydrol., 355, 123–130, https://doi.org/10.1016/j.jhydrol.2008.03.010, 2008.

Kibria, K., Ahiablame, L., Hay, C., and Djira, G.: Stream- flow Trends and Responses to Climate Variability and Land Cover Change in South Dakota, Hydrology, 3, https://doi.org/10.3390/hydrology3010002, 2016.

Kottek, M., Grieser, J., Beck, C., Rudolf, B., and Rubel, F.: World Map of the Köppen-Geiger climate classification updated, Meteorol. Z., 15, 259–263, https://doi.org/10.1127/0941- 2948/2006/0130, 2006.

Kreiling, R. M. and Houser, J. N.: Long-term decreases in phosphorus and suspended solids, but not nitrogen, in six upper Mississippi River tributaries, 1991–2014, Environ. Monit. Assess., 188, 1–19, https://doi.org/10.1007/s10661-016-5464-3, 2016.

Kronvang, B., Andersen, H. E., Larsen, S. E., and Audet, J.: Importance of bank erosion

for sediment input, storage and export at the catchment scale, J. Soils Sediments, 13, 230–241, https://doi.org/10.1007/s11368-012-0597-7, 2013.

Labat, D., Ababou, R., and Mangin, A.: Introduction of Wavelet Analyses to Rainfall/Runoffs Relationship for a Karstic Basin: The Case of Licq-Atherey Karstic System (France), Ground Water, 39, 605–615, https://doi.org/10.1111/j.1745- 6584.2001.tb02348.x, 2001.

Lauer, J. W., Echterling, C., Lenhart, C., Belmont, P., and Rausch, R.: Air-photo based change in channel width in the Minnesota River basin: Modes of adjustment and implications for sediment budget, Geomorphology, https://doi.org/10.1016/j.geomorph.2017.09.005, in press, 2017.

Lenhart, C., Titov, M., Ulrich, J., Nieber, J., and Suppes, B.: The role of hydrologic alteration and riparian vegetation dynamics in channel evolution along the lower Minnesota River, T. Am. Soc. Agric. Biol. Eng., 56, 549–561, 2013.

Lenhart, C. F., Peterson, H., and Nieber, J.: Increased Streamflow in Agricultural Watersheds of the Midwest: Implications for Man- agement, Watershed Sci. Bull., 2, 25–31, 2011.

Lenhart, C. F., Verry, E. S., Brooks, K. N., and Magner, J. A.: Adjustment of prairie pothole streams to land-use, drainage and climate changes and consequences for turbidity impairment, River Res. Appl., 28, 1609–1619, https://doi.org/10.1002/rra.1549, 2012.

Letey, J., Blair, J. W., Devitt, D., Lund, L. J., and Nash, P.: Nitrate-Nitrogen in Effluent from Agricultural Tile Drains in California, Hilgardia, 45, 289–319, 1977.

Lian, Y., You, J.-Y., Sparks, R., and Demissie, M.: Impact of Human Activities to Hydrologic Alterations on the Illinois River, J. Hydrol. Eng., 17, 537–546, https://doi.org/10.1061/(ASCE)HE, 2012.

Liu, R. Q., Jacobi, C., Hoffmann, P., Stober, G., and Merzlyakov, E. G.: A piecewise linear model for detecting climatic trends and their structural changes with application to mesosphere/lower thermosphere winds over Collm, Germany, J. Geophys. Res., 115, D22105, https://doi.org/10.1029/2010JD014080, 2010.

Livneh, B., Rosenberg, E. A., Lin, C., Nijssen, B., Mishra, V., An- dreadis, K. M., Maurer, E. P., and Lettenmaier, D. P.: A Long- Term Hydrologically Based Dataset of Land Surface Fluxes and States for the Conterminous United States: Update and Extensions, J. Climate, 26, 9384–9392, 2013.

Magner, J. A., Payne, G. A., and Steffen, L. J.: Drainage effects on stream nitrate-n and hydrology in south-central Minnesota (USA), Environ. Monit. Assess., 91, 183–198, 2004.

Marschner, F.: The original vegetation of Minnesota, a map compiled in 1930 by F. J. Marschner under the direction of M. L. Heinselman of the United States Forest Service, scale 1:500,000, 1974.

Martin, L.: The Physical Geography ofWisconsin, Third, The University ofWisconsin Press, Madison, WI, 1965.

Maurer, E. P., Wood, A. W., Adam, J. C., Lettenmaier, D. P., and Nijssen, B.: A Long-Term Hydrologically Based Dataset of Land Surface Fluxes and States for the Conterminous United States, J. Climate, 15, 3237–3251, https://doi.org/10.1175/1520- 0442(2002)015<3237:ALTHBD>2.0.CO;2, 2002.

McCorvie, M. R. and Lant, C. L.: Drainage district formation and the loss of midwestern wetlands, 1850–1930, Agr. Hist., 67, 13– 39, 1993.

McIsaac, G. F., David, M. B., and Illinois, C. A. M. U.: Miscanthus and switchgrass production in central Illinois: impacts on hydrology and inorganic nitrogen leaching, J. Environ. Qual., 39, 1790, https://doi.org/10.2134/jeq2009.0497, 2010.

Meyles, E., Williams, A., Ternan, L., and Dowd, J.: Runoff generation in relation to soil moisture patterns in a small Dartmoor catchment, Southwest England, Hydrol. Process., 17, 251–264, https://doi.org/10.1002/hyp.1122, 2003.

Miller, J. E. and Frink, D. L.: Changes in flood response of the Red River of the North basin, North Dakota-Minnesota, US Geol. Surv. Water-Supply Pap. 2243, 103 pp., 1984.

Mueller, N. D., Butler, E. E., McKinnon, K. A., Rhines, A., Tingley, M., Holbrook, N. M., and Huybers, P.: Cooling of US Midwest summer temperature extremes from cropland intensification, Nature Climate Change, 6, 317–322, https://doi.org/10.1038/nclimate2825, 2015.

Naz, B. S., Ale, S., and Bowling, L. C.: Detecting subsurface drainage systems and estimating drain spacing in intensively managed agricultural landscapes, Agr. Water Manage., 96, 627– 637, https://doi.org/10.1016/j.agwat.2008.10.002, 2009.

Novotny, E. V. and Stefan, H. G.: Stream flow in Minnesota: Indicator of climate change, J. Hydrol., 334, 319–333, https://doi.org/10.1016/j.jhydrol.2006.10.011, 2007.

O'Connell, E., Ewen, J., O'Donnell, G., and Quinn, P.: Is there a link between agricultural land-use management and flooding?, 11, 96–107, 2007.

Palmer, J. A., Schilling, K. E., Isenhart, T. M., Schultz, R. C., and Tomer, M. D.: Streambank erosion rates and loads within a single watershed: Bridging the gap between temporal and spatial scales, Geomorphology, 209, 66–78,

https://doi.org/10.1016/j.geomorph.2013.11.027, 2014.

Penna, D., Tromp-van Meerveld, H. J., Gobbi, A., Borga, M., and Dalla Fontana, G.: The influence of soil moisture on threshold runoff generation processes in an alpine headwater catchment, Hydrol. Earth Syst. Sci., 15, 689–702, https://doi.org/10.5194/hess-15-689-2011, 2011.

PRISM Climate Group: Oregon State University, available at: http: //prism.oregonstate.edu (last access: 19 September 2017), 2004.

Randall, G. W. and Mulla, D. J.: Nitrate Nitrogen in Surface Waters as Influenced by Climatic Conditions and Agricultural Practices, J. Environ. Qual., 30, 337–344, 2001.

R Core Team: R: A language and environment for statistical com- puting, available at: http://www.r-project.org/ (last access: 19 September 2017), 2013.

Robinson, M.: Impact of improved land drainage on river flows, Oxon, UK, 1990.

Rockström, J., Falkenmark, M., Allan, T., Folke, C., Gordon, L., Jägerskog, A., Kummu, M., Lannerstad, M., Meybeck, M., Molden, D., Postel, S., Savenije, H., Svedin, U., Turton, A., and Varis, O.: The unfolding water drama in the Anthropocene: towards a resilience based perspective on water for global sustainability, Ecohydrology, 7, 1249–1261, https://doi.org/10.1002/eco.1562, 2014.

Rosenberg, D. M., Chambers, P. A., Culp, J. M., Franzin, W. G., Nelson, P. A., Salki, A. G., Stainton, M. P., Bodaly, R. A., and Newbury, R. W.: Nelson and Churchill River Basins, in Rivers of North America, edited by: Benke, A. C. and Cushing, C. E., Elsevier/Academic Press, Boston, 853–901, 2005.

Royer, T. V., David, M. B., and Gentry, L. E.: Timing of Riverine Export of Nitrate and Phosphorus from Agricultural Watersheds in Illinois?: Implications for Reducing Nutrient Loading to the Mississippi River, Environ. Sci. Technol., 40, 4126–4131, 2006.

Schaffrath, K. R., Belmont, P., and Wheaton, J. M.: Landscape-scale geomorphic change detection: Quantifying spatially variable uncertainty and circumventing legacy data issues, Geomorphology, 250, 334–348, https://doi.org/10.1016/j.geomorph.2015.09.020, 2015.

Schilling, K. E. and Libra, R. D.: Increased baseflow in Iowa over the second half of the 20th century, J. Am. Water Resour. As., 39, 851–860, https://doi.org/10.1111/j.1752- 1688.2003.tb04410.x, 2003.

Schilling, K. E., Kult, K., Wilke, K., Streeter, M., and Vo- gelgesang, J.: Nitrate reduction in a reconstructed floodplain oxbow fed by tile drainage, Ecol. Eng.,

102, 98–107, https://doi.org/10.1016/j.ecoleng.2017.02.006, 2017.

Schottler, S. P., Ulrich, J., Belmont, P., Moore, R., Lauer, J. W., Engstrom, D. R., and Almendinger, J. E.: Twentieth century agricultural drainage creates more erosive rivers, Hydrol. Process., 28, 1951–1961, https://doi.org/10.1002/hyp.9738, 2014.

Seuront, L. and Strutton, P. G.: Handbook of scaling methods in aquatic ecology: measurement, analysis, simulation, CRC Press, Boca Raton, FL, 2003.

Simon, A., Rinaldi, M., and Hadish, G.: Channel evolution in the loess area of the Midwestern United States, in Proceedings of the Sixth Federal Interagency Sedimentation Conference, Las Vegas, Nevada, p. III-86–III-93, Federal Interagency Sedimentation Conference, Reston, VA, 1996.

Sims, J. T., Simard, R. R., and Joern, B. C.: Phosphorus Loss in Agricultural Drainage: Historical Perspective and Current Research, J. Environ. Qual., 27, 277–293, 1998.

Skaggs, R., Gilliam, J., Sheets, T., and Barnes, J.: Effects of agricultural land development on drainage waters in the North Carolina tidewater region, Water Resour. Res. Institute, Rep. No. 159, Univ. North Carolina, Raleigh, 1980.

Skaggs, R., Brevé, M., and Gilliam, J.: Hydrologic and water quality impacts of agricultural drainage, Crit. Rev. Environ. Sci. Tech- nol., 24, 1–32, 1994.

Stark, J. R., Andrews, W. J., Fallon, J. D., Fong, A. L., Goldstein, R. M., Hanson, P. E., Kroening, S. E., and Lee, K. E.: Water-Quality Assessment of Part of the Upper Mississippi River Basin, Min- nesota and Wisconsin-Environmental Setting and Study Design, US Geol. Surv. Water-Resources Investig. Rep., 96–4098, 1996.

Stoner, J. D., Lorenz, D. L., Wiche, G. J., and Goldstein, R. M.: Red River of the North Basin, Minnesota, North Dakota, and South Dakota, Water Resour. Bull., 29, 575–615, 1993.

Stout, J. C., Belmont, P., Schottler, S. P., and Willenbring, J. K.: Identifying Sediment Sources and Sinks in the Root River, Southeastern Minnesota, Ann. Assoc. Am. Geogr., 104, 20–39, https://doi.org/10.1080/00045608.2013.843434, 2014.

Sugg, Z.: Assessing U S Farm Drainage?: Can GIS Lead to Better Estimates of Subsurface Drainage Extent?, World Resour. Inst., 1–8, available at: http://pdf.wri.org/assessing_farm_drainage.pdf (last access: 19 September 2017), 2007.

Sullivan, M., VanToai, T., Fausey, N., Beuerlein, J., Parkinson, R., and Soboyejo, A.: Crop ecology, production & management: Evaluating on-farm flooding impacts on soybean, Crop Sci., 41, 93–100, https://doi.org/10.2135/cropsci2001.41193x,

2001.

Tomé, A. R. and Miranda, P. M. A.: Piecewise linear fitting and trend changing points of climate parameters, Geophys. Res. Lett., 31, L02207, https://doi.org/10.1029/2003GL019100, 2004.

Torrence, C. and Compo, G. P.: A Practical Guide to Wavelet Analysis, B. Am. Meteorol. Soc., 79, 61–78, 1998.

Trimble, S. W.: Decreased rates of alluvial sediment storage in the Coon Creek Basin, Wisconsin, 1975–93, Science, 285, 1244– 1246, https://doi.org/10.1126/science.285.5431.1244, 1999.

Trimble, S. W. and Crosson, P.: U.S. Soil Erosion Rates: Myth and Reality, Science, 289, 248–250, 2000.

United States Army Corps of Engineers: National Inventory of Dams, available at: http://nid.usace.army.mil (last access: 16 Jan- uary 2017), 2016.

US Bureau of the Census: Irrigation and drainage: General report and analytical tables and reports for states, with statistic for counties, Volume 7, in Fourteenth Census of the United States Taken in the year 1920, United States Department of Commerce, Government Printing Office, Washington, DC, 1922.

US Bureau of the Census: Drainage of agricultural lands, Volume 4, in Sixteenth Census of the United States: 1940, United States Department of Commerce, Government Printing Office, Washington, DC, 1942.

US Bureau of the Census: Drainage of agricultural lands, Volume 4, in United States Census of Agriculture: 1950, United States Department of Commerce, Government Printing Office, Washington, DC, 1952.

US Bureau of the Census: Drainage of agricultural lands, Volume 4, in United States Census of Agriculture: 1959, United States Department of Commerce, Government Printing Office, Wash- ington, DC, 1961.

US Bureau of the Census: Drainage of agricultural lands, Volume 5, Part 5, in 1978 Census of Agriculture, United States Department of Commerce, Government Printing Office, Washington, DC, 1981.

US Department of Agriculture Bureau of Agricultural Economics Crop Reporting Board: Crop Production Annual Summary, 1949, Washington, DC, 1949.

US Department of Agriculture National Agricultural Statistics Service Agricultural Statistics Board: Crop Production Annual Summary, 1989, Washington, DC, 1990.

US Department of Agriculture National Agricultural Statistics Service: Special tabulation: county-level land drained by tile and ditches, 2012 Census Agric., 2014a.

US Department of Agriculture National Agricultural Statistics Service: Summary and state data, 2012 Census Agric., 1, 2014b.

USDA National Agricultural Statistics Service Cropland Data Layer: Published crop-specific data layer, available at: https: //nassgeodata.gmu.edu/CropScape/ (last accessed: 1 November 2016), 2013.

Vandegrift, T. R. and Stefan, H. G.: Annual stream runoff and climate in Minnesota's river basins, Minneapolis, 2010.

Verbesselt, J., Hyndman, R., Newnham, G., and Culvenor, D.: Detecting trend and seasonal changes in satellite image time series, Remote Sens. Environ., 114, 106–115, https://doi.org/10.1016/j.rse.2009.08.014, 2010.

Vörösmarty, C., Lettenmaier, D., Leveque, C., Meybeck, M., Pahl- Wostl, C., Alcamo, J., Cosgrove, W., Grassl, H., Hoff, H., Kabat, P., Lansigan, F., Lawford, R., and Naiman, R.: Humans transforming the global water system, Eos, Trans. Am. Geophys. Union, 85, 509–514, https://doi.org/10.1029/2004EO480001, 2004.

Wilcock, P.: Identifying sediment sources in the Minnesota River Basin, Minnesota River Sediment Colloq., 16, available at: http://www.pca.state.mn.us/index.php/view-document.html? gid=8099 (last access: 19 September 2017), 2009.

Willett, C. D., Lerch, R. N., Schultz, R. C., Berges, S. A., Peacher, R. D., and Isenhart, T. M.: Streambank erosion in two watersheds of the Central Claypan Region of Missouri, United States, J. Soil Water Conserv., 67, 249–263, https://doi.org/10.2489/jswc.67.4.249, 2012.

Wolf, R. A. and Market, P. S.: On the impact of corn and soybeans to the local moisture budget in Iowa, Natl. Weather Dig., 31, 3–7, 2007.

Wuebker, E. F., Mullen, R. E., and Koehler, K.: Flooding and temperature effects on soybean germination, Crop Sci., 41, 1857– 1861, https://doi.org/10.2135/cropsci2001.1857, 2001.

Xu, X., Scanlon, B. R., Schilling, K., and Sun, A.: Relative importance of climate and land surface changes on hydrologic changes in the US Midwest since the 1930s: Implications for biofuel production, J. Hydrol., 497, 110–120, https://doi.org/10.1016/j.jhydrol.2013.05.041, 2013.

Zeileis, A., Kleiber, C., Krämer, W., and Hornik, K.: Testing and dating of structural changes in practice, Comput. Stat. Data An., 44, 109–123,

https://doi.org/10.1016/S0167-9473(03)00030-6, 2003.

Zeri, M., Hussain, M. Z., Anderson-Teixeira, K. J., Delucia, E., and Bernacchi, C. J.: Water use efficiency of perennial and annual bioenergy crops in central Illinois, J. Geophys. Res. Biogeo., 118, 581–589, https://doi.org/10.1002/jgrg.20052, 2013.

Zhang, Y. K. and Schilling, K. E.: Increasing streamflow and baseflow in Mississippi River since the 1940s: Effect of land use change, J. Hydrol., 324, 412–422, https://doi.org/10.1016/j.jhydrol.2005.09.033, 2006.

Tables

Table 2-1. United States Geological Survey (USGS) stream gauge stations listed by study basin.

USGS gauge station	Station name	Period of record	Length (years)	Notes
Chippewa River basin (9 gauges)				
05356000	Chippewa River at Bishops Bridge, near Winter, WI	1929-2013	85	Mainstem river
05356500	Chippewa River near Bruce, WI	1929-2013	85	Mainstem river
05360500	Flambeau River near Bruce, WI	1952-2013	62	
05362000	Jump River at Sheldon, WI	1929-2013	85	
05365500	Chippewa River at Chippewa Falls, WI	1929-2013	81	Missing data: 1983 - 1986
05369000	Red Cedar River at Menomine, WI	1929-2013	85	
05368000	Hay River at Wheeler, WI	1951-2013	63	
05370000	Eau Galle River at Spring Valley, WI	1945-2013	69	
05369500	Chippewa River at Durand, WI	1929-2013	85	Mainstem river - Downstream gauge
Illinois River basin (20 gauges)				
05552500	Fox River at Dayton, IL	1929-2013	85	
05543500	Illinois River at Marseilles, IL	1929-2013	85	Mainstem river
05555300	Vermilion River near Leonore, IL	1932-2013	82	†
05556500	Big Bureau Creek at Princeton, IL	1937-2013	77	†
05554500	Vermilion River at Pontiac, IL	1943-2013	71	†
05569500	Spoon River at London Mills, IL	1943-2013	71	
05567500	Mackinaw River near Congerville, IL	1945-2013	69	†
05568500	Illinois River at Kingston Mines, IL	1940-2013	74	Mainstem river
05570000	Spoon River at Seville, IL	1929-2013	85	
05584500	La Moine River at Colmar, IL	1945-2013	69	
05585000	La Moine River at Ripley, IL	1929-2013	85	
05583000	Sangamon River Near Oakford, IL	1929-2013	79	Missing data: 1934 - 1939
05582000	Salt Creek near Greenview, IL	1942-2013	72	

Table 2-1. (cont.)

05580000	Kickapoo Creek at Waynesville, IL	1948-2013	66	† *
05578500	Salt Creek near Rowell, IL	1943-2013	71	
05572000	Sangamon River at Monticello, IL	1929-2013	85	†
05576000	South Fork Sangamon River near Rochester, IL	1950-2013	64	
05577500	Spring Creek at Springfield, IL	1949-2013	65	†
05586100	Illinois River at Valley City, IL	1939-2013	75	Mainstem river - Downstream gauge
05587000	Macoupin Creek near Kane, IL	1929-2013	77	Missing data: 1933 - 1940
Minnesota River basin (12 gauges)				
05291000	Whetstone River near Big Stone City, SD	1932–2013	82	
05292000	Minnesota River at Ortonville, MN	1939–2013	75	Mainstem river
05304500	Chippewa River near Milan, MN	1938-2013	76	
05311000	Minnesota River at Montevideo, MN	1930-2013	84	Mainstem river
05313500	Yellow Medicine River near Granite Falls, MN	1940-2013	74	
05315000	Redwood River near Marshall, MN	1941-2013	73	
05316500	Redwood River near Redwood Falls, MN	1936-2013	78	
05317000	Cottonwood River near New Ulm, MN	1939-2013	75	
05320000	Blue Earth River near Rapidan, MN	1950-2013	64	
05320500	Le Sueur River near Rapidan, MN	1950-2013	64	
05325000	Minnesota River at Mankato, MN	1930-2013	84	Mainstem river
05330000	Minnesota River near Jordan, MN	1935-2013	79	Mainstem river - Downstream gauge
Red River of the North basin (22 gauges)				
05050000	Bois de Sioux River near White Rock, SD	1942-2013	72	
05046000	Otter Tail River near Fergus Falls, MN	1931-2013	83	
05051500	Red River of the North at Wahpeton, ND	1944-2013	70	Mainstem river
05053000	Wild Rice River near Abercrombie, ND	1933-2013	81	
05056000	Sheyenne River near Warwick, ND	1950-2013	64	
05057000	Sheyenne River near Cooperstown, ND	1945-2013	69	
05058000	Sheyenne River below Baldhill Dam, ND	1950-2013	64	
05059000	Sheyenne River near Kindred, ND	1950-2013	64	
05059500	Sheyenne River at West Fargo, ND	1930-2013	84	
05054000	Red River of the North at Fargo, ND	1929-2013	85	Mainstem river
05060500	Rush River at Amenia, ND	1947-2013	67	
05062000	Buffalo River near Dilworth, MN	1932-2013	82	
05066500	Goose River at Hillsboro, ND	1935-2013	79	
05064000	Wild Rice River at Hendrum, MN	1945-2013	67	Missing data: 1984 - 1985
05069000	Sand Hill River at Climax, MN	1947-2013	65	Missing data: 1984 - 1985
05074500	Red Lake River near Red Lake, MN	1934-2013	74	Missing data: 1994 - 1999
05075000	Red Lake River at High Landing near Goodridge, MN	1930-1999	70	Missing data: 2000 - 2013

Table 2-1. (cont.)

05076000	Thief River near Thief River Falls, MN	1929-2013	83	Missing data: 1981 - 1982
05078000	Clearwater River at Plummer, MN	1940-2013	70	Missing data: 1979 - 1982
05078500	Clearwater River at Red Lake Falls, MN	1935-2013	77	Missing data: 1981 - 1982
05079000	Red Lake River at Crookston, MN	1929-2013	85	
05082500	Red River of the North at Grand Forks, ND	1929-2013	85	Mainstem river - Downstream gauge

† Tributary gauges, predominantly agricultural, not influenced by major dams
* Mean Annual Flow and Seven Day Low Flow Winter 1949-2013

Table 2-2. Site details for AmeriFlux sites used for comparison with Livneh et al. (2013) evapotranspiration data (L13), where L13(JJA) represents 17% reduction in ET during summer months June, July, and August. Average annual difference is positive when L13/L13(JJA) ET is greater than Ameriflux ET and negative when less than. Nearest study watersheds are abbreviated: Chippewa River basin (CRB), Illinois River basin (IRB), Minnesota River basin (MRB), and Red River of the North basin (RRB).

Site name	**Willow Creek, WI**	**Bondville, IL**	**Rosemount, MN**	**Brookings, SD**
AmeriFlux site no.	US-WCr	US-Bo1	US-Ro1	US-Bkg
Latitude	45.8059	40.0062	44.7143	44.3453
Longitude	-90.0799	-88.2904	-93.0898	-96.8362
Nearest watershed[s]	CRB	IRB	MRB [CRB]	MRB [RRB]
Distance to nearest watershed (km)	0.463	13.049	43.807 [74.169]	25.949 [129.688]
Years	1999-2002	2003-2008	2004-2009	2004-2009
Vegetation	Deciduous broadleaf forest	Croplands	Croplands	Grasslands
Average difference L13-Ameriflux	+31%	+17%	+14%	-29%
Average difference L13(JJA)-Ameriflux	+19%	+7%	+5%	-34%

Table 2-3. Summary of the breakpoint years identified from land cover transition (LCT) (Fig. 2-3), piecewise linear regression (PwLR) of precipitation (P) and streamflow (Q), and continuous wavelet transform (CWT) of P and Q (Fig. 2-4).

	LCT (Fig. 2-3)	P (PwLR)	Q (PwLR)	P (CWT, Fig. 2-4)	Q (CWT, Fig. 2-4)
Red River of the North basin	2003/2004	1987/1988	1989/1990	No change	1995
Minnesota River basin	1978/1979	1958/1959	1967/1968	No change	1980
Illinois River basin	1961/1962	1981/1982	1981/1982	No change	1975
Chippewa River basin	2009/2010	1995/1996	1995/1996	No change	No change

Table 2-4. Observed average annual precipitation (P), flow (Q), evapotranspiration (ET) and storage $\left(\frac{dS}{dt}\right)$ depths (cm y^{-1}) for each basin during the pre-period (a) and post-period (b) split by 1974/1975 (1) and land cover transition (LCT) (2) breakpoints.

		Years	P_{mean} (cm y^{-1})	Q_{mean} (cm y^{-1})	ET_{mean} (cm y^{-1})	$\frac{dS}{dt}_{mean}$ (cm y^{-1})
Minnesota River basin	1a	1935-1974	65.1	7.2	60.9	-3.0
	1b	1975-2011	70.0	13.4	64.2	-7.5
	2a	1935-1978	64.8	7.0	60.6	-2.8
	2b	1979-2011	71.0	14.4	65.0	-8.4
	1a†	1935-1974			55.6	2.3
	1b†	1975-2011			58.7	-2.0
	2a†	1935-1978			55.4	2.4
	2b†	1979-2011			59.3	-2.7
Red River of the North basin	1a	1935-1974	53.4	3.7	45.1	4.7
	1b	1975-2011	57.7	6.7	47.4	3.5
	2a	1935-2003	54.5	4.6	45.6	4.4
	2b	2004-2011	63.3	10.1	51.6	1.5
	1a†	1935-1974			41.1	8.6
	1b†	1975-2011			43.3	7.6
	2a†	1935-2003			41.6	8.4
	2b†	2004-2011			47.4	5.8
Illinois River basin	1a	1939-1974	90.5	27.3	73.2	-10.0
	1b	1975-2011	95.2	33.0	75.1	-13.0
	2a	1939-1961	89.5	25.9	72.8	-9.3
	2b	1962-2011	94.4	32.2	74.8	-12.5
	1a†	1939-1974			66.9	-3.7
	1b†	1975-2011			68.7	-6.6

Table 2-4. (cont.)

	2a†	1939-1961			66.5	-3.0
	2b†	1962-2011			68.4	-6.1
Chippewa River basin	1a	1935-1974	80.0	29.7	61.8	-11.5
	1b	1975-2011	82.1	29.8	62.7	-10.5
	2a	1935-2009	80.8	29.6	62.1	-11.0
	2b	2010-2011	88.4	33.3	68.5	-13.4
	1a†	1935-1974			56.5	-6.2
	1b†	1975-2011			57.4	-5.2
	2a†	1935-2009			56.8	-5.7
	2b†	2010-2011			62.3	-7.3

† 17% reduction in ET during summer months (JJA)

CHAPTER 3

HIGH RESOLUTION MONITORING OF RIVER BLUFF EROSION REVEALS FAILURE MECHANISMS AND GEOMORPHICALLY EFFECTIVE FLOWS[2]

Abstract

Using a combination of SfM and timelapse photogrammetry, we document rapid river bluff erosion occurring in the Greater Blue Earth River (GBER) basin, a muddy tributary to the sediment-impaired Minnesota River in south-central Minnesota. Our datasets elucidated dominant bluff failure mechanisms and rates of bluff retreat in a transient system responding to ongoing streamflow increases and glacial legacy impacts. Specifically, we document the importance of fluvial scour, freeze-thaw, as well as other drivers of bluff erosion. We find that even small flows, a mere 30% of the 2 year recurrence interval flow, are capable of causing bluff erosion. During our study period (2014 – 2017), the most erosion was associated with two large flood events with 13 and 25 year return periods. However, based on the frequency of floods and magnitude of bluff face erosion associated with floods over the last 78 years, the 1.2 year return interval flood has likely accomplished the most cumulative erosion, and is thus more geomorphically effective than larger magnitude floods. Flows in the GBER basin are non-stationary, increasing across the full range of return intervals. We find that management implications differ considerably depending on whether the bluff erosion ~ runoff power law exponent, γ, is greater than, equal to, or less than 1. Previous research

[2]Kelly, S. A., & Belmont, P. (2018). High resolution monitoring of river blufferosion reveals failure mechanisms and geomorphically effective flows. Water, 10(4). https://doi.org/10.3390/w10040394

has recommended installation of water retention sites in tributaries to the Minnesota River in order to reduce flows and sediment loading from river bluffs. Our findings support the notion that water retention would be an effective practice to reduce sediment loading and highlight the importance of managing for both runoff frequency and magnitude.

Keywords: Structure-from-Motion 1; photogrammetry 2; bluff erosion 3; geomorphic change detection 4; geomorphically effective flows 5; freeze-thaw 6; fine sediment 7; Minnesota River 8

1. Introduction

Humans have profoundly changed water and sediment fluxes in rivers worldwide [1–7]. Fluxes of fine sediment (clay, silt and fine sand) in particular have been directly affected by dam construction, urbanization, agriculture, fire suppression, mining, dredging, and logging [6]. Pervasive changes in watershed hydrology, due to anthropogenic climate change as well as land and water management actions, have indirectly amplified and damped sediment loading [8–11]. Such alterations in riverine fine sediment fluxes have important implications for channel and floodplain morphology [12,13], nutrient and contaminant transport [14–16], and aquatic habitat [17,18].

Problems of excess sediment and phosphorous affect a growing number of lakes and rivers globally, especially in agricultural landscapes [19]. Currently, fifteen percent of all river miles in the USA are impaired by excess sediment [20]. Thus, effective strategies for reducing sediment loads are greatly needed. In order to develop effective sediment reduction strategies, it is essential to identify the sediment sources and factors

causing excessive erosion [21]. Pinpointing the cause of excessive sediment loading is often complicated by the immense variability of climate and land use in both time and space, thresholds and non-linear processes governing erosion, transport and deposition throughout a landscape, and a severe lack of sediment monitoring data, especially at small spatial scales [22]. Multiple, independent lines of information are often needed to properly constrain a sediment budget or watershed hydro-erosion model, in order to inform policy and management actions [7,23].

The Minnesota River basin (MRB) has been identified as a dominant contributor to sediment impairments in the Upper Mississippi River basin [24–26]. Ambitious sediment and nutrient reduction targets have been established for the MRB [27]. Thus, a suite of conservation measures are currently being considered to reduce sediment loading [28]. The hydro-climate of south-central Minnesota, like large swaths of the Midwest, is becoming wetter and on-going increases in artificial agricultural drainage continue to increase river runoff [11,10], creating more erosive flows.

Several studies document strong coupling between discharge and erosion of near-channel sediment sources (NCSS), such as streambanks and bluffs, at broad spatial (10^3+ km^2) and temporal (semi-annual to decadal) scales in the Minnesota River basin [7,9,10,29–31]. However, mechanistic linkages between NCSS erosion and streamflows have received less attention at finer spatial (101-102 m^2) and temporal (daily to seasonal) scales. If sediment loading from NCSS is to be reduced in an effort to meet regional sediment reduction goals [27], then we need to better understand when and how these sources erode [21] in response to external drivers such as temperature, precipitation, and streamflow, all of which are changing due to shifts in climate and land use.

River bluffs are the dominant features contributing sediment in the Le Sueur River basin, which is the sub-basin of the MRB with the highest flow-weighted sediment loads [7,32]. Thus, reducing bluff erosion is essential for reducing sediment loading and improving water quality. Using repeat Terrestrial Laser Scanner (TLS) surveys, Day et al. (2013a) measured higher annual bluff retreat rates when surveys bracketed larger magnitude flood events [33]. We build on these findings by answering several important questions: 1) Which physical processes accomplish the most bluff erosion?; 2) Is there a threshold flow magnitude required to erode bluffs?; and 3) Considering tradeoffs between frequency and magnitude of erosional events [34], what is the most geomorphically effective flow for bluff erosion? In an effort to inform sediment reduction strategies for the MRB [27,28] we present direct observations and high resolution measurements of river bluff erosion, the results of which allowed us to identify dominant failure mechanisms and geomorphically effective flows.

2. Methods

2.1. Study Sites

The 9200 km2 Greater Blue Earth River (GBER) watershed is a geomorphically transient basin with flat agricultural uplands and deeply incised river valleys in the lower portions of the watershed (Figure 3-1). The GBER is a major tributary to the MRB and is underlain by 15-100 m [35] of easily erodible glacial till, weakly lithified sandstones, and lacustrine deposits. The Blue Earth River and tributaries, including the Watonwan, Maple, Cobb, and Le Sueur rivers, erode tall (3 – 70 m) bluffs and terraces within the actively incising “knickzone”, the upper extent of which is marked by the green line in Figure 3-1. River and ravine incision began approximately 13,400 cal BP following

paleo-flooding of Glacial River Warren (the modern-day Minnesota River) and continues at present [36,37]. Though riverine bluffs have dominated watershed sediment budgets in this basin since the end of the Pleistocene, erosion of bluffs has been further exacerbated by exceptionally high flows over the past few decades [7,21,38].

We monitored bluff erosion at 20 sites: 3 along the Blue Earth River, 7 along the Maple River, and 10 along the Le Sueur River (Figure 3-1). Surface areas are provided for all sites in Appendix B. Sites were selected to include a range of slope aspects and various material types (Appendix B, Table B1); priority was given to sites previously monitored by Day et al. 2013a and landowner access was required in all cases, as sites were located on private lands. See Appendix B,Table B1 for site descriptions.

2.2. Data Aquisition

2.2.1. Daily Timelapse Photographs

In June 2013, we installed six Canon PowerShot SX110 IS cameras in weatherproof cases, three each at sites LS9 and LS10. These cameras took one bluff photo per day and ran off of a solar panel configuration in summer, and an air alkaline battery configuration in winter. In early June 2015, we installed less expensive Cabela's Outfitter 12MP IR HD Trail Cameras at all 20 sites. Each camera, powered year-round by eight AA batteries, took a photo every three hours, recording photo time, date, and air temperature. Both types of cameras required manual data downloading.

2.2.2. Repeat Topographic Surveys using Structure-from-Motion Photogrammetry

We conducted 7 repeat photo surveys at each of two sites (LS9 and LS10) between June 2014 and May 2017 (Table 3-1). During each site visit we obtained 46-110

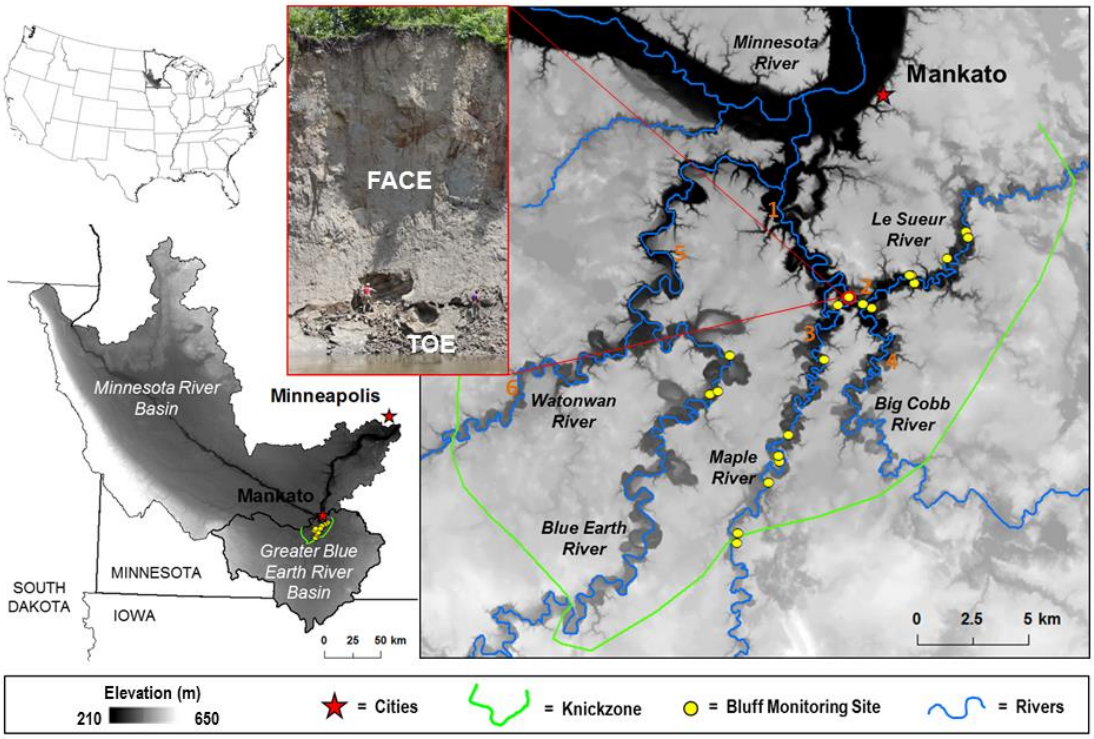

Figure 3-1. Locations of bluff study sites within the Greater Blue Earth River basin. Inset photo corresponds with bluff site LS10, a 20 m tall bluff composed of overly consolidated glacial till; 1.8 m tall person for scale. Streamflow gages are labeled by number (1: Le Sueur River gage near Rapidan, MN (USGS 5320500), 2: Le Sueur River near Highway 8 (MPCA/MDNR site 32076001), 3: Maple River at Highway 35 (MPCA/MDNR site 32072001), 4: Big Cobb River near Beauford (MPCA/MDNR site 32071001), 5: Blue Earth River near Rapidan (USGS 05320000), 6: Watonwan River near Garden City (MPCA/MDNR site 31051001)). Photo taken following a large flood event in June 2014 (credit: Shayler Levine).

photographs from the bank opposite each bluff using a Panasonic Lumix® DMC-TS4 12.1 megapixel digital camera. Our image acquisition techniques in the field were consistent with Structure-from-Motion with Multi-View Stereo (SfM-MVS) guidelines outlined by (Smith et al., 2015). Based on average point cloud density (1.25 pts/cm^2), ground control root-mean-square-error (0.027 m), as well as SfM-MVS post-processing time (30 hrs/survey for automated steps, and 10+ hours/survey for manual steps), we

found surveys containing ~100 photos were most effective for bluff surveys, each of which covered approximately 2500 m^2.

Image acquisition surveys were conducted within several hours (up to 24 hours) of total station ground control surveys, using a Leica TPS 1200. Prior to each bluff photo survey we installed 9 to 13 ground control points (GCPs) – pieces of rebar (0.95 cm diameter; 61 cm length), each with a 5.8 cm diameter orange cap. We surveyed the center location of each rebar cap using the total station in reflectorless mode to avoid rodman error and risk of injury. Total station survey closing error was < 1 cm. Permanent benchmarks could not be established on either bank due to frequent, large erosion and/or deposition events. Therefore, new total station benchmarks were established at the start of each survey with coordinates obtained using a Leica CS15 and GS15 rtkGPS. GPS coordinates were obtained in real time while referencing the Minnesota Department of Transportation Continuously Operating Reference Network, typically achieving ± 2-3 cm horizontal accuracy, and ± 4-5 cm vertical accuracy. Easting and Northing coordinates reference NAD83 UTM Zone 15N and elevation coordinates reference NAVD88 ellipsoid heights.

2.3. Data Analysis

2.3.1. Inventory and Classification of Bluff Erosion Events

For each site we manually viewed daily photographs, deleting blurry and obstructed images. On average, 89% of days contained useable images; Table B1 in Appendix B reports the percent of days with photographs for each site. In total we kept 12,608 images, all of which can be accessed with other raw data in the Supplemental Material.

Table 3-1. Repeat Structure-from-Motion photo survey information. Abbreviations used for ground control points (GCPs) and root mean square error (RMSE).

Site Name	Survey Date	Number of Survey Photos	Number of GCPs	GCP RMSE (m)	Total Dense Cloud Points ($x10^6$)	Average Cloud Density (pts/cm^2)
LS9[1]	6/15/2014	46	9	0.024	28.4	1.4
LS9	7/3/2014	52	11	0.087	35.1	1.5
LS9	5/8/2015	55	9	0.013	30.3	1.3
LS9	7/12/2015	60	11	0.028	17.9	0.6
LS9	5/24/2016	54	10	0.031	17.7	0.7
LS9	10/22/2016	100	11	0.024	22.0	0.8
LS9	5/17/2017	108	10	0.010	47.1	1.6
LS10[2]	6/15/2014	51	9	0.015	31.9	2.2
LS10	7/3/2014	110	13	0.018	35.1	1.7
LS10	5/9/2015	51	11	0.010	38.6	2.0
LS10	7/10/2015	50	11	0.073	19.9	0.7
LS10	5/24/2016	63	10	0.018	26.1	1.0
LS10	10/22/2016	100	13	0.018	20.6	0.7
LS10	5/17/2017	91	5[3]	0.016	38.7	1.3

[1] Bluff LS 9 average survey area: 2100 m^2
[2] Bluff LS 10 average survey area: 2000 m^2
[3] Field survey contained 12 GCPs, but only 5 GCPs were recovered post-survey due to instrument damage.

For each day between June 8, 2015 and May 15, 2017 we indicated whether a photo existed and whether a large or small failure had occurred, based on repeat visual inspection by both an undergraduate researcher and S. Kelly. Daily photographs at site LS9 and LS10 extend back to June 2013, though the photo collection prior to May 2015 is less complete. The distinction between large and small failures was made based on size of the affected area, with large failures being those that exceeded 1 m^2. The largest failures were further classified as either face or toe erosion events. Face erosion events occurred sub-aerially via mass wasting, block fall, slumping, or cantilever failure, primarily affecting in-situ till and/or Holocene terrace alluvium that caps the bluff. By contrast, toe erosion events coincided with high flow events, often removed failed colluvium, and occasionally eroded in-situ till at the base of the bluff via fluvial abrasion

or scour (Figure 3-1). For the 347 largest events we classified whether failures were caused (based on photograph interpretations) by precipitation, freeze-thaw, sapping, rising limb flows, falling limb flows, ice breakup floods, structural instabilities (from previous failures), a combination of causes, or an unknown cause. Additionally, we categorically documented the duration of time that failed face material persisted at the toe of the bluff: one day to one week; one week to one month; one month to six months; six months to one year; and greater than one year.

2.3.2. Measuring Bluff Erosion using Structure-from-Motion Photogrammetry

We post-processed field-collected photo surveys using Agisoft PhotoScan Professional following best-practice methods outlined by (Carrivick et al., 2016; Fonstad et al., 2013; Smith et al., 2015; Westoby et al., 2012). For each survey we imported all non-blurry images; created photo masks; grouped photos by cameras based on focal length; aligned photos to create a sparse cloud, key point limit 100,000 and tie point limit 0; semi-automatically removed noisy points from sparse point clouds using gradual selection with a reconstruction uncertainty of 100; optimized cameras; manually removed noisy points, which were generally introduced from vegetation; re-optimized cameras; georeferenced point clouds using surveyed GCP coordinates; again re-optimized cameras; and finally reconstructed dense point clouds with ultra-high and mild depth filtering settings. Point clouds were manually edited for erroneous points (<10% of total points) usually introduced from vegetation, exported from PhotoScan as text files (.xyz), and then imported to CloudCompare to obtain bluff domain coordinates for point cloud rotations (Girardeau-Montaut, 2015).

Bluff point clouds were built in real-world coordinates, however bluffs are near vertical features, often with overhangs, that erode in a direction normal to the bluff aspect and therefore perpendicular to the z coordinate axis. We rotated all point cloud coordinates using a Matlab script (Appendix B) so that the measured direction of change in the z direction would capture erosion normal to the bluff aspect.

Once rotated, dense clouds were decimated to a 10 cm x 10 cm grid using the Topographic Analysis Toolkit (ToPCAT), developed by (Brasington et al., 2012) and available from OpenTopography. This tool creates an output shapefile containing the mean, maximum, minimum, detrended standard deviation, as well as other statistics, associated with the subsampled point cloud. Subsampled points were computed using a minimum of 4 dense cloud points. Then we created 2.5-D rasters in ArcMap using the point to raster tool (10 cm grid) and differenced rasters using the Geomorphic Change Detection (GCD) tool (Wheaton et al., 2010). Although terrestrial and aerial lidar surveys often build rasters using the zmin, or last returned/bare earth, elevation, Structure-from-Motion does not necessarily provide bare earth elevations using zmin, especially in heavily vegetated areas. Error can occur all three dimensions; therefore we used zmean to build survey elevation rasters.

We constrained our final areal and volumetric change by probabilistically (99% CI) thresholding the DEM of difference (DoD) with a spatially propagated error surface generated for each survey. The error surface was created from the survey point cloud detrended standard deviation, or roughness, and the GCD defined SfM surveying uncertainty, 0.12 m. Where roughness was greater than 0.12 m, we assigned the roughness value to each error surface pixel, and where roughness was less than 0.12 m,

we assigned the error surface pixel the value 0.12 m. Because we used the ground control points to georeference the dense point cloud, the GCP root-mean-square-error (RMSE) reported in Table 3-1 is not an independent measure of point cloud accuracy. Therefore, we validated our topographic models using 9-20 check points that were withheld from dense point cloud georeferencing and found an average survey RMSE of 0.11 m. Thus, it seems reasonable for a conservative assessment of change to assume 0.12 m as a minimum level of detection in areas of low roughness.

2.3.3. Estimating Bluff Erosion using Daily Photographs and Volume ~ Area Scaling Relation

Although repeat Structure-from-Motion photogrammetric surveys are relatively inexpensive, quick to acquire, and require minimal expertise to post-process using commercially available software packages, trade-offs exist between time spent in the field and lab and the overall accuracy of the survey (Castillo et al., 2012; Smith et al., 2015). Given that SfM surveys were not feasible at all 20 sites due to financial and time constraints, we developed a relation between bluff erosion volumes and areas based on SfM DoDs and repeat terrestrial laser scanner (TLS) surveys conducted by (Day et al., 2013b). This allowed us to estimate bluff erosion volumes from digitizing areas of change for daily timelapse photographs. We find that mass wasting of riverine bluffs exhibit a power-law volume ~ area relation and compare the scaling exponent of our relation to the range of scaling exponents found for soil- and bedrock-cored landslides by (Larsen et al., 2010; Lavé and Burbank, 2004; N et al., 1997; Stark and Guzzetti, 2009) in Section 4.

Areas of change were manually digitized using the daily photographs for all of the large (>1 m^2) erosional events. Depositional areas were excluded in order to measure face erosion and toe erosion separately, while minimizing the possibility of double-counting material. For large toe erosion events occurring over multiple days during a flood, we indicated small toe erosion events during the rising and falling limb flows and assigned the large toe erosion event to the date of the flood peak. Photographs from before and after each erosional event were imported to ArcMap 10.4 and erosional areas were digitized as shapefiles for the largest 347 events on record. For scale, we also digitized 1 to 4 orange rebar caps in each photograph. We used the average number of pixels per cap at each site and the measured rebar cap size ($2.64\ x\ 10^{-3}\ m^2$) to estimate the average size of bluff failures ($\overline{n} = 46\ caps/site$). Areas of bluff face erosion were converted to volumes of change using the previously described power-law, volume ~ area relation. Volumes of change were subsequently scaled by measured bluff area to calculate a spatially averaged (per 1 m x 1 m) bluff face retreat rate (m/day). Given the sum of all large events at each site we also calculated an average annual retreat rate for the period June 2015 – May 2017.

We did not extrapolate bluff erosion volumes from areas of change for toe events because fluvial erosion of the toe occurs by a different set of processes (e.g. plucking, abrasion, dissolution), and volume ~ area scaling of toe erosion was poorly constrained in this study. Given that till erosion rates are likely set by rates of colluvium removal at the bluff toe, it is reasonable to assume that long-term average till and toe retreat rates are equal such that the bluff face slope retreats in parallel through time.

In Appendix B we present an assessment of the general accuracy of the volume ~ area scaling method for estimating bluff face erosion. Figure B1 compares measured areas and volumes of erosion from four SfM surveys at site LS10 that primarily capture bluff face erosion (6/15/2014 - 7/3/2014, 7/3/2014 - 5/9/2015, 5/9/2015 - 7/10/2015, and 10/22/2016 – 5/17/2017) to the sum of timelapse photo estimated face erosion for all events between SfM surveys.

2.3.4. Identifying Geomorphically Effective Flows

In order to identify geomorphically effective flows (Doyle et al., 2007; Wolman and Miller, 1960) for bluff retreat we calculated the exceedance probability and average runoff depth for mean daily flow values, then related daily flow values to each failure based on the failure observation date. For each bluff site, we calculated mean daily discharge exceedance probabilities based on a 10-year record: October 1, 2007 – September 30, 2017. For each site, we referenced the nearest streamflow gage on the respective river, as discussed in Appendix B. Appendix B also presents Log-Pearson III flood frequency analysis for a longer gage record, 1980 – 2016, for the Le Sueur River near Rapidan, MN (USGS 5320500) gage (Figure B5). Some results are discussed in relation to this gage in Section 4.

3. Results

Section 3.1 summarizes bluff failures observed in timelapse photos and discusses mechanisms of failure. Section 3.2 details measured bluff erosion volumes, retreat distances, and retreat rates obtained from repeat Structure-from-Motion surveys. The bluff erosion volume and area scaling relation is presented in Section 3.3. Finally section

3.4 presents daily timelapse bluff erosion results in relation to river streamflow. Results identify geomorphically effective flows for bluff erosion, as well as minimum flows necessary for measureable toe erosion. Overall the results highlight the importance of streamflow and freeze-thaw processes, and furthermore indicate that bluff toe erosion occurs at flows much less than the "bankfull" flow that is typically considered the most geomorphically effective flow defining channel hydraulic geometry. Section 4 discusses these results in the context of using flow reductions to achieve sediment loading reductions in the Minnesota River Basin.

3.1. Daily Photographs Reveal Bluff Erosion Timing, Frequency, and Seasonal Failure Mechanisms

Between June 2015 and May 2017 we observed 2705 failures, of which 347 were classified as large (>1 m^2). Of the 347 large events, 169 were large face events. Considering all failures, the greatest frequency of failures occurred in March when failures occur nearly half of all days (Figure 3-2a). Based only on frequency of occurrence, bluff failures peak seasonally during early spring months, February – May (Figure 3-2a), coinciding with diurnal freeze-thaw cycles, snowmelt and ice break up floods, and late spring thaw driven by consecutive above-freezing temperature days.

The frequency of large failure events followed a different seasonal pattern compared with all failures (Figure 3-2a, 3-2b). For example, large failures were most frequently observed in September, not March. This result is explained almost entirely by a single extreme flood event (25 year return period) that occurred in late September 2016. The impact of this event is further discussed in Sections 3.2 and 4. Large failures were also

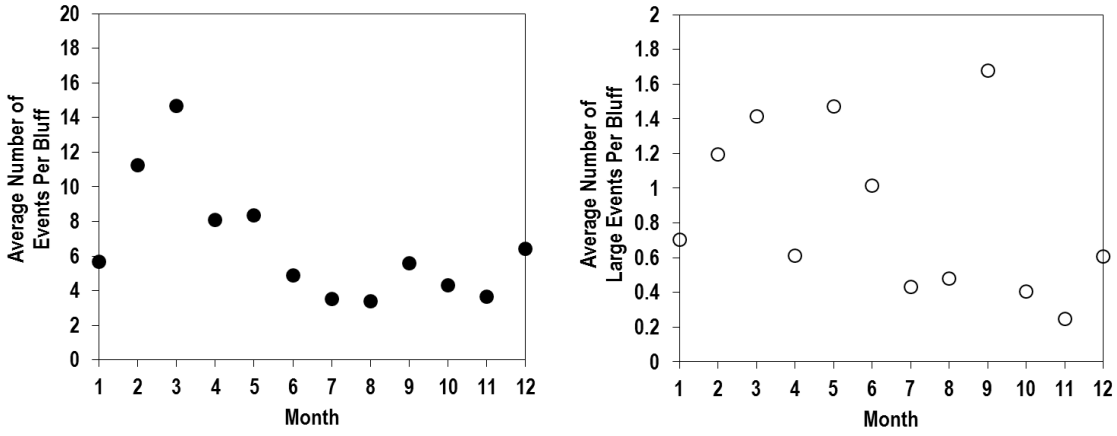

(**a**) (**b**)

Figure 3-2. (**a**) Average number of failure days per month for a bluff of average size 250 m^2 (along stream length x height). Number of observations: 2705; (**b**) Average number days with large failures per month. Number of observations: 347. Months are labeled in order from January (1) to December (12).

common in May and March, when many failures occur in both till and toe material as a result of seasonal spring thaw and snowmelt floods.

The overall pattern of seasonal bluff erosion frequency (Figure 3-2a, 3-2b) was consistent with individual patterns we observed for each of the three rivers on which we monitored bluffs (Appendix B, Figure B2). Slight differences among rivers, for example in the frequency of large events in September for the Le Sueur versus Blue Earth River, can be explained by local storm severity. Flood peaks were higher on the Le Sueur River than the Maple and Blue Earth rivers in September 2016 and consequently bluff erosion was more severe on the Le Sueur River bluffs (Minnesota Department of Natural Resources, 2017).

Despite local variation in streamflow magnitudes and weather patterns, bluff erosion responded in a predictable manner to primary controls, such as normalized streamflow magnitudes (see section 3.4) and aspect. We observed a significant positive regression

relation between bluff aspect, measured in degrees from 180 degrees south, and the frequency of bluff failures for January ($p = 0.0006$, $r^2 = 0.49$, $F = 17.3$) and February ($p = 0.0037$, $r^2 = 0.38$, $F = 11.1$). During these months, generally northern facing bluffs remain snow-covered, while southern facing bluffs experience multiple snowfall and snowmelt events and frequent diurnal freeze thaw cycles based on interpretations from photographs and camera-recorded daytime and nighttime temperatures.

Interestingly, April ($p = 0.0407$, $r^2 = 0.24$, $F = 4.95$) and November ($p = 0.0289$, $r^2 = 0.24$, $F = 5.64$) exhibit weak, slightly significant negative regressions between bluff aspect and frequency of erosion, while March and December exhibit no significant relation ($p>0.05$). It is likely that March and December are transitional months between winter and spring/fall. We did not observe any significant relation between bluff erosion frequency and aspect between May – October, likely because streamflow processes dominate erosion events and freeze-thaw is rare during these months. For further discussion of bluff erosion seasonality, see Appendix B, and Figure B3.

3.2. Structure-from-Motion Measured Bluff Erosion Volumes, Distances, and Rates

Figure 3-3 shows measured bluff erosion volumes and distances calculated from seven repeat Structure-from-Motion surveys at two monitoring sites, LS9 and LS10. For tabular results, reference Appendix B, Table B2. It should be noted that between our initial SfM survey in June 2014 and our final survey in May 2017 two major floods occurred. Based on Log-Pearson Type III analysis of peak flows (1980-2016) at the Le Sueur River gage near Rapidan, MN (USGS 5320500), downstream of all camera sites, the June 2014 and September 2016 floods were equivalent to 13 and 25 year recurrence interval floods, respectively (Appendix B). Not surprisingly, we measured the most

volumetric change for surveys bracketing the September 2016 flood (2220-3510 m^3 net erosion per site), which accounted for 74% (LS9) and 53% (LS10) of the total erosional change measured at each site over the three year study period. Surveys bracketing the June 2014 flood captured the second largest net loss of material (~1080 m^3 net erosion per site). In total, these two events accounted for 97% (LS9) and 79% (LS10) of the net erosion measured over the three year study period.

June 2014 and September 2016 floods caused significant toe erosion at both sites (top left and bottom center panel in Figure 3-3a and 3-3b). Significant face erosion occurred at site LS10 during the June 2014 flood and at site LS9 during the September 2016 flood (Figure 3-3). To provide context for the size of these events, a local resident, who previously relocated her home due to erosion at site LS10, claims to have heard the failure and felt her house shake during the failure triggered on June 18, 2014. Three cameras installed on 4 in x 4 in x 8 ft fence posts buried 4 ft deep on the sand bar opposite bluff LS10 were disconnected from their power source and posts supporting the cameras were significantly slanted towards the floodplain, likely due to the transverse wave generated by the exceptionally large failure event (Figure 3-3). We previously observed a transverse wave at site LS10 following a considerably smaller face failure on June 2, 2014 (Supplemental Material, Video S1).

Daily timelapse photos revealed that toe erosion caused by the June 2014 and September 2016 floods affected both colluvium and in-situ till at the toe of all sites monitored. During, and following these large flood events, a clear pattern of significant face erosion (2-6 m, locally) and toe deposition (2-4 m, locally) was evident at site LS10 and to a lesser extent at site LS9 (Figure 3-3). Site LS9 has a large colluvial fan that has

persisted along the bluff toe since 2010. Much of the erosion at site LS9 occurred along the bluff toe, especially on the upstream side of the colluvial fan (Figure 3-3a). During spring thaw, sub-daily moving earthflows occurred on the upstream side of the colluvial toe (Figure 3-3a). At both sites, little erosion occurred between July 12, 2015 and May 24, 2016, a period of low flow. Based on daily timelapse photos, most of the change during this period occurred in March 2016, coinciding with spring thaw. Still, July 2015 – May 2016 change was an order of magnitude less than the erosion associated with the June 2014 and September 2016 floods (Figure 3-3). Figure 3-3a shows that net deposition occurred on the bluff face at site LS9 between July 2015 and May 2016. Daily timelapse photos revealed erosion of upslope material at this site. Heavily forested, upslope areas were edited out of site LS9 SfM generated point clouds because dense vegetation introduces too much uncertainty to accurately measure change. Therefore, it is reasonable to end up with net deposition at site LS9 if sandy upslope material is eroded and deposited on the bluff colluvial toe.

By contrast, net deposition measured at site LS10 during relatively low flow period, October 2016 and May 2017, is likely due to differences in bulk density between in-situ till and toe colluvium (Figure 3-3b). Toe colluvium necessarily has a lower bulk density compared to in situ, overly consolidated till due to macropores between blocks of failed till. Additionally, the September 2016 flood undercut the bluff toe with irregularity, which may have left open spaces between the in-situ till and the colluvial apron that could not feasibly be measured in the field. Both of these mechanisms would bias our GCD results in the direction of a small apparent volumetric gain despite conservation of mass. Day et al. 2013a found some sites with apparent net deposition between 2007 and

2009, when peak annual flows were modest (< 2 year recurrence interval), though the cause of this apparent volumetric gain is not explicitly discussed.

Deposits of toe colluvium generally persist for short time periods (discussed in section 3.4), and net erosion was predominant throughout the entire study period. Spatially-averaged bluff retreat rates for sites LS9 and LS10 were 1.10 m/yr and 1.28 m/yr, respectively, per 1 m tall x 1 m along stream bluff surface area. Withholding the exceptionally high rates measured between June 15, 2014 and July 3, 2014 surveys, which bracket the 13 year recurrence interval flood by less than three weeks, measured annual rates are closer to 0.58 m/year. An even more conservative estimate, ignoring erosion caused by the September 2016 flood, puts average, quasi-background retreat rates at approximately 0.28 m/yr. Given all survey SfM data collected between 2014 and 2017, sites LS9 and LS10 eroded on average 1.19 m/yr.

3.3. SfM- and TLS-Derived Geometry Relations for Estimating Bluff Erosion from Daily Photographs

Based on SfM survey results (Appendix B, Table B2) and previously collected TLS surveys from Appendix B of Day et al. 2013a, we developed a bluff erosion volume ~ area power law scaling relation:

$$V = \alpha A^{\gamma} \quad , \tag{1}$$

where the volume of the failure, V, is a function of the failure area, A, a scaling exponent, γ, and intercept, α. Figure 3-4 presents the volume ~ area relation between net survey erosion volume and bluff survey area using data from this study and Day et al. 2013a (Figure 3-4a) as well as between the locally measured erosion volume and area (i.e., the footprint of the failures themselves, Figure 3-4b). Day et al. 2013a only report net change

and did not parse out erosion specifically in their results. Therefore, we did not want to assume that we could use the Day et al. 2013a data (Figure 3-4a) to create a volume ~ area scaling relation to convert our timelapse photo measurements of erosional areas to erosional volumes. Instead, we used the volume ~ area scaling relation constrained by our SfM measurements of erosion only, where $\gamma = 1.4$ and $\alpha = 0.12$ (Figure 3-4b).

Although the scaling relations shown in Figure 3-4 were developed using different data sets, it turns out that both indicate a similar scaling exponent, γ, between 1.37-1.40. This is remarkable given that Figure 3-4a accounts for net erosion (erosion and deposition) and is spatially averaged across the entire bluff face and toe, while Figure 3-4b only accounts for areas of erosion of face material, or till. Similarity between gamma values suggests that deposition is essentially a negligible component of the overall signal, which is entirely consistent with our qualitative observations that erosion predominates bluff change. Virtually none of the sediment that eroded during our study was stored throughout the study period.

Observations at sites LS9 and LS10 covered a narrow range of areas, but fit well within the variability observed by Day et al. 2013a (Figure 3-4a). Thus, good agreement between the scaling exponents, regardless of the data used to build Figures 3-4a and 3-4b, suggests that we have likely covered enough local variability in erosion to apply the erosion scaling relation (Figure 3-4b) to areas of erosion measured from timelapse photos beyond sites LS9 and LS10. After scaling up the timelapse photo survey areas to those surveyed using SfM, there is reasonable agreement between SfM measured erosion and cumulative timelapse photo measured erosion for events that mostly affected the bluff

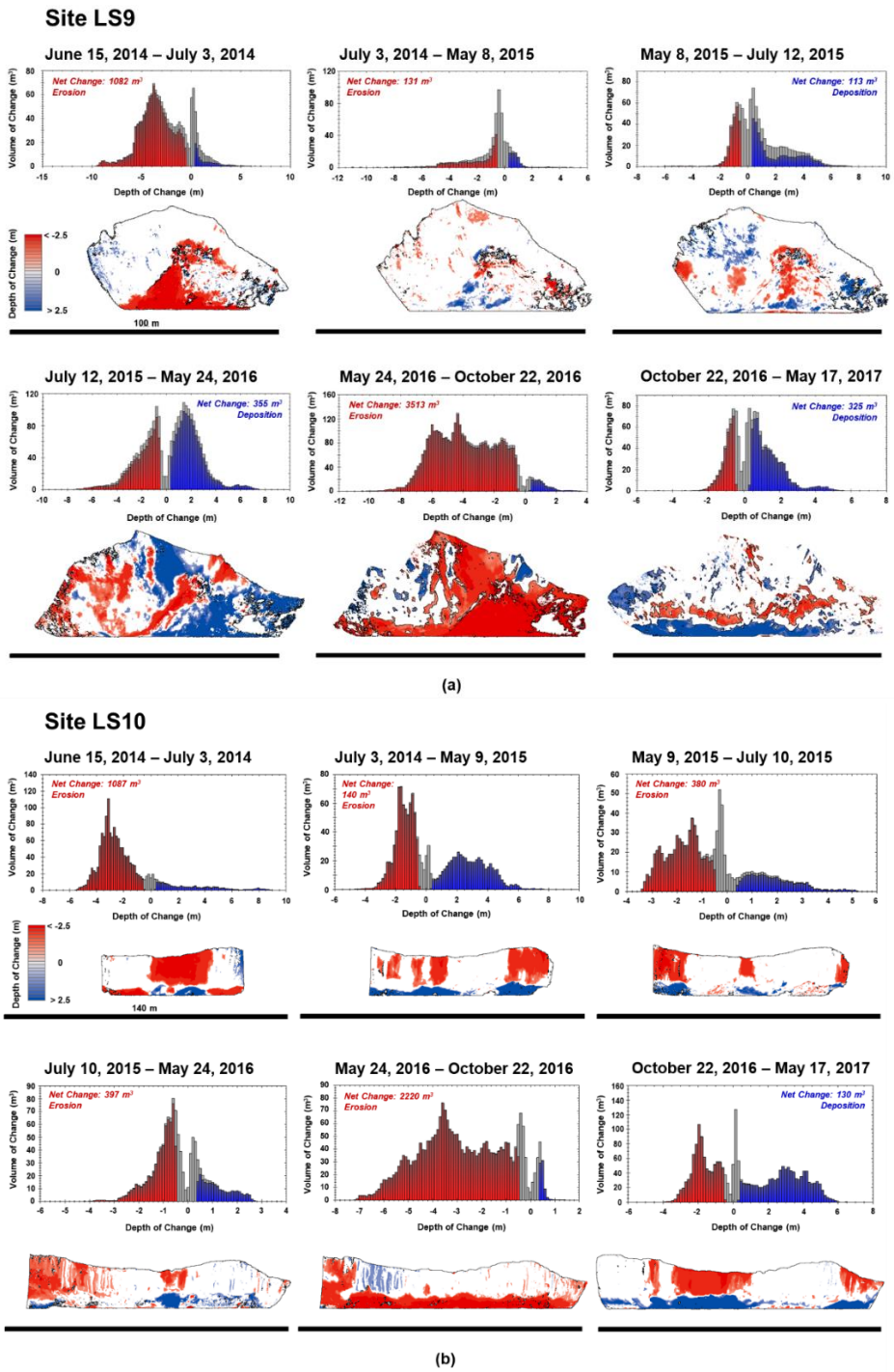

Figure 3-3. Panels of change from seven repeat Structure from Motion survey generated DEMs of difference (below) and distributions of volumetric change (m^3) as a function of depth of change (m) (above) for site LS9 **(a)** and LS10 **(b)**; outputs from ArcMap 10.4, Geomorphic Change Detection software 5.0. All survey areas are plotted relative to the same black bar indicating approximately the maximum length of each bluff surveyed. Bluff geomorphic change surveys shown perpendicular to the streamwise direction; flow direction from left to right for site LS9, and right to left for site LS10.

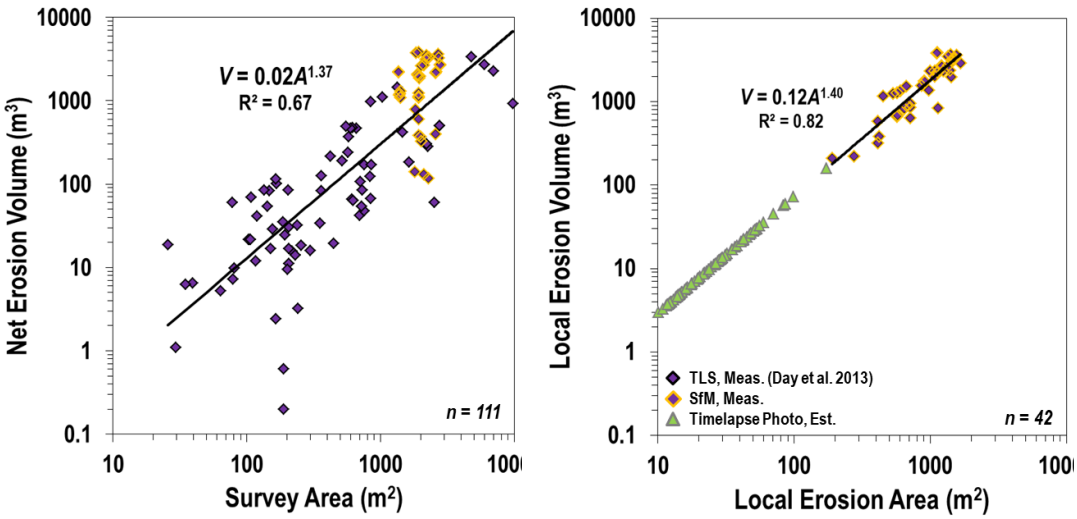

(**a**) (**b**)

Figure 3-4. (**a**) Bluff retreat scaling relation (black line) between net bluff erosion volume (*V*) and bluff survey area (*A*) from repeat SfM surveys and Day et al. 2013a TLS surveys, 111 total observations. (**b**) Local scaling relation between measured total bluff erosion volume (*V*) and bluff erosion survey area (*A*) from repeat SfM surveys, 42 total observations. Data represented by green triangles were estimated using the locally measured erosion relation.

face during SfM survey intervals (Appendix B, Figure B1). Estimated (from timelapse photos) and measured (from repeat SfM surveys) erosion rates are within the same order of magnitude. Further, estimated volumes are robust to digitization error (one standard deviation) of photo-estimated areas. Overall, we feel the scaling relation developed in this study is robust enough to estimate bluff erosion from areas of digitized erosion in order to determine the magnitude of geomorphically effective flows, presented in section 3.4.

3.4. Geomorpically Effective Flows for Bluff Erosion

Due to the short timescale of this study (June 2015 – May 2017) and the fact that we happened to capture an extreme flow event in September 2016, the erosion caused by the largest flood was much greater than anything measured in absence of this flood (Table

B2). However, because an event of the magnitude of the 2016 flood occurs so infrequently (25 year return period), over long timescales, small floods (1-2 year return period) may in fact be more geomorphically effective. To begin to evaluate that hypothesis, we identified threshold flows for bluff toe and till erosion and examined the persistence of failed material.

Figure 3-5 shows the distribution of large bluff failures (separated by toe and face events) in relation to flow duration exceedance probabilities. There is a clear threshold for measureable (>1 m^2) bluff toe erosion at 15% exceedance probability flows (1.3 – 2 mm/day of basin runoff). Not surprisingly, bluff face erosion has a much wider distribution because face erosion events, a) may be directly related to oversteepening that occurs during toe erosion events, but are delayed in time, and b) may be triggered by processes that are not directly related to streamflow, such as changes in matric suction or pore pressures as well as freeze thaw. That said, the fact that the vast majority of large face erosion events occur when flows are below 30% exceedance probability (> 1 mm/day basin runoff) suggests that many face erosion events are triggered before, during, or after toe erosion events (Appendix B, Figure B4).

Based on the volume ~ area relation presented in Figure 3-4b, we calculated average bluff retreat rates (m/day) for face events and plotted retreat rates, event frequency, and total retreat against month (Figure 3-6a). Figure 3-6b shows large bluff failure frequency, event magnitude, and total retreat as a function of daily flow exceedance probabilities. Peaks in total retreat in March, June, and September in Figure 3-6a underscore the geomorphic importance of the September 2016 and June 2014 floods, as well as freeze-thaw, echoing the results of Section 3.2.

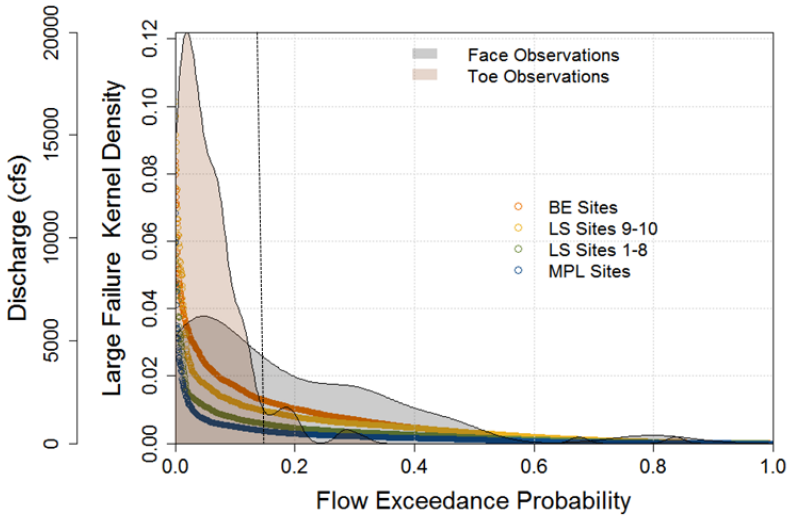

Figure 3-5. Distributions of large toe and face failures plotted as kernel density functions of flow exceedance probabilities. Dashed vertical line indicates 15% exceedance probability flows. Behind the kernel density functions, four flow duration curves are plotted, corresponding to gages for each of the bluff sites (described in Section 2.3.4); BE: Blue Earth River sites, LS: Le Sueur River sties, MPL: Maple River sties.

Daily photographs allowed us to differentiate between toe and face events. Therefore we could measure the persistence time of failed face material once it became toe alluvium. In general, face retreat rates measured at this daily or event timescale show greater retreat during lower exceedance probability flows (Figure 3-7a). This is especially true for events that persist for short amounts of time.

In general (95% of observations) face material does not persist as toe colluvium for longer than six months (Figure 3-7b). This is yet another line of evidence indicating that bluff erosion responds even to modest floods (less than 1 year recurrence interval). Face material that persists for the shortest amount of time (one day to one week) is generally small in size and/or coincides with larger flow events (Figure 3-7a, 3-7b).

Figure 3-7c also shows a positive power-law relation between bluff retreat rate and daily runoff depth (daily discharge volume normalized by basin area). This relation is

stronger if we only include face events that occurred above a threshold discharge of 1 mm/day or <30% exceedance probability (Figure 3-7d), and stronger still when only examining the material that persisted from one day to one week (Figure 3-7e). Interestingly, the material that did not persist (i.e., failed face material that only persisted as toe material for very short periods of time), clusters at discharges near or above the 1 mm/day threshold.

Based on the power law relation between daily runoff depth (Q, mm/day) and timelapse photo estimated bluff erosion rate (E, m/day) developed in Figure 3-7d:

$$E = \alpha Q^{\gamma}, \quad (2)$$

as well as the frequency of daily flow events, we calculated the magnitude x frequency product in order to identify geomorphically effective flows for the periods, June 2014 – May 2017 and January 1940 – December 2017 (Figure 3-8). Diamonds in Figure 3-8 indicate the product of magnitude and frequency with the large diamond representing the highest value computed. Several insights emerge from Figure 3-8.

Figure 3-8a suggests that the 1.3 year return period flow (1.9 mm/day) is the most geomorphically effective based on flow frequency and bluff erosion magnitude during the period 2014 - 2017. However, the flow frequency data is noisy during the short record, 2014 – 2017. The 1.2 year return interval flow (1.5 mm/day) produced on average 6.9 cm/year of erosion while the 1.3 year return interval flood accomplished on average 7.8 cm/year of bluff face erosion. These low flow magnitudes correspond well with the previously identified minimum measureable flows for bluff toe erosion, or 15% exceedance probability flows (equivalent to 1.5 mm/day at the Le Sueur River gage near Rapidan, MN (USGS 5320500).

The 1.2 year recurrence interval flood (1.5 mm/day) appears to have been the most geomorphically effective flood for bluff erosion in the Greater Blue Earth River basin during the period 1940 – 2017 (Figure 3-8b). The product of runoff event frequency and bluff erosion magnitude is mostly driven by event frequency, which mostly declines with increasing runoff. Bluff erosion magnitude increases, but at a slower rate when discharge increases according to the power law exponent 0.67. When event frequency is constant, the product follows the same non-linear increase as the bluff erosion magnitude curve (Figure 3-8).

4. Discussion

4.1. Bluff Failure Timing, Frequency, and Seasonality

Based on frequency of events, March is an especially active time of year for bluff erosion, when bluffs erode nearly half of all days (Figure 3-2a). These events occur from a combination of sub-aerial and fluvial processes, including freeze-thaw and ice break up floods (Figure B3). Overall, soil moisture is high and temperatures are transitioning towards mostly positive degree days (Figure B3). Despite major post-winter activity during spring thaw, events in March are generally small (Figure 3-2b; Figure 3-6a). Therefore, the greatest occurrence of large failures was in September (Figure 3-2b; Figure 3-6a), and the most total erosion occurred during September (Figure 3-6a). A 25-year recurrence interval flood occurred in September 2016. In absence of large floods, the relative importance of winter freeze-thaw and spring snowmelt on bluff erosion increases. These insights were made possible through an immense amount of manual digitization on

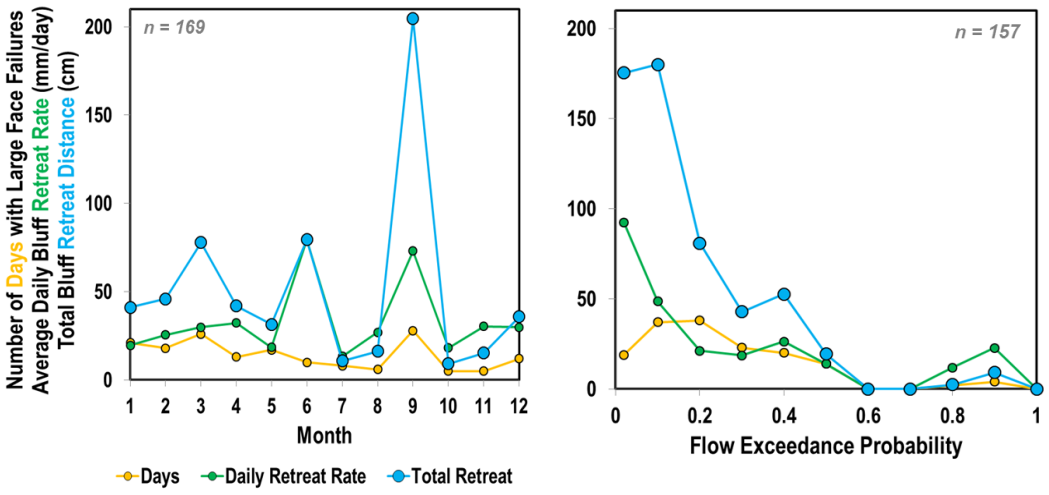

(**a**) (**b**)

Figure 3-6. (**a**) Large face failure frequency (total number of days per month), average daily retreat rate for a 250 ± 95 m^2 bluff in a given month, and their product, total bluff retreat, measured across 20 timelapse photo monitored sites, 169 total observations. (**b**) Same data as 6a, only plotted against daily flow exceedance probability. Data binned every 10 percentile except percentiles binned 0 – 2 and 2 – 10. Data binned as 0 – 0.02 exceedance probability only include June 2014 and September 2016 flood peaks, when 12% of all large failures occurred. Total bluff face erosion during the two flood peaks account for 45% of all face erosion from June 2014 – May 2017. Data represented by one hundred fifty seven total observations since 12 large face failures occurred when daily flow data were unavailable due to winter ice affected gages.

time-lapse photographs. Given the value of this information, it would be beneficial for future studies to develop image processing workflows to automate the process of identifying and quantifying failures.

4.2. Measured Bluff Erosion

Structure from Motion measured bluff erosion rates (1.19 m/yr) were much higher than those measured by Day et al. 2013a (0.20 m/yr) – based on repeat TLS surveys (2007-2010) at 15 sites along the Le Sueur, Maple, and Big Cobb rivers. Day et al. 2013a measured bluff change immediately following a 12 year recurrence interval flood in

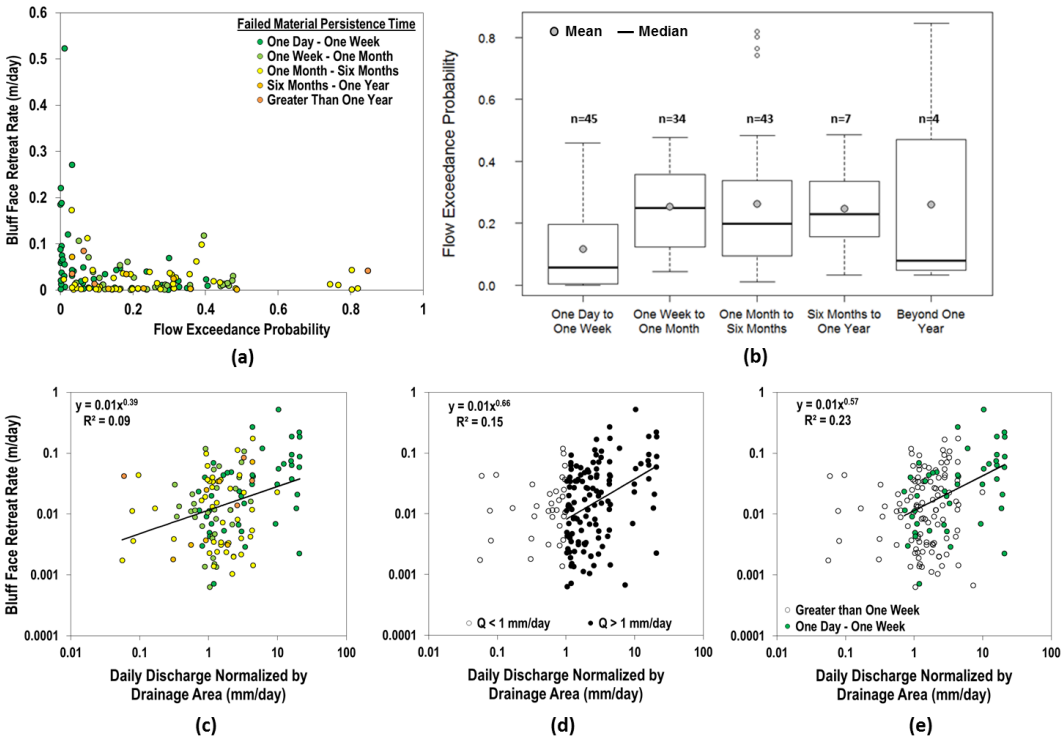

Figure 3-7. (**a**) Spatially averaged event retreat rate (m/day) from timelapse photo estimated erosion versus the failure date flow exceedance probability. Points are color coded by the persistence time of the failed till material; (**b**) Box and whiskers (25% and 75%) plots of flow exceedance probabilities associated with categorical failed till persistence times. Black bar and grey circle indicate median and mean descriptive statistics, respectively, and n indicates the number of observations in each category; **(c)** Till event retreat rate versus daily discharge normalized by drainage area upstream of gauge. Line indicates a weak power law relation between event size and discharge; **(d)** Same as (c), but regression applied only to events when daily discharge was greater than 1 mm/day; **(e)** Same as (c), but regression applied only to events that persisted for less than one week.

March 2010. However, they captured that event at the end of their study period and therefore may have missed subsequent failures that occurred due to instabilities or oversteepening as a result of that event. In contrast, we captured a 13 year flood event at the beginning of our study period. Based on spatial patterns of bluff erosion at site LS10, extensive face erosion occurred during the two years following the June 2014 flood (Figure 3-3b). Had Day et al. 2013a continued to measure erosion in the years following

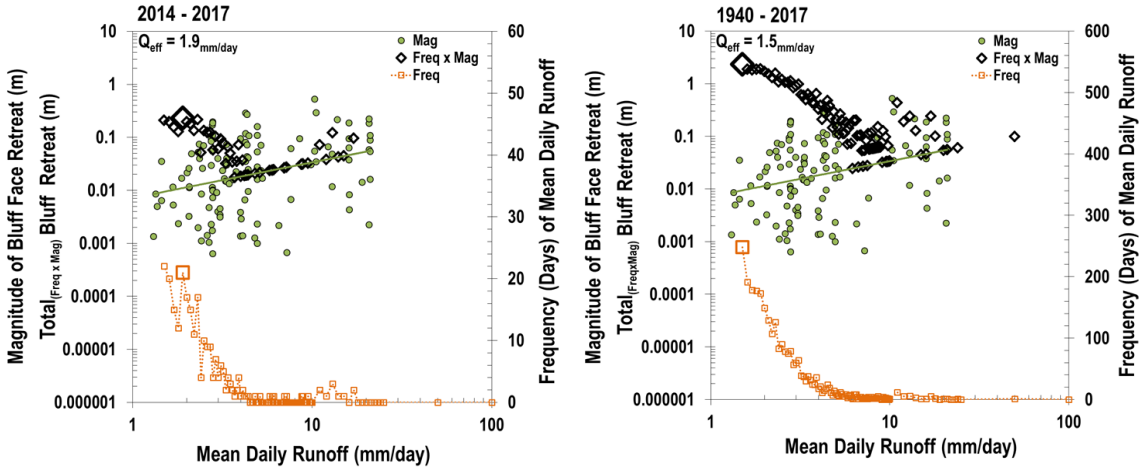

(a) **(b)**

Figure 3-8. Streamflow frequency, days greater than 1.5 mm/day runoff (orange); bluff erosion magnitude, given the bluff erosion (E) ~ discharge (Q) power law relation $E = 0.01Q^{0.67}$ (green line fitted through green points); and the product of bluff erosion magnitude and streamflow frequency versus river basin runoff (mm/day), during the periods **(a)** 2014 – 2017 and **(b)** 1940 – 2017. Mean daily runoff values for the Le Sueur River gage near Rapidan, MN (USGS 5320500).

the March 2010 flood, perhaps their bluff erosion rates would have been higher, as toe erosion caused by large floods seems to perpetuate erosion of the bluff face, even long after flood peaks have receded.

4.3. Generalizability of our volume ~ area scaling relation

Measured bluff erosion exhibited a clear volume ~ area scaling relation and this relation was consistent between SfM and TLS (Day et al., 2013b) measured erosion, despite differences in areal extents and net erosion vs erosion and deposition (Figure 3-4a; Figure 3-4b). Remarkably, an extensive analysis of 4,231 individual landslide geometries conducted by Larsen et al. 2010 found γ=1.1-1.3 for soil-based and γ=1.3-1.6 for bedrock landslides, suggesting that γ is a property of the landslide material. The well

consolidated till material in our study sites falls at the low end of bedrock in terms of mechanical properties, so an exponent of 1.4 is entirely consistent with the Larsen et al., 2010 scaling relation.

4.4. Geomorpically Effective Flows for Bluff Erosion

The Greater Blue Earth River basin makes up about 21% of the MRB watershed area and contains about 25% of the bluff surface area within the MRB (S. Day, unpublished data). Therefore reducing sediment loading in the GBER basin could have a substantial effect on sediment loading in the entire MRB. It is clear from our results that flow exerts a primary control on bluff erosion, with abrasion and scouring of the bluff toe causing oversteepening and eventual failure of the bluff face. Moderately high flows (1 – 2 mm/day) appear sufficiently capable of removing colluvial material deposited at the toe of the bluff. One of the primary sediment reduction strategies being considered in Minnesota involves reducing high flows via installation of water retention structures. Therefore, it is essential to understand which flows cause the most bluff erosion over time, considering both frequency and magnitude.

During our study period, the flow that caused the most erosion (based on SfM and timelapse photo results) was the September 2016, 25 year recurrence interval flood. Over long periods of time, this flood should be rare. At the lower end of geomorphically effective flows, we found flows less than 15% exceedance probabilities are effective at eroding bluff toe colluvium and in-situ till. Fifteen percent exceedance probability is equivalent to 1 – 2 mm/day of runoff at each watershed outlet in the Greater Blue Earth River watershed. This flow threshold agrees well with a 1 mm/day threshold identified for erosion of near channel sediment sources by Cho (Cho, 2017).

We found that the 1.2 year recurrence interval flood should have been the most geomorphically effective flow during the period 1940 – 2017. However, the traditional Wolman and Miller type event frequency x response magnitude approach may underestimate the importance of very large events, which affect the geomorphic response long after the flood peak. To explore this idea further we discuss the sensitivity of the "geomorphically effective" flow to the erosion power law scaling relation exponent, γ.

Although it may seem reasonable to have identified the 1.2 year return interval flood as the most geomorphically effective flood during the period 1940 – 2017, it is harder to reconcile the 1.3 year flood being the most geomorphically effective during the period 2014 – 2017, given our daily timelapse and repeat SfM surveys. There are two reasons that likely explain why we found the 1.3 year return interval flood as the most geomorphically effective flow instead of the 13 or 25 year return interval floods. First, the 13 and 25 year floods also produce several days of lower magnitude flows, such as the 1.2 or 1.3 year flow, and very few days of substantially higher magnitude flows. Therefore, the impact of these events is diminished in a traditional Wolman and Miller style, magnitude – frequency approach. Second, the Q estimated bluff erosion approach likely underestimates the impact of large floods, as we only estimated bluff face erosion from timelapse photos and excluded bluff toe erosion, in volumetric terms, from our empirical data fit to equation 2. Additional material removed during floods from fluvial scour and abrasion of glacial in-situ till and failed colluvium below the water level is likely underestimating the impact of large flood events. Therefore, the exponent on the power-law relation presented in Figure 3-7d (0.67) may in fact be higher due to

underestimated erosion totals during large floods. If the exponent is greater than 1, the importance of and implications for managing large food events become even greater.

Using the magnitude of the 1.2 year recurrence interval flow (1980 – 2016) on the Le Sueur River near Rapidan, MN (USGS gage 5320500), we found the average occurrence (58 days/year) of this magnitude event during the period June 2014 – May 2017 (Appendix B, Figure B6). By comparison, there were 20 and 45 days per year exceeding 1.2 year return interval flood during the periods 1940 – 1979 and 1980 – 2017, respectively (Figure B6). In general, reducing the number of days each year with flows meeting or exceeding the 1.2 year recurrence interval flow should reduce annual loading from bluff erosion (Figure 3-8b). Future work should investigate tradeoffs between event frequency and magnitude, and additionally try to constrain bluff toe erosion as a function of discharge to inform sediment management strategies within the Minnesota River Basin.

5. Conclusions

Results of measured Structure-from-Motion photogrammetry and estimated timelapse photo bluff erosion rates lead us to several conclusions:

- Fluvial erosion was much more important than freeze-thaw and other sub-aerial processes during our study period, 2014 -2017. The 13- and 25-year flood events caused 79% - 97% of the total erosion measured at two bluff sites on the Le Sueur River. Fluvial erosion is also the dominant long-term process driving bluff erosion, as toe colluvium must be removed by flows in order to continue bluff face erosion. In this way, the process of bluff erosion is very similar to landslide erosion, in which erosion rates are controlled by fluvial incision and uplift rates (Larsen et al., 2010).

- Freeze – thaw and spring snowmelt influence bluff erosion rates between November and April. These processes exert greater influence on annual bluff erosion rates during low flow years. It is uncertain how climate change may amplify or dampen the importance of freeze – thaw processes in the Midwest USA, presenting opportunities for future researchers to expand upon frontiers in hillslope and fluvial geomorphology.
- Bluff erosion follows a power-law volume ~ area scaling relation with an exponent of 1.4, which is consistent with volume ~ area scaling found by Larsen et al. 2010 for landslides in weak bedrock (Larsen et al., 2010).
- We captured two very large floods during a relatively short study period and thus measured 5.5 x higher rates of annual bluff erosion than Day et al. 2013a and 2013b.
- Modest, 15% exceedance probability, floods (30% of the 2 year recurrence interval flow), are capable of inducing bluff erosion.
- Considering only the relatively short period of time that we directly monitored bluff erosion, we found that the vast amount of geomorphic work was done by the 13- and 25-year recurrence interval flows.
- Using daily runoff frequency, estimated bluff face erosion magnitude, and their product as a function of daily runoff, the most “geomorphically effective” flow for bluff erosion from 1940 – 2017 was the 1.5 mm/day or 1.2 year recurrence interval flood. Coincidently, this is the minimum flow necessary for measureable toe erosion, though future work should better constrain bluff toe erosion as a function of discharge.

Several major tributaries of the Minnesota River basin are responding to human and climate driven flow increases, as well as glacial legacy impacts by increasing river width, which recruits fine sediment from till deposits along the river valley margin. Bluffs will continue to erode, even if current hydrologic conditions do not change, until the channel geometry comes into equilibrium with the flow regime. If geomorphically effective peak flow magnitudes and/or their occurrence continue to increase, as they have in many river basins of the Midwest, USA during the late 20th and early 21st centuries, then managing erosion of near channel sediment sources may only become more challenging in the future. Sediment-targeted management strategies in the Greater Blue Earth River basin and other MRB tributary basins should explicitly account for tradeoffs between streamflow timing, frequency, and magnitude, as well as the effects of freeze-thaw and flood events (which are often underrepresented) on overall bluff erosion under future human and climate scenarios.

References

1. Wilkinson, B. H.; McElroy, B. J. The impact of humans on continental erosion and sedimentation. Bull. Geol. Soc. Am. 2007, 119, 140–156, doi:10.1130/B25899.1.

2. Montgomery, D. R. Is agriculture eroding civilization's foundation? GSA Today 2007, 17, 4–9, doi:10.1130/GSAT01710A.1.

3. Hooke, R. L. On the history of human as geomorphic agent. Geology 2000, 28, 843–846, doi:10.1130/0091-7613(2000)28<843.

4. Wilkinson, B. H. Humans as geologic agents: A deep-time perspective. Geology 2005, 33, 161–164, doi:10.1130/G21108.1.

5. Syvitski, J. P. M.; Vörösmarty, C. J.; Kettner, A. J.; Green, P. Impact of humans on the flux of terrestrial sediment to the global coastal ocean. Science 2005, 308, 376–380, doi:10.1126/science.1109454.

6. Owens, P. N.; Batalla, R. J.; Collins, A. J.; Gomez, B.; Hicks, D. M.; Horowitz, A. J.; Kondolf, G. M.; Marden, M.; Page, M. J.; Peacock, D. H.; Petticrew, E. L.; Salomons, W.; Trustrum, N. A. Fine-grained sediment in river systems: environmental significance and management issues. River Res. Appl. 2005, 21, 693–717, doi:10.1002/rra.878.

7. Belmont, P.; Gran, K. B.; Schottler, S. P.; Wilcock, P. R.; Day, S. S.; Jennings, C.; Lauer, J. W.; Viparelli, E.; Willenbring, J. K.; Engstrom, D. R.; Parker, G. Large shift in source of fine sediment in the upper Mississippi River. Environ. Sci. Technol. 2011, 45, 8804–8810, doi:10.1021/es2019109.

8. Dean, D. J.; Schmidt, J. C. The role of feedback mechanisms in historic channel changes of the lower Rio Grande in the Big Bend region. Geomorphology 2011, 126, 333–349, doi:10.1016/j.geomorph.2010.03.009.

9. Schottler, S. P.; Ulrich, J.; Belmont, P.; Moore, R.; Lauer, J. W.; Engstrom, D. R.; Almendinger, J. E. Twentieth century agricultural drainage creates more erosive rivers. Hydrol. Process. 2014, 28, 1951–1961, doi:10.1002/hyp.9738.

10. Lauer, J. W.; Echterling, C.; Lenhart, C.; Belmont, P.; Rausch, R. Air-photo based change in channel width in the Minnesota River basin: Modes of adjustment and implications for sediment budget. Geomorphology 2017, 297, 170–184, doi:https://doi.org/10.1016/j.geomorph.2017.09.005.

11. Kelly, S. A.; Takbiri, Z.; Belmont, P.; Foufoula-Georgiou, E. Human amplified changes in precipitation-runoff patterns in large river basins of the Midwestern United States. Hydrol. Earth Syst. Sci. Discuss. 2017, 1–37, doi:10.5194/hess-2017-133.

12. Nakamura, F.; Seo, J. Il; Akasaka, T.; Swanson, F. J. Large wood, sediment, and flow regimes: Their interactions and temporal changes caused by human impacts in Japan. Geomorphology 2017, 279, 176–187, doi:10.1016/j.geomorph.2016.09.001.

13. Call, B. C.; Belmont, P.; Schmidt, J. C.; Wilcock, P. R. Changes in floodplain inundation under nonstationary hydrology for an adjustable, alluvial river channel. Water Resour. Res. 2017, 53, 3811–3834, doi:10.1002/2016WR020277.

14. Walling, D. E.; Owens, P. N.; Carter, J.; Leeks, G. J. L.; Lewis, S.; Meharg, A. A.; Wright, J. Storage of sediment-associated nutrients and contaminants in river channel and floodplain systems. Appl. Geochemistry 2003, 18, 195–220, doi:10.1016/S0883-2927(02)00121-X.

15. Peck, M.; Gibson, R. W.; Kortenkamp, A.; Hill, E. M. Sediments Are Major Sinks of Steroidal Estrogens in Two United Kingdom Rivers. Environ. Toxicol. Chem. 2004, 23, 945, doi:10.1897/03-41.

16. Perks, M. T.; Owen, G. J.; Benskin, C. M. W. H.; Jonczyk, J.; Deasy, C.; Burke, S.; Reaney, S. M.; Haygarth, P. M. Dominant mechanisms for the delivery of fine sediment and phosphorus to fluvial networks draining grassland dominated headwater catchments. Sci. Total Environ. 2015, 523, 178–190, doi:10.1016/j.scitotenv.2015.03.008.

17. Wood, P.; Armitage, P. Biological Effects of Fine Sediment in the Lotic Environment. Environ. Manage. 1997, 21, 203–17, doi:10.1007/s002679900019.

18. Bilotta, G. S.; Brazier, R. E. Understanding the influence of suspended solids on water quality and aquatic biota. Water Res. 2008, 42, 2849–2861, doi:10.1016/j.watres.2008.03.018.

19. Bennett, E. M.; Carpenter, S. R.; Caraco, N. F. Human Impact on Erodable Phosphorus and Eutrophication: A Global Perspective. Bioscience 2001, 51, 227, doi:10.1641/0006-3568(2001)051[0227:HIOEPA]2.0.CO;2.

20. USEPA (United States Environmental Protection Agency) National Water Quality Inventory: Report to Congress. EPA 841-R-16-011 2017, 30.

21. Belmont, P.; Foufoula-Georgiou, E. Solving water quality problems in agricultural landscapes: New approaches for these nonlinear, multiprocess, multiscale systems. Water Resour. Res. 2017, 53, 2585–2590, doi:10.1002/2017WR020839.

22. Burt, T. P.; Allison, R. J. Sediment Cascades: An Integrated Approach. Sediment Cascades An Integr. Approach 2009, 1–471, doi:10.1002/9780470682876.

23. Smith, S. M. C.; Belmont, P.; Wilcock, P. R. Closing the Gap Between Watershed Modeling, Sediment Budgeting, and Stream Restoration. In Stream Restoration in Dynamic Fluvial Systems: Scientific Approaches, Analyses, and Tools; Simon, A., Bennett, S., JM, C., Eds.; AGU: Washington, DC, 2011; pp. 293–317.

24. Kelley, D. W.; Brachfeld, S. A.; Nater, E. A.; Wright, H. E. Sources of sediment in Lake Pepin on the Upper Mississippi River in response to Holocene climatic changes. J. Paleolimnol. 2006, 35, 193–206, doi:10.1007/s10933-005-8686-x.

25. Kelley, D. W.; Nater, E. A. Source apportionment of lake bed sediments to watersheds in an Upper Mississippi basin using a chemical mass balance method. Rivers 2000, 277–292.

26. Wilcock, P. Identifying sediment sources in the Minnesota River Basin. Minnesota River Sediment Colloq. 2009, 16.

27. Gunderson, L.; Finley, R.; Bourne, H.; Lofton, D. Sediment reduction strategy for

the Minnesota River basin and South Metro Mississippi River: Establishing a foundation for local watershed planning to reach sediment TMDL goals; Saint Paul, MN, 2014;

28. Gran, K.; Belmont, P.; Bevis, M.; Cho, S. J.; Heitkamp, B.; Hobbs, B.; Marr, J.; Mielke, S.; Mitchell, N.; Kumarasamy, K.; Wilcock, P. Collaborative for Sediment Source Reduction : Greater Blue Earth River Basin Summary of Findings. Collab. Sediment Source Reduct. 2017, 1–4.

29. Vaughan, A. A.; Belmont, P.; Hawkins, C. P.; Wilcock, P. Near-Channel Versus Watershed Controls on Sediment Rating Curves. J. Geophys. Res. Earth Surf. 2017, 122, 1901–1923, doi:10.1002/2016JF004180.

30. Cho, S. J. Development of data-driven, reduced-complexity watershed simulation models to address agricultural non-point source sediment pollution in southern Minnesota, Johns Hopkins University, PhD Dissertation, 2017.

31. Ellison, C. A.; Savage, B. E.; Johnson, G. D. Suspended-sediment concentrations, loads, total suspended solids, turbidity, and particle-size fractions for selected rivers in Minnesota, 2007 through 2011. U.S. Geol. Surv. Sci. Investig. Rep. 2014, 5205, 43.

32. Day, S. S.; Gran, K. B.; Belmont, P.; Wawrzyniec, T. Measuring bluff erosion part 2: Pairing aerial photographs and terrestrial laser scanning to create a watershed scale sediment budget. Earth Surf. Process. Landforms 2013, 38, 1068–1082, doi:10.1002/esp.3359.

33. Day, S. S.; Gran, K. B.; Belmont, P.; Wawrzyniec, T. Measuring bluff erosion part 1: Terrestrial laser scanning methods for change detection. Earth Surf. Process. Landforms 2013, 38, 1055–1067, doi:10.1002/esp.3353.

34. Wolman, M. G.; Miller, J. P. Magnitude and Frequency of Forces in Geomorphic Processes. J. Geol. 1960, 1, 54–74.

35. Runkel, A. C.; Meyer, G. N.; Lusardi, B. A. C-26 Geologic Atlas of Blue Earth County, Minnesota [Part A]. Minnesota Geol. Surv. Cty. Atlas Ser. [44] 2011.

36. Gran, K. B.; Belmont, P.; Day, S. S.; Finnegan, N.; Jennings, C.; Lauer, J. W.; Wilcock, P. R. Landscape evolution in south-central Minnesota and the role of geomorphic history on modern erosional processes. GSA Today 2011, 21, 7–9, doi:10.1130/G121A.1.

37. Gran, K. B.; Belmont, P.; Day, S. S.; Jennings, C.; Johnson, A.; Perg, L.; Wilcock, P. R. Geomorphic evolution of the Le Sueur River, Minnesota, USA, and implications for current sediment loading. In Management and Restoration of Fluvial Systems with Broad Historical Changes and Human Impacts: Geological

Society of America Special Paper 451; James, L. A., Rathburn, S. L., Whittecar, G. R., Eds.; 2009; pp. 119–130 ISBN 0072-1077r978-0-8137-2451-5.

38. Schaffrath, K. R.; Belmont, P.; Wheaton, J. M. Landscape-scale geomorphic change detection: Quantifying spatially variable uncertainty and circumventing legacy data issues. Geomorphology 2015, 250, 334–348, doi:10.1016/j.geomorph.2015.09.020.

39. Smith, M. W.; Carrivick, J. L.; Quincey, D. J. Structure from motion photogrammetry in physical geography. Prog. Phys. Geogr. 2015, 40, 247–275, doi:10.1177/0309133315615805.

40. Westoby, M. J.; Brasington, J.; Glasser, N. F.; Hambrey, M. J.; Reynolds, J. M. "Structure- from- Motion" photogrammetry: A low- cost, effective tool for geoscience applications. Geomorphology 2012, 179, 300–314, doi:10.1016/j.geomorph.2012.08.021.

41. Fonstad, M. A.; Dietrich, J. T.; Courville, B. C.; Jensen, J. L.; Carbonneau, P. E. Topographic structure from motion: A new development in photogrammetric measurement. Earth Surf. Process. Landforms 2013, 38, 421–430, doi:10.1002/esp.3366.

42. Carrivick, J. L.; Smith, M. W.; Quincey, D. J. Structure from Motion in the Geosciences; Wiley-Blackwell: Singapore, 2016; ISBN 978-1-118-89584-9.

43. Girardeau-Montaut, D. Cloud Compare—3d point cloud and mesh processing software. Open Source Project. 2015.

44. Brasington, J.; Vericat, D.; Rychkov, I. Modeling river bed morphology, roughness, and surface sedimentology using high resolution terrestrial laser scanning. Water Resour. Res. 2012, 48, doi:10.1029/2012WR012223.

45. Wheaton, J. M.; Brasington, J.; Darby, S. E.; Sear, D. A. Accounting for uncertainty in DEMs from repeat topographic surveys : improved sediment budgets. Earth Surf. Process. Landforms 2010, 35, 136–156, doi:10.1002/esp.1886.

46. Castillo, C.; Pérez, R.; James, M. R.; Quinton, J. N.; Taguas, E. V.; Gómez, J. A. Comparing the Accuracy of Several Field Methods for Measuring Gully Erosion. Soil Sci. Soc. Am. J. 2012, 76, 1319, doi:10.2136/sssaj2011.0390.

47. Larsen, I. J.; Montgomery, D. R.; Korup, O. Landslide erosion controlled by hillslope material. Nat. Geosci. 2010, 3, 247–251, doi:10.1038/ngeo776.

48. N, H.; CP, S.; PA, A. Sediment flux from a mountain belt derived by landsliding mapping. Geology 1997, 25, 231–234, doi:10.1130/0091-

7613(1997)025<0231:SFFAMB>2.3.CO;2.

49. Lavé, J.; Burbank, D. Denudation processes and rates in the Transverse Ranges, southern California: Erosional response of a transitional landscape to external and anthropogenic forcing. J. Geophys. Res. Earth Surf. 2004, 109, doi:10.1029/2003JF000023.

50. Stark, C. P.; Guzzetti, F. Landslide rupture and the probability distribution of mobilized debris volumes. J. Geophys. Res. Earth Surf. 2009, 114, 1–16, doi:10.1029/2008JF001008.

51. Doyle, M. W.; Shields, D.; Boyd, K. F.; Skidmore, P. B.; Dominick, D. Channel-Forming Discharge Selection in River Restoration Design. J. Hydraul. Eng. 2007, 133, 831–837, doi:10.1061/(ASCE)0733-9429(2007)133:7(831).

52. Minnesota Department of Natural Resources September 20-22, 2016 Heavy Rain Available online: http://www.dnr.state.mn.us/climate/journal/160921_22_heavy_rain.html (accessed on Jan 10, 2018).

CHAPTER 4

BEDLOAD SUPPLY AND TRANSPORT CONTROLS ON MORPHODYNAMICS OF A TRANSIENT SAND BED RIVER[3]

Abstract

Rivers are dynamic, self-organized systems that respond readily to changes in water and sediment supply. The Minnesota River, USA has experienced considerable increases in water and sediment supply over the past few decades. Such large changes, in an exceptionally well-monitored river system with distinct process domains, can be viewed as a rare opportunity to study factors controlling channel form and dynamics in a sand bed river. We document a distinct transition in the form and dynamics along the lower 175 kilometers of the river. Specifically, a longitudinal discontinuity in both bed and suspended sediment transport occurs approximately 85 km upstream from the mouth of the river, due to declining slope. Bedload transport diminishes to negligible amounts below the slope break at river km 85. Coincident with decreased bedload transports is an abrupt grain size transition as well as an increase in amplitude and decrease in width of bars. Floodplain characteristics, backwater from the Mississippi River, and lack of bedload supply appear to suppress rates of channel migration and widening in the lowermost 65 km of the Minnesota River. Above the backwater reach the channel migrates and widens faster, especially near tributary junctions, where large inputs of coarse sand and fine gravel provide sufficient bedload for maintaining alternate and point bars. Broad, bedload built, higher roughness alternate bars occur upstream of river

[3]Kelly, S. A., Belmont, P., & Wilcock, P. (in prep). Bedload supply and transport controls on morphodynamics of a transient sand bed river. Geomorphology.

kilometer 85 and appear to be more effective at promoting meander migration than the narrow, suspended-sediment built, low roughness bars like those found in the downstream reach. The results of this study highlight interactions between sediment supply, transport capacity, bar dynamics, and meander migration, and underscore the necessity for a mechanistic understanding of how sediment supply and transport affects river meandering.

1. Introduction

Understanding how and why rivers adjust to changing water and sediment boundary conditions is a fundamental question in geomorphology. Rivers frequently experience changes in water and sediment supply, and in spite of this, often display striking persistence in their morphology. Determining what factors most strongly influence river geomorphology – including form and dynamics – is challenging in natural rivers because river change may be not be directly linked in time or space to changes in climate and/or land use (Burt and Allison, 2010), and sediment transport is a variable and often pulsed process, whereby slugs of sediment containing a range of grain sizes from multiple sources are transported downstream intermittently (Nicholas et al. 1995). Yet understanding what dictates river form and dynamics is often critical for risk management (e.g., flood risk, navigation, and infrastructure safety) and stream restoration.

In this paper, form and morphology both refer to channel cross-sectional geometry (width and depth), river planform (braided, meandering, straight, anastomosing), slope, bed grain size distribution, sinuosity, and/or spatial arrangement and size of topographic features, such as pools and bars. Channel dynamics refers to the

movement of sediment or the channel boundary, including transport of bedload or suspended load, bedform development and migration, meander migration, channel widening or narrowing, and bed aggradation or degradation. Both channel form and dynamics respond to flow and sediment supply drivers.

One factor on which river morphology depends is a balance between transport capacity and sediment supply. This relation was described by Lane (1955) in the following form:

$$Q_s D_s \propto Q_w S \tag{1}$$

where Q_s is sediment discharge, D_s is grain size, Q_w is water discharge, and S is bed slope. A specific relation among these variables was further quantified by Henderson (1966) as:

$$q_s D^{3/2} \propto q S^{1/2} \tag{2}$$

While this proportionality is a useful starting point for predicting aggradation or degradation, it fails to capture the myriad modes by which river channels may adjust morphology or dynamics to balance supply and transport capacity of both water and sediment.

Flow and sediment supply are known to be the primary factors influencing channel morphology (Li et al., 2015; Wilkerson and Parker, 2011). While alluvial morphology and sediment transport have each been studied extensively, links between the two are insufficiently investigated (Church, 2006). Much progress has been made over the last century to better understand river and sediment dynamics, especially through numerical simulations and flume experiments (Best, 1988; Blanckaert, 2010; Call et al., 2017; Friedkin, 1945; Menard, 1950; Podolak and Wilcock, 2013; Recking et al., 2016;

Van Dijk et al., 2012; Venditti et al., 2012; Zhang et al., 2018). However, relatively few field-scale studies have quantified the importance of sediment supply and transport in shaping channel and bedform topography or in determining rates of channel adjustment (Church and Rice, 2009; Erwin, 2013; Harrison et al., 2011; Massong and Montgomery, 2000; Pitlick, 1993; Venditti and Church, 2014). This is in part due to the challenges in locating an appropriate study system that will exhibit sufficiently large and predictable changes, and complicated further by difficulties obtaining field measurements of sediment transport and bathymetric surveys that constrain spatial and temporal variability.

Many field studies of the effect of sediment surplus or deficit on channel form have tended to focus on coarse (> 1-2mm) sediment in wadeable streams (Hoffman and Gabet, 2007; Lane et al., 2008; Nelson et al., 2009). Studies of gravel-sand transitions have advanced understanding of how rapid transitions in bed grain size can arise (Ferguson, 2003; Jerolmack and Brzinski, 2010; Lamb and Venditti, 2016; Paola et al., 1992; Venditti and Church, 2014). But far less work has been conducted to explain the organization and patterns of behavior in lowland sand bed rivers (Dietrich et al., 1999; Frings, 2008; Nanson, 1980; Ramirez and Allison, 2013).

Meandering sand bed rivers are very common; thus, there is a need to explain patterns of channel form and adjustment in these systems for further understanding of river science and management. We investigate factors controlling river form and dynamics in a sand bed river, specifically a 175 km section of the Minnesota River in south central Minnesota. The Minnesota River is a major tributary to the Upper Mississippi River in a watershed dominated by intensively managed agricultural uplands.

Globally, agricultural expansion has profoundly changed where sediment is produced, how sediment is routed, and where sediment is stored in many low relief landscapes (Wilkinson and McElroy 2007, Montgomery 2007). The Minnesota River is an example of such a landscape where increases in streamflow have caused considerable increases in both fine and coarse sediment loads. According to the 2018 draft of the Impaired Waters List for Minnesota, the Minnesota River basin has 128 impairments for turbidity and total suspended solids (Minnesota Pollution Control Agency, 2018). Large increases in flows in the Minnesota River basin during the 20th and 21st centuries are the result of agricultural tile drainage and climate change (Belmont et al., 2016; Foufoula-Georgiou et al., 2016, 2015; Kelly et al., 2017; Schottler et al., 2014). These increases in flow have created more powerful and erosive rivers (Belmont et al., 2011; Lauer et al., 2017; Lenhart et al., 2013). For example, bluff erosion on Minnesota River tributaries is sensitive to the magnitude and frequency of streamflow (Kelly and Belmont, 2018). Bluffs supply a large fraction of the total sediment load to these tributaries (Belmont et al., 2011). Given that large increases in flow or sediment supply are known to cause changes in channel form and/or dynamics (Kondolf et al., 2002; Lach and Wyga, 2002; Macdonald et al., 2003), we ask:

- can sediment supply and transport (drivers) explain some of the spatial patterns in bar morphology (length, width, height, grain size) in different reaches?
- have increased flows and sediment supply (drivers of geomorphic change) caused changes in channel dynamics, specifically increased channel width

and meander migration rate (response variables) in the mainstem Minnesota River?

We explain spatial patterns in form and dynamics using analysis of flow and sediment drivers including streamflow, a sediment budget, measurement and calculation of sediment transport, slope analysis, and floodplain characteristics.

2. Study Area: Lower 175 km of the Minnesota River, USA

The 43,000 km^2 Minnesota River Basin is underlain by several packages of glacial till and glacio-lacustrine deposits from the late Pleistocene (Clayton and Moran, 1982; Jennings, 2010). The basin is responding to two post-glacial perturbations: glacial isostatic adjustment and mainstem incision triggering tributary erosion. Since the Wisconsinan deglaciation, northern Minnesota and southern Canada have been rebounding at rates of a couple mm/yr while southern Minnesota has been subsiding due to forebulge collapse at approximately 1 mm/yr (Sella et al., 2007). In addition, the mainstem Minnesota River incised 70 m around 13,400 years ago when glacial Lake Agassiz drained catastrophically (Gran et al., 2009; Teller et al., 2005). Incision of the mainstem Minnesota River Valley caused a substantial base level fall for Minnesota River tributaries, which have been rapidly incising through glacial sediments at rates of several mm per year for the last ~13,000 years (Gran et al., 2013). As a result, a steep knickzone is present in the lower reaches of each major tributary (Belmont, 2011; Gran et al., 2013; Wilcock et al., 2009).

Watershed hydrology is another transient factor affecting basin dynamics. During the past 80 years, these rivers have seen large increases in streamflow. Kelly et al. 2017, among others, showed that a combination of precipitation increases combined with

increases in the extent and density of agricultural tile drainage have increased low flows, high flows, and extreme flows by roughly 50% – 250% within the Minnesota River Basin (Foufoula-Georgiou et al., 2015; Novotny and Stefan, 2007; Schottler et al., 2014). Kelly and Belmont (2018), among others, have demonstrated that increases in high flows substantially amplify erosion of near-channel sediment sources (Belmont et al., 2011; Lauer et al., 2017; Schottler et al., 2014).

We examine the lower 175 km of the Minnesota River from Mankato, MN, near of one of the largest sediment exporting tributaries (the Blue Earth River), to Fort Snelling, MN where the Minnesota River joins the Mississippi River (Figure 4-1). This section of river contains three USGS gages, each with several years of sediment transport data. Gages are located at Mankato (05325000), Jordan (05330000), and Fort Snelling (05330920) (Figure 4-1). The location of the gages are well situated for this study because most major tributaries contributing sediment enter the Minnesota River upstream of Jordan, MN. Thus, we generally split the study area into an 'upstream' reach (Mankato to Jordan) and 'downstream' reach (Joran to Fort Snelling).

The unique glacial history of the Minnesota River and its tributaries combined with recent, dramatic increases in streamflow and sediment supply present a well constrained an opportunity to study how a large river responds to significant changes in water and sediment supply. There is a large body of research for the Minnesota River basin, which we will leverage throughout this paper. Fluxes of water and sediment have been well-monitored and changes in morphology and dynamics have been extensively documented via cross section surveys, repeat bathymetry surveys and historical air photos (Gran et al., in review; Groten et al., 2016; Lauer et al., 2017; Lenhart et al., 2013; Libby,

2018). Thus, the lower Minnesota River represents a rare, well-constrained case that provides an extraordinary opportunity to answer the questions posed here.

Previous work on the lower Minnesota River has examined historical patterns of channel width and meander migration using aerial photograph analysis, and found that channel widening and migration have contributed substantially to sediment loads in the lower Minnesota (Lauer et al., 2017). Lenhart et al. (2013) investigated floodplain and point bar deposition in the lower Minnesota and found that modern point bar deposition rates are less than they were a century ago. Additionally, average bed shear stresses have increased in some cases by as much as 144% (Lenhart et al., 2013). Both studies highlight the importance of streamflow increases on channel response. However, neither study investigated the spatial variability in their results along the length of the lower Minnesota River.

3. Methods

3.1. Response in Channel Form – Bar Topography and Bed Grain Size

To characterize longitudinal patterns in grain size, twenty-one samples were collected from 8 sites along the lower Minnesota River during low flow in August 2014. At each site, one or more bar samples were collected using a shovel. Additionally, a thalweg sample was collected at each site using a shovel and a submerged 1-gallon ziplock bag to minimize the loss of fines. Where appropriate, samples were collected below a surface armor layer. Bars of uniform grain size were sampled once from the center of the bar. Bars with multiple facies were sampled from the center of each facies. Samples were sieved at ½ ϕ resolution.

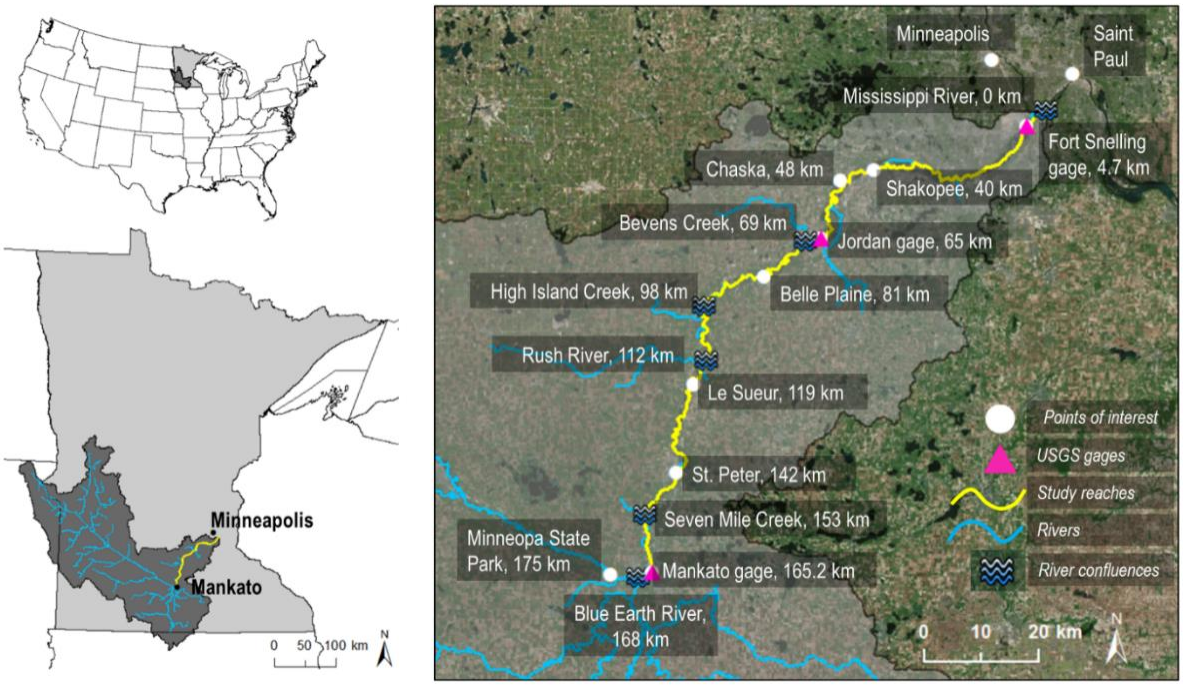

Fig. 4-1. Lower Minnesota River (yellow) with several points of interest, including gage and grain size sample locations, as well as river confluences.

Between June 2013 and June 2016 we mapped a total of 234 km for river bathymetry during high flow conditions using a Teledyne River Ray ADCP and a Leica GS15 rtkGPS (Kelly et al., 2018). Further information about the bathymetric surveys can be found at http://dx.doi.org/10.4211/hs.6cd3728f69cb4cb39c6f11baac1734ec and in Appendix C. We delineated pools and bars manually, from 8 surveyed reaches, in ArcGIS's ArcMap 10.6 using bathymetric elevation, slope, hillshade, and feature shape as indicators of these large-scale features. Bar boundaries were drawn either to the edge of the thalweg or until the bed elevation no longer declined with distance. We calculate the polygon area for bars and pools separately, and report the percent of the total channel area with pools and bars. Bar amplitude is calculated as the minimum elevation minus the maximum elevation within each bar polygon. Bar length is calculated using the Bounding

Containers toolbox for ArcMap with a rectangle bounding box. Average bar width is derived from dividing the bar area by the bar length.

Bar height measurements provide even more insight into bar geometry when compared to bank heights. We calculate bank heights using 1 m lidar from Blue Earth (2012), Le Sueur (2011), and Scott (2011) County, Minnesota (Available from: http://www.mngeo.state.mn.us/chouse/elevation/lidar.html). Bank heights are calculated as the maximum bounding container clipped DEM elevation minus the minimum bar clipped bathymetry elevation.

3.2. Response in Channel Dynamics – Channel Width and Meander Migration

We calculated meander migration rates and channel widening rates from historical aerial photographs from 1937, 1951, 1964, 1980, 1991, 2010, 2013, and 2017. Libby (2018) georeferenced historic photos, digitized banklines, and calculated migration rates for all years except 2010 and 2017. We followed the same methods as Libby, 2018, digitizing banklines at a scale of 1:2000 and using the ArcGIS 10.2 Planform Statistics toolbox to generate centerlines and calculate widths and migration distances (Lauer and Parker, 2008).

In addition to planform dynamics, we evaluate potential changes in bed elevation using a gage height analysis, as well as repeat bathymetry surveys. For the gage height analysis, we calculated mean bed elevation for every field-collected discharge measurement in the USGS gage record. Mean bed elevation is calculated as:

$$Z_M = \frac{Z_D + H}{\left[\frac{A}{W}\right]} \quad (3)$$

where Z_M is the mean bed elevation, Z_D is the gage datum elevation, H is the gage height, A is the channel area, and W is the channel width at the time of the discharge measurement (Smelser and Schmidt, 1998). None of the gages reported a datum shift during the period of record.

We couple gage height analysis with measured bathymetric change to better understand bed dynamics in the lower Minnesota River. We differenced repeat bathymetry using the Geomorphic Change Detection tool for ArcGIS (Wheaton et al., 2010). Based on the data uncertainty, we used a 25 cm minimum level of detection for repeat surveys.

3.3. Streamflow Change as a Driver of Channel Form and Dynamics

Previous studies have quantified 20th and 21st century streamflow changes in the Minnesota River basin in detail (Foufoula-Georgiou et al., 2015; Kelly et al., 2017; Novotny and Stefan, 2007; Schottler et al., 2014). We are interested in along-river changes in streamflow and therefore leverage three USGS gages along the lower Minnesota River (Figure 4-1). To analyze the entire range of flows, we calculated flow duration curves for two time periods at Mankato and Jordan gages: 1936-1976 and 1977-2017, and then computed the ratio at each exceedance percentile. The gage at Fort Snelling began operation in January 2004, so we also calculated flow duration curve ratios at each of the three gages for the periods 2004-2010 and 2011-2017.

3.4. Sediment Supply as a Driver of Channel Form and Dynamics

Sediment budgets are mass balances that account for sediment inputs, outputs and changes in storage over a given domain (Dietrich and Dunne, 1978; Reid and Dunne,

2016). They reveal the significance of sediment sources and sinks over vast areas (e.g. Belmont et al., 2011; Erwin et al., 2012; Trimble, 1999). We balance a sediment budget for the period 2011 to 2016 for the upstream and downstream reach, Mankato to Jordan and Jordan to Fort Snelling, respectively. Budget sediment inputs (tons/year) for each reach include: 1) USGS measured bedload and suspended load at the upstream end of each reach, 2) USGS measured tributary bedload and suspended load for the Mankato to Jordan reach, 3) sand inputs from bank erosion due to meander migration, and 4) sand inputs from channel widening. Budget sediment outputs (tons/year) for each reach include: 1) USGS measured bedload and suspended load at the downstream end of each reach, 2) floodplain deposition of sand, 3) sand deposited on point bars due to meander migration, and 4) channel dredging for the Jordan to Fort Snelling reach. Detail for each budget input and output term calculation is presented in Appendix C.

To close the average annual sediment budget we reduce all budget values, except those at the Jordan gage, by a fraction of their uncertainty until the sum of all inputs and outputs equals zero, consistent with Belmont et al., 2011. This approach allows better constrained (less uncertain) values to be changed less than less well constrained (more uncertain) values in the budget. Importantly, interpretations from the raw and closed sediment budget are in agreement (Figures C2 & 4-10, respectively). For the closed budget we reduced all values in the Mankato to Jordan budget by 1.7% of each value's uncertainty and all values in the Jordan to Fort Snelling budget by 11.6% of each value's uncertainty. We held the average values at the Jordan gage constant for both budgets so that the outputs of the upstream budget would equal the inputs of the downstream budget. We calculated gage uncertainty for Mankato, Jordan, and High Island gages from the

95% confidence interval on the power law rating relation exponent and coefficient. See Appendix C for Matlab script containing calculations of weighted non-linear least squares fit and 95% confidence intervals. Because the Fort Snelling data were fit using an independent sediment transport model, we calculated uncertainty by varying the median grain size from 0.125 mm to 0.5 mm. Migration and widening uncertainty combines aerial photograph uncertainty from Libby (2018), with bulk density and grain size uncertainty from Lenhart et al. (2013). We used floodplain deposition uncertainty from Lenhart et al. (2013) and assumed 5% uncertainty on reported dredging.

3.5. Channel Slope as a Driver of Channel Form and Dynamics

We measure channel slope from a USGS 1:24,000 scale level 2 DEM with 30 m resolution. We use the 2017 channel centerline (derived from aerial photographs, as explained in section 3b) to extract water surface elevations along this line. We also measure water surface slope and bed slope for 6, 6, and 12 km reaches near Mankato, Jordan, and Shakopee, respectively, using field surveyed DEMs. We calculate bathymetric slope from the average elevation within a 1 km window at the upstream and downstream end of each reached surveyed. We divide the elevation difference by the reach length measured from the centroid of each circle.

3.6. Sediment Transport Regimes as a Driver of Channel Form and Dynamics

In addition to sediment gaging information, we expect that any spatial discontinuities in channel form and/or dynamics may be explained by the sediment transport regimes. We calculated Rouse Number, formative shear velocity, relative settling velocity, particle Reynolds Number, and Shields Number for a range of flows

from 3.5 m depth to 6.0 m depth for the Mankato to Jordan and Jordan to Fort Snelling reaches. We calculated Rouse numbers according to the following definitions:

$$Z_R = \frac{\nu_s}{\kappa u_*} \quad (4)$$

where Z_R is the Rouse number, ν_s is the particle fall velocity as defined by Dietrich (1982), κ is the von Kármán constant taken as 0.4, and u_* is the shear velocity defined as $u_* = \sqrt{gHS}$, where g is the acceleration due to gravity, H is the flow depth, and S is the slope. Relative settling velocities are calculated similar to equation 4, but removing the von Kármán constant from the denominator.

Formative shear velocities were calculated consistent with methods of Lamb and Venditti (2016) only using D_{84} instead of D_{90} as they were approximately the same. The relation for formative shear velocity is defined as:

$$u_{*f}^2 = fRgD_{84}\tau_{c50}^* \left(\frac{D_{84}}{D_{50}}\right)^{-\gamma} \quad (5)$$

where u_{*f} is the formative bed shear velocity, f =1.5, R is the submerged specific gravity of quartz = 1.65, g = 9.81 m/s^2, D_{84} and D_{50} are the 84th and 50th percentile grain size diameters in meters, γ = 0.9, and τ^*_{c50} is the critical Shields number for the median grain size calculated as $\tau_{c50}^* = \frac{u_*^2}{RgD_{50}}$.

Particle Reynolds number is calculated for a range of grain sizes, every phi increment between and including ¼ mm and 8 mm, and defined by the shear velocity (u_*), grain diameter in meters (D), and kinematic viscosity of water (ν = 0.000001 m^2/s), as:

$$Re^* = \frac{u_* D}{\nu} \quad . \quad (6)$$

Finally, Shields stress was calculated for a range of grain sizes, every phi increment between and including ¼ mm and 8 mm as:

$$\tau^* = \frac{\tau}{g(\rho_s - \rho)D} \quad (7)$$

where $\tau = \rho gHS$, $\rho = 1000$ kg/m^3, and $\rho_s = 2650$ kg/m^3.

4. Results

4.1. Characterizing Channel Form: Slope, Bed Grain Size, and In-Channel Topography

Basic understanding of river form and organization may be gleaned from a longitudinal profile. Figure 4-2a shows river elevation as a function of distance upstream from the Mississippi River confluence. A major break in slope occurs around river kilometer 85. Water surface slope measured from field surveyed data is consistent with measured bed slope and slope extracted from the 30 m DEM (Table 4-1). Slope measured near Jordan is more similar to Shakopee than to Mankato, suggesting that the slope break is located upstream of Jordan, which is consistent with Figure 4-2a. In general, the

Table 4-1. Field surveyed channel bed and water surface slope for reaches near Mankato, Jordan, and Shakopee, and water surface slope for reaches from Mankato to Jordan and Jordan to Fort Snelling derived from USGS 30 m DEM.

Field Measured Slope				**30 m DEM Derived Slope**		
Site	Reach Length (km)	Bathymetry Bed Slope	Water Surface Slope	Site	Reach Length (km)	DEM Water Surface Slope
Mankato	6	0.000156	0.000200	Mankato to Jordan	102	0.000176
Jordan	6	0.000102	0.000092	Jordan to Shakopee	65	0.000079
Shakopee	12	0.000089	0.000105			

downstream reach has a slope of 0.0001, approximately half the slope of the upstream reach (Table 4-1).

Bed grain size systematically changes longitudinally, as shown in Figure 4-2b. Upstream of the Blue Earth River (Minneopa State Park sites), thalweg D_{50} is approximately 0.5 mm. However, downstream of the Blue Earth River confluence, thalweg D_{50} increases to roughly 3 mm. Thalweg D_{50} declines rapidly from Mankato to Belle Plaine. Downstream from Belle Plaine, bed grain size does not vary much within and between sites, and the D_{50} is approximately 0.25 mm (Figure 4-2b). Full grain size distributions for the channel thalweg as well as bars are plotted in Figure 4-3. Bar samples were not consistently finer or coarser than thalweg samples (dashed vs solid lines). Bed grain size variability increases between Minneopa State Park (SP) and Lime Township, where the Greater Blue Earth River joins the Minnesota River (Figure 4-3). Grain size variability is lowest between Belle Plaine and Shakopee (Figure 4-3).

Much like slope and grain size, the number of pools, bars, and bar amplitude also change systematically along the lower Minnesota River (Figure 4-2d). Upstream of the Blue Earth River (river kilometer 175), bars and pools make up 9% and 18% of the channel, respectively. In the channelized reach through downtown Mankato (river kilometer 165), bars and pools combined comprise 20% of the channel area. Downstream, the area of bars reaches a maximum of 38%, and pool area is 18% (river kilometer 153). The area of bars decreases in St. Peter to 14% (river kilometer 142). Bar area increases in Belle Plaine and Jordan to 23% (river kilometers 81 and 65), then decreases to 10% and less in Chaska and Shakopee (river kilometers 48 and 40). Overall,

the presence of pools is fairly consistent across sites, only varying between 12% and 23% of the channel area.

Bar amplitude is very different upstream versus downstream of Belle Plaine (Figure 4-2d). Upstream of Belle Plaine bar amplitude is about 2.3 m, except in the channelized reach through downtown Mankato, where bars are 1.5 m tall. Bars reach a maximum average height of 5.7 m in Belle Plaine and decrease to 3.8 m in Shakopee. Bar height variability was greatest in Belle Plaine and Jordan (Figure 4-2d). Bar lengths range in size between 200 m and 700 m (Figure 4-2d). In general bars are longer downstream of the Greater Blue Earth River, though there is no emergent relation between bar length and distance from the Mississippi River confluence (Figure 4-2d). However, bar width changes systematically along the lower Minnesota River, increasing from roughly 30 m upstream of the Greater Blue Earth River to 40-50 m downstream of the tributary confluences through Mankato, St. Peter, Belle Plaine, and Jordan (Figure 4-2d). Further downstream, river kilometers 48 and 40, bar width decreases to roughly 20 m.

Bar height can be directly compared to adjacent bank height to understand how close bars are to becoming floodplain. Bars upstream of Belle Plain (river kimometer 81) are relatively short, bank heights generally increase in the downstream direction, and thus bars become shorter relative to their banks in the downstream direction (Figure 4-4). Near Belle Plain and Jordan (river kilometers 81 and 65), bars reach average heights that are 70% of the bank height (Figure 4-4). Downstream in Chaska and Shakopee (river kimometers 48 and 40), bar heights are 45% of bank heights (Figure 4-4). Bar heights are only 40% of bank heights upstream of Belle Plaine.

In general, bars in the upstream reach are broad and short while bars in the downstream reach are narrow, tall, and in places close to bank heights. Based on the product of bar length, width, and height, bars are largest near a transition in bar size that occurs near Belle Plaine and Jordan (river kilometers 81 and 65). Dramatic differences in bar morphology may be explained by differences in sediment supply and transport. This idea will be explored further in the discussion.

4.2. Longitudinal Variability in Channel Dynamics: Widening, Migration and Bed Elevation Change

Spatial variability in channel form discussed above covaries with measures of channel dynamics. From 1937 to 2017 the lower Minnesota River widened extensively (Figure 4-5a). The greatest widening occurred in the section upstream of Jordan. From Mankato (165 km) to Jordan (65 km) the average widening rate from 1937 to 2013 was 0.72 m/yr. While from Jordan to Fort Snelling (0 km) the channel has widened at a rate of 0.36 m/yr. Mean widening rates are significantly different between the two reaches ($p<<<0.01$) at alpha = 0.05 (student's t-test). We also calculated widening rates for a more recent interval 2010 – 2017 and found even greater average widening rates for these two reaches. Between Mankato and Jordan the average widening rate was 0.83 m/yr, and 0.67 m/yr between Jordan and Fort Snelling. Table 4-2 lists the average channel width in each reach for every year digitized. Of particular note is the fact that the upstream reach is currently wider than the downstream reach by nearly 17 m. However, the Minnesota River has not always exhibited downstream narrowing. In 1937, the downstream reach was wider than the upstream reach by 11.5 m. In 1951, both reaches were approximately 80 m (Table 4-2).

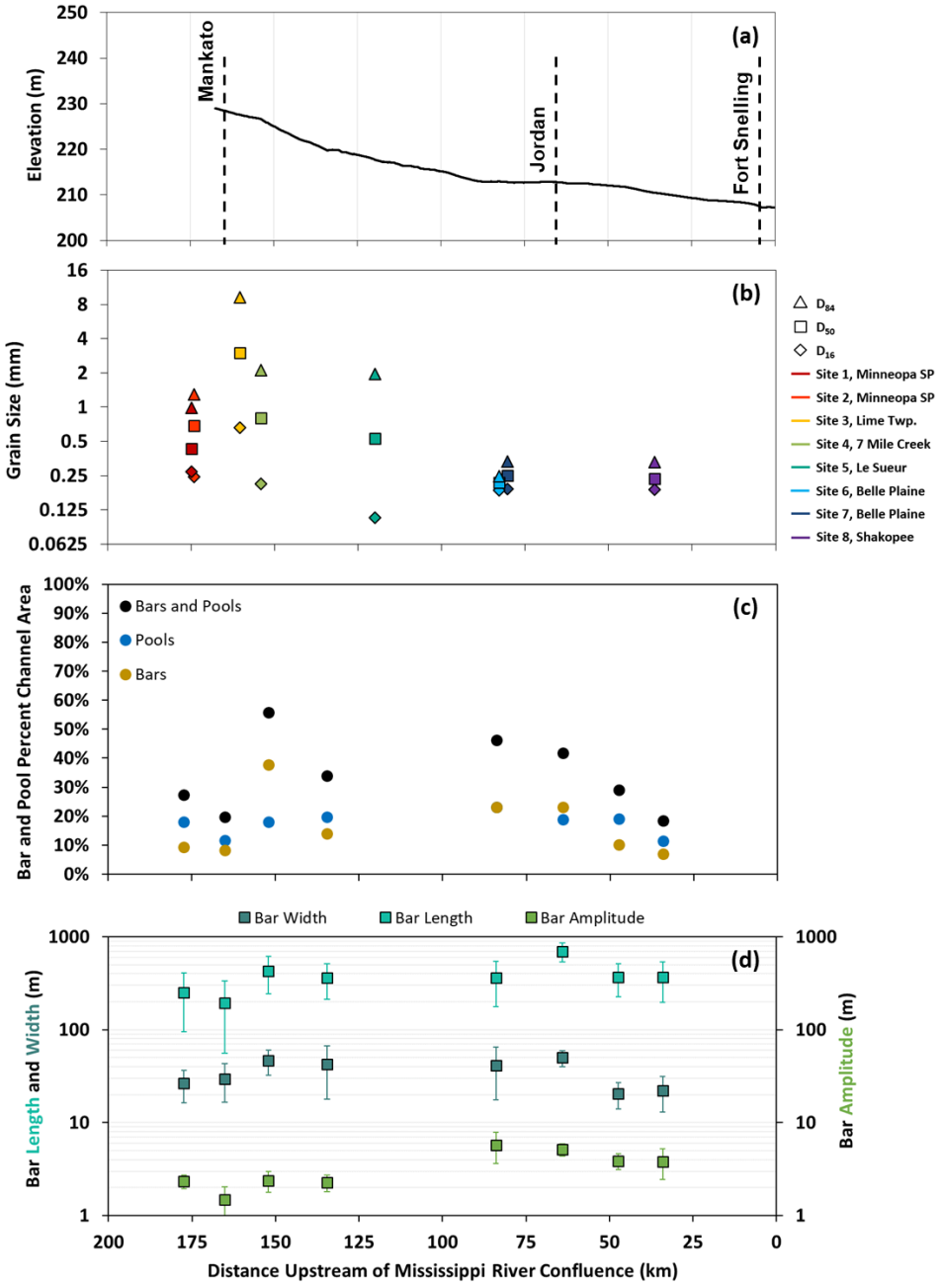

Fig. 4-2. a) Channel water surface elevation (m) versus distance upstream of the Mississippi River (km) derived from USGS 30 m DEM with 20 km smoothing window b) Channel thalweg subsurface D_{16}, D_{50}, and D_{84} grain size for 8 sites along the lower Minnesota River. c) Percent surveyed channel area with bars, pools, and bars plus pools for 8 sites along the lower Minnesota River. d) Average bar length (m), width (m), and amplitude (m) ± one standard deviation for eight sights along the lower Minnesota River. For panels b-d, the upstream most site is upstream of the Greater Blue Earth River confluence. The second most upstream site is located in downtown Mankato, and is heavily engineered with levees. The four downstream sites are all downstream of tributaries Rush River and High Island Creek.

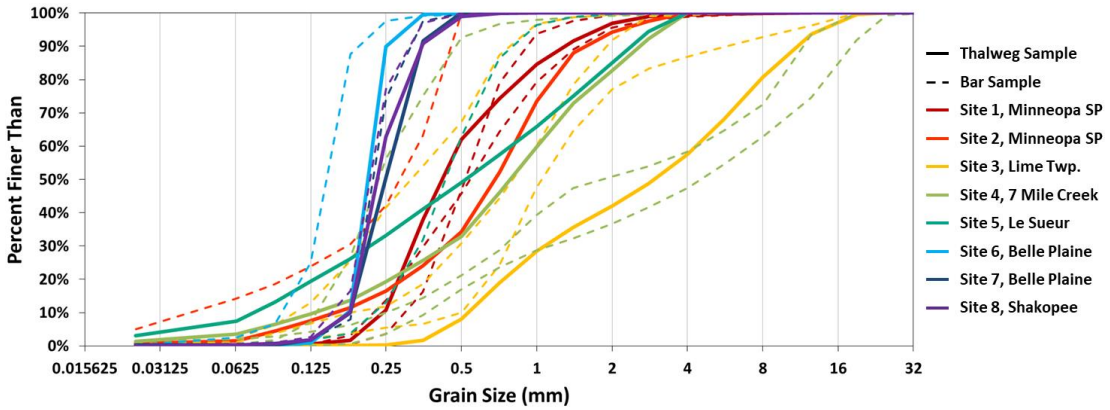

Fig. 4-3. Cumulative percent finer than grain size distributions for 8 sites along the lower Minnesota River. The two Minneopa State Park (SP) sites are located upstream of the Blue Earth River. All samples were collected from the subsurface (below the armor layer) during low flow conditions.

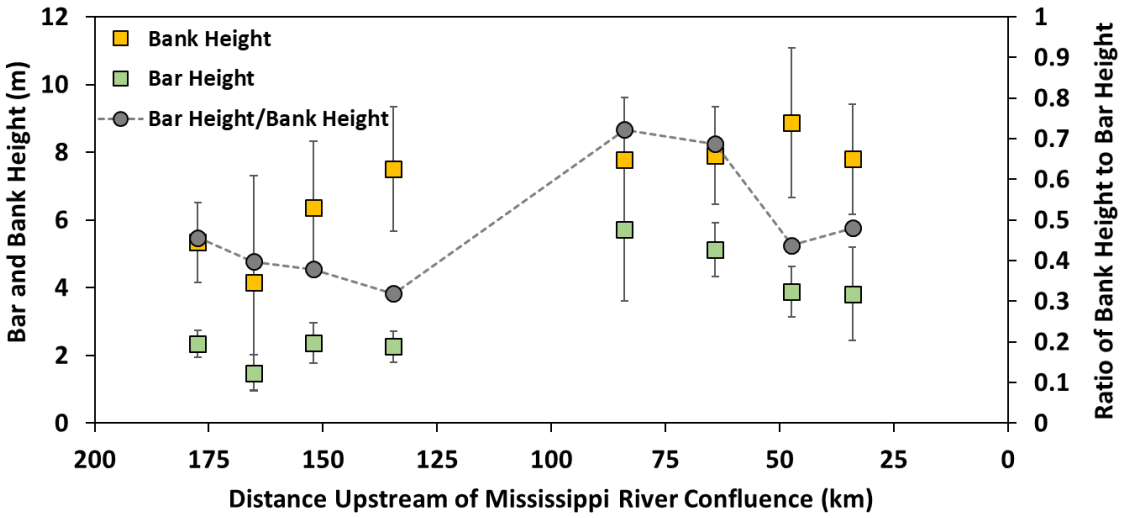

Fig. 4-4. Bar and bank height (m) ± 1 standard deviation and ratio of bar height to bank height for 8 sites along the lower Minnesota River.

In addition to extensive and heterogeneous widening, the channel has migrated substantially in both reaches. Current migration rates (2010 -2017) are 1.50 m/yr and 0.57 m/yr for the Mankato to Jordan, and Jordan to Fort Snelling reaches respectively. When scaled by channel width, this migration is equivalent to 1.2 and 0.5 percent channel width per year respectively. Figure 4-5b shows that migration has occurred throughout all

decades, much like the observed widening. Notably, migration rates above Jordan have been consistently higher than those measured downstream of Jordan (Figure 4-5b). Migration has also led to several channel cutoffs, denoted by stars in Figure 4-5b. A disproportionate number of cutoffs have occurred in the reach upstream of Jordan.

In addition to measuring channel planform change, we attempted to constrain aggradation or degradation. This is important because the sediment budget contains fluxes from horizontal as well as vertical channel sources. Over a short timescale, we observed aggradation in Mankato and Belle Plaine according to repeat bathymetry surveys (Figures 4-6 & 4-7). Average bed aggradation between Mankato and Seven Mile Creek was 21 cm between 2013 and 2014, and 31 cm between 2014 and 2016. Aggradation was measured throughout the reach in both years. Near Belle Plaine average deposition was 74 cm between 2014 and 2016. One explanation for the large average deposition in this reach is due to local deposition downstream of a bridge pier following a large flood (Figure 4-7). We surveyed a large 20+ m scour hole behind a bridge pier during an out-of-bank flood in 2014. By 2016, this hole had completely filled in.

We calculated the mean streambed elevation at each gage (Mankato, Jordan, and Fort Snelling) for every field streamflow measurement in the USGS gage record (Figure 4-8). River gage height analysis showed considerable variability in mean stream bed elevation, but no systematic shifts are observed. It is plausible that bed elevations in the Minnesota fluctuate on the order of a meter within a given year as dunes and bars migrate through the measurement cross section. Out-of-bank flows are largely responsible for the large deviations from the average conditions, or high elevations. Average conditions are

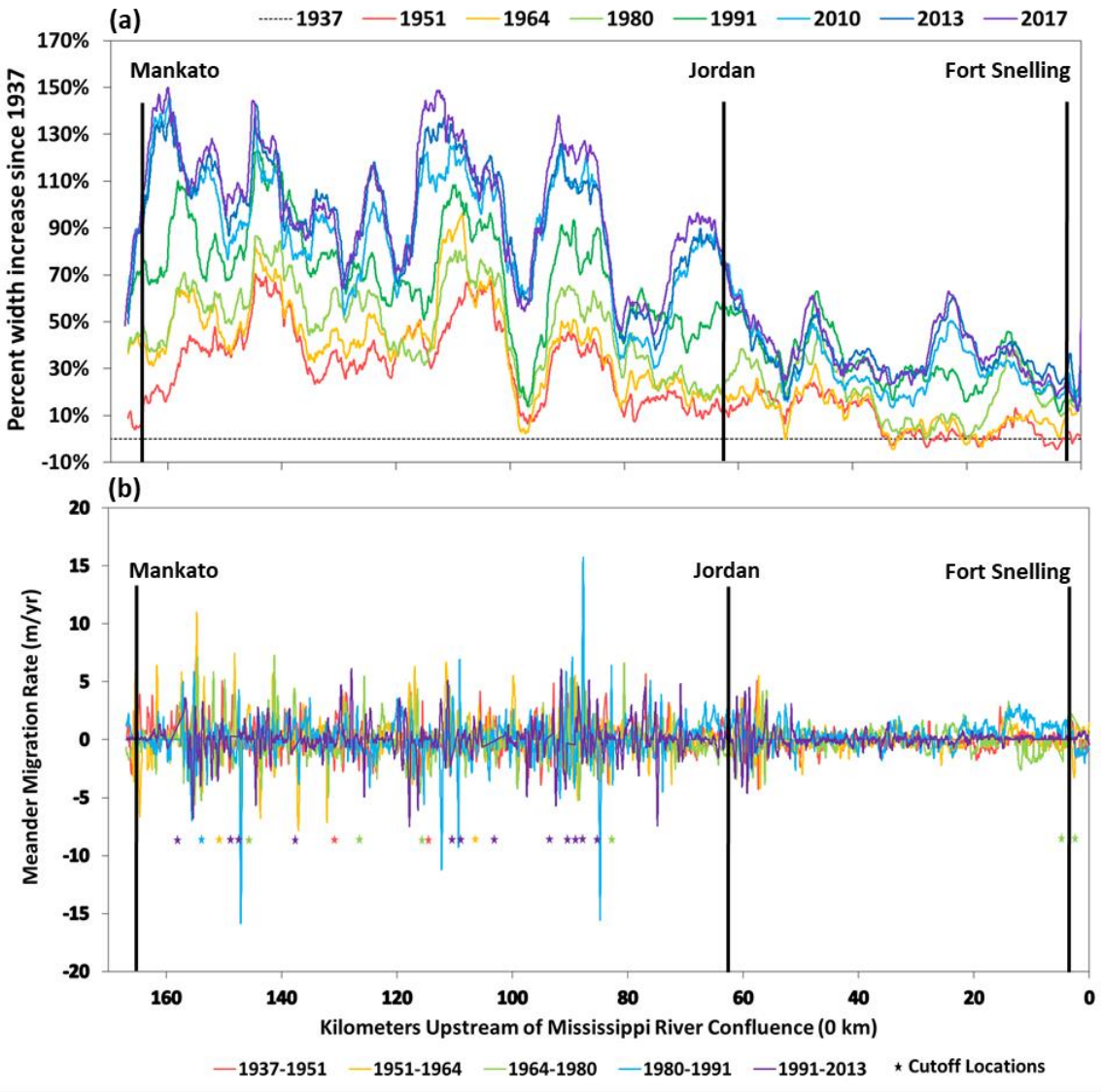

Fig. 4-5. a) Percent increase in width between 1937 and 1951, 1964, 1980, 1991, 2010, 2013, and 2017 along the Minnesota River from the Mississippi River confluence (0 km) to the Blue Earth River confluence (168 km). Widths were measured at 10 m intervals, and percent differences are plotted using a 5 km average smoothing window. b) Average channel migration rate, m/yr, along the Minnesota River for five aerial photograph intervals. Positive and negative migration rates indicate movement of the channel centerline towards river left and river right, respectively. The Mississippi River confluence is located at 0 km, and the Blue Earth River confluence is located at 168 km.

Table 4-2. Average channel width in meters measured from 8 aerial photograph derived banklines for the reach between Mankato and Jordan (MtoJ), and Jordan and Fort Snelling (JtoFS).

Year	MtoJ Width (m)	JtoFS Width (m)
1937	64.4	75.9
1951	81.8	80.4
1964	87.2	81.8
1980	91.8	88.2
1991	104.6	98.9
2010	115.5	99.7
2013	118.8	103.4
2017	121.3	104.4

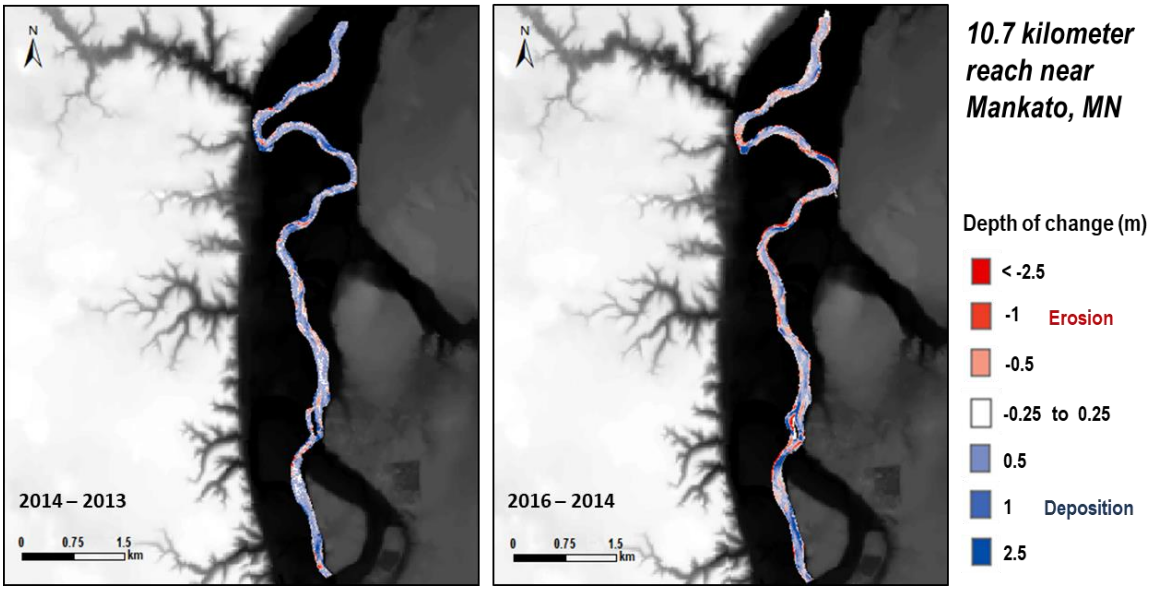

Fig. 4-6. DEMs of difference for a 10.7 km reach between Mankato and Seven Mile creek, shown between 2013 and 2014 (left) and 2014 and 2016 (right). Erosion is red, deposition is blue, and change below a 25 cm minimum level of change is white. Spatially averaged volume of change is 0.21 m of deposition between 2013 and 2014 and 0.31 m of deposition between 2014 and 2016.

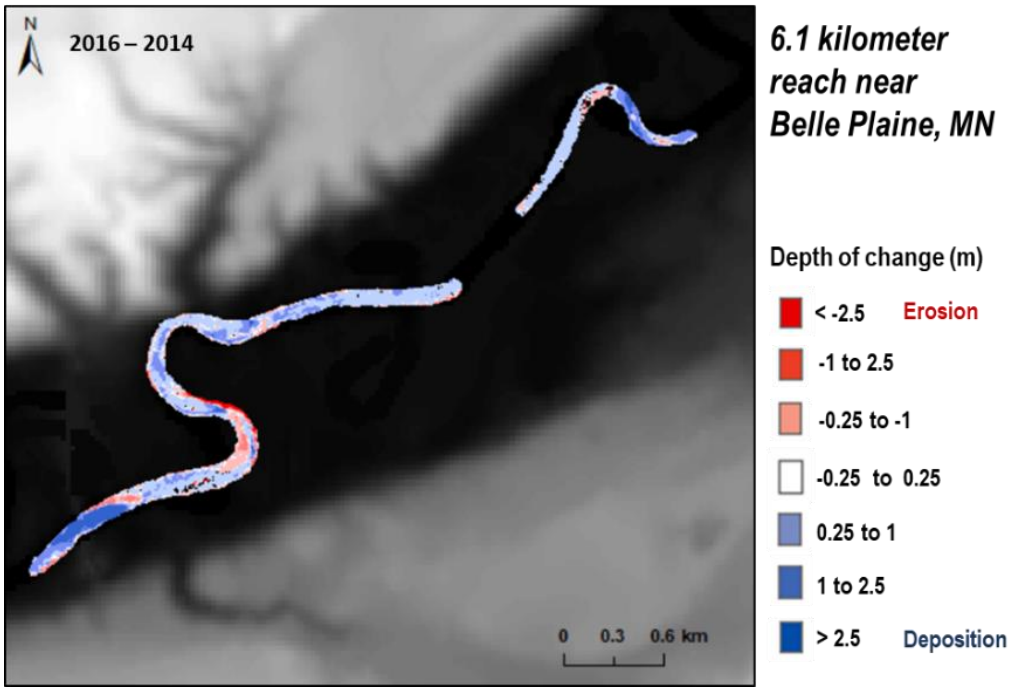

Fig. 4-7. DEM of difference for a 6.1 km reach near Belle Plaine, between 2014 and 2016. Erosion is red, deposition is blue, and change below a 25 cm minimum level of change is white. Spatially averaged volume of change is 0.74 m of deposition between 2014 and 2016.

not visibly different through time at each gage (Figure 4-8). If we compare the short and long term records of bed elevations, we find that the short term aggradation captured by the repeat bathymetry falls within the bed elevation variability captured at the gage. Therefore, bed elevation change will not be included as a significant flux in the sediment budgets.

4.3. Flow Duration Curves Show Streamflow Increase

From 1936-1976 to 1977-2017 the magnitude of flows associated with the full range of exceedance probabilities have increased substantially at the Mankato and Jordan gages (Figure 4-9). Flows associated with a twenty percent and smaller exceedance probabilities have increased between 1.5 and 2 times at both gages. Flows between 20%

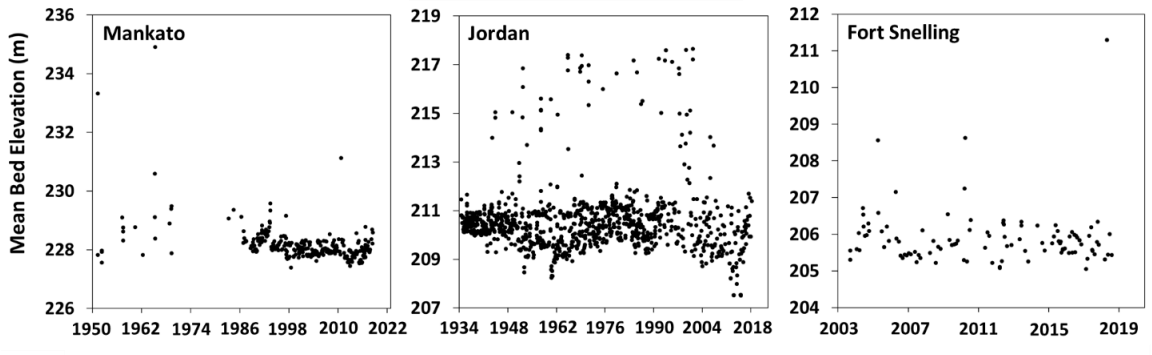

Fig. 4-8. Mean streambed elevation (m) calculated from available channel geometry collected during field discharge measurements at Mankato, Jordan, and Fort Snelling gages.

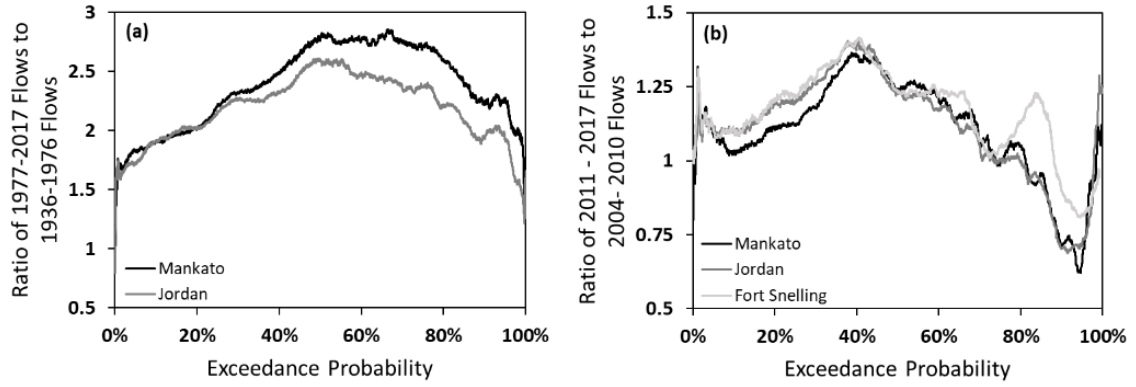

Fig. 4-9. a) Ratio of 1977 – 2017 flow magnitude to 1936 – 1976 flow magnitude for the same exceedance probabilities at Mankato and Jordan gages, and b) ratio of 2011 – 2017 flow magnitude to 2004 – 2010 flow magnitude at Mankato, Jordan, and Fort Snelling gages.

to 95% exceedance probabilities have increased the most at both sites, 2 to nearly 3 times at Mankato and 2 to 2.5 times at Jordan. Flows greater than 95% exceedance probability have also increased in magnitude, but to a lesser degree.

More recently flows have continued to increase at Mankato, Jordan, and Fort Snelling (Figure 4-9). From 2004-2010 to 2011-2017 flows have increased for exceedance probabilities less than 80% at Mankato and Jordan and less than 90% at Fort

Snelling. Both the short and long term records suggest non-stationary hydrology with increasing streamflow for all sections of the lower Minnesota River.

4.4. Annual Sediment Supply and Transport: 2011 – 2016

4.4.1. Upstream Reach (Mankato to Jordan) –Mixed Load

The average annual sediment supply (2011-2016) of combined bedload and suspended sands to the Mankato to Jordan reach is 1.29 million tons per year (Figure 4-10). The transport of sediment past the Jordan gage is 658,000 tons per year. Thus, 49% of the annual sediment supply in the Mankato to Jordan reach is stored within the channel and floodplain. Point bar deposition from meander migration is the largest depositional sink in the reach (Figure 4-10a). Channel widening and net erosion from meander migration contribute more sediment than the Minnesota River at Mankato and tributary gages combined, and together comprise 53% of the sediment inputs.

The coarse bedload supply is almost entirely stored within the Mankato to Jordan reach. At Mankato, 0.5-2 mm and 2-8 mm bedload comprises 19% of the total load. However, in Jordan less than 0.1% of the total supply is bedload. At Mankato, the Minnesota River is a mixed load river, but by Jordan the river has shifted to a predominately suspended load regime (Dade and Friend, 1998). Eighty percent of the total bedload supply enters the reach at the Mankato gage, with Rush River, High Island Creek, and Bevens Creek tributaries supplying the other 20% of the bedload material. Given the grain size distributions of the Minnesota River upstream of the Blue Earth River confluence, it seems likely that the Mankato gravel and coarse sand supply comes almost exclusively from the Blue Earth River and its tributaries.

4.4.2. Downstream Reach (Jordan to Fort Snelling) – Suspended Load Dominant

The average annual sediment supply to the downstream reach is 887,000 tons per year (Figure 4-10b). Transport of sediment past the Fort Snelling gage is 699,000 tons per year. Thus, 20% of the annual sediment supply is stored within the channel and floodplain. Floodplain deposition is the largest sediment sink in the reach (Figure 4-10a). Meander migration erosion and channel widening contribute 26% of sediment in the downstream reach. Therefore, most of the sediment supply comes directly from the upstream reach (Figure 4-10b).

4.4.3. Transport Regimes – Bedload, Suspended Load, or Mixed Load Transport?

Spatial discontinuities in channel form and dynamics might be explained by differences in transport regimes. We compare transport regimes identified from the sediment budget to those characterized by relations from the literature. The sediment budget reveals that 19% of the total load at Mankato is bedload (Figure 4-10). Using a 10 - 20% bedload threshold for dividing suspended load and mixed load transport, the upstream reach falls at the transition from suspended-dominant to mixed load transport (Dade and Friend, 1998). The downstream reach has a bedload supply that is less than half a percent of the total supply and bedload transport is essentially zero, therefore this reach is suspended load dominant. According to the relative settling ratio for the median grain size and a range of depths in the upstream and downstream reach, the lower Minnesota River should be a mixed load river (Figure 4-11a). The location of the data on the Shields diagram indicates a mixed load regime for both the upstream and downstream reach (Figure 4-11b). Although transport may occur as mixed bedload and suspended load upstream, there is no indication of bedload transport at Fort Snelling and little

transport at Jordan. Using only the median grain size of the downstream reach (0.25 mm), the empirical fit of Dade and Friend (1998) indicates that the downstream reach is correctly classified as suspended load dominant. In contrast, the transport regime for the upstream reach (D_{50} = 1 mm) is mixed load dominant. Bedload transport falls from 19% to nearly zero in the upstream reach suggesting significant storage of bedload material in bars. This suggests that bedload supply is greater than the transport capacity in the upstream reach. In the downstream reach, bedload supply is absent and suspended load material is finer than the upstream reach according to calculated Rouse numbers.

Rouse numbers calculated for the upstream reach suggest partial suspension transport of 0.5 mm sands and finer, but only partial transport of 0.25 mm sands and finer in the downstream reach (Table 4-3). The absence of 0.5 mm sands in the bed of the downstream reach suggest that it may no longer be transported in suspension, and may be deposited rapidly near the slope break (Figures 4-2 & 4-3). The formative bed shear velocities are consistent with Rouse number results. Calculated for every location with bed grain size data and for a range of depths, formative shear velocities decline longitudinally to at or below the threshold value for suspended sands, 0.1, identified by Lamb and Venditti (2016) (Figure 4-12). The location of this decrease, downstream of Saint Peter but upstream of Belle Plaine, coincides with the slope break (Figure 4-2). Coincidently, this is also where the bed significantly fines (Figure 4-2 & 4-12). Photo insets in Figure 4-12a show bar texture in the upstream reach near Mankato and in the downstream reach near Shakopee.

5. Discussion

Many studies of flow and sediment transport investigate steady, uniform, or equilibrium conditions, especially in physical and mathematical modeling. This theory is often applied to natural rivers, which may experience dis-equilibrium conditions more often than equilibrium conditions (Andrews and Nelson, 1989). The Minnesota River is a sand-bed dis-equilibrium river that has been extensively monitored. Despite the variability inherent to a natural system, we found distinct differences in morphology and dynamics between the upstream and downstream reaches. Here we attempt to explain those differences using a variety of approaches based on theoretical understanding of sediment transport and meandering rivers.

5.1. Can Hydrologic Change Explain Differences in Form and Dynamics?

The Minnesota River basin has experienced profound increases in flow over the past 80 years. Geomorphologically, the most important of these increases is probably the 1.5 to 2 fold increases in high flows (<20% exceedance flows). Notably, very similar increases are observed in the upstream and downstream reaches. While we might expect increased widening or migration associated with flow increases (Bradley and Smith, 1984; Lauer et al., 2017; Schottler et al., 2014), widening and migration rates have remained relatively constant in both reaches since 1937 (Figure 4-5). Thus, while increased flows have likely sustained river widening and migration in both reaches, they cannot explain the spatial differences in morphology and dynamics between the upstream and downstream reach. Similarly, migration rates in the adjacent Root River watershed have not increased despite increasing streamflow trends (Donovan and Belmont, 2019). It is clear that other

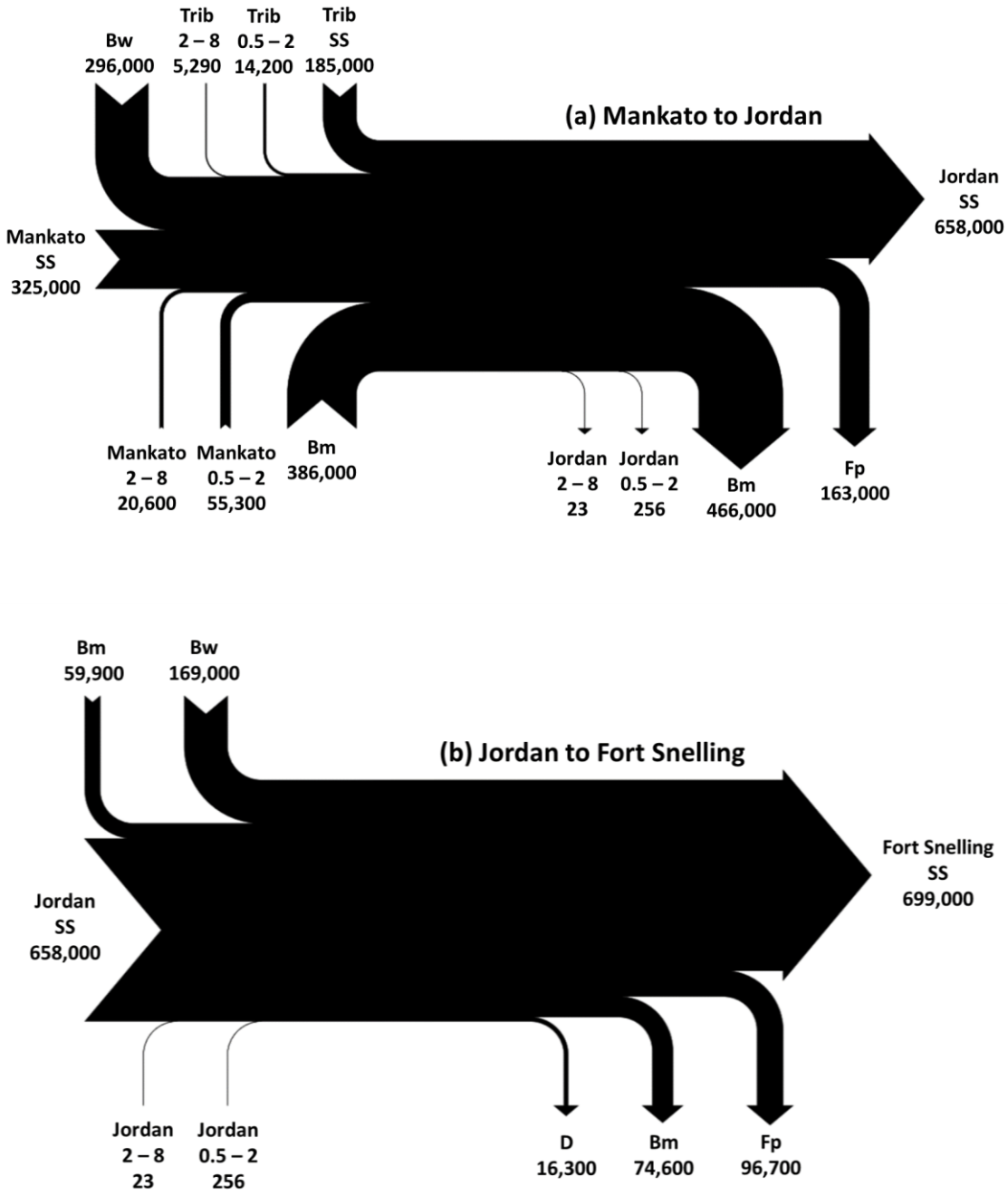

Fig. 4-10. Average annual sediment budget computed between 2011 and 2016 for a) the reach between Mankato and Jordan, and b) Jordan to Fort Snelling on the lower Minnesota River. Sediment inputs are arrow tails and sediment outputs are arrow heads. Abbreviations reflect suspended sands (SS), coarse bedload sands (0.5-2 mm), fine bedload gravels (2-8 mm), tributaries (Trib), channel migration (Bm), channel widening (Bw), floodplain deposition (Fp) and dredging (D). All values reported as tons/year and rounded to three significant digits. Small budget deficits are an artifact of rounding.

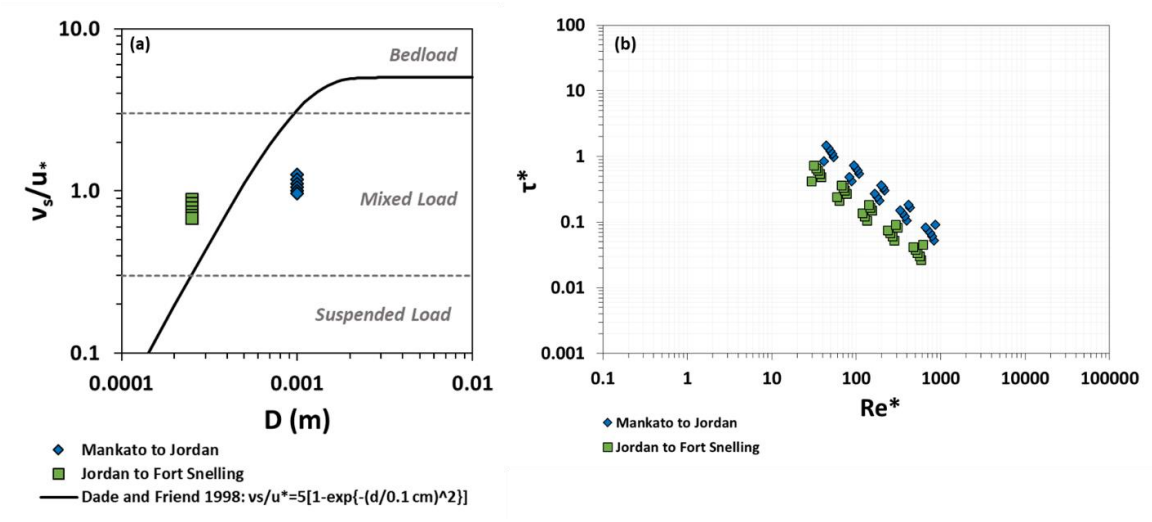

Fig. 4-11. a) Particle fall velocity (v_s) divided by shear velocity (u_*) for median grain sizes (D) for the Mankato to Jordan and Jordan to Fort Snelling reaches. There are multiple values for a given grain size, which represent depths from 3.5 m to 6 m. The lowest depths correspond to the greatest fall velocity to shear velocity ratios. Black and grey lines are from Dade and Friend 1998 and represent the relation between grain size in cm and v_s/u_*, and breaks between suspended load, mixed load, and bedload rivers, respectively. b) Shields stress versus grain Reynold's number for the same range of flow depths at the Mankato to Jordan and Jordan to Fort Snelling reaches.

Table 4-3. Rouse numbers calculated for a range of flow depths (900 – 50,000 cfs) and grain sizes for the Mankato to Jordan (M to J) and Jordan to Fort Snelling (J to FS) reaches. Italicized values highlight Rouse numbers indicative of 50% transport in suspension. Non-italicized values are indicative of bedload transport.

		Grain Size (m)					
Site	**Depth (m)**	**0.00025**	**0.0005**	**0.001**	**0.002**	**0.004**	**0.008**
M to J	3.5	*1.6*	*2.2*	3.2	4.5	6.3	8.9
M to J	4.0	*1.5*	*2.1*	3.0	4.2	5.9	8.4
M to J	4.5	*1.4*	*2.0*	2.8	3.9	5.6	7.9
M to J	5.0	*1.3*	*1.9*	2.6	3.7	5.3	7.5
M to J	5.5	*1.3*	*1.8*	2.5	3.6	5.0	7.1
M to J	6.0	*1.2*	*1.7*	*2.4*	3.4	4.8	6.8
J to FS	3.5	*2.2*	3.2	4.5	6.3	8.9	12.6
J to FS	4.0	*2.1*	3.0	4.2	5.9	8.4	11.8
J to FS	4.5	*2.0*	2.8	3.9	5.6	7.9	11.1
J to FS	5.0	*1.9*	2.6	3.7	5.3	7.5	10.6
J to FS	5.5	*1.8*	2.5	3.6	5.0	7.1	10.1
J to FS	6.0	*1.7*	*2.4*	3.4	4.8	6.8	9.6

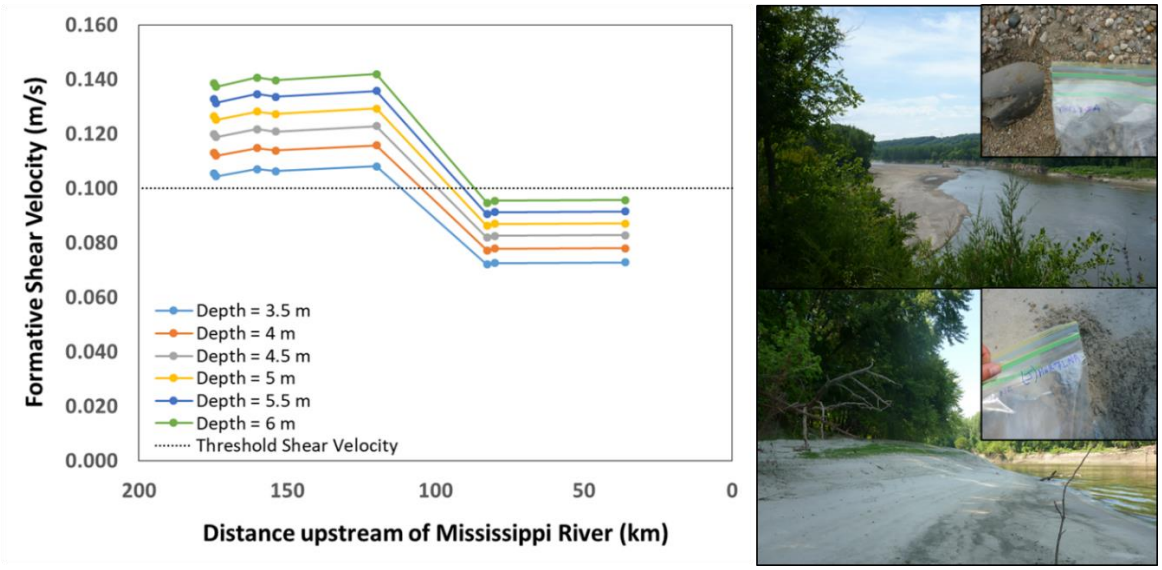

Fig. 4-12. Formative shear velocities for eight grain size measured bars. Threshold shear velocity for suspended sands shown by dashed line at 0.1 m/s. Values less than this threshold indicated suspended sand fallout; values greater than 0.1 m/s indicate suspension transport of sand. Photos show characteristic bars upstream and downstream of Belle Plaine, MN. Upstream of Belle Plaine, bars are short and have a coarse texture, while downstream of Belle Plaine, bars are tall and comprised almost exclusively of fine to medium sand.

factors are necessary to explain why the upstream reach has relatively wider and shallower bars and has migrated and widened twice as fast as the downstream reach.

5.2. Difference in Channel Form is Due to a Discontinuity in Sediment Supply and Transport

Spatial patterns in sediment supply and transport exert strong control over channel morphology and dynamics. Our sediment budgets reveal that 19% of the total load at Mankato is bedload, while less than one percent of this bedload material passes the gage at Jordan (Figure 4-10a) and there is essentially zero bedload transport at Fort Snelling (Figure 4-10b). Twenty percent of the bedload supply in the upstream reach comes from incising and migrating tributary rivers. Although the remaining bedload supply enters the reach at Mankato, the large difference in observed grain sizes above and below the Blue

Earth River confluence suggests that the Blue Earth River, and other large tributaries that enter along this reach, are important sources of coarse bedload material for the Minnesota River. The downstream reach has a lack of large tributaries that directly enter the Minnesota River, and consequently has virtually no bedload supply or transport, according to the sediment budget. This means that virtually all of the bedload entering the reach remains stored within the upstream reach. Suspended sediment transport is similarly heterogeneous along the lower Minnesota River, but for a different reason, as discussed below.

Discontinuity in channel slope is almost always associated with discontinuity in sediment transport. The slope of the Minnesota River decreases by about a factor of two between Mankato and Fort Snelling, with a distinct slope break located upstream of Jordan near river kilometer 85 (Figure 4-2a). Rouse numbers calculated for 0.25 and 0.5 mm sand suggest that roughly 50% of the material is carried in suspension in the upstream reach (Table 4-3). Formative shear velocities indicate that sand should be carried in suspension from Mankato until the slope break that is approximately 20 km upstream of Jordan (Figure 4-12). The Rouse numbers for the downstream reach indicate that 0.5 mm sand is no longer carried in suspension.

Many of the differences in grain size and bar topography can be explained by the differences in supply and transport, upstream and downstream of the slope break. Bars are common topographic features in actively migrating rivers. The presence of unvegetated channel bars indicates the storage of material that was previously active in transport. Sediment supply is necessary for bar maintenance; when sediment supply decreases, the presence of bars diminishes (Venditti et al., 2012). In this case, the loss of

coarse sediment supply (bedload and coarse sand in suspension) downstream of the slope break is associated with a substantial change in bar characteristics.

Bars in Belle Plaine and downstream are tall and go from wide (50 m) at the upstream end of this reach to narrow (20 m) at the downstream end (Figure 4-2d), with a narrow grain size distribution and D_{100} approximately equal to 0.5 mm (Figure 4-3). The observation that half millimeter sands are largely absent from the bed and from the suspended load suggests that bars located at and downstream from Belle Plaine are built from material carried in suspension. Bars located upstream of Belle Plaine are broad, short, and coarser than those downstream. Based on the grain size distributions and Rouse numbers, bars in the upstream reach are built by a combination of bedload and suspended load material, with the relative contribution of bedload greatest at river kilometer 160 and declining downstream (Figure 4-2b). Bedload deposits are wide and shallow in contrast to suspended load deposits (Church, 2006). Bedload is usually coarser than suspended load, and is transported laterally along the river bed rather than vertically in the water column. Therefore bars built by bedload are unlikely to reach the same heights as suspended load built bars. Thus it is reasonable to expect greater bar heights in the downstream reach, consistent with Figure 4-2d. Near Belle Plaine and Jordan, bar heights are close to bank heights, but further upstream and downstream they are not (Figure 4-4). One explanation for this difference is that bar deposition may not be able to keep pace with channel migration (Braudrick et al., 2009). Regardless of the cause, the major driver of bar geometry and bed roughness change in the lower Minnesota is the change in transport and suspension fallout due to the slope break. The slope break is

likely both the cause and effect of the change in sediment transport, and is most certainly linked to the spatial patterns in river morphology and dynamics.

5.3. Difference in Channel Dynamics Explained by Multiple Mechanisms

The upstream reach has consistently exhibited more rapid meander migration rates and has widened considerably more than the downstream reach in response to recent increases in water and sediment supply. The difference in responses could be explained by several mechanisms, which may be working in combination. Three mechanisms are described in detail in the following paragraphs.

First, we observe differences in floodplain characteristics. The downstream reach is less sinuous (1.2) than the upstream reach (1.4), and has an abundance of floodplain lakes present within the alluvial valley. The presence of floodplain lakes indicates that the downstream reach has experienced lower migration rates over Holocene time. As floodplain lakes fill with sediments transported in suspension away from the channel; this creates thick packages of cohesive, fine-grained material in the floodplain. Cohesive bank materials restrict migration and lead to square-like, rather than loop-like, meander bends, which are abundant in the downstream reach. Thus the downstream reach is characterized by confined free meanders, and only migrates within part of the alluvial valley (Ikeda 1989).

The downstream reach also has relatively few cutoffs compared to the upstream reach (Figure 4-5b). The fact that the downstream reach carries nearly all of its load in suspension may explain why the downstream reach has fewer cutoffs, or at least fewer chute cutoffs. Vertical accretion of bars by suspension fallout may prevent the development and growth of chutes between the bar and the floodplain (Braudrick et al.,

2009; Church, 2006). Cutoffs like those seen in the upstream reach shorten the channel and create locally steeper slopes, which may act to increase stress locally and promote bank erosion.

A second possible explanation for the difference in meandering and widening dynamic is that the water surface slope of the downstream reach is controlled by a backwater effect from the Mississippi River. Water surface slopes measured between USGS gages for a range of flows are presented in Table 4-4. In the Mankato to Jordan reach, water surface slopes are near or above measured bed slopes. In contrast, water surface slopes between Jordan and Fort Snelling are below measured bed slopes for all flows. USGS field measurements of hydraulic geometry and velocity at each gage suggest a downstream trend in increasing depth and decreasing velocity for the same discharge at each gage. Thus, it is reasonable to explore the possibility that the downstream backwater affected reach might be associated with lower average and near bank stresses and therefore migrate and widen more slowly than the upstream reach in response to similar flow increases.

So, what might be controlling the downstream end of the backwater affected reach? The backwater from the Mississippi may not have always been important in the evolution of the lower Minnesota given that the Jordan to Fort Snelling channel was wider than the Mankato to Jordan reach in 1937 (Table 4-2). Lock and Dam #2 is located 43 km downstream from the confluence of the Minnesota and Mississippi Rivers, and was constructed in 1930 with additional work in 1948 due to settling (U.S. Army Corps of Engineers, n.d.). Army Corps of Engineers stage record for the pool at Lock & Dam 2 indicates approximately 3 m of stage increase since 1932. Assuming the Mississippi

River slope is similar to the downstream reach of the Minnesota River, 0.0001, and depth is 6 m according to USGS hydraulic geometry (gage 05331000), 3 m of stage increase would increase the backwater length from 60 km to 90 km (Paola and Mohrig, 1996). Considering construction of the dam in 1930 and the recorded 3 m stage increase between 1932 and 1948, the total stage increase experienced by the lower Minnesota River since 1930 was likely closer to 6 m. Thus the total length of the Minnesota River affected by the Lock and Dam #2 backwater is approximately 120 km, which includes the entire Jordan to Fort Snelling reach. The timing of the stage increase on the Mississippi coincides with slowed widening on the Minnesota River in the Jordan to Fort Snelling reach. By 1951, the Mankato to Jordan reach was slightly wider than the Jordan to Fort Snelling Reach. The backwater may also explain size selective suspended transport (Table 4-3) and observed downstream fining (Figure 4-2b) (Wright and Parker, 2005).

A third explanation for the disparities in widening and migration rates along the Minnesota River involves the interactions between flow, sediment supply, and bar topography. Increased sediment supply has been associated with higher bank erosion rates through field and flume studies, but has yet to be linked in a predictive framework. Constantine et al. (2014) found higher migration rates associated with higher sediment supply in the Amazon basin. The downstream reach has a smaller sediment budget, does not have a bedload supply, and exhibits a lower slope and reduced migration and widening. Flume experiments by Friedkin (1945) showed that a lack of sand feed, or bedload supply, led to channel deepening and eventual slope reduction that slowed bank erosion. Similar results were reported by Venditti et al. (2012), where flume sediment supply termination resulted in bar erosion, slope reduction, and reduction in boundary

shear stress. Slope reduction has been associated with decreased meander migration rates in field and flume studies (Dietrich et al., 1999; Friedkin, 1945). Thus the lack of bedload supply in the downstream reach could be the cause, rather than effect of the reduction in slope.

Although the bars in the downstream reach are taller than the upstream reach, they are considerably narrower once downstream of Jordan (Figure 4-2d, Figure 4-13). If these bars are forced by planform curvature, it may be that suspended load may only deposit in narrow shear zones on the inside of the bend. The topographic steering effect of these narrow bars may be diminished, even though they are tall, if they do not sufficiently "push" the thalweg and zone of maximum shear stress towards the outer bank. Dietrich and Whiting (1989) investigated point bars and their effect on local flow accelerations, stresses, and transport in meandering rivers. Following from their work, we investigate how bar form may be influencing sediment transport.

For meandering sand-bed rivers, the cross stream sediment transport component should be negligible except for rivers with pools at the upstream end of the bend, high width to depth ratios and a minimum elevation near the channel center, and bars with flat tops (Dietrich and Whiting, 1989). In the upstream reach of the Minnesota River, bars are broad and relatively flat because they are primarily composed of bedload material (Figure 4-13). Stage dependent bar aggradation leads to temporary decrease in the cross stream transport during stage rise, and local scour of the pool (Dietrich and Whiting, 1989). Once the pool has sufficiently deepened to steepen the transverse bar slope, net outward transport of sediment to the pool may resume. This phenomenon likely oversteepens, and even leads to scour of, the outside bank, encouraging meander migration. Therefore tall

but narrow bars composed of suspended load may be less effective at bar push than broad short bars, like those located further upstream. Although this idea cannot be fully tested in this paper, it does offer a possible explanation for variation in migration and widening rates between the two reaches. Future work should investigate what mechanistic links exist between sediment supply, transport state, and meander migration.

6. Conclusion

Leveraging existing datasets combined with new data we found that spatial variation in slope, sediment supply and transport, floodplain characteristics, and backwater effects can explain many of the observed differences in form and dynamics between the upstream reach and downstream reach of the lower Minnesota River. The transition in channel grain size as well as bar amplitude and extent between the upstream and downstream reach coincides with a slope break that results in larger Rouse numbers and smaller formative shear velocities in the downstream reach. Thus, suspended sands may readily be deposited in the downstream reach. The tall, but narrow bars in the downstream reach are likely forced due to channel curvature induced flow separation and comprised exclusively of suspended load fallout.

Table 4-4. Water surface slopes measured between gages at different discharges, ranging from low flows to out of bank flows (40,000 cfs). The last row presents bathymetry measured bed slopes at the upstream (right) and downstream (left) end of each reach.

Discharge (cfs)	Mankato to Jordan	Jordan to Fort Snelling
5000	0.000166	0.000057
10000	0.000168	0.000076
20000	0.000152	0.000086
40000	0.000146	0.000083
Bed Slope	0.000102 - 0.000156	0.000089 - 0.000102

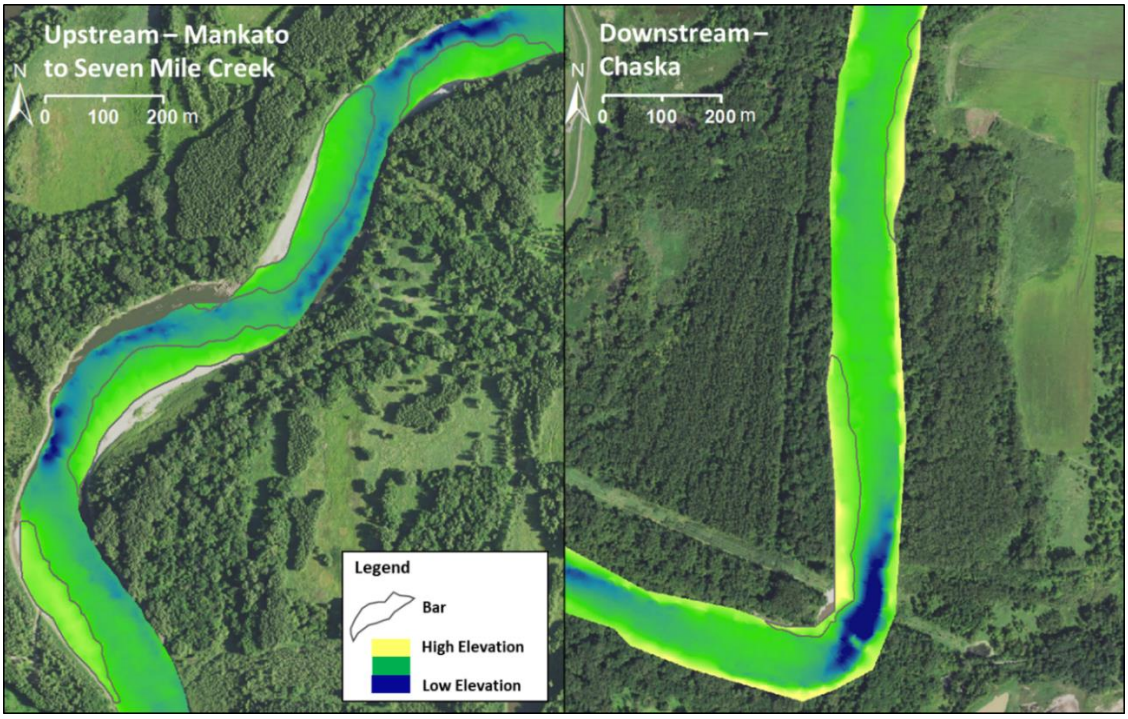

Fig. 4-13. Bar and bend geometry at an upstream section near Mankato and a downstream section near Chaska. Elevation color scheme is relative as it does not relate to the bar and bend geometry.

The downstream reach is migrating and widening more slowly than the upstream reach. The presence of thick fine-grained sediments in floodplain lakes in the downstream reach may explain why the channel is eroding its banks more slowly. Additionally, the downstream reach is affected by backwater effects from the Mississippi River. The timing of slowed widening in the downstream reach coincides with the construction of Lock & Dam 2, which raised the elevation of the Mississippi by at least 3 m. Another explanation for the difference in dynamics is that the downstream reach lacks a bedload supply and the presence of narrow forced bars in the downstream reach are less effective at bar "push" than bedload built alternate and point bars in the upstream reach. This idea should be explored further by future flume and/or field experiments.

In conclusion, the Minnesota River is dynamically responding to 20th and 21st century streamflow increases through meander migration and widening. Modern migration rates in the upstream and downstream reach are 1.2 and 0.5 percent of channel widths per year, respectively. Since 1937, the upstream reached has widened by as much as 150% while the downstream reach has widened less than 70%. The degree of dynamism is spatially discontinuous, as are changes in channel form. Though sediment supply and transport likely explains channel form, linking the dynamics to sediment supply and transport is not straightforward. Understanding how sediment supply and transport influence channel dynamics is critical for the Minnesota River and other rivers that are experiencing systematic changes in flow and bedload supply from tributaries. This understanding improves our ability to predict river dynamics and make informed restoration and/or risk mitigation decisions. In the case of the Minnesota River, flow increases should be mitigated when possible to reduce flood risk and property loss while the channel transiently responds through migration and widening so to establish a new equilibrium.

References

Abad, J.D., García, M.H., 2006. Discussion of "Efficient Algorithm for Computing Einstein Integrals" by Junke Guo and Pierre Y. Julien. J. Hydraul. Eng. 132, 332–334. https://doi.org/10.1061/(ASCE)0733-9429(2006)132:3(332)

Andrews, E.D., Nelson, J.M., 1989. Topographic Response of a Bar in the Green River, Utah to Variation in Discharge, in: Ikeda, S., Parker, G. (Eds.), River Meandering. American Geophysical Union, Washington D.C., pp. 463–485.

Belmont, P., 2011. Floodplain width adjustments in response to rapid base level fall and knickpoint migration. Geomorphology 128, 92–101. https://doi.org/10.1016/j.geomorph.2010.12.026

Belmont, P., Gran, K.B., Schottler, S.P., Wilcock, P.R., Day, S.S., Jennings, C., Lauer,

J.W., Viparelli, E., Willenbring, J.K., Engstrom, D.R., Parker, G., 2011. Large shift in source of fine sediment in the upper Mississippi River. Environ. Sci. Technol. 45, 8804–8810. https://doi.org/10.1021/es2019109

Belmont, P., Stevens, J.R., Czuba, J.A., Kumarasamy, K., Kelly, S.A., 2016. Comment on "Climate and agricultural land use change impacts on streamflow in the upper midwestern United States," by Satish C. Gupta et al. Water Resour. Res. 52, 7523–7528. https://doi.org/10.1002/2015WR018476

Best, J.L., 1988. Sediment transport and bed morphology at river channel confluences. Sedimentology 35, 481–498.

Blanckaert, K., 2010. Topographic steering, flow recirculation, velocity redistribution, and bed topography in sharp meander bends. Water Resour. Res. 46, 1–23. https://doi.org/10.1029/2009WR008303

Bradley, C., Smith, D.G., 1984. Meandering channel response to altered flow regime: Milk River, Alberta and Montana. Water Resour. Res. 20, 1913–1920. https://doi.org/10.1029/WR020i012p01913

Braudrick, C.A., Dietrich, W.E., Leverich, G.T., Sklar, L.S., 2009. Experimental evidence for the conditions necessary to sustain meandering in coarse-bedded rivers. Proc. Natl. Acad. Sci. 106, 16936–16941. https://doi.org/10.1073/pnas.0909417106

Burt, T.P., Allison, R.J., 2010. Sediment cascades in the environment: an integrated approach, in: Burt, T.P., Allison, R.J. (Eds.), Sediment Cascades: An Integrated Approach. John Wiley and Sons Ltd, West Sussex, United Kingdom, pp. 1–15.

Call, B.C., Belmont, P., Schmidt, J.C., Wilcock, P.R., 2017. Changes in floodplain inundation under nonstationary hydrology for an adjustable, alluvial river channel. Water Resour. Res. 53, 3811–3834. https://doi.org/10.1002/2016WR020277

Church, M., 2006. Bed Material Transport and the Morphology of Alluvial River Channels. Annu. Rev. Earth Planet. Sci. 34, 325–354. https://doi.org/10.1146/annurev.earth.33.092203.122721

Church, M., Rice, S.P., 2009. Form and growth of bars in a wandering gravel-bed river. Earth Surf. Process. Landforms 34, 1422–1432. https://doi.org/10.1002/esp

Clayton, L., Moran, S.R., 1982. Chronology of late wisconsinan glaciation in middle North America. Quat. Sci. Rev. 1, 55–82. https://doi.org/10.1016/0277-3791(82)90019-1

Constantine, J.A., Dunne, T., Ahmed, J., Legleiter, C., Lazarus, E.D., 2014. Sediment

supply as a driver of river meandering and floodplain evolution in the Amazon Basin. Nat. Geosci. 7, 899–903. https://doi.org/10.1038/ngeo2282

Dade, W.B., Friend, P.F., 1998. Grain Size, Sediment Transport Regime, and Channel Slope in Alluvial Rivers. J. Geol. 106, 661–676. https://doi.org/10.1086/516052

Dietrich, W.E., 1982. Settling velocity of natural particles. Water Resour. Res. 18, 1615–1626. https://doi.org/10.1029/WR018i006p01615

Dietrich, W.E., Day, G., Parker, G., 1999. The Fly River, Papua New Guinea: Inferences about River Dynamics, Floodplain Sedimentation and Fate of Sediment, in: Miller, A.J., Gupta, A. (Eds.), Varieties of Fluvial Form. Wiley, pp. 345–376.

Dietrich, W.E., Whiting, P., 1989. Boundary Shear Stress and Sediment Transport in River Meanders of Sand and Gravel, in: Ikeda, S., Parker, G. (Eds.), River Meandering. American Geophysical Union, Washington D.C., pp. 1–50.

Dietrich, W.E., Dunne, T., 1978. Sediment budget for a small catchment in mountainous terrain. Z. Geomorph. N. F., Suppl. Bd. 29, 191–206.

Donovan, M., Belmont, P., 2019. Timescale Dependence in River Channel Migration Measurements. Earth Surf. Process. Landforms. https://doi.org/10.1002/esp.4590

Erwin, S.O., 2013. Development of sediment budgets at multiple scales. Utah State University.

Erwin, S.O., Schmidt, J.C., Wheaton, J.M., Wilcock, P.R., 2012. Closing a sediment budget for a reconfigured reach of the Provo River, Utah, United States. Water Resour. Res. 48, 1–13. https://doi.org/10.1029/2011WR011035

Ferguson, R.I., 2003. Emergence of abrupt gravel to sand transitions along rivers through sorting processes. Geology 31, 159–162. https://doi.org/10.1130/0091-7613(2003)031<0159:EOAGTS>2.0.CO;2

Foufoula-Georgiou, E., Belmont, P., Wilcock, P., Gran, K., Finlay, J.C., Kumar, P., Czuba, J.A., Schwenk, J., Takbiri, Z., 2016. Comment on “Climate and agricultural land use change impacts on streamflow in the upper midwestern United States” by Satish C. Gupta et al. Water Resour. Res. 52, 7536–7539. https://doi.org/10.1002/2015WR018494

Foufoula-Georgiou, E., Takbiri, Z., Czuba, J.A., Schwenk, J., 2015. The change of nature and the nature of change in agricultural landscapes: Hydrologic regime shifts modulate ecological transitions. Water Resour. Res. 51, 6649–6671. https://doi.org/10.1002/2015WR017637

Friedkin, J.F., 1945. A Laboratory Study of the Meandering of Alluvial Rivers. Vicksburg, Mississippi.

Frings, R.M., 2008. Downstream fining in large sand-bed rivers. Earth-Science Rev. 87, 39–60. https://doi.org/10.1016/j.earscirev.2007.10.001

Garcia, M.H., 1999. Sedimentation and Erosion Hydraulics, in: Mays, L. (Ed.), Hydraulic Design Handbook. McGraw-Hill Inc.

Garcia, M.H., 2008. Sediment Transport and Morphodynamics, in: Garcia, M. (Ed.), Sedimentation Engineering. American Society of Civil Engineers, Reston, VA, pp. 21–163. https://doi.org/10.1061/9780784408148

Garcia, M., Parker, G., 1991. Entrainment of Bed Sediment into Suspension. J. Hydraul. Eng. 117, 414–435. https://doi.org/10.1061/(ASCE)0733-9429(1991)117:4(414)

Gran, K., Dolph, C., Baker, A., Bevis, M., Cho, S.J., Czuba, J.A., Dalzell, B., Hansen, A., Kelly, S., Lang, Z., Schwenk, J., Belmont, P., Finlay, J.C., Kumar, P., Rabotyagov, S., Roehrig, G., Wilcock, P., Foufoula-Georgiou, E., In review. Data synthesis for collaborative, multidisciplinary research in an intensively managed agricultural landscape: the Minnesota River Basin environmental observatory. Water Resour. Res.

Gran, K.B., Finnegan, N., Johnson, A.L., Belmont, P., Wittkop, C., Rittenour, T., 2013. Landscape evolution, valley excavation, and terrace development following abrupt postglacial base-level fall. Geol. Soc. Am. Bull. https://doi.org/10.1130/B30772.1

Gran, K.B., Belmont, P., Day, S.S., Jennings, C., Johnson, A., Perg, L., Wilcock, P.R., 2009. Geomorphic evolution of the Le Sueur River, Minnesota, USA, and implications for current sediment loading, in: James, L.A., Rathburn, S.L., Whittecar, G.R. (Eds.), Management and Restoration of Fluvial Systems with Broad Historical Changes and Human Impacts. Geological Society of America.

Groten, J.T., Ellison, C.A., Hendrickson, J.S., 2016. Suspended-Sediment Concentrations, Bedload, Particle Sizes, Surrogate Measurements, and Annual Sediment Loads for Selected Sites in the Lower Minnesota River Basin, Water Years 2011 through 2016, U.S. Geological Survey Scientific Investigations Report 2016-5174. Reston, VA.

Harrison, L.R., Legleiter, C.J., Wydzga, M.A., Dunne, T., 2011. Channel dynamics and habitat development in a meandering, gravel bed river. Water Resour. Res. 47, 1–21. https://doi.org/10.1029/2009WR008926

Henderson, F.M., 1966. Open Channel Flow. Macmillan, New York.

Hoffman, D.F., Gabet, E.J., 2007. Effects of sediment pulses on channel morphology in a gravel-bed river. Bull. Geol. Soc. Am. 119, 116–125. https://doi.org/10.1130/B25982.1

Ikeda, H., 1989. Sedimentary Controls on Channel Migration and Origin of Point Bars in Sand-Bedded Meandering Rivers, in: Ikeda, S., Parker, G. (Eds.), River Meandering. American Geophysical Union, Washington D.C., pp. 51–68.

Jennings, C.E., 2010. OFR10-03, Geomorphology and Reconnaissance Surficial Geology of the Le Sueur River Watershed.

Jerolmack, D.J., Brzinski, T.A., 2010. Equivalence of abrupt grain-size transitions in alluvial rivers and eolian sand seas: A hypothesis. Geology 38, 719–722. https://doi.org/10.1130/G30922.1

Kelly, S., Call, B., Levine, S., Belmont, P., Larson, P., 2018. Minnesota River Bathymetry: 2013 - 2016 [WWW Document]. HydroShare. URL http://dx.doi.org/10.4211/hs.6cd3728f69cb4cb39c6f11baac1734ec%0A

Kelly, S.A., Takbiri, Z., Belmont, P., Foufoula-Georgiou, E., 2017. Human amplified changes in precipitation-runoff patterns in large river basins of the Midwestern United States. Hydrol. Earth Syst. Sci. 1–37. https://doi.org/10.5194/hess-2017-133

Kelly, S.A., Belmont, P., 2018. High resolution monitoring of river blufferosion reveals failure mechanisms and geomorphically effective flows. Water 10. https://doi.org/10.3390/w10040394

Kondolf, G.M., Piégay, H., Landon, N., 2002. Channel response to increased and decreased bedload supply from land use change: Contrasts between two catchments. Geomorphology 45, 35–51. https://doi.org/10.1016/S0169-555X(01)00188-X

Lach, J., Wyga, B., 2002. Channel incision and flow increase of the upper Wisłoka river, Southern Poland, subsequent to the reafforestation of its catchment. Earth Surf. Process. Landforms 27, 445–462. https://doi.org/10.1002/esp.329

Lamb, M.P., Venditti, J.G., 2016. The grain size gap and abrupt gravel-sand transitions in rivers due to suspension fallout. Geophys. Res. Lett. 43, 3777–3785. https://doi.org/10.1002/2016GL068713

Lane, E.W., 1955. The importance of fluvial morphology in hydraulic engineering. Proceedings, Am. Soc. Civ. Eng. 18, 1–17.

Lane, S.N., Reid, S.C., Tayefi, V., Yu, D., Hardy, R.J., 2008. Reconceptualising coarse sediment delivery problems in rivers as catchment-scale and diffuse. Geomorphology 98, 227–249. https://doi.org/10.1016/j.geomorph.2006.12.028

Lauer, J.W., Parker, G., 2008. Net local removal of floodplain sediment by river meander

migration. Geomorphology 96, 123–149. https://doi.org/10.1016/j.geomorph.2007.08.003

Lauer, J.W., Echterling, C., Lenhart, C., Belmont, P., Rausch, R., 2017. Air-photo based change in channel width in the Minnesota River basin: Modes of adjustment and implications for sediment budget. Geomorphology 297, 170–184. https://doi.org/https://doi.org/10.1016/j.geomorph.2017.09.005

Lenhart, C.F., Titov, M.L., Ulrich, J.S., Nieber, J.L., Suppes, B., 2013. The Role of Hydrologic Alteration and Riparian Vegetation Dynamics in Channel Evolution along the Lower Minnesota River. Trans. Am. Soc. Agric. Biol. Eng. 56, 549–561.

Li, C., Czapiga, M.J., Eke, E.C., Viparelli, E., Parker, G., 2015. Variable Shields number model for river bankfull geometry: Bankfull shear velocity is viscosity-dependent but grain size-independent. J. Hydraul. Res. 53, 36–48. https://doi.org/10.1080/00221686.2014.939113

Libby, D., 2018. Assessing historical planform channel change in an altered watershed with quantification of error and uncertainty present in a GIS/aerial photography-based analysis; case study: Minnesota River, Minnesota, USA. Minnesota State University.

Macdonald, J.S., Beaudry, P.G., MacIsaac, E. a, Herunter, H.E., 2003. The effects of forest harvesting and best management practices on streamflow and suspended sediment concentrations during snowmelt in headwater streams in sub-boreal forests of British Columbia, Canada. Can. J. For. Res. 33, 1397–1407. https://doi.org/10.1139/x03-110

Massong, T.M., Montgomery, D.R., 2000. Influence of sediment supply, lithology, and wood debris on the distribution of bedrock and alluvial channels. GSA Bull. 112, 591–599. https://doi.org/10.1130/0016-7606(2000)112<591

Menard, H.W., 1950. Sediment Movement in Relation to Current Velocity. J. Sediment. Petrol. 20, 148–160.

Minnesota Pollution Control Agency, 2018. Minnesota's Proposed 2018 Impaired Waters List.

Montgomery, D.R., 2007. Is agriculture eroding civilization's foundation? GSA Today 17, 4–9. https://doi.org/10.1130/GSAT01710A.1

Nanson, G.C., 1980. Point bar and floodplain formation of the meandering Beatton River, northeastern British Columbia, Canada. Sedimentology 27, 3–29. https://doi.org/10.1111/j.1365-3091.1980.tb01155.x

Nelson, P.A., Venditti, J.G., Dietrich, W.E., Kirchner, J.W., Ikeda, H., Iseya, F., Sklar, L.S., 2009. Response of bed surface patchiness to reductions in sediment supply. J. Geophys. Res. Earth Surf. 114, 1–18. https://doi.org/10.1029/2008JF001144

Nicholas, A.P., Ashworth, P.J., Kirkby, M.J., Macklin, M.G., Murray, T., 1995. Sediment slugs: large-scale fluctuations in fluvial sediment transport rates and storage volumes. Prog. Phys. Geogr. 19, 500–519. https://doi.org/10.1177/030913339501900404

Novotny, E. V., Stefan, H.G., 2007. Stream flow in Minnesota: Indicator of climate change. J. Hydrol. 334, 319–333. https://doi.org/10.1016/j.jhydrol.2006.10.011

Paola, C., Mohrig, D., 1996. Palaeohydraulics revisited: palaeoslope estimation in coarse-grained braided rivers. Basin Res. 8, 243–254.

Paola, C., Parker, G., Seal, R., Sinha, S.K., Southard, J.B., Wilcock, P.R., Paola, C., Parker, G., Seal, R., Sinha, S.K., Southard, J.B., Wilcock, P.R., 1992. Downstream Fining by Selective Deposition in a Laboratory Flume. Science 258, 1757–1760.

Pitlick, J., 1993. Response and recoveiy of a subalpine stream. Geol. Soc. Am. Bull. 105, 657–670. https://doi.org/10.1130/0016-7606(1993)105<0657

Podolak, C.J.P., Wilcock, P.R., 2013. Experimental study of the response of a gravel streambed to increased sediment supply. Earth Surf. Process. Landforms 38, 1748–1764. https://doi.org/10.1002/esp.3468

Ramirez, M.T., Allison, M.A., 2013. Suspension of bed material over sand bars in the Lower Mississippi River and its implications for Mississippi delta environmental restoration. J. Geophys. Res. Earth Surf. 118, 1085–1104. https://doi.org/10.1002/jgrf.20075

Recking, A., 2016. A generalized threshold model for computing bed load grain size distribution. Water Resour. Res. 52, 9274–9289. https://doi.org/10.1002/2016WR018977.Received

Reid, L., Dunne, T., 2016. Sediment budgets as an organizing framework in fluvial geomorphology, in: Kondolf, G.M., Piégay, H. (Eds.), Tools in Fluvial Geomorphology. John Wiley and Sons Ltd, Chichester, United Kingdom, pp. 357–379.

Schottler, S.P., Urlich, J., Belmont, P., Moore, R., Lauer, J.W., Engstrom, D.R., Almendinger, J.E., 2014. Twentieth century agricultural drainage creates more erosive rivers. Hydrol. Process. 28, 1951–1961. https://doi.org/10.1002/hyp.9738

Sella, G.F., Stein, S., Dixon, T.H., Craymer, M., James, T.S., Mazzotti, S., Dokka, R.K.,

2007. Observation of glacial isostatic adjustment in “stable” North America with GPS. Geophys. Res. Lett. 34, 1–6. https://doi.org/10.1029/2006GL027081

Smelser, M.G., Schmidt, J.C., 1998. An assessment methodology for determining historical changes in mountain streams. Fort Collins, CO.

Teller, J.T., Boyd, M., Yang, Z., Kor, P.S.G., Fard, A.M., 2005. Alternative routing of Lake Agassiz overflow during the Younger Dryas: New dates, paleotopography, and a re-evaluation. Quat. Sci. Rev. 24, 1890–1905. https://doi.org/10.1016/j.quascirev.2005.01.008

Trimble, S.W., 1999. Decreased Rates of Alluvial Sediment Storage in the Coon Creek Basin, Wisconsin, 1975-93. Science (80-.). 285, 1244–1246. https://doi.org/10.1126/science.285.5431.1244

Van Dijk, W.M., Van De Lageweg, W.I., Kleinhans, M.G., 2012. Experimental meandering river with chute cutoffs. J. Geophys. Res. 117, 1–18. https://doi.org/10.1029/2011JF002314

Venditti, J.G., Nelson, P.A., Minear, J.T., Wooster, J., Dietrich, W.E., 2012. Alternate bar response to sediment supply termination. J. Geophys. Res. 117, 1–18. https://doi.org/10.1029/2011JF002254

Venditti, J.G., Church, M., 2014. Morphology and controls on the position of a gravel-sand transition: Fraser River, British Columbia. J. Geophys. Res. Earth Surf. 119, 1959–1976. https://doi.org/10.1002/2014JF003147.Received

Wheaton, J.M., Brasington, J., Darby, S.E., Sear, D.A., 2010. Accounting for uncertainty in DEMs from repeat topographic surveys: Improved sediment budgets. Earth Surf. Process. Landforms 35, 136–156. https://doi.org/10.1002/esp.1886

Wilcock, P., Baskfield, P., Belmont, P., Birr, A., Cooper, P., Engstrom, D., Jennings, C., Kiesling, R., Matteson, S., Mulla, D., Nieber, J., Regan, C., Schottler, S., 2009. Identifying sediment sources in the Minnesota River Basin. Minnesota River Sediment Colloq. 1–16.

Wilkerson, G. V., Parker, G., 2011. Physical Basis for Quasi-Universal Relationships Describing Bankfull Hydraulic Geometry of Sand-Bed Rivers. J. Hydraul. Eng. 137, 739–753. https://doi.org/10.1061/(ASCE)HY.1943-7900.0000352

Wilkinson, B.H., McElroy, B.J., 2007. The impact of humans on continental erosion and sedimentation. Bull. Geol. Soc. Am. 119, 140–156. https://doi.org/10.1130/B25899.1

Wright, S., Parker, G., 2005. Modeling downstream fining in sand-bed rivers. II:

application. J. Hydraul. Res. 43, 621–631. https://doi.org/10.1080/00221680509500382

Zhang, L., Stark, C., Schumer, R., Kwang, J., Li, T., Fu, X., Wang, G., Parker, G., 2018. The Advective-Diffusive Morphodynamics of Mixed Bedrock-Alluvial Rivers Subjected to Spatiotemporally Varying Sediment Supply. J. Geophys. Res. Earth Surf. https://doi.org/10.1029/2017JF004431

CHAPTER 5

CONCLUSION

This dissertation explores the linkages between agricultural drainage, streamflows (chapter 2), and sediment problems in the Minnesota River Basin (chapters 3 & 4). Our findings that agricultural drainage increases flows and exacerbates erosion of near channel sources, which in turn amplify channel morphodynamics suggest that gains in water quality will require flow reductions and cooperation with farmers and agricultural drainage districts. In chapters 2-4, I demonstrate that agricultural drainage has indeed amplified streamflow, and larger streamflows have increased the erosion of near channel sources through bluff erosion, channel migration and widening. In this chapter, I discuss the main findings from each chapter in the context of their implications for the science and management of riverine sediment.

Since the early twentieth century artificial drainage extent and agricultural production have both increased significantly throughout the upper Midwestern US. Extensively drained river basins have experienced a high degree of streamflow increase. The water budgets in chapter 2 reveal that while precipitation has increased, temporary storage of surface and sub-surface water has decreased significantly in intensively drained basins throughout the upper Midwest. In the Minnesota River basin, flows have more than doubled, while precipitation only increased 10% between the pre- and post-land use land cover periods. Annual water budgets compiled for 1935-1978 and 1979-2011 demonstrate that ground, lake, and/or soil water storage in the Minnesota River Basin have decreased on the order of, and perhaps by more than, 200%. Although the adjacent Red River of the North basin has exhibited slightly greater flow increases,

precipitation increases were also greater and expansion of artificial has occurred more recently. Thus, the 1935-2003 and 2004-2011 water budgets demonstrate that storage in the Red River of the North has decreased by 30%. These results are qualitatively supported by the notion that the Red River of the North basin is less extensively drained than the Minnesota River basin. The Illinois River basin is also heavily agricultural, and has experienced a 100% decrease in ground, lake, and/or soil water storage from 1939-1961 to 1962-2011. The results of this chapter suggest that enhanced hydrologic connectivity imparted by artificial agricultural drainage appears to have amplified the streamflow response to precipitation increases in the Midwest. Better documentation of tile drainage density would greatly enhance our ability to understand and predict the effects of artificial drainage on streamflows at large spatial scales. Recognizing that tile drainage has likely played a large role in the increased crop yields that have been documented in the upper Midwestern US over the past few decades, it is unlikely that they would be removed. And given their role in desiccating soils and therefore reducing surface water runoff and associated sheet and rill erosion, their removal is not necessarily desirable. An alternative approach to counteracting the downstream impacts of tile drainage would be to divert tile lines to temporary water detention basins. Diversion of tile lines to detention basins is especially needed in spring and early summer months, when precipitation events are large and fields are soggy and bare, to dampen large runoff events (Cho et al., 2019; Mitchell et al., 2018).

Bluffs are particularly sensitive to erosion during large flood events, precipitation events, and seasonal freeze-thaw. Chapter 3 investigates the influence of several erosion processes on bluffs and determined that fluvial scour was the most important mechanism

for near channel erosion of river bluffs. Larger floods caused more erosion, but occur less frequently than smaller floods. Even small flows, a mere 30% of the two-year recurrence interval flow, are capable of causing bluff erosion. Therefore, based on analysis of daily flows over the past 78 years, I found that the 1.2 year return interval flood accomplishes the most cumulative erosion and is thus more geomorphically effective than other flood magnitudes. The frequency of this flood event has increased from 20 days/yr (1940-1979) to 45 days/yr (1980-2017). Given bluff erosion sensitivity to fluvial scour, flow reductions through drainage water retention should lead to sediment reductions from bluffs. The empirical bluff erosion relation developed here can be used by the Minnesota Pollution Control Agency, Minnesota Board of Soil and Water Resources, or restoration practitioners to determine magnitude-frequency tradeoffs between flow reductions and sediment reductions in order to guide conservation and restoration efforts.

The Minnesota River Basin provides an extraordinary opportunity to study watershed sediment dynamics from sources, such as bluffs, to sinks, such as the lower Minnesota River. Few other river systems have been as extensively monitored and exhibit such a wide range of geomorphic environments, from some of the most rapidly incising rivers in the world, to actively aggrading reaches and from highly dynamic reaches that change on an annual basis to reaches that have remained relatively static for decades. Leveraging existing datasets with new data, chapter 5 identifies a spatial discontinuity in slope, sediment supply and transport, floodplain characteristics, and backwater effects along lower Minnesota River, explores the cause of this discontinuity, and discusses the implications for river channel morphology and dynamics. Specifically, I quantify substantial differences in channel morphology and dynamics between the

lowermost 65 kilometers of the Minnesota River, essentially from Fort Snelling to Jordan, Minnesota, and the preceding 100 kilometers of the river, essentially from Jordan to Mankato, Minnesota. The sediment budgets I compiled for each of these distinct reaches reveal that a considerable amount of sediment exchange occurs in the upper reach, via channel migration and widening, and relatively little sediment exchange occurs in the lower reach. Notably, channel widening and meander migration were the largest sources of sediment to the upstream reach, and this reach was the largest source of sediment to the downstream reach. The upstream reach has a considerable bedload supply and is a mixed (bed and suspended) load river system, while the downstream reach is suspended load dominated. A spatial discontinuity in sediment supply and transport, due to fewer tributaries and a break in slope around river kilometer 85 is associated with an abrupt grain size transition as well as a change in the amplitude of bars between the upstream and downstream reach. Floodplain characteristics, backwater from the Mississippi River, and a lack of bedload supply slow rates of channel migration and widening in the downstream reach of the Minnesota River. Above the backwater reach the channel migrates and widens faster, and is met by several tributaries, which provide coarse sand and fine gravel bedload for maintaining alternate and point bars. I propose that broad, bedload-built alternate bars may be more effective at promoting channel migration than narrow, suspended load-built forced bars. The results of this study highlight the importance of sediment supply and transport on river morphology, and underscores the necessity for a mechanistic understanding of how sediment supply and transport affect river meander migration. Flow reductions in the Minnesota River Basin would likely dampen rates of migration and widening, and thus reduce rates of sediment

recruitment from near channel sources, including tributary bluffs and Minnesota River streambanks.

The combined results of this work have important science and management implications for Midwest rivers. Accounting for specific processes and understanding how they may change over different spatiotemporal scales is challenging and yet necessary in river science and management. Although tile drainage effects are well understood at the field scale (Hillel, 1998), much less is known about their effect over large scales. Better, publicly available documentation of tile drainage would greatly enhance our ability to directly account for drainage effects over large scales.

Game cameras captured two large streamflow events during the bluff erosion study. These events were important for identifying the geomorphically effective flows for bluff erosion, especially over the last 78 years. In the absence of these large events, the ability to predict bluff erosion for large magnitude flood events in the past and/or future would not be as robust. Thus, there is a need for more long-term monitoring, more spatially distributed monitoring of actively eroding features, and better modeling and analytical techniques to estimate erosion associated with large events in the absence of direct measurements.

Development of bars from either bedload or suspended load may explain differences in meander migration and widening rates. There is a need to mechanistically understand how sediment supply (quantity, grain size, and mode of transport) influences channel dynamics in large, sediment-impaired rivers so that effective sediment reduction strategies may be developed. For the Minnesota River basin, if bedload supply from incising and migrating tributaries is amplifying channel dynamics and therefore recruiting

sediment from the channel margins, then reducing flows and erosion of near-channel sediment sources via water retention in upland agricultural fields may be an effective management action to reduce overall sediment loading and risks posed to infrastructure by rapidly migrating river channels.

In the Minnesota River Basin, drastic sediment reduction measures are needed to achieve an 80-90% sediment load reduction to meet the current total daily maximum load (TMDL) target (Gunderson et al., 2014) set by the Minnesota Pollution Control Agency (MPCA), Minnesota's regulatory agency for environmental and water quality. MPCA's current Sediment Reduction Strategy for the Minnesota River Basin and South Metro Mississippi River has set two interim benchmarks towards achieving the TMDL: 25% reduction in sediment loading by 2025 and 50% reduction by 2030. Model results suggest that, in order to meet the TMDL, sediment loads must be reduced by approximately 1 million tons per year (Gunderson et al., 2014). With much of the sediment in the basin coming from near channel sources, meeting this load reduction will be a challenging, if not impossible task without streamflow management (Cho et al., 2019; Lenhart et al., 2018).

Streamflow management may be a viable sediment reduction option for the Minnesota River Basin given the available resources in the state. In 2008, Minnesota passed a sales tax under the Clean Water, Land and Legacy Amendment (CWLLA), to improve the State's water quality with an annual fund of approximately $90 million (Eshenaur et al., 2014). One of the specific goals for rivers and streams is to increase the index of biological integrity (IBI) for fish communities. The goal for the Minnesota River is to increase IBI by 16%, and is the most ambitious for the state (Eshenaur et al., 2014).

Part of the CWLLA's funds support the MPCA, who have financially supported research on sediment sources within the Minnesota River Basin. Now that the MPCA has been monitoring water quality to establish baseline conditions for several years, strategies for restoration can be designed and implemented.

The work presented in this dissertation provides historical context for current conditions and a basis for developing water reduction strategies in the basin. Streamflows have increased as a result of climate and land use change and erosion of near channel sources is the largest sediment source for tributaries, as well as the mainstem Minnesota River. Temporarily detaining tile drainage water so the landscape drains more slowly appears to be an essential approach for reducing sediment loads. Implementing targeted water detention throughout a large watershed such as the Minnesota River Basin will require that the MPCA work with individual farmers and agricultural drainage districts to dedicate land for detention basins and to divert tile lines to detention basins.

Results from the Minnesota River basin are reasonably applicable to many other landscapes that have relatively weak bedrock with significant base level changes, especially if they have experienced recent changes in hydrology. Incising rivers appear to be more vulnerable to perturbations such as land use and hydrologic change (Gran et al. 2009). Large areas of the Midwest have been cleared and drained for agricultural development. Furthermore, large areas of the Midwest are underlain by easily erodible material such as till and loess. Therefore, the story of streamflow increase and rapid channel adjustment is not limited to the Minnesota River Basin. Simon and Rinaldi (2000) documented channel enlargement through incision, channel widening, and meander extension in several loess streams throughout the Midwest in response to

channel straightening and agricultural land development during the 19th and 20th centuries. Although tile drainage was not explicitly mentioned in their work, the implications of my own work suggests that agricultural drainage may be influencing channel adjustment across the Midwest. Notably, bank erosion is a larger sediment source than field erosion in many alluvial rivers (Kronvang et al., 2013; Palmer et al., 2014; Schaffrath et al., 2015; Simon et al., 1996; Stout et al., 2014; Willett et al., 2012). Furthermore, bank erosion is sensitive to streamflow increase. Therefore, sediment management in a wetter Midwestern USA will require management of streamflow timing and magnitude in order to protect river health and minimize river excess streambank erosion, especially in those basins with artificial arteries, such as tile drains (Gran et al., 2013).

References

Cho, S.J., Wilcock, P.R., Belmont, P., Gran, K., Hobbs, B., 2019. Simulation model for collaborative decision-making on sediment source reduction in an intensively managed watershed. Water Resour. Res. https://doi.org/10.1029/2018WR024324

Eshenaur, T., Wagner, M., Westerlund, J. (Eds.), 2014. Minnesota's Clean Water Roadmap: setting long-range goals for Minnesota's water resources.

Gran, K.B., Belmont, P., Day, S.S., Jennings, C., Johnson, A., Perg, L., Wilcock, P.R., 2009. Geomorphic evolution of the Le Sueur River, Minnesota, USA, and implications for current sediment loading, in: James, L.A., Rathburn, S.L., Whittecar, G.R. (Eds.), Management and Restoration of Fluvial Systems with Broad Historical Changes and Human Impacts. Geological Society of America.

Gran, K.B., Finnegan, N., Johnson, A.L., Belmont, P., Wittkop, C., Rittenour, T., 2013. Landscape evolution, valley excavation, and terrace development following abrupt postglacial base-level fall. Geol. Soc. Am. Bull. https://doi.org/10.1130/B30772.1

Gunderson, L., Finley, R., Bourne, H., Lofton, D., 2014. Sediment reduction strategy for the Minnesota River basin and South Metro Mississippi River: Establishing a foundation for local watershed planning to reach sediment TMDL goals, Minnesota Pollution Control Agency. Saint Paul, MN.

Hillel, D., 1998. Groundwater drainage and pollution, in: Environmental Soil Physics. Academic Press, San Diego, CA, pp. 471–505.

Kronvang, B., Andersen, H.E., Larsen, S.E., Audet, J., 2013. Importance of bank erosion for sediment input, storage and export at the catchment scale. J. Soils Sediments 13, 230–241. https://doi.org/10.1007/s11368-012-0597-7

Lenhart, C.F., Smith, D.J., Lewandowski, A., Belmont, P., Gunderson, L., Nieber, J.L., 2018. Assessment of stream restoration for reduction of sediment in a large agricultural watershed. J. Water Resour. Plan. Manag. 144, 1–13. https://doi.org/10.1061/(ASCE)WR.1943-5452.0000908

Mitchell, N., Kumarasamy, K., Cho, S.J., Belmont, P., Dalzell, B., Gran, K., 2018. Reducing high flows and sediment loading through increased water storage in an agricultural watershed of the upper Midwest, USA. Water 10, 1–21. https://doi.org/10.3390/w10081053

Palmer, J.A., Schilling, K.E., Isenhart, T.M., Schultz, R.C., Tomer, M.D., 2014. Streambank erosion rates and loads within a single watershed: Bridging the gap between temporal and spatial scales. Geomorphology 209, 66–78. https://doi.org/10.1016/j.geomorph.2013.11.027

Schaffrath, K.R., Belmont, P., Wheaton, J.M., 2015. Landscape-scale geomorphic change detection: Quantifying spatially variable uncertainty and circumventing legacy data issues. Geomorphology 250, 334–348. https://doi.org/10.1016/j.geomorph.2015.09.020

Simon, A., Rinaldi, M., Hadish, G., 1996. Channel evolution in the loess area of the Midwestern United States, in: Proceedings of the Sixth Federal Interagency Sedimentation Conference, Las Vegas, Nevada. Federal Interagency Sedimentation Conference, Reston, VA, p. III-86–III-93.

Simon, A., Rinaldi, M., 2000. Channel instability in the loess area of the midwestern United States. J. Am. Water Resour. Assoc. 36, 133–150. https://doi.org/10.1111/j.1752-1688.2000.tb04255.x

Stout, J.C., Belmont, P., Schottler, S.P., Willenbring, J.K., 2014. Identifying Sediment Sources and Sinks in the Root River, Southeastern Minnesota. Ann. Assoc. Am. Geogr. 104, 20–39. https://doi.org/10.1080/00045608.2013.843434

Willett, C.D., Lerch, R.N., Schultz, R.C., Berges, S. a., Peacher, R.D., Isenhart, T.M., 2012. Streambank erosion in two watersheds of the Central Claypan Region of Missouri, United States. J. Soil Water Conserv. 67, 249–263. https://doi.org/10.2489/jswc.67.4.249

APPENDICES

APPENDIX A – CHAPTER 2 SUPPLEMENTAL MATERIAL

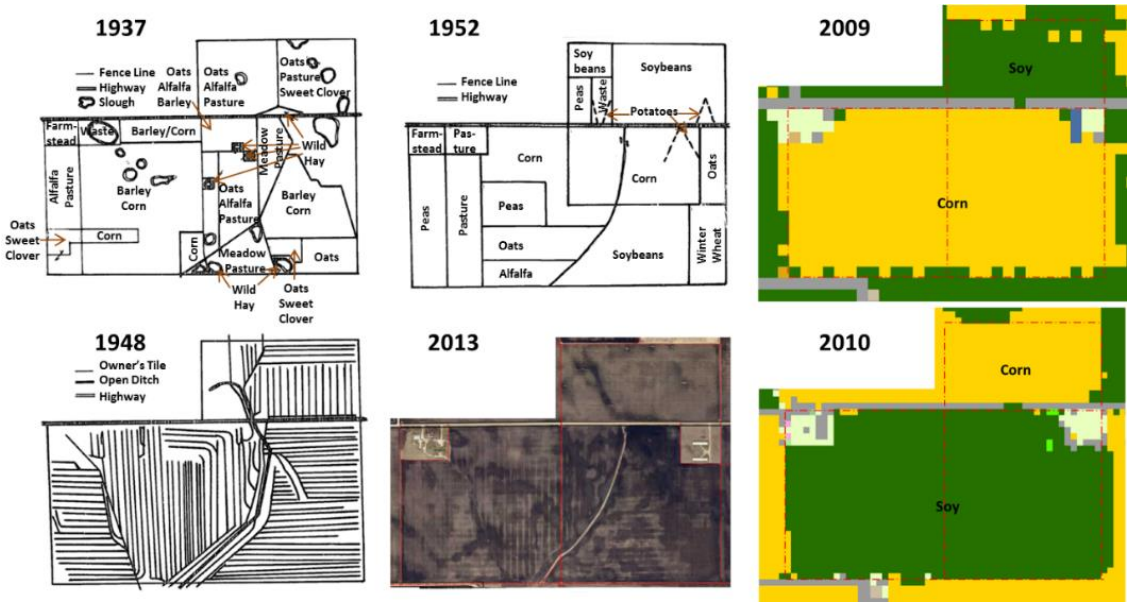

Figure A1: Field land use and tile arrangement before (1937) and after (1952) tile installation (1948) near Mapleton, MN (adapted from Burns, 1954); aerial photograph flown in spring 2013 shows the modern tile pattern remains relatively unchanged with a corn-soybean crop rotation (2009-2010), from the Cropland Data Layer (USDA NASS , 2013).

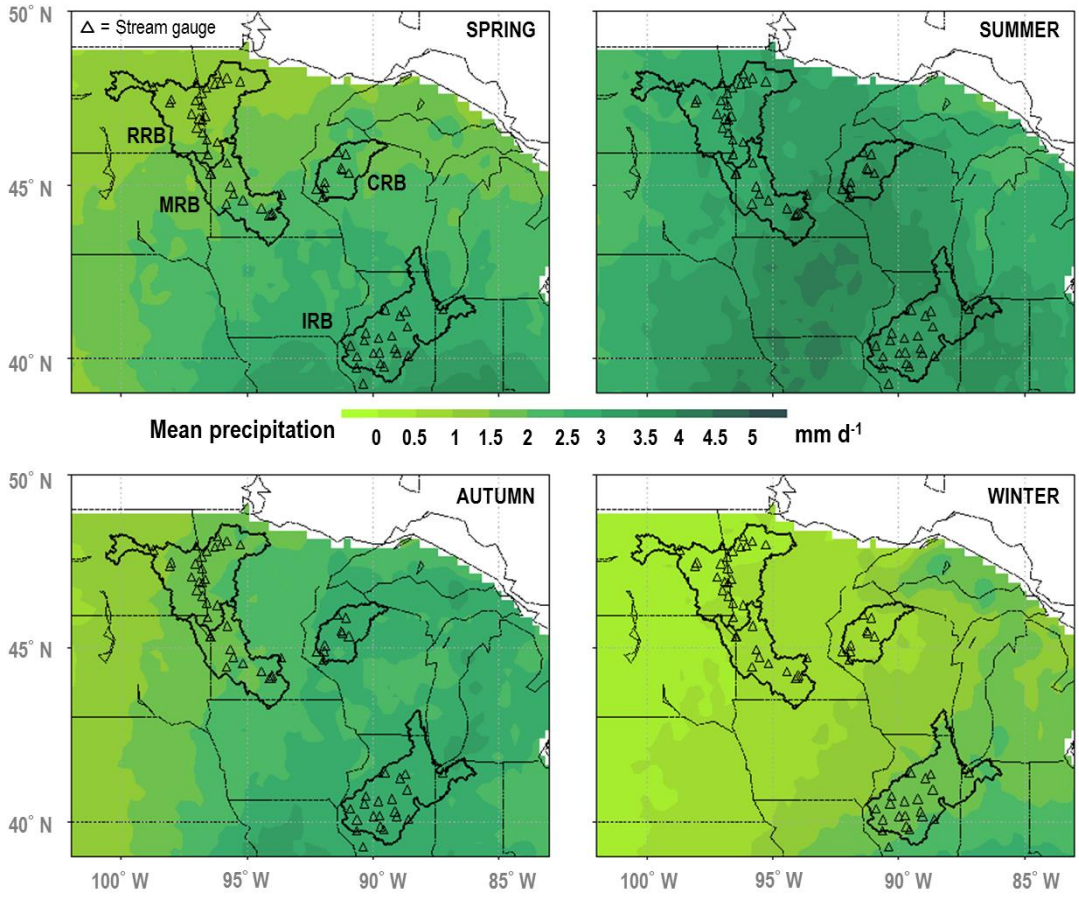

Figure A2. Seasonally averaged long term daily Parameter elevation Regression on Independent Slopes Model (PRISM) precipitation means (1981-2010) across the Upper Midwest: spring (MAM), summer (JJA), autumn (SON), and winter (DJF); USGS gauge locations for each study basin (Table 2-1) indicated by open triangles (PRISM Climate Group, 2004). Study basin acronyms are defined as: Red River of the North basin (RRB), Minnesota River basin (MRB), Chippewa River basin (CRB), and Illinois River basin (IRB).

Supplement of Section 3.2 - Climate records: precipitation and evapotranspiration

Comparison of monthly precipitation total reported as an average depth (cm) from Parameter elevation Regression on Independent Slopes Model (PRISM), used in this study, and Livneh et al. (2013) (L13) for each watershed is shown in Figure A3. If PRISM and L13 precipitation depths were equivalent in every month, then all points

would plot on the 1:1 line. On average (1935-2011) the difference between the two monthly precipitation datasets is 1% for each study watershed.

Figure A4 shows a comparison of monthly (March-November during 2001-2011) ET_a estimates produced by Livneh et al. (2013) (L13) with ET_p estimates (available from: http://agwx.soils.wisc.edu/uwex_agwx/sun_water/et_wimn) produced following the methods of Diak et al. (1998) (D98) for a location in the Minnesota River basin (MRB), 44 N, 94 W and the Chippewa River basin (CRB), 45.2 N, 91.6 W. On average, the estimates of ET_a are 19% (raw) and 26% (17% reduction in JJA ET_a) lower than estimates of ET_p in the MRB, and 16% (raw) and 24% (17% reduction in JJA ET_a) lower than estimates of ET_p in the CRB.

Figure A5 shows average monthly ET_a from Livneh et al. (2013) compared against four AmeriFlux sites near the study watersheds (Table 2-2) as well as data from Bryan et al. (2015). In general, the L13 data show an earlier peak in ET_a for the cropland sites in Rosemount, MN and Bondville, IL, and overestimate average annual ET_a by 17% (raw) and 7% (17% reduction in JJA) for Bondville and 14% (raw) and 5% (17% reduction in JJA) for Rosemount. The L13 data overestimate ET_a at Willow Creek, WI (broadleaf deciduous forest) by as much as 31% (raw) and 19% (17% reduction in JJA) annually, and underestimate ET_a at Brookings, SD (grassland) by 29% (raw) and 34% (17% reduction in JJA) annually.

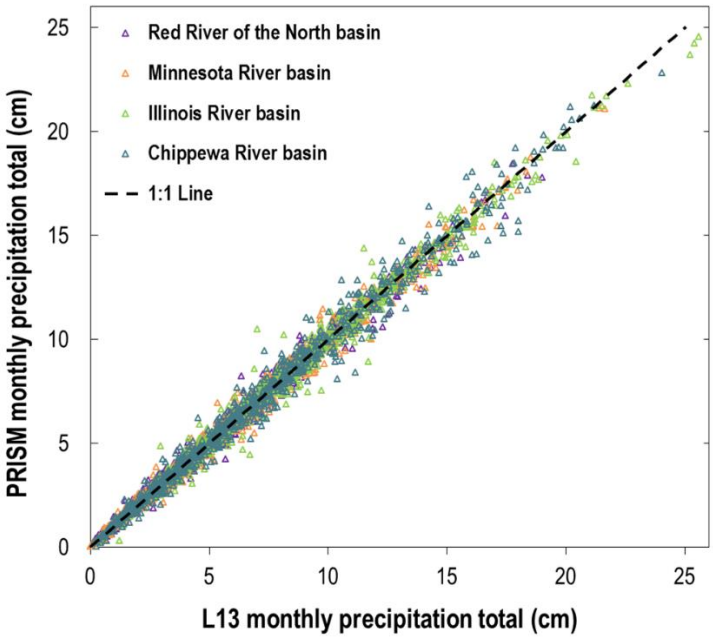

Figure A3. Spatially averaged, total monthly (cm) precipitation (1935-2011) for each watershed from Parameter elevation Regression on Independent Slopes Model (PRISM Climate Group, 2004) and Livneh et al. 2013 (L13) plotted with 1:1 line.

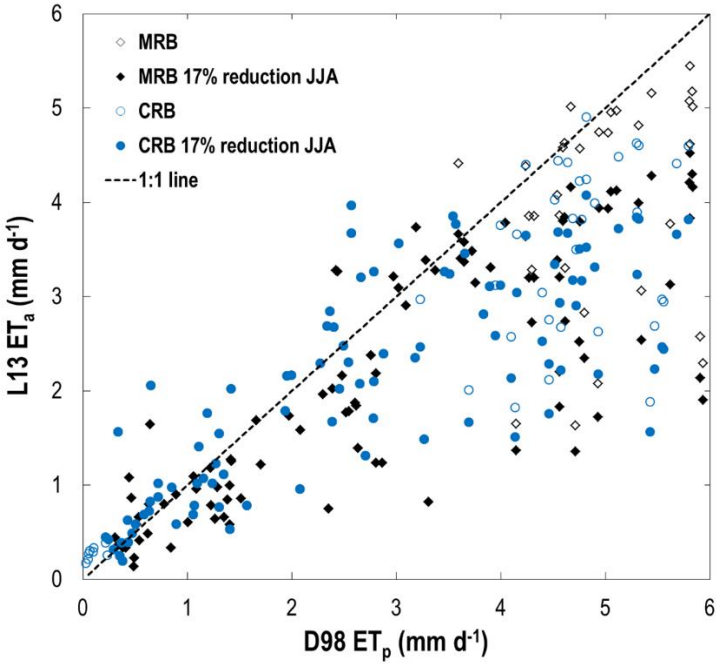

Figure A4. Monthly (March-November) average daily (mm d^{-1}) estimates of ET_p following methods of Diak et al., 1998 (D98) versus estimates of ET_a from Livneh et al., 2013 (L13) during 2001-2011.

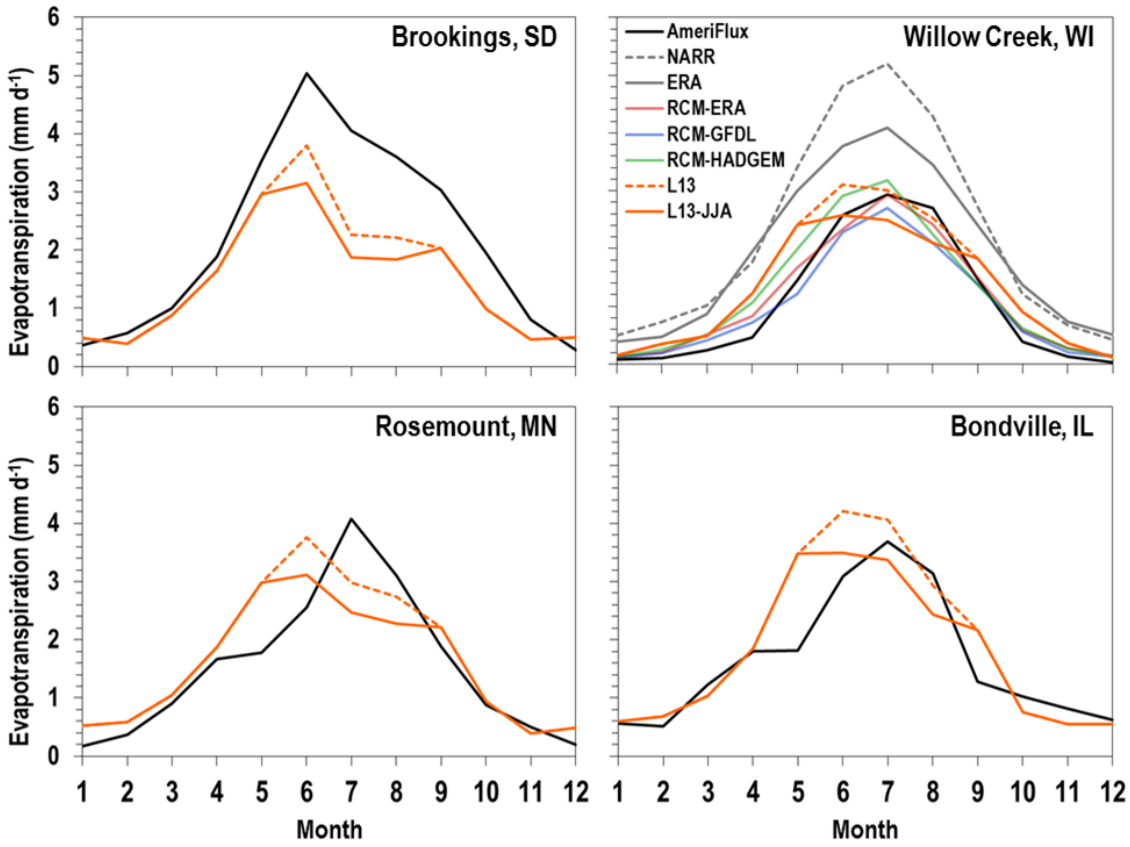

Figure A5. Average monthly evapotranspiration rate (mm d^{-1}) at four AmeriFlux sites (see Table 2-2) compared to modeled evapotranspiration rates used in this study (L13 & L13-JJA) and Bryan et al. 2015.

The L13 ET_a estimates were calculated in VIC using the Hansen et al. (2000) static global vegetation classification, and did not consider artificial drainage, Therefore, the dominant mechanism for losing soil water in May and June is expected to be through ET_a loss according to the L13 estimates. In contrast, ET_a losses in May and June at Ameriflux sites are relatively low since crops are absent or very young and soil water likely drains primarily via artificial drainage. We expect that the effects of drainage influence ET_a during the peak growing season as well. Because drainage improves crop growing conditions early in the growing season, late growing season ET_a may be higher in drained fields than undrained fields. This would be an interesting further line of study.

Regardless, it seems reasonable that the L13 ET_a estimates would seasonally mismatch the Rosemount and Bondville Ameriflux station ET_a estimates, given the presence/absence of artificial drainage.

ET_a estimates may dramatically underestimate Ameriflux ET_a estimates in Brookings, SD due to differences in crop coefficients or misclassification of grasslands and croplands; corn has been found to have lower ET_a rates than some grasses (Hickman et al., 2010). Due to the coarse resolution of the global vegetation input for the L13 VIC model, parts of southern Wisconsin appear to be misclassified as broadleaf deciduous forest instead of cropland. Some studies in the Great Lakes region report broadleaf deciduous forest to have slightly higher annual ET_a rates than cropland (Mao and Cherkauer, 2009; Mishra et al., 2010). Likely of larger significance is that Livneh et al. (2013) and Maurer et al. (2002) do not suggest that they considered lake and wetland effects on evapotranspiration, which in the Great Lakes region can be significant (Bryan et al., 2015). Furthermore, the Hansen et al. (2000) global vegetation classification masks bodies of water, as the land cover input.

The fact that the L13 ET_a estimates mismatch Ameriflux estimates seasonally provides assurance that the L13 ET_a estimates are appropriate for testing our hypothesis. The lack of artificial drainage is what allows us to test whether factors beyond climate contribute to modern streamflow increases in the Midwestern US.

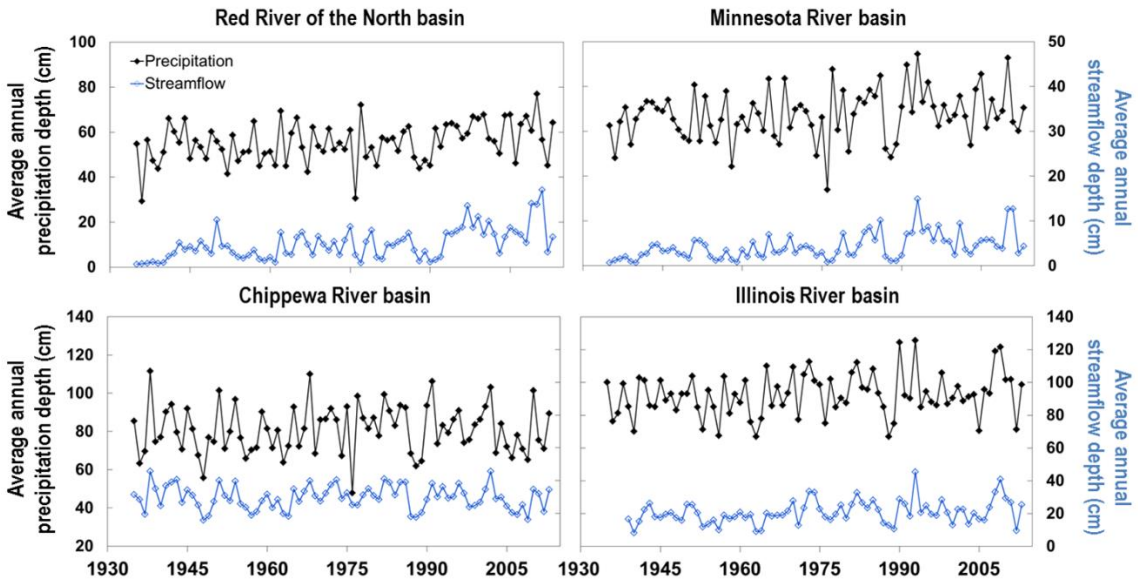

Figure A6. Annual, spatially averaged watershed precipitation and streamflow depths (cm) for each study basin.

Table A1. Resulting p-values of 624 statistical tests (t-test and Kolmogorov–Smirnov [KS]-test) comparing pre-period and post-period flow and precipitation based on the 1974/1975, piecewise linear regression (PwLR), and land cover transition (LCT) breakpoints for each basin (Table 2-3). P-values are highlighted based on their significance: bolded values are p-values with 95% confidence level or greater, grey values are p-values with less than a 95% confidence level, and black values are p-values where significance depends on the breakpoint. Italicized grey values reported for the CRB are not reliable because the post-period includes fewer than 10 years of data.

		Flow: t-test			Flow: KS-test			Precipitation: t-test			Precipitation: KS-test		
		74/75	**PwLR**	**LCT**	**74/75**	**PwLR**	**LCT**	**74/75**	**PwLR**	**LCT**	**74/75**	**PwLR**	**LCT**
Chippewa River basin	January	0.341	0.893	*0.846*	0.653	0.958	*0.902*	0.278	0.097	*0.214*	0.223	0.050	*0.082*
	February	0.372	0.680	*0.851*	0.449	0.878	*0.953*	0.337	0.039	*0.309*	0.446	0.071	*0.367*
	March	0.566	0.871	*0.525*	0.219	0.749	*0.205*	0.188	0.369	*0.574*	0.234	0.348	*0.700*
	April	0.468	0.267	*0.719*	0.506	0.152	*0.416*	0.192	0.277	*0.258*	0.169	0.308	*0.575*
	May	0.826	0.485	*0.264*	0.482	0.311	*0.622*	0.933	0.374	*0.187*	0.906	0.697	*0.445*
	June	0.900	0.552	*0.211*	0.908	0.628	*0.142*	0.833	0.434	*0.117*	0.945	0.587	*0.246*
	July	0.706	0.775	*0.308*	0.584	0.893	*0.606*	0.463	0.609	*0.358*	0.567	0.794	*0.360*
	August	0.174	0.508	*0.364*	0.354	0.450	*0.200*	0.496	0.945	*0.769*	0.760	1.000	*0.856*
	September	0.517	0.990	*0.723*	0.357	0.958	*0.654*	0.286	0.912	*0.752*	0.657	0.925	*0.654*
	October	0.103	0.778	*0.593*	0.110	0.887	*0.817*	**0.022**	**0.026**	*0.304*	0.097	0.073	*0.423*
	November	0.240	0.894	*0.713*	0.337	0.887	*0.902*	0.510	0.905	*0.806*	0.375	0.944	*0.874*
	December	0.263	0.973	*0.806*	0.387	0.971	*0.931*	0.380	0.135	*0.062*	0.337	0.175	*0.045*
	Annual	0.499	0.793	*0.340*	0.721	0.918	*0.291*	0.243	0.571	*0.295*	0.246	0.764	*0.614*

Table A1 (cont.)

Illinois River basin	January	0.123	0.030	0.092	0.136	0.079	0.265	0.543	0.250	0.529	0.454	0.425	0.211
	February	0.355	0.082	0.184	0.353	0.043	0.216	0.224	0.108	0.764	0.433	0.359	0.899
	March	0.035	0.062	0.045	0.104	0.114	0.099	0.649	0.777	0.619	0.619	0.836	0.828
	April	0.174	0.438	0.158	0.335	0.479	0.353	0.780	0.832	0.588	0.883	0.947	0.638
	May	0.182	0.344	0.155	0.126	0.398	0.161	0.212	0.113	0.326	0.063	0.063	0.138
	June	0.105	0.077	0.280	0.082	0.071	0.117	0.798	0.742	0.845	0.811	0.643	0.954
	July	0.451	0.411	0.525	0.518	0.436	0.614	0.453	0.585	0.214	0.585	0.519	0.443
	August	0.090	0.249	0.212	0.181	0.508	0.259	0.054	0.408	0.257	0.037	0.475	0.108
	September	0.004	0.062	0.009	0.003	0.111	0.041	0.511	0.465	0.118	0.685	0.728	0.113
	October	0.074	0.147	0.065	0.082	0.139	0.142	0.142	0.072	0.363	0.113	0.143	0.378
	November	**0.034**	**0.007**	**0.041**	0.075	0.008	0.074	0.023	0.004	0.109	0.053	0.013	0.045
	December	**0.021**	**0.011**	**0.010**	**0.040**	**0.019**	**0.022**	0.122	0.081	0.039	0.136	0.203	0.050
	Annual	**0.011**	**0.019**	**0.017**	**0.012**	**0.018**	**0.020**	0.086	0.075	0.085	0.117	0.141	0.183
Minnesota River basin	January	**0.000**	**0.000**	**0.000**	**0.001**	**0.000**	**0.000**	0.096	0.520	0.182	0.369	0.672	0.338
	February	**0.000**	**0.000**	**0.000**	**0.002**	**0.000**	**0.000**	0.722	0.842	0.659	0.540	0.938	0.604
	March	**0.007**	**0.005**	**0.002**	0.089	0.055	0.074	0.017	0.394	0.060	0.107	0.515	0.148
	April	**0.041**	**0.039**	**0.016**	**0.011**	**0.034**	**0.003**	0.159	0.164	0.239	0.489	0.344	0.684
	May	**0.000**	**0.001**	**0.000**	**0.001**	**0.001**	**0.001**	0.716	0.366	0.469	0.807	0.657	0.636
	June	**0.000**	**0.000**	**0.000**	**0.000**	**0.000**	**0.000**	0.500	0.957	0.418	0.807	0.879	0.677
	July	**0.002**	**0.007**	**0.000**	**0.021**	**0.020**	**0.003**	0.300	0.107	0.151	0.351	0.230	0.223
	August	**0.008**	**0.012**	**0.000**	**0.017**	**0.040**	**0.001**	0.239	0.641	0.133	0.097	0.806	0.064
	September	0.017	0.062	0.001	0.106	0.225	0.015	0.224	0.077	0.242	0.334	0.112	0.261
	October	**0.002**	**0.001**	**0.000**	**0.012**	**0.007**	**0.002**	0.082	0.015	0.029	0.115	0.088	0.116
	November	**0.001**	**0.000**	**0.000**	**0.006**	**0.000**	**0.001**	0.262	0.418	0.380	0.260	0.519	0.445
	December	**0.000**	**0.000**	**0.000**	**0.002**	**0.000**	**0.000**	0.435	0.138	0.385	0.608	0.457	0.413
	Annual	**0.000**	**0.000**	**0.000**	**0.001**	**0.001**	**0.000**	0.033	0.072	0.011	0.098	0.199	0.051
Red River of the North basin	January	**0.000**	**0.000**	**0.005**	**0.005**	**0.000**	**0.013**	0.117	0.169	0.412	0.112	0.105	0.368
	February	**0.000**	**0.000**	**0.016**	**0.003**	**0.000**	**0.034**	0.155	0.321	0.050	0.246	0.326	0.183
	March	0.006	0.012	0.171	0.011	0.005	0.217	0.050	0.108	0.021	0.062	0.247	0.054
	April	0.069	0.079	0.036	0.105	0.102	0.115	0.981	0.902	0.619	0.974	0.823	0.574
	May	**0.016**	**0.003**	**0.004**	0.059	0.013	0.014	0.321	0.039	0.046	0.312	0.129	0.186
	June	**0.015**	**0.000**	**0.001**	**0.038**	**0.002**	**0.001**	0.170	0.138	0.351	0.105	0.032	0.569
	July	**0.000**	**0.000**	**0.001**	**0.001**	**0.000**	**0.005**	0.288	0.251	0.886	0.244	0.418	0.943
	August	**0.000**	**0.000**	**0.013**	**0.000**	**0.000**	**0.043**	0.687	0.551	0.681	0.598	0.650	0.786
	September	**0.002**	**0.000**	**0.024**	0.002	0.000	0.084	0.094	0.036	0.047	0.009	0.013	0.081
	October	**0.003**	**0.000**	**0.010**	0.003	0.002	0.053	**0.010**	**0.015**	**0.002**	**0.011**	**0.003**	**0.004**
	November	**0.000**	**0.000**	**0.001**	**0.000**	**0.000**	**0.003**	0.409	0.560	0.918	0.270	0.341	0.943
	December	**0.000**	**0.000**	**0.000**	**0.001**	**0.000**	**0.013**	0.487	0.058	0.000	0.639	0.071	0.002
	Annual	**0.000**	**0.000**	**0.000**	**0.000**	**0.000**	**0.005**	**0.019**	**0.004**	**0.009**	**0.010**	**0.008**	**0.027**

References for Appendix A

Bryan, A. M., Steiner, A. L. and Posselt, D. J.: Regional modeling of surface-atmosphere interactions and their impact on Great Lakes hydroclimate, J. Geophys. Res. D Atmos., 120(3), 1044–1064, doi:10.1002/2014JD022316, 2015.

Burns, B. E.: Artificial Drainage in Blue Earth County, Minnesota, University of Nebraska., 1954.

Diak, G. R., Anderson, M. C., Bland, W. L., Norman, J. M., Mecikalski, J. M. and Aune, R. M.: Agricultural-Management Decision Aids Driven by Real-Time Satellite Data, Bull. Am. Meteorol. Soc., 79(7), 1345–1355, doi:10.1175/1520-0477(1998)079<1345:AMDADB>2.0.CO;2, 1998.

Hansen, M. C., DeFries, R. S., Townshend, J. R. and Sohlberg, R.: Global land cover classification at 1 km spatial resolution using a classification tree approach, Int. J. Remote Sens., 21(6–7), 1331–1364 [online] Available from: http://data.globalforestwatch.org/datasets/7876b225f8034a0ebba79fad4afb80ad, 2000.

Hickman, G. C., Vanloocke, A., Dohleman, F. G. and Bernacchi, C. J.: A comparison of canopy evapotranspiration for maize and two perennial grasses identified as potential bioenergy crops, GCB Bioenergy, 2, 157–168, doi:10.1111/j.1757-1707.2010.01050.x, 2010.

Livneh, B., Rosenberg, E. A., Lin, C., Nijssen, B., Mishra, V., Andreadis, K. M., Maurer, E. P. and Lettenmaier, D. P.: A Long-Term Hydrologically Based Dataset of Land Surface Fluxes and States for the Conterminous United States: Update and Extensions, J. Clim., 26, 9384–9392, 2013.

Mao, D. and Cherkauer, K. A.: Impacts of land-use change on hydrologic responses in the Great Lakes region, J. Hydrol., 374(1–2), 71–82, doi:10.1016/j.jhydrol.2009.06.016, 2009.

Maurer, E. P., Wood, A. W., Adam, J. C., Lettenmaier, D. P. and Nijssen, B.: A Long-Term Hydrologically Based Dataset of Land Surface Fluxes and States for the Conterminous United States*, J. Clim., 15(22), 3237–3251, doi:10.1175/1520-0442(2002)015<3237:ALTHBD>2.0.CO;2, 2002.

Mishra, V., Cherkauer, K. A., Niyogi, D., Lei, M., Pijanowski, B. C., Ray, D. K., Bowling, L. C. and Yang, G.: A regional scale assessment of land use/land cover and climatic changes on water and energy cycle in the upper Midwest United States, Int. J. Climatol., 30(13), 2025–2044, doi:10.1002/joc.2095, 2010.

PRISM Climate Group: Oregon State University, [online] Available from: http://prism.oregonstate.edu, 2004.

USDA National Agricultural Statistics Service Cropland Data Layer. {2013}. Published crop-specific data layer [Online]. Available at https://nassgeodata.gmu.edu/CropScape/ (accessed {1 Oct 2016}; verified {19 May 2017}). USDA-NASS, Washington, DC.

APPENDIX B – CHAPTER 3 SUPPLEMENTAL MATERIAL

Data Availability: The following are available online at https://usu.box.com/s/o7l0fzez7ln7ujqb6s14ti8ufe7wug4i, Video S1: Bluffs-Downstream- Camera B Timelapse.mp4, Video S2,: Bluffs- Upstream- Camera A Timelapse.mp4, Video S3: bluff_failure.m4v. Raw data, including all photos, SfM surveys, derivative files and spreadsheets used for analysis.

Conflicts of Interest: Patrick Belmont, a co-author, is the Guest Editor for the Water Special Issue: Watershed Hydrology, Erosion and Sediment Transport Processes but recused himself from the review process for this paper. Funding sources had no role in the design of the study; in the collection, analyses, or interpretation of data; in the writing of the manuscript, or in the decision to publish the results.

Site information and bluff erosion data

Table B1. Timelapse camera site information. Easting and Northing coordinates reference datum NAD83, and projection UTM Zone 15N

Site Name[1]	Site Description[2]	Aspect (°)	Survey Dimensions L(m)xH(m)	Easting (m)	Northing (m)	Photo Dates	Days w/ Photos (%)
BE1	NC, TS, FA	153	22 x 7	412910	4877097	6/9/2015-5/16/2017	98
BE2	NC, IS, OC	229	26 x 14	413266	4877247	6/8/2015-5/16/2017	83
BE3	NC, IS, OC	174	24 x 11	413786	4878851	6/9/2015-5/16/2017	100
MPL1	NC, IS, OC	274	20 x 10	414108	4870395	6/4/2015-5/12/2017	94
MPL2	NC, IS, OC	180	20 x 11	414145	4870844	6/5/2015-5/12/2017	100

Table B1 (cont.)

MPL3	OC	193	22 x 9	415540	4873137	6/7/2015-5/13/2017	99
MPL4	NC, TS, FA	69	21 x 6	416018	4874079	6/7/2015-5/13/2017	92
MPL5	NC, TS, FA	116	17 x 6	415988	4874321	6/8/2015-5/13/2017	100
MPL6	OC	166	21 x 13	416435	4875258	6/8/2015-3/16/2016	70
MPL7	OC, TS, IS	170	20 x 14	418051	4878666	6/8/2015-3/29/2017	99
LS1	OC	292	18 x 7	424457	4884466	5/22/2015-5/18/2017	80
LS2	NC, TS, FA	228	23 x 12	424533	4884155	7/11/2015-5/13/2017	95
LS3	NC, IS, OC	118	23 x 17	423608	4883232	6/7/2015-5/14/2017	91
LS4	NC, OC	36	23 x 13	422105	4882098	6/7/2015-5/14/2017	84
LS5	OC, TS, FA	180	20 x 6	421975	4882474	6/7/2015-5/13/2017	58
LS6	OC, TS, FA	138	20 x 9	421918	4882463	6/8/2015-5/14/2017	98
LS7	OC, TS, FA	262	28 x 11	420202	4881018	6/7/2015-5/13/2017	99
LS8	OC, TS, FA	222	23 x 7	419815	4881174	6/7/2015-3/10/2016	68
LS9	NC, IS	70	21 x 20	418666	4881123	6/3/2014-5/15/2017	82
LS10	OC, TS, FA	270	21 x 16	419186	4881486	6/2/2014-5/15/2017	93

[1] Site names abbreviated for each river: Blue Earth River (BE), Maple River (MPL), and Le Sueur River (LS). Site numbers correspond to independent sites from upstream to downstream (1, 2, 3…).

[2] Site descriptions are reported as general stratigraphic units from bluff base to crest. Abbreviations correspond to the following: normally consolidated till (NC); overly consolidated till (OC), interglacial sands (IS), terrace strath (TS), floodplain alluvium (FA).

Table B2. Geomorphic change detection results from repeat SfM surveys at two bluffs sites on the Le Sueur River. Average annual retreat rates calculated as net volume lost (erosion positive) divided by entire survey area, divided by the amount of time, in years, between surveys. Right two columns report results for areas of erosion only.

Site Name	Survey 1 Date	Survey 2 Date	Survey Area (m^2)	Net Volume Lost (m^3)	Retreat Rate (m/yr)	Erosion Area (m^2)	Erosion Volume (m^3)
LS9	6/15/2014	7/3/2014	1,938.8	1,082.0	11.3	451.0	1,163.0
LS9	6/15/2014	5/8/2015	1,928.3	1,229.0	0.71	538.0	1,254.0
LS9	6/15/2014	7/12/2015	1,930.3	1,132.6	0.55	604.0	1,335.0
LS9	6/15/2014	5/24/2016	1,834.0	785.0	0.22	667.0	1,524.0
LS9	6/15/2014	10/22/2016	1,931.6	3,826.0	0.84	1,129.0	3,837.0
LS9	6/15/2014	5/17/2017	1,857.9	3,759.0	0.69	1,119.0	3,785.0
LS9	7/3/2014	5/8/2015	2,111.3	131.2	0.07	191.0	207.0
LS9	7/3/2014	7/12/2015	2,297.2	117.2	0.05	424.0	381.0
LS9	7/3/2014	5/24/2016	2,138.7	-224.1	-0.06	716.0	841.0
LS9	7/3/2014	10/22/2016	2,318.4	3,275.3	0.61	1,533.0	3,279.0
LS9	7/3/2014	5/17/2017	2,190.0	3,117.3	0.50	1,452.0	3,146.0
LS9	5/8/2015	7/12/2015	2,157.2	-113.0	-0.29	276.0	221.0
LS9	5/8/2015	5/24/2016	2,037.8	-481.6	-0.23	576.0	655.0
LS9	5/8/2015	10/22/2016	2,130.4	2,674.6	0.86	1,217.0	2,682.0
LS9	5/8/2015	5/17/2017	2,037.0	2,597.7	0.65	1,229.0	2,626.0
LS9	7/12/2015	5/24/2016	2,385.2	-355.0	-0.17	646.0	817.0
LS9	7/12/2015	10/22/2016	2,713.6	3,598.3	1.04	1,562.0	3,604.0
LS9	7/12/2015	5/17/2017	2,756.5	3,256.9	0.64	1,488.0	3,292.0
LS9	5/24/2016	10/22/2016	2,227.2	3,513.2	3.81	1,419.0	3,662.0
LS9	5/24/2016	5/17/2017	2,250.5	3,240.0	1.47	1,358.0	3,462.0
LS9	10/22/2016	5/17/2017	2,616.1	-324.6	-0.22	412.0	316.0
LS10	6/15/2014	7/3/2014	1,420.6	1,086.7	15.5	574.0	1,270.0
LS10	6/15/2014	5/9/2015	1,396.9	1,210.0	0.97	870.0	1,551.0
LS10	6/15/2014	7/10/2015	1,410.9	1,302.0	0.85	916.0	1,729.0
LS10	6/15/2014	5/24/2016	1,390.9	1,174.0	0.43	908.0	1,751.0
LS10	6/15/2014	10/22/2016	1,372.1	2,225.0	0.69	1,140.0	2,242.0
LS10	6/15/2014	5/17/2017	1,363.2	2,182.0	0.55	1,003.0	2,291.0
LS10	7/3/2014	5/9/2015	1,807.6	139.9	0.09	582.0	686.0
LS10	7/3/2014	7/10/2015	2,021.3	325.0	0.16	1,144.0	831.0
LS10	7/3/2014	5/24/2016	2,005.3	366.0	0.10	983.0	1,365.0
LS10	7/3/2014	10/22/2016	1,984.9	1,958.0	0.43	1,436.0	1,965.0

Table B2 (cont.)

LS10	7/3/2014	5/17/2017	1,969.9	1,857.0	0.33	1,258.0	2,329.0
LS10	5/9/2015	7/10/2015	1,947.7	380.3	1.08	414.0	582.0
LS10	5/9/2015	5/24/2016	1,941.6	599.0	0.30	718.0	949.0
LS10	5/9/2015	10/22/2016	1,915.8	2,009.0	0.72	1,085.0	2,011.0
LS10	5/9/2015	5/17/2017	1,901.9	2,070.0	0.55	1,148.0	2,237.0
LS10	7/10/2015	5/24/2016	2,587.2	396.7	0.18	719.0	628.0
LS10	7/10/2015	10/22/2016	2,807.7	2,691.0	0.75	1,371.0	2,708.0
LS10	7/10/2015	5/17/2017	2,800.3	2,650.0	0.51	1,671.0	2,852.0
LS10	5/24/2016	10/22/2016	2,607.7	2,219.6	2.06	1,082.0	2,293.0
LS10	5/24/2016	5/17/2017	2,580.9	2,127.0	0.84	1,401.0	2,340.0
LS10	10/22/2016	5/17/2017	2,890.8	-130.3	-0.08	673.0	895.0

Table B3. Daily discharge (Q) estimated bluff erosion magnitude x observed Q (mm/day) frequency (right four columns) – estimated using different daily erosion ~ discharge power law scaling exponents, gamma – validated against measured retreat rates from Day et al 2013a (D13a) and 2013b (D13b) and Kelly and Belmont, this paper (K&B) collected data. Italicized estimated retreat rates that are also underlined fall with the 95% confidence interval of measured, non-italicized measured retreat rates.

Survey Dates	**Data, authors / source / method**	**Measured, retreat (m/yr) ± 95% CI**	**Q (mm/d), est. retreat (m/yr), γ = 0.66**	**Q (mm/d), est. retreat (m/yr), γ = 0.67**	**Q (mm/d), est. retreat (m/yr), γ = 1.00**	**Q (mm/d), est. retreat (m/yr), γ = 1.35**
Jan 1938 – Dec 2005	D13b / AP / Crest retreat	0.14 ± 0.02	*0.47**	*0.42**	*0.68**	*1.03**
Jul 2007 – Jun 2010	D13a / TLS / Site ero.	0.20 ± 0.04	*0.68*	*0.62*	*1.03*	*1.67*
Jun 2014 – May 2017	K&B / SfM / Site ero.	1.19 ± 0.87	*1.32*	*1.20*	*1.99*	*3.26*

* Q record available beginning 1940 and missing data 1945 - 1949.

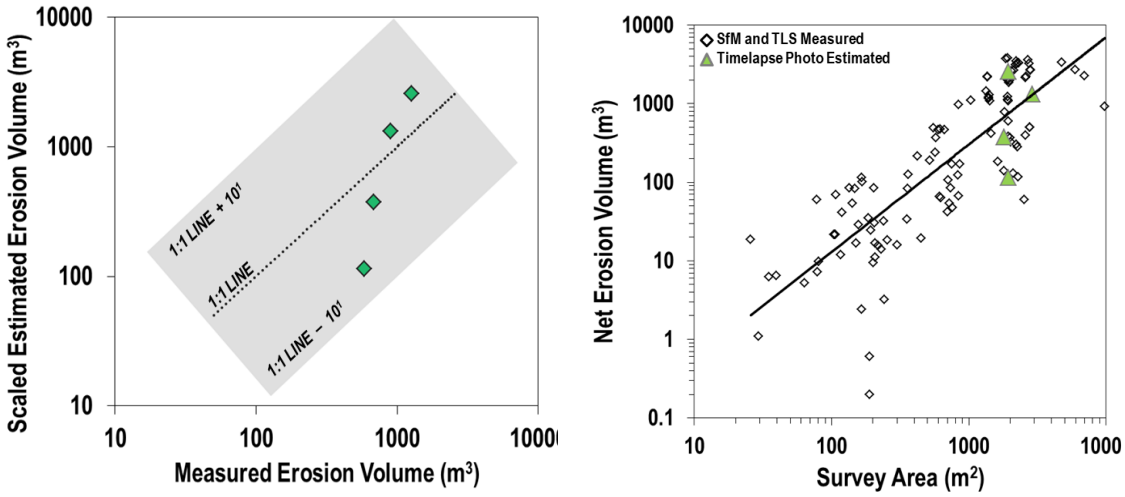

(a) **(b)**

Figure B1. (**a**) Measured bluff erosion from four SfM surveys, 6/15/2014 - 7/3/2014, 7/3/2014 - 5/9/2015, 5/9/2015 - 7/10/2015, and 10/22/2016 – 5/17/2017, which primarily capture bluff face erosion vs the sum of timelapse photo estimated erosion, using the scaling relation, $V = 0.12A^{1.4}$. (**b**) Bluff survey area vs net erosion volume for SfM and TLS measured surveys (black diamonds) and timelapse photo estimated areas and volumes (green triangles). Estimated erosion is within the same order of magnitude as SfM measured erosion for the same time periods.

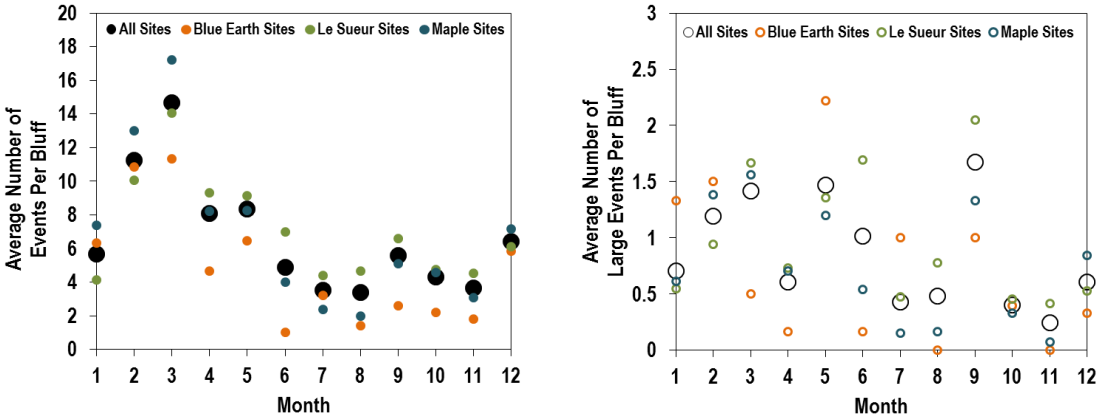

(**a**) (**b**)

Figure B2. (**a**) Average number of failure days per month for a bluff of average size 250 m^2 (length x height). Average monthly days with failures are plotted for sites grouped by each river and for all bluff sites. Total number of observations: 2705 events; (**b**) Average number days with large failures per month for sites grouped by each river and for all bluff sites. Number of observations: 347 events.

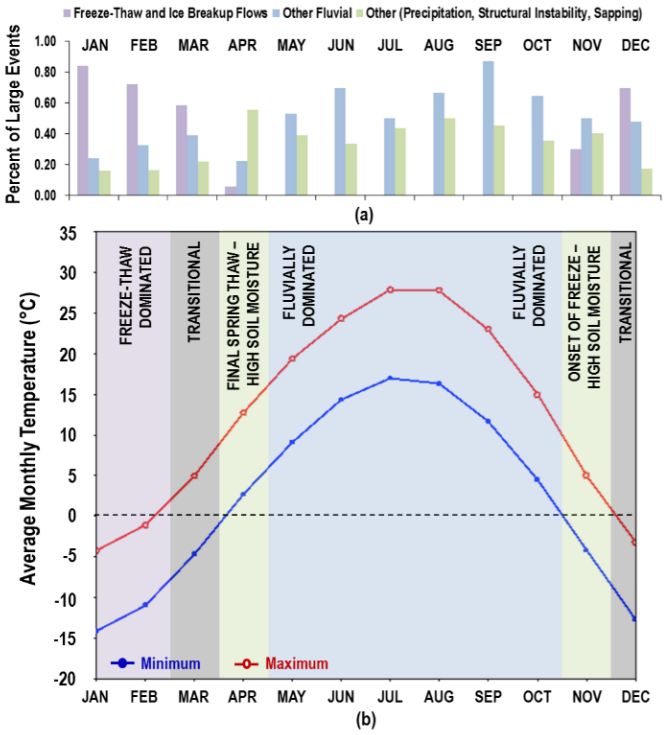

Figure B3. (**a**) Percent of large events likely triggered by freeze-thaw and ice breakup floods (purple), other ice-free floods (blue), and other processes including precipitation, structural instability, and seepage/sapping (green), based on qualitative photographic interpretations. Total number of observations: 347 events. Monthly percentages do not sum to 1 because some events were triggered by multiple processes and for some events, the cause of failure could not be determined; (**b**) Average monthly maximum (red) and minimum (blue) temperatures based on long term mean (1981 – 2010), 4x daily temperatures measured 2 m above the land surface for Good Thunder, MN. Temperature data from NCEP-NCAR Reanalysis 1. Dashed line indicates 0° C. Months binned by interpretations made in section 3.1.

Discussion of Figure B3:

One possible explanation for seasonal reversals between erosion frequency of north and south facing bluffs is that north facing bluffs likely have higher water content than south facing bluffs, and therefore a higher heat capacity in months such as November and April when diurnal temperatures often oscillate between below-freezing and above-freezing temperatures (Figure B3). The increased heat capacity of wetter, more northerly facing bluffs may prevent these sites from freezing entirely and allow for more erosion

events than south facing bluffs due to fluctuations in matric suction. Once temperatures drop below freezing for several days to weeks (usually December), north facing bluffs remain frozen, while south facing bluffs likely experience repeated freeze-thaw cycles through January and February (Figure B3). Though these rivers are often several meters deep during spring and summer peak flows, typical winter water depths are less than a meter; furthermore, all river gradients are low, and ambient air temperatures are low, often freezing the rivers entirely. Therefore, fluvial toe erosion is rare during January and February, until the onset of ice-breakup floods in late February, early March (Figure B3).

During the spring, a similar aspect related effect may occur. March is a transitional, but generally thawing month, when significant toe and face erosion occurs across all bluffs. However, in April north facing bluffs again may retain more moisture and heat than south facing bluffs. North facing bluffs may be prone to more fluctuations in matric suction, and thus more erosion in months such as April and November. Spring and summer months are when most precipitation falls in these basins (Kelly et al., 2017), and therefore fluvial processes are likely much more important than fluctuations in matric suction on the bluff face, though obviously both play a role. The lack of a regression relation between aspect and erosion frequency in summer and fall months (May – October) in part supports the idea that high flows are at least a seasonally dominant erosion mechanism (Figure B3). This idea is discussed further in Section 3.4. Streamflow can often remain high during summer months further facilitating bluff toe erosion, but in some years summer streamflow is quite low. In drought years, such as summer 2015, erosion caused both fluctuations in matric suction and fluvial toe erosion is rare due to low rainfall totals. Minnesota has seen a recent shift towards wetter fall months

(September – October) in some basins (Schottler et al., 2014a), and therefore a combination of bluff toe and face processes are likely occurring during these months before the onset of winter. See Figure B3 for further detail.

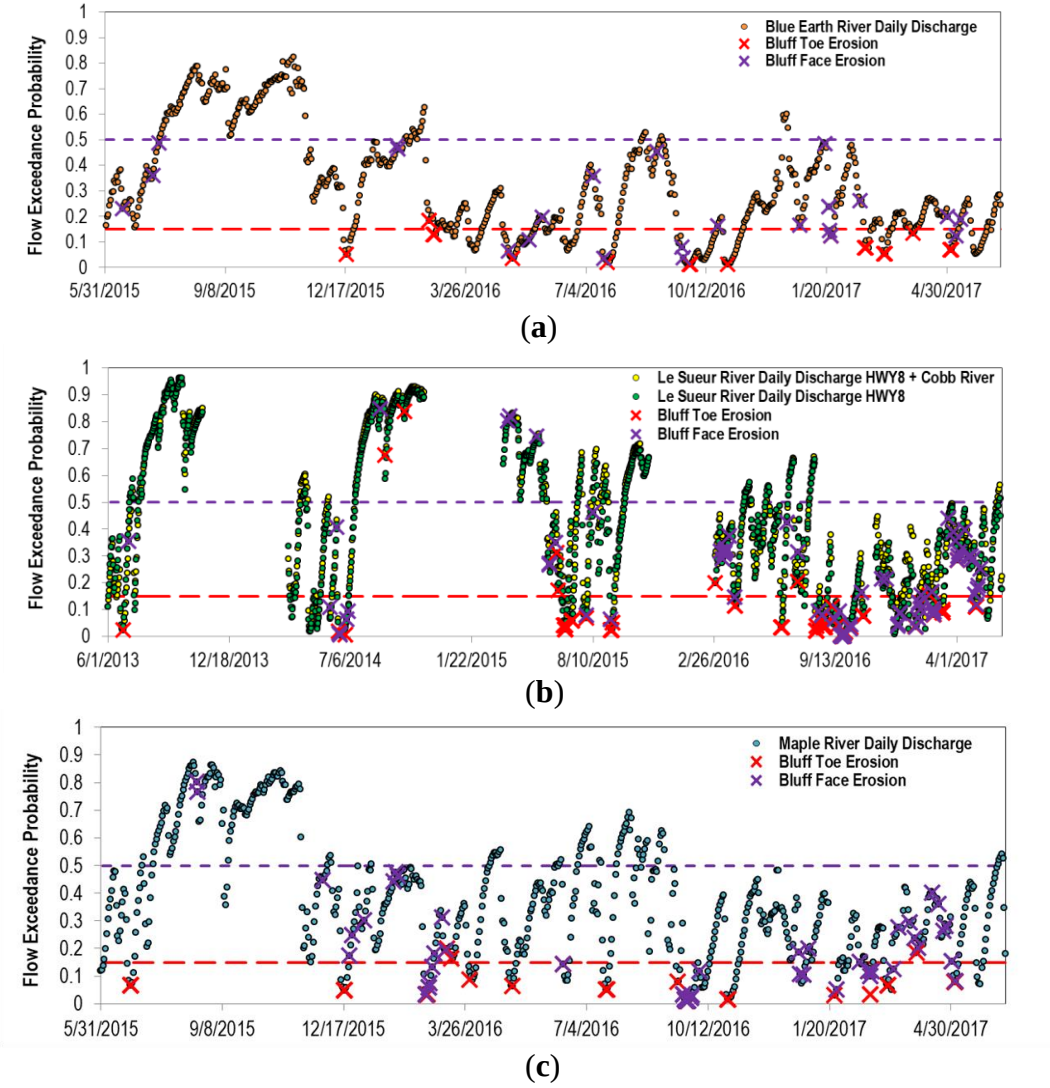

Figure B4. Daily river discharge plotted as flow exceedance probability (2007 – 2017 gage record) with the timing of toe and face bluff failures marked by red and purple X's respectively. Dashed purple line indicates 50% flow exceedance probability, below which most face failures occur. Dashed red line indicates 20% flow exceedance probability, below which most toe failures occur for: (**a**) Blue Earth River sites (gages 05319500 and 05320000, USGS); (**b**) Le Sueur River sites (gages 32076001 and 32071001, MN DNR/MPCA Cooperative Stream Gaging); (**c**) Maple River sites (gage 32072001, MN DNR/MPCA Cooperative Stream Gaging).

Matlab script for Agisoft .xyz point cloud rotation

```
% Code to reorient XYZ data of a subvertical bluff so that the bluff
% face is oriented perpendicular to z-axis and erosional differencing
% can be calculated relative to the azimuthal direction of bluff erosion.
% Requires .xyz input file, bluff aspect angle, and XYZ coordinates at the
% edges of bluff base.
% Created by Brendan Murphy, 08/13/2017

clear
close all

%% Inputs

%Bluff XYZ coordinates, .xyz file format, no headers, in meters
inputfilename = 'PP_Check_Points_161022.txt';

%Average Bluff Aspect (perpendicular to erosion direction), in degrees
Bluff_Aspect = 70;
%Distance of Rotational Axis Behind Bluff, meters
length = 200;

% XYZ Coordinates at the Edges of the bluff base - as column array
% Projected to become rotational axis
% Note: Z-values must be equal
BaseEdge_Left = [418834.012; 4881069.887; 215.140]; % meters
BaseEdge_Right = [418788.854; 4881162.019; 215.140]; % meters

%% Read-in Data
Coords = importdata(inputfilename);
Coords = Coords';

%% Project and Create Rotational Axis
RotAx(1,1) = BaseEdge_Left(1)+length*sind(Bluff_Aspect+180);
RotAx(2,1) = BaseEdge_Left(2)+length*cosd(Bluff_Aspect+180);
RotAx(3,1) = BaseEdge_Left(3);

RotAx(1,2) = BaseEdge_Right(1)+length*sind(Bluff_Aspect+180);
RotAx(2,2) = BaseEdge_Right(2)+length*cosd(Bluff_Aspect+180);
RotAx(3,2) = BaseEdge_Right(3);

%% Plot Initial XYZ
figure(1)
subplot(1,2,1)
hold on
```

```
plot3(Coords(1,:),Coords(2,:),Coords(3,:),'o','MarkerFaceColor','r')
plot3(RotAx(1,:),RotAx(2,:),RotAx(3,:),'k-o','LineWidth',1.5,'MarkerFaceColor','k')
grid on
box on
view(140,10)
xlabel('x')
ylabel('y')
zlabel('z')

%% Translate Left Coordinate of Rotational Axis to Origin
Coords(1,:) = Coords(1,:)-RotAx(1,1);
Coords(2,:) = Coords(2,:)-RotAx(2,1);
Coords(3,:) = Coords(3,:)-RotAx(3,1);
RotAx(1,:) = RotAx(1,:)-RotAx(1,1);
RotAx(2,:) = RotAx(2,:)-RotAx(2,1);
RotAx(3,:) = RotAx(3,:)-RotAx(3,1);

%% Replot (Optional)
% plot3(Coords(1,:),Coords(2,:),Coords(3,:),'o','MarkerFaceColor','r')
% plot3(RotAx(1,:),RotAx(2,:),RotAx(3,:),'k-
o','LineWidth',1.5,'MarkerFaceColor','k')

%% Calcluate XY Rotation Angle
if Bluff_Aspect < 90 || Bluff_Aspect > 270
   Theta = 180-atand(RotAx(2,2)/RotAx(1,2));
else
   Theta = -atand(RotAx(2,2)/RotAx(1,2));
end

%% Create XY Rotation Matrix
RotMat1 = [cosd(Theta) -sind(Theta); sind(Theta) cosd(Theta)];

%% Rotate All in XY to Align Rotational Axis with X-axis
Coords(1:2,:)=RotMat1*Coords(1:2,:);
RotAx_temp = RotMat1*RotAx(1:2,:);
RotAx(1,:) = RotAx_temp(1,:);
RotAx(2,:) = RotAx_temp(2,:);

%% Replot (Optional)
% plot3(Coords(1,:),Coords(2,:),Coords(3,:),'o','MarkerFaceColor','r')
% plot3(RotAx(1,:),RotAx(2,:),RotAx(3,:),'k-
o','LineWidth',1.5,'MarkerFaceColor','k')

%% Create YZ Rotation Matrix
RotMat2 = [cosd(-90) -sind(-90); sind(-90) cosd(-90)];
```

```
%% Rotate in YZ to Orient Bluff Perpendicular to Z-axis
Coords(2:3,:)=RotMat2*Coords(2:3,:);

%% Plot Final Transformation
subplot(1,2,2)
hold on
plot3(Coords(1,:),Coords(2,:),Coords(3,:),'o','MarkerFaceColor','r')
plot3(RotAx(1,:),RotAx(2,:),RotAx(3,:),'k-o','LineWidth',1.5,'MarkerFaceColor','k')
grid on
box on
view(140,10)
xlabel('x')
ylabel('y')
zlabel('z')
zlim = zlim;
set(gca,'zlim',[0 zlim(2)])
%% Export Final Transformation
Coords = Coords';
dlmwrite('PP_Check_Points_161022_append.txt', Coords)
```

Hydrologic data and streamflow return intervals

In this paragraph, we explain which gages were used to estimate flows at each of the bluff monitoring sites. For the 3 Blue Earth River sites, we referenced USGS gages 05319500 and 05320000 (Watonwan River near Garden City, MN and Blue Earth River near Rapidan, MN, respectively). Bluff sites along the Blue Earth River are upstream of the Watonwan River, therefore daily Watonwan River discharge values were subtracted from daily Blue Earth River discharge values. Because there is a hydroelectric dam upstream of the Blue Earth River gage, though it is almost completely filled with sediment, in some cases (16 out of 3653 daily records) discharge on the Blue Earth River was less than the discharge on the Watonwan River, leading to negative values. For these cases, which affected fall and winter low flows, daily discharge was assumed to be 0 cfs. For the 7 Maple River bluff sites, we referenced daily discharge values from gage site 32072001 (Maple River near Rapidan, CR35 Minnesota) maintained by the DNR/MPCA

Cooperative Stream Gaging network. Daily discharge for Le Sueur River bluff sites 1-8 references gage site 32076001 (Le Sueur River near Rapidan, CR8), also maintained by the DNR/MPCA. Daily discharge values for Le Sueur bluff sites 9 and 10, downstream of the Big Cobb River, but upstream of the Maple River, were calculated as the sum of daily discharges at reference sites 32076001 and 32071001 (Big Cobb River near Beauford, CSAH16).

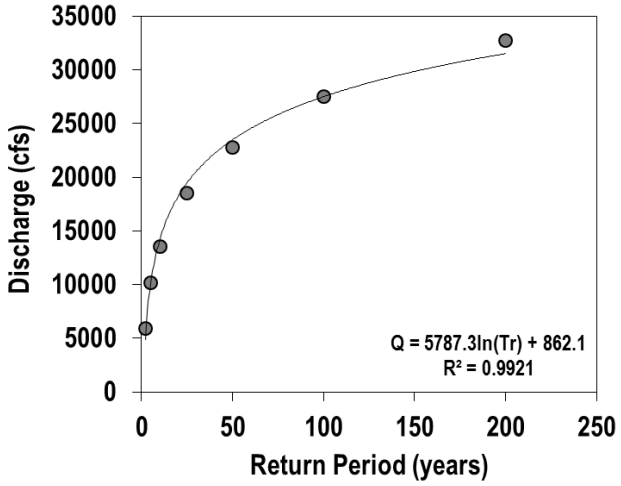

Figure B5. Log Pearson Type III discharge (cfs) vs recurrence interval (years). Equation for annual peak discharge (Q) as a function of return period (Tr).

Log-Pearson Type III analysis of peak annual flows (1980-2016) was computed for the Le Sueur River gage near Rapidan, MN (USGS 5320500). This site was selected over gages used for the flow duration curve analysis because it has greater than 10 years of data and is downstream of all Maple and Le Sueur river camera sites. We used a standard flood frequency approach (e.g. the Oregon State University Streamflow Tutorial – Flood Frequency Analysis) to create Figure B5. Based on this analysis, the June 2014

and September 2016 floods were equivalent to 13 and 25 year recurrence interval floods, respectively. The magnitude of the 1.2 year event is 1.5 mm/day and or 1762 cfs.

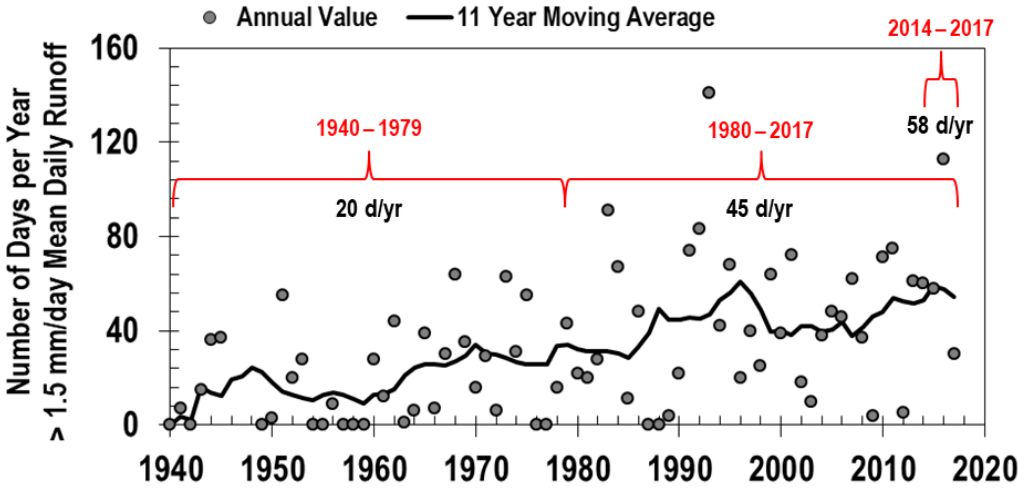

Figure B6. Number of days each year when mean daily flows are greater than the magnitude of the 1.5 mm/day or 1.2 year recurrence interval event. Daily data from USGS gage 5320500. Black line indicates an 11 year moving window average through the annual data points. Red bars indicate average annual values for the periods 1940 – 1979, 1980 – 2017, and 2014 – 2017.

APPENDIX C – CHAPTER 4 SUPPLEMANTAL MATERIAL

River Bathymetry Data Post-Processing

Bruce Call's WinRiver Post-Processing Scripts (2 parts)

```
###PART 1
import pandas as pd
import numpy as np
import arcpy

#####Import master file of points#####
output_dir = r"C:\Users\Sara Kelly\Documents\Utah State University\Belmont Lab Projects\SummerFieldwork2014\2014BellePlainGeoid09"
fn = r"C:\Users\Sara Kelly\Documents\Utah State University\Belmont Lab Projects\SummerFieldwork2014\2014BellePlainGeoid09\WINRIVER\final_points.txt"

# Specify spatial reference names
LatLong_ref = "NAD 1983"
UTM_ref = "NAD 1983 UTM Zone 15N"

data = pd.read_csv(fn, header=None, skip_footer=0, engine="python")
data.columns = ["year", "month", "day", "hour", "minute",
        "second", "centisecond", "ensembleID", "average_depth",
        "beam1_d", "beam2_d", "beam3_d", "beam4_d",
        "roll", "pitch", "heading", "long", "lat", "altitude",
        "GPS_quality", "HDOP"]

#####Filter data#####
print "Filtering points"
```

```
# Filter out data with GPS quality != 4
data = data[data.GPS_quality == 4]
data.drop("GPS_quality", axis=1, inplace=True)

# Filter out data with HDOP > 5
data = data[data.HDOP < 5.0]
data.drop("HDOP", axis=1, inplace=True)

# Filter out depth values < 0
data = data[data.average_depth > 0]

#####Assign each point a unique code#####
print "Assigning unique point codes"

# Clean up formating for time fields
data.drop("hour", axis=1, inplace=True)
data.drop("minute", axis=1, inplace=True)
data.drop("second", axis=1, inplace=True)
data.drop("centisecond", axis=1, inplace=True)
data[["year", "month", "day", "ensembleID"]] = data[["year", "month", "day", "ensembleID"]].astype(int)
data[["year", "month", "day", "ensembleID"]] = data[["year", "month", "day", "ensembleID"]].astype(str)

# Assign unigue code
data["ensembleTimeId"] = data["year"] + "_" + data["month"] + "_" + data["day"] + "_" + data["ensembleID"]
```

```
# Delete time columns
data.drop("year", axis=1, inplace=True)
data.drop("month", axis=1, inplace=True)
data.drop("day", axis=1, inplace=True)
data.drop("ensembleID", axis=1, inplace=True)

#####Correct depths for pitch and roll#####
print "Correcting depths"

data["theta1"] = (90 - (20 + data["roll"])) / 180.0 * np.pi
data["theta2"] = (90 - (20 - data["roll"])) / 180.0 * np.pi
data["theta3"] = (90 - (20 + data["pitch"])) / 180.0 * np.pi
data["theta4"] = (90 - (20 - data["pitch"])) / 180.0 * np.pi

# Backcalculate raw beam parallel distance to bed for each beam factor for backcalculating beam length is depth/sin(70)
data["bpd1"] = data["beam1_d"] / np.sin(70 / 180.0 * np.pi)
data["bpd2"] = data["beam2_d"] / np.sin(70 / 180.0 * np.pi)
data["bpd3"] = data["beam3_d"] / np.sin(70 / 180.0 * np.pi)
data["bpd4"] = data["beam4_d"] / np.sin(70 / 180.0 * np.pi)

# Compute distances to translate coordinates along beams and cross beams along beam offsets are forced to be positive, cross beam can be + or - where + is toward front (beam 3) or toward left (beam 1)
data["ABoffset1"] = data["bpd1"] * np.cos(data["theta1"])
data["CBoffset1"] = data["bpd1"] * np.sin(data["theta1"]) * np.sin(data["pitch"] / 180.0 * np.pi)

data["ABoffset2"] = data["bpd2"] * np.cos(data["theta2"])
```

```
data["CBoffset2"] = data["bpd2"] * np.sin(data["theta2"]) * np.sin(data["pitch"] / 180.0 * np.pi)


data["ABoffset3"] = data["bpd3"] * np.cos(data["theta3"])

data["CBoffset3"] = data["bpd3"] * np.sin(data["theta3"]) * np.sin(data["roll"] / 180.0 * np.pi)


data["ABoffset4"] = data["bpd4"] * np.cos(data["theta4"])

data["CBoffset4"] = data["bpd4"] * np.sin(data["theta4"]) * np.sin(data["roll"] / 180.0 * np.pi)


# Compute new depths for each beam

data["Depth1"] = data["bpd1"] * np.sin(data["theta1"]) * np.cos(data["pitch"] / 180.0 * np.pi)

data["Depth2"] = data["bpd2"] * np.sin(data["theta2"]) * np.cos(data["pitch"] / 180.0 * np.pi)

data["Depth3"] = data["bpd3"] * np.sin(data["theta3"]) * np.cos(data["roll"] / 180.0 * np.pi)

data["Depth4"] = data["bpd4"] * np.sin(data["theta4"]) * np.cos(data["roll"] / 180.0 * np.pi)


#relative beam azimuth for all beams

data["A"] = data["heading"] / 180 * np.pi


#compute x and y translations for each

data["dy1"] = data["ABoffset1"] * np.sin(data["A"]) + data["CBoffset1"] * np.cos(data["A"])

data["dx1"] = -data["ABoffset1"] * np.cos(data["A"]) + data["CBoffset1"] * np.sin(data["A"])


data["dy2"] = -data["ABoffset2"] * np.sin(data["A"]) + data["CBoffset2"] * np.cos(data["A"])
```

```
data["dx2"] = data["ABoffset2"] * np.cos(data["A"]) + data["CBoffset2"] * np.sin(data["A"])

data["dy3"] = data["ABoffset3"] * np.cos(data["A"]) + data["CBoffset3"] * np.sin(data["A"])
data["dx3"] = data["ABoffset3"] * np.sin(data["A"]) - data["CBoffset3"] * np.cos(data["A"])

data["dy4"] = -data["ABoffset4"] * np.cos(data["A"]) + data["CBoffset4"] * np.sin(data["A"])
data["dx4"] = -data["ABoffset4"] * np.sin(data["A"]) - data["CBoffset4"] * np.cos(data["A"])

# Drop no-longer needed columns to keep things tidy
data.drop("average_depth", axis=1, inplace=True)
data.drop("beam1_d", axis=1, inplace=True)
data.drop("beam2_d", axis=1, inplace=True)
data.drop("beam3_d", axis=1, inplace=True)
data.drop("beam4_d", axis=1, inplace=True)

data.drop("roll", axis=1, inplace=True)
data.drop("pitch", axis=1, inplace=True)
data.drop("heading", axis=1, inplace=True)

data.drop("theta1", axis=1, inplace=True)
data.drop("theta2", axis=1, inplace=True)
data.drop("theta3", axis=1, inplace=True)
data.drop("theta4", axis=1, inplace=True)

data.drop("bpd1", axis=1, inplace=True)
```

```
data.drop("bpd2", axis=1, inplace=True)
data.drop("bpd3", axis=1, inplace=True)
data.drop("bpd4", axis=1, inplace=True)

data.drop("ABoffset1", axis=1, inplace=True)
data.drop("ABoffset2", axis=1, inplace=True)
data.drop("ABoffset3", axis=1, inplace=True)
data.drop("ABoffset4", axis=1, inplace=True)

data.drop("CBoffset1", axis=1, inplace=True)
data.drop("CBoffset2", axis=1, inplace=True)
data.drop("CBoffset3", axis=1, inplace=True)
data.drop("CBoffset4", axis=1, inplace=True)

data.drop("A", axis=1, inplace=True)

#####Calculate Eastings and Northings#####

print "Converting lat/long points to UTM coordinates"

#Output file for projection
LatLongOut = pd.DataFrame(data[["lat", "long"]])
out_path4 = "{0}\LatLongOut.csv".format(output_dir)
LatLongOut.to_csv(out_path4)

# Use Arcpy to convert lat/long points to UTM coordinates
arcpy.MakeXYEventLayer_management(out_path4, "lat", "long", "out_layer",
arcpy.SpatialReference(LatLong_ref))
```

```
arcpy.Project_management("out_layer", "{0}\projected.shp".format(output_dir),
arcpy.SpatialReference(UTM_ref))

arcpy.Delete_management("out_layer")

arcpy.AddXY_management("{0}\projected.shp".format(output_dir))


#####Output file for use in part 2######

print "Outputing file for part 2"

out_path1 = "{0}\part1_output.csv".format(output_dir)

data.to_csv(out_path1, index=False)


#####Output file for Geoid Correction######

print "Outputing file for Geoid Correction"

data["lat"] = np.abs(data["lat"])

geoid_output = pd.DataFrame(data[["long", "lat"]])

out_path2 = "{0}\GeoidOutput.asc".format(output_dir)

geoid_output.to_csv(out_path2, index=False, header=False, sep=" ")


print "Finished"


###PART 2

 import pandas as pd

import arcpy


# User specified paramaters

output_dir = r"C:\Users\Bruce\Desktop\Test"

fn = r"C:\Users\Bruce\Desktop\Bathymetry\part1_output.csv"

geoid_corrected = r"C:\Users\Bruce\Desktop\Bathymetry\GeoidOutputOut.ASC"

UTM_coordinates = r"C:\Users\Bruce\Desktop\Test\UTM.txt"

antenna_height = 0.17
```

```
Z_threshold = 1000

# Specify spatial reference names
UTM_ref = "NAD 1983 UTM Zone 15N"

# Import data from part 1
data = pd.read_csv(fn)

# Import geoid corrected heights
df = pd.read_table(geoid_corrected, header=None, delim_whitespace=True)

#####Reclaculate heights using Geoid corrections#####
print "Recalcuating heights using Geoid corrections"

data["correction"] = df[6]
data["ortho_height"] = data["altitude"] + antenna_height - data["correction"]
data.drop("altitude", axis=1, inplace=True)
data.drop("correction", axis=1, inplace=True)

# Import UTM Coordinates
df1 = pd.read_csv(UTM_coordinates, thousands=",")
df1 = df1[["POINT_X", "POINT_Y"]]

# Join UTM coordinates
data[["Northing", "Easting"]] = df1[["POINT_Y", "POINT_X"]]
data.drop("lat", axis=1, inplace=True)
data.drop("long", axis=1, inplace=True)
```

```
# Calculate new coordinates
data["X1"] = data["Easting"] + data["dx1"]
data["Y1"] = data["Northing"] + data["dy1"]
data["Z1"] = data["ortho_height"] - data["Depth1"]

data["X2"] = data["Easting"] + data["dx2"]
data["Y2"] = data["Northing"] + data["dy2"]
data["Z2"] = data["ortho_height"] - data["Depth2"]

data["X3"] = data["Easting"] + data["dx3"]
data["Y3"] = data["Northing"] + data["dy3"]
data["Z3"] = data["ortho_height"] - data["Depth3"]

data["X4"] = data["Easting"] + data["dx4"]
data["Y4"] = data["Northing"] + data["dy4"]
data["Z4"] = data["ortho_height"] - data["Depth4"]

data.drop("Depth1", axis=1, inplace=True)
data.drop("Depth2", axis=1, inplace=True)
data.drop("Depth3", axis=1, inplace=True)
data.drop("Depth4", axis=1, inplace=True)
data.drop("dx1", axis=1, inplace=True)
data.drop("dy1", axis=1, inplace=True)
data.drop("dx2", axis=1, inplace=True)
data.drop("dy2", axis=1, inplace=True)
data.drop("dx3", axis=1, inplace=True)
data.drop("dy3", axis=1, inplace=True)
data.drop("dx4", axis=1, inplace=True)
```

```
data.drop("dy4", axis=1, inplace=True)

"""
#####Calculate single beam data#####
data["Z_Average"] = (data["Z1"] + data["Z2"] + data["Z3"] + data["Z4"]) / 4.0

single_beam = data[["Easting", "Northing", "Z_Average", "ensembleTimeId"]]
single_beam.columns = ["X", "Y", "Z", "ensembleTimeId"]
out_path = r"{0}\single_beam.csv".format(output_dir)
single_beam.to_csv(out_path, index=False)

# Convert points to shapefile
arcpy.MakeXYEventLayer_management(out_path, "X", "Y", "single_beam", UTM_ref,
"Z")
arcpy.CopyFeatures_management("single_beam",
"{0}\single_beam.shp".format(output_dir))
arcpy.Delete_management("single_beam")
"""

#####Calculate four beam data#####
print "Calculating four beam data"
beam1 = pd.DataFrame(data[["X1", "Y1", "Z1", "ensembleTimeId"]])
beam2 = pd.DataFrame(data[["X2", "Y2", "Z2", "ensembleTimeId"]])
beam3 = pd.DataFrame(data[["X3", "Y3", "Z3", "ensembleTimeId"]])
beam4 = pd.DataFrame(data[["X4", "Y4", "Z4", "ensembleTimeId"]])

beam1.columns = ["X", "Y", "Z", "ensembleTimeId"]
beam2.columns = ["X", "Y", "Z", "ensembleTimeId"]
beam3.columns = ["X", "Y", "Z", "ensembleTimeId"]
```

```
beam4.columns = ["X", "Y", "Z", "ensembleTimeId"]

beam1["ensembleTimeId"] = beam1["ensembleTimeId"] + "_1"
beam2["ensembleTimeId"] = beam2["ensembleTimeId"] + "_2"
beam3["ensembleTimeId"] = beam3["ensembleTimeId"] + "_3"
beam4["ensembleTimeId"] = beam4["ensembleTimeId"] + "_4"

frames = [beam1, beam2, beam3, beam4]
four_beam = pd.concat(frames)
four_beam = four_beam[four_beam.Z < 30000]

out_path1 = r"{0}\four_beam.csv".format(output_dir)
four_beam.to_csv(out_path1, index=False)

# Convert points to shapefile
print "Converting points to shapefile...make take awhile"

arcpy.MakeXYEventLayer_management(out_path1, "X", "Y", "four_beam",
arcpy.SpatialReference(UTM_ref), "Z")
arcpy.CopyFeatures_management("four_beam",
r"{0}\four_beam.shp".format(output_dir))

arcpy.Delete_management("four_beam")

print "Finished"
```

Sediment Rating Curves and Sediment Budgets

Methods for Quantifying Sediment Supply

The USGS collected suspended sediment and bedload sediment samples at each of these three gage locations between 2011 and 2016 (Groten et al., 2016). Suspended load samples were separated into percent sand and percent silt and clay. Bedload samples were sieved at one ϕ resolution between 0.0625 mm and 16 mm. To build each sediment budget we separate bedload measurements into two size fractions: 0.5 – 2 mm and 2 – 8 mm, to differentiate potential suspended load from bedload, respectively. For each gage, we develop sediment rating curves for the two bedload fractions and the suspended sands. At Mankato and Jordan, we fit a weighted, non-linear (power law), least squares regression to observations of daily bedload and suspended load discharge (tons/day) with mean daily discharge (cfs), consistent with methods of Groten et al. (2016) (Appendix B). For the Minnesota River at Jordan, we remove a single outlier (more than an order of magnitude larger than similar measurements) from the 2 – 8 mm fraction.

Observations of bedload at Fort Snelling were exceptionally small, despite uncertainties inherent in sampling low transport rates on large rivers (Personal Communication Joel Groten, August 2018). Therefore, we assume bedload discharge at Fort Snelling to be negligible. Suspended load measurements made at flows greater than 19,000 cfs were made on the falling limb of the hydrograph and are therefore less representative of average conditions. Removing these few points and fitting a weighted nonlinear least squares regression to the suspended load data (consistent with Groten et al., 2016) resulted in an unreasonable exponential fit for high discharges. Therefore, we

fit the suspended load data using the Garcia and Parker (1991) dimensionless suspended sediment entrainment function:

$$E_s = \frac{A\, Z_u^5}{\left(1+\frac{A}{0.3}Z_u^5\right)} \quad \text{(B1)}$$

where E_s is the dimensionless entrainment rate, A is equal to 1.3×10^{-7}, and Z_u is the skin friction shear velocity, u_{*s}, divided by the particle fall velocity, ν_s, multiplied by particle Reynolds number, R_{ep}, raised to the 0.6 power; and the Garcia (1999) volumetric suspended sediment transport per unit width formula:

$$q_s = \frac{1}{\kappa}\bar{c_b}u_* H\left[J_1\, ln\left(30\frac{H}{k_c}\right) + J_2\right] \quad \text{(B2)}$$

where q_s is the volumetric transport rate per unit width, is the von Karmen constant 0.4, $\bar{c_b}$ is the near bed sediment concentration, u_* is the total friction velocity, H is the flow depth, k_c is the composite roughness, and J_1 and J_2 are approximated from a regression analysis using seven coefficients and the computed Rouse number, Z_R (Abad and García, 2006; Garcia, 2008). Channel width, depth, and velocity for a given discharge are calculated using the empirical, power law fit between USGS field measurments of discharge and each variable made between 9/8/2003 and 8/9/2018. Measurments made on 5/1/2018 and 4/1/2010 are exculeded from power law relations since reported channel widths on these days are greater than three standard deviations above the mean channel width for all field measurements. Power law coeffiecients for channel width, depth, and velocity are reported in Table C2. Slope at Fort Snelling is approximately 0.0001 based on USGS 30 m DEM derived slope. We fit the suspended sediment transport model by adjusting the grain size until there was a visual match between model and data; the best fit model assumes grain size equal to 0.15 mm.

The USGS also made sediment transport measurements at High Island Creek, a tributary that enters the Minnesota River near river kilometer 98, towards the lower end of the upstream reach. We use the drainage area-normalized sediment loads from High Island Creek to estimate sediment loads from unsampled Rush River and Bevens Creek. Sand Creek was excluded as a sediment input to the Minnesota mainstem because it terminates in a floodplain lake in the downstream reach between Jordan and Chaska.

We couple 2011 to 2016 sediment discharge observations with measurements of meander migration and channel widening made between 2010 and 2017 (nearest aerial photo dates) to compute volumes of sand lost from channel widening and outer bank erosion due to meander migration, as well as volumes of sand deposited from inner bank bar deposition. To calculate sediment inputs from channel widening we multiplied the average widening rate (m/yr) by bank height (m), reach length (m), average streambank bulk density of 1350 kg/m^3, and a streambank sand content of 46%, following the methods of Lauer et al. (2017). Assumed values for the calculation of sediment inputs from channel widening are reported in Table C3. We computed sediment contributions from meander migration in a similar fashion, using the average migration rate (m/yr) minus half of the average widening rate. Point bar deposition was calculated as the average migration rate (m/yr) minus half of the widening rate (m/yr), multiplied by the bar height (m), reach length (m), average point bar bulk density of 1590 kg/m^3, and a bar sand content of 81% (Lauer et al., 2017). Our bar grain size data suggest a similar sand content of 82%. See Table C3 for more detail.

Annual floodplain deposition was taken to be 0.8 mm/yr, given the range of values presented by Lenhart et al. (2013). The downstream most 20 km of the Minnesota

River is dredged for navigation purposes. Therefore, annual average dredging (2010 – 2017), 16,403.6 tons/yr, was included in the Jordan to Fort Snelling budget based on Army Corps of Engineers Record of Dredging Events (Personal Communication Rebecca Seal-Soileau, September 12, 2018).

Table C1. Weighted non-linear least squares regression coefficients (a) and exponents (b) for the power law function $Q_b = aQ^b$ between gage discharge and daily sediment load measured at Mankato, High Island Creek, and Jordan gages.

Site	Transport	a	b	Comments
Mankato	2-8 mm	1.07E-04	1.46E+00	
Mankato	0.5-2 mm	6.38E-02	8.91E-01	
Mankato	Suspended Sands	9.84E-04	1.51E+00	
High Island Creek	2-8 mm	9.96E-02	8.13E-01	
High Island Creek	0.5-2 mm	3.36E+00	3.62E-01	
High Island Creek	Suspended Sands	3.11E-02	1.56E+00	
Jordan	2-8 mm	3.57E-06	1.09E+00	Removed single outlier at 4740 cfs
Jordan	0.5-2 mm	3.24E-05	1.11E+00	
Jordan	Suspended Sands	1.32E-06	2.21E+00	

Table C2. Power law coefficients (a) and exponents (b) for the function $Q = aX^b$ between gage discharge (Q) in cfs and field measured width, depth, and velocity (X) in US customary units at the Fort Snelling gage (USGS 05330920).

Variable	a	b
Width	221.45	0.0554
Depth	4.5514	0.1353
Velocity	0.0010	0.8067

Table C3. Lengths and rates for Mankto to Jordan and Jordan to Fort Snelling reaches for the calculation of sediment budget inputs and outputs from channel widening and meander migration.

Site	Widening Rate (m/yr)	Migration Rate (m/yr)	Reach Length (km)	Bank Height (m)
Mankato to Jordan	0.8329	1.50	102.17	5
Jordan to Fort Snelling	0.6696	0.57	65	5

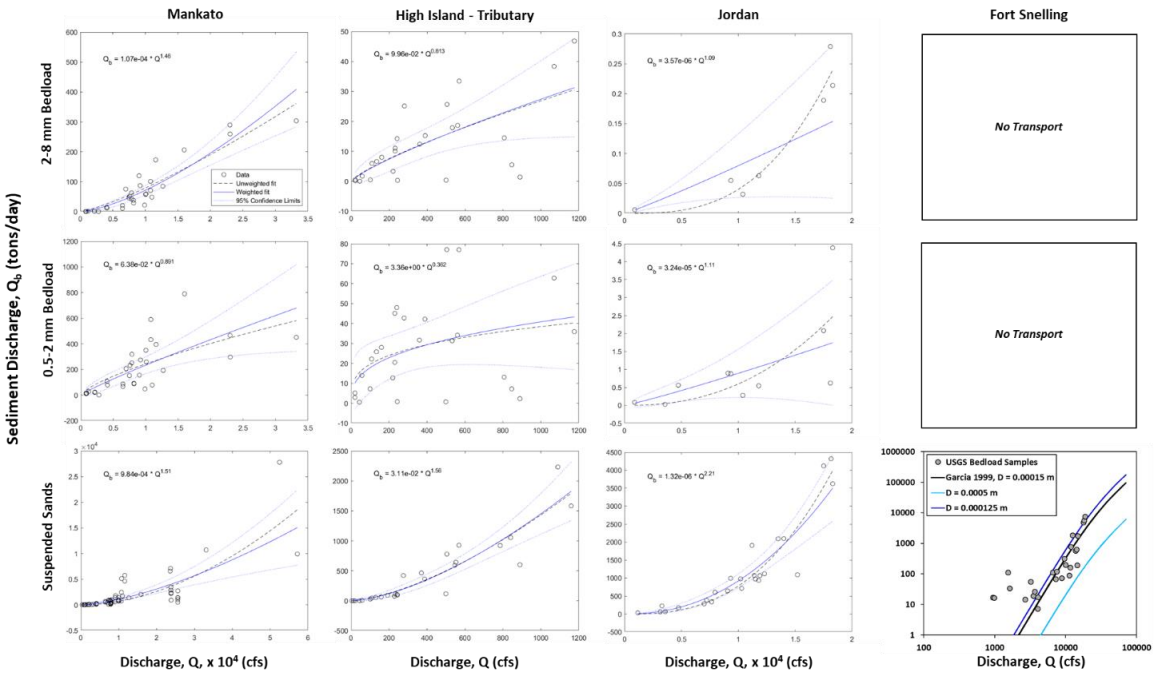

Fig. C1. Sediment rating curves for USGS bedload and suspended load measurements at four gages for different grain size fractions. For Mankato, High Island, and Jordan rating relations were best fit by a weighted non-linear least squares regression of power-law form. For Fort Snelling, suspended sand measurements were best fit by the Garcia and Parker 1991 and Garcia 1999 models (Equations B1 & B2).

Matlab Script for Sediment Rating Curves and Confidence Intervals

Developed by Brendan P. Murphy, Utah State University, October 3, 2018

This script is intended for fitting a weighted, non-linear (power law), least squares regression between the dependent variable, sediment discharge in tons/day, and the independent variable, sampling discharge in cubic feet per second. Sediment data from Groten et al. 2016 and lumped into daily suspended load, bedload from 0.5 – 2 mm, and bedload from 2 – 8 mm fractions. Confidence intervals are calculated for the 95th percentile.

```
%% Filenames

%In
input_filename1 = 'Mankato_ss.xls'; %needs format extension
input_filename2 = 'Mankato_Flow.xls'; %needs format extension

%Out
outputfilename = 'Mankato_Output_SSsums.xls'; %needs format extension
outputfilename2 = 'Mankato_Output_SSall.xls'; %needs format extension
figurefilename  = 'Mankato_SSfit'; %no format extension

%% Read in Excel Files
[num1,~,~] = xlsread(input_filename1);
[num2,txt2,~] = xlsread(input_filename2);

%% Create Variables
x = num1(:,1);
y = num1(:,2);
Q = num2(:,1);
date = txt2(2:end,1);
% Fitting Predictor (for plotting)
xx = linspace(min(x),max(x))';

%% Creating Nonlinear Least Squares Model Fits

%Unweighted Model Fit
modelFun = @(b,x) b(1)*x.^b(2);
beta0 = [2.605e-5 1.861];
mdl = fitnlm(x,y,modelFun,beta0);

%Plotting
figure
hold on
plot(x,y,'ko'); %Plot Data
line(xx,predict(mdl,xx),'linestyle','--','color','k') %Plot Unweighted Fit
```

```
% Calculate Weights from Unweighted Fit Parameter
wt_b = mdl.Coefficients.Estimate(2);
w = 1./(x.^wt_b);

% Weighted Model Fit
wmdl = fitnlm(x,y,modelFun,beta0,'Weight',w);

% Plotting Weighted Model Fit w/ 95% CI
[ypred,ypredci] = predict(wmdl,xx,'Simultaneous',true);
plot(xx,ypred,'b-', xx,ypredci,'b:');

xL = xlim;
yL = ylim;
funname = ['Q_b = ',num2str(wmdl.Coefficients.Estimate(1),'%10.2e\n'),' *
Q^{',num2str(wmdl.Coefficients.Estimate(2),3),'}'];

text(0.1*xL(2),0.85*yL(2),funname)
xlabel('Discharge,cfs'); ylabel('Suspended Sediment, tons/day');
legend({'Data', 'Unweighted fit', 'Weighted fit', '95% Confidence
Limits'},'location','SouthEast');
box on

print(figurefilename,'-dtiffn')

%% Calculating Predicted SS Loads

[SSpred,SSpredci] = predict(wmdl,Q,'Simultaneous',true);

% Plotting
figure
plot(Q,SSpred,'ko', Q,SSpredci,'ko');

% Total Predicted Loads w/ CI
SS_Total = sum(SSpred);
SS_5th = sum(SSpredci(:,1));
SS_95th = sum(SSpredci(:,2));

%% Write Output
output =
table(SS_Total,SS_5th,SS_95th,'VariableNames',{'Predicted','Fifth','NinetyFifth'});
writetable(output,outputfilename)

output2 =
table(date,Q,SSpred,SSpredci(:,1),SSpredci(:,2),'VariableNames',{'Date','Discharge','Pred
icted_all','Fifth_all','NinetyFifth_all'});
writetable(output2,outputfilename2)
```

Original Sediment Budget: Budget Closed by Reducing all Budget Values. Jordan Suspended Sands Different in Upstream and Downstream Reach

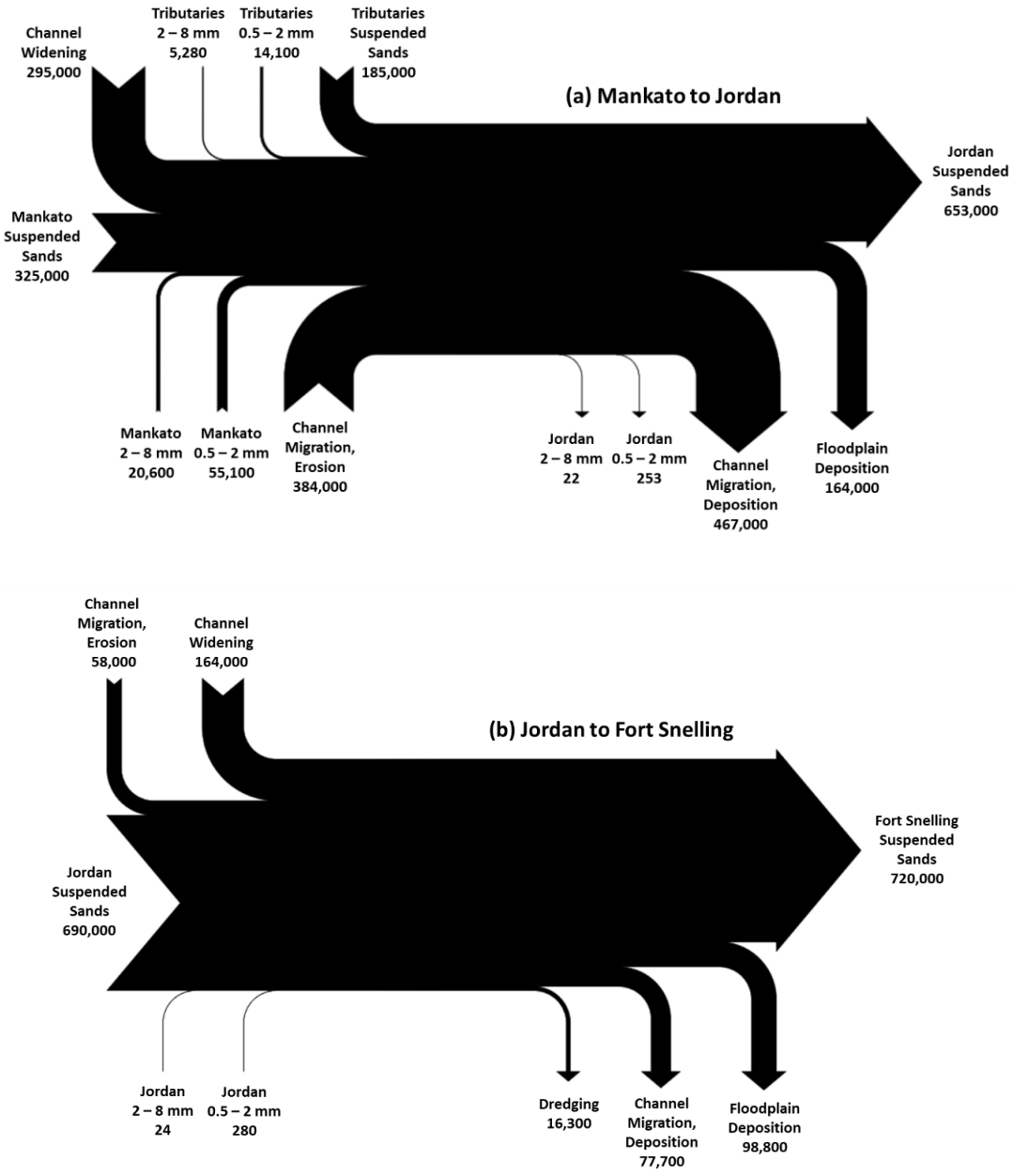

Fig. C2. Average annual sediment budget computed between 2011 and 2016 for a) the reach between Mankato and Jordan, and b) Jordan to Fort Snelling on the lower Minnesota River. Sediment inputs are arrow tails and sediment outputs are arrow heads. Sediment sources differentiated between suspended sands, coarse bedload sands (0.5-2 mm), and fine bedload gravels (2-8 mm). Values are reported in tons/year and rounded to three significant digits. Small budget deficits are an artifact of rounding.

APPENDIX D – PERMISSION TO REPRINT WATER

February 20, 2019

Zeinab Takbiri
1730 Larpenteur AVE W, APT 2H,
Falcon heights, MN, 55113

Dear Zeinab:

I am in the process of preparing my dissertation in the Watershed Sciences department at Utah State University. I hope to complete my degree program in the coming days to weeks. I am requesting your permission to include the material published Hydrology and Earth Systems Sciences as my second dissertation chapter. I have included you in my dissertation acknowledgments, cited our work at the beginning of the chapter and included copyright and reprint rights information in a special appendix. The bibliographic citation will appear as shown: Kelly, S. A., Takbiri, Z., Belmont, P., & Foufoula-Georgiou, E. (2017). Human amplified changes in precipitation-runoff patterns in large river basins of the Midwestern United States. Hydrology and Earth System Sciences, 1–37. https://doi.org/10.5194/hess-2017-133

Please advise me of any changes you require. Please indicate your approval of this request by signing in the space provided, attaching any other form or instruction necessary to confirm permission. If you have any questions, please call me at the number below.

I hope you will be able to reply immediately.

Thank you for you cooperation,

Sara Kelly

(714) 348-2609

I hereby give permission to Sara Kelly to reprint the following material in her dissertation:
Kelly, S. A., Takbiri, Z., Belmont, P., & Foufoula-Georgiou, E. (2017). Human amplified changes in precipitation-runoff patterns in large river basins of the Midwestern United States. Hydrology and Earth System Sciences, 1–37. https://doi.org/10.5194/hess-2017-133

Signed: Zeinab Takbiri

APPENDIX E – PERMISSION TO REPRINT HYDROLOGY AND EARTH SYSTEMS SCIENCES

© 2018 by the authors. Submitted for possible open access publication under the terms and conditions of the Creative Commons Attribution (CC BY) license (http://creativecommons.org/licens

CURRICULUM VITAE

Sara Ann Kelly

Watershed Sciences PhD Candidate

sara.kelly@aggiemail.usu.edu
http://www.cnr.usu.edu/wats
Tel: (714) 348-2609
Fax: (435) 797-1871

Dept. of Watershed Sciences
Utah State University
5210 Old Main Hill
Logan, UT 84322-5210

RESEARCH AND TEACHING INTERESTS

My interests lie in understanding the processes which govern river dynamics and landscape evolution over human and geologic timescales. Beyond being a personal passion that I wish to share with students, scholars, and those outside the scientific community through teaching, research, and outreach, interdisciplinary knowledge of watershed sciences is critical for addressing global problems of climate change, natural hazards, and food and water security. The focus of my most recent research includes deconvolving climate and agricultural land use impacts on watershed hydrology; identifying dominant failure mechanisms and thresholds for large river bluff erosion using inexpensive, high resolution surveying techniques; and determining the role of sediment supply on rates and modes of river channel adjustment in a transient basin responding to human-amplified streamflow. My education and training has prepared me well for teaching courses such as Watershed Sciences, Hydrology, Fluvial Geomorphology, Natural Hazards, and Geographic Information Systems.

EDUCATION

Ph.D. Watershed Science
2012 – present, anticipated graduation May 2019
Department of Watershed Sciences
Utah State University, Logan, UT
Dissertation: River hydrology, morphology, and dynamics in an intensively managed, transient landscape

B.S. Environmental Science Technology and Policy
2012, Summa Cum Laude with Distinction in Major
Minor, Outdoor Education and Recreation
Division of Science & Environmental Policy
California State University Monterey Bay, Seaside, CA
Honors Thesis: Geomorphic change in the Upper Carmel River, CA: effects of the 2008 Basin Complex Fire

PEER-REVIEWED PUBLICATIONS *Citations 137; h-index 4*

Kelly SA, Belmont P, Wilcock P (*in prep*aration). Bedload supply and transport controls on morphodynamics of a transient sand bed river. Geomorphology, *to be submitted May 2019*

2019 Gran K, Dolph C, Baker A, Bevis M, Cho SJ, Czuba JA, Dalzell B, Danesh-Yazdi M, Hansen A, **Kelly S**, Lang Z, Schwenk J, Belmont P, Finlay JC, Kumar P, Rabotyagov S, Roehrig G, Wilcock P, Foufoula-Georgiou E. (2019). The power of environmental observatories for advancing multidisciplinary research, outreach, and decision support: the case of the Minnesota River Basin. Water Resources Research, 55.

2018 **Kelly SA**, Belmont P. (2018). High resolution monitoring of river bluff erosion reveals dominant failure mechanisms and geomorphically effective flows. Water 10(4), doi: 10.3390/w10040394

2017 **Kelly SA**, Takbiri Z, Belmont P, Foufoula-Georgiou E. (2017). Human amplified changes in precipitation-runoff patterns in large river basins of the Midwestern United States. Hydrology and Earth System Sciences 21: 5065–5088, doi: 10.5194/hess-2017-133

2016 Belmont P, Stevens JR, Czuba JA, Kumarasamy, K, **Kelly SA** (2016). Comment on "Climate and agricultural land use change impacts on streamflow in the upper midwestern United States" by Satish C. Gupta et al. Water Resources Research 52(9): 7523-7528, doi: 10.1002/2015WR018476

2015 Passalacqua P, Belmont P, Staley DM, Simley JD, Arrowsmith JR, Bode CA, Crosby C, DeLong SB, Glenn NF, **Kelly SA**, Lague D, Sangireddy H, Schaffrath K, Tarboton DG, Wasklewicz T, Wheaton JM. (2015). Analyzing high resolution topography for advancing the understanding of mass and energy transfer through landscapes: A review. Earth-Science Reviews 148: 174-193, doi: 10.1016/j.earscirev.2015.05.012

AWARDS AND HONORS

2016 Best Student Oral Presentation, 26 November 2016, Fourth Irish Geomorphology Scientific Workshop, University College Cork, Ireland

2014 National Science Foundation, Graduate Research Fellowship Program - $138,000

2014 Geological Society of America, Graduate Student Research Grant - $1,500

2013 Geological Society of America, Rocky Mountain Section Student Travel Grant - $140

2012 California State University Monterey Bay, Service Learning Award, Environmental Science, Technology and Policy

2012 Association for Women Geoscientists, Outstanding Women in Geosciences Student Award, San Francisco Bay Area Chapter - $100

PRESENTATIONS – INVITED

2018 **Kelly SA**, Belmont P. River hydrology, morphology, and dynamics in an intensively managed, transient landscape. Franklin and Marshall College ENE Lite Lunch Series; 2 November, 2018; Lancaster, PA.

2017 **Kelly SA**, Belmont P. Minnesota River channel geometry mapping. Minnesota Invasive Carp Forum; 29 March, 2017; Bloomington, MN.

2015 **Kelly SA**. Unraveling the complexity of sediment cascades: the role of valley setting, sediment supply, and hydrology on river form, processes, and morphodynamics. Geography Department, Minnesota State University; 2015 October 28; Mankato, MN.

2014 Belmont P, Kumarasamy K, **Kelly SA**, Schaffrath KR, Beach TJ. The cascade of non-stationarity. American Geophysical Union Fall Meeting. 2014 December; San Francisco, CA.

2014 Belmont P, Kumarasamy K, **Kelly SA**, Schaffrath KR, Beach TJ. The cascade of non-stationarity. University of Tennessee, Knoxville Distinguished Lecturer Series.

PRESENTATIONS – PROFESSIONAL MEETINGS

Oral Presentations

2017 **Kelly S**, Belmont P. High resolution monitoring of large river bluff failures and implications for downstream channel morphodynamics. American Geophysical Union Fall Meeting. 2017 December 13; New Orleans, LA.

2016 **Kelly SA**, Belmont P. River bluff erosion responds rapidly to high streamflow events. Fourth Irish Geomorphology Scientific Workshop; 2016 November 26; University College Cork, Ireland

2015 **Kelly S**, Belmont P. Patterns and processes of width adjustment to increased streamflow in semi-alluvial rivers. American Geophysical Union Fall Meeting; 2015 Dec 15; San Francisco, CA.

2013 **Kelly S**, Belmont P. Mapping bathymetry in a large meandering river above and below a significant sediment input. Geological Society of America Annual Meeting; 2013 Oct 30; Denver, CO.

Poster Presentations

2016 **Kelly S**, Belmont, P. Human and Climate Amplified Rapid River Bluff Erosion: an Application of Terrestrial-Based Structure-from-Motion and Time-Lapse Photogrammetry in the Midwestern USA. 13 Dec 2016; San Francisco, CA.

2014 **Kelly S**, Belmont P. Topographic signatures of meandering rivers with differences in outer bank cohesion. American Geophysical Union Fall Meeting; 19 Dec 2014; San Francisco, CA.

2014 **Kelly S**, Belmont P. Application of terrestrial-based structure-from-motion (SFM) photogrammetry to the measurement and monitoring of river bluff erosion.

Geological Society of America Annual Meeting; 2014 Oct 22; Vancouver, BC, Canada.

2013 **Kelly S**. Mapping bathymetry in a large meandering river above and below a significant sediment input. ADCPs in Action! The 2013 Teledyne RD Instruments Users' Conference; 2013 Sept 29 – Oct 2; San Diego, CA.

2012 **Kelly S**, Richmond S, Smith D. Quantifying geomorphic change in the Upper Carmel River following the 2008 Basin Complex Fire. From Lions to Luminescence: Linking Land and Sea. Monterey Bay National Marine Sanctuary, Sanctuary Currents Symposium; 2012 Apr 14; Seaside, CA.

2011 **Kelly S**, Flores D, Jordan J, Lutey A, Barrett K, Galster J, Ophori D. Hydrologic budget assessment of a small forested lake in northwestern NJ. American Geophysical Union Fall Meeting; 2011 Dec 8; San Francisco, CA.

2011 **Kelly S**, Nicol C. Assessing salmonid passage through culverts in the Coast Dairies, CA. Ripple Effects: The Far-Reaching Impacts of Local Ocean Research. Monterey Bay National Marine Sanctuary, Sanctuary Currents Symposium; 2011 Apr 9; Seaside, CA.

2010 **Kelly S**. Assessing anadromous fish passage through culverts in the Coast Dairies, CA. Society for the Advancements in Chicanos and Native Americans in Science National Conference; 2010 Oct 1; Anaheim, CA.

PRESENTATIONS – DEPARTMENTAL TALKS

2017 Human and climate amplified, rapid river bluff erosion. Department of Watershed Sciences Graduate Student Research Symposium, Utah State University; 2017 April 7; Logan, UT.

2015 Sediment contributions from bluff erosion caught on camera in the Le Sueur River, south central Minnesota. Department of Watershed Sciences Graduate Student Research Symposium, Utah State University; 2015 April 10; Logan, UT.

2013 Profound hydrologic changes in the Minnesota River Basin: Towards an improved understanding of how humans and climate influence natural processes. Department of Watershed Sciences Graduate Student Research Symposium, Utah State University; 2013 March 22; Logan, UT.

TEACHING EXPERIENCE

Utah State University, Logan, UT

2017 Primary Instructor, Fundamentals of Watershed Science (Spring)

2016 Teaching Assistant, Watershed Sciences Graduate Induction Course (Summer)

2016 Co-Instructor, Fundamentals of Watershed Science (Spring)

2015 Teaching Assistant, Watershed Sciences Graduate Induction Course (Summer)

2015 Teaching Assistant, Small Watershed Hydrology (Spring)

2013 Assistant-Teaching Assistant, Small Watershed Hydrology (Spring)

California State University Monterey Bay, Seaside, CA
2012 Mathematics Tutor, Academic Skills and Achievement Program (2009-2012)

RESEARCH EXPERIENCE

Belmont Hydrology and Fine Sediment Lab, Utah State University, Logan, UT

- Measuring frequent bluff erosion using structure-from-motion (SfM) and timelapse photogrammetry, GIS, and empirical landslide geometry relations to determine the importance of streamflow vs other process on bluff erosion rates, as well as to constrain geomorphically effective flow magnitudes
- Evaluating climate and agricultural land use effects on hydrologic change in large river basins of the Upper Midwest, USA
- Topographic and bathymetric surveying, specifically of fluvial environments using satellite-GPS and echo sounding technologies; interest in inexpensive, accurate methods for building and differencing topography using Matlab, Python, and Geographic Information Systems
- Determining patterns and processes of channel width, depth, migration, sinuosity, and grain size in equilibrium and transient river basins

Watershed Geology Lab, California State University, Monterey Bay, Seaside, CA

- Quantifying geomorphic effects of wildfire in the Upper Carmel River basin, post-2008 Basin-Complex Fire, Los Padres National Forest, CA
- Determining the limit of anadromy for salmonid spawning in six coastal California streams using topographic and hydraulic surveying, as well as HEC-RAS 1-D flow modeling

National Science Foundation, Research Experience for Undergraduates, New Jersey School of Conservation, Montclair State University, Branchville, NJ

- Developing a hydrologic budget for a small forested lake in northwest New Jersey

Alaska Wildlands Studies, Wrangell Mountain Center, McCarthy, AK

- Mapping current and historical glacial terminus extent to determine factors influencing glacial retreat rates for six glaciers in the Wrangell Mountains, AK

DEPARTMENTAL, UNIVERSITY, AND COMMUNITY SERVICE

2016 Graduate Student Council Committee, Quinney College of Natural Resources, Utah State University, Logan, UT
2015 Science Fair Volunteer Judge, Hillcrest Elementary School, Logan, UT
2014 Aquatic/Riparian Ecology Faculty Search Committee, Department of Watershed Sciences and Ecology Center, Utah State University, Logan, UT

2014 Graduate Student Council Committee, Quinney College of Natural Resources, Utah State University, Logan, UT
2013 Reviewer Graduate Enhancement Award, Utah State University Student Association, Logan, UT
2012-2014 Cyberseminar coordinator for NSF Water Sustainability and Climate REACH research group
2010-2012 Youth in Wilderness Program Trail Leader, Ventana Wilderness Alliance, Santa Cruz, CA
2009- 2011 Composting Outreach Volunteer, Monterey Peninsula Regional Waste Management District, Marina, CA
2009 YW-Teens After School Program Volunteer, YWCA, Watsonville, CA

EXTRACURRICULAR WORKSHOPS AND TRAININGS

2016 Mathematical Modeling of Earth's Dynamic Systems (July 31 – Aug 5)
Pennsylvania State University, State College, PA
2015 Workshop on Modeling Mixed-Sediment River Morphodynamics (May 27-29)
Delft University of Technology, Delft, Netherlands
2013 Hydromorphodynamics Modeling using Delft3D Open Source (December 16-17)
Consulate General of the Kingdom of the Netherlands, San Francisco, CA
2013 Software Carpentry Boot Camp (March 23-24)
Utah State University, Logan, UT
2012 Summer Institute on Earth-Surface Dynamics (August 8-17)
National Center for Earth-Surface Dynamics, Minneapolis, MN

PROFESSIONAL MEMBERSHIPS

Geological Society of America, American Geophysical Union, Society for the Advancements of Chicanos and Native Americans in Science

PROFESSIONAL REFERENCES

Patrick Belmont (Major Advisor)
Professor of Hydrology and Geomorphology
Department of Watershed Sciences
Utah State University
5210 Old Main Hill, Logan, UT 84322-5210
Office: 435-797-3794 | Cell: 435-374-8574
patrick.belmont@usu.edu

Peter Wilcock
Department Head

Department of Watershed Sciences
Utah State University
5210 Old Main Hill, Logan, UT 84322-5210
Office: 435-797-2463 | Cell: 443-564-6253
wilcock@usu.edu

Efi Foufoula-Georgiou
Distinguished Professor
Department of Civil and Environmental Engineering
University of California, Irvine
Engineering Hall 5400, Irvine, CA 92697-2175
Office: 949-824-9643 | Cell: 651-470-2038
efi@uci.edu